2018-05-15

Engineered Exosomes for Delivery of Therapeutic siRNAs to Neurons

Reka A. Haraszti
University of Massachusetts Medical School

ENGINEERED EXOSOMES FOR DELIVERY OF THERAPEUTIC siRNAS TO NEURONS

A Dissertation Presented

By

REKA AGNES HARASZTI

Submitted to the Faculty of the

University of Massachusetts Graduate School of Biomedical Sciences, Worcester

In partial fulfillment of the requirements for the degree of

DOCTOR OF PHILOSOPHY

May 15th, 2018

Translational Science Program

ENGINEERED EXOSOMES FOR DELIVERY OF THERAPEUTIC siRNAS TO NEURONS

A Dissertation Presented

By

REKA AGNES HARASZTI

This work was undertaken in the Graduate School of Biomedical Sciences

Translational Science Program

Under the mentorship of

Anastasia Khvorova, Ph.D., Thesis Advisor

Neil Aronin, M.D., Member of the Committee

Jonathan Watts, Ph.D., Member of the Committee

Terence Flotte, M.D., Member of the Committee

Xandra O. Breakefield, Ph.D., External Member of the Committee

Miguel Sena-Esteves, Ph.D., Chair of Committee

Mary Ellen Lane, Ph.D.,

Dean of the Graduate School of Biomedical Sciences

May 15th, 2018

DEDICATION

Dedicated to the memory of Szabó Szabolcs,
an inspiring chemistry teacher in my high school,
who first taught me about the importance of humility in science.

ACKNOWLEDGEMENT

Anastasia believed in me from my rotation interview on throughout this adventure. She always appreciated and fostered my interest in translational science and was open to my sometimes-crazy ideas. Her faith kept me going even in difficult times. She has been very good at motivating me and building a tolerant, creative and cooperative team to work with. She helped me get public exposure at numerous conferences. I am immensely thankful to have Anastasia as my "science-mother".

Neil has taught me a lot about scientific writing and understanding point of views different from mine. This experience made me a better communicator. He pushed the limits of my knowledge and scientific skills, making me grow. He also encouraged me to present my data at various meetings. I enjoyed his stories about medicine and life a lot. I am very thankful having had Neil as my co-mentor.

The Khvorova and Aronin labs were my family in a land far away from home. I thank Marie, Bruno, Julia, Dimas, Maire, Matt, Andy, Rachael, Anton, Sarah, Soki, James, Chantal and Annabelle to be there for me in times of sorrow and laughter. For fruitful scientific conversations, for overcoming your personal frustrations, for crying with me in the kitchen, for drinking tea and liquor together. For dancing, paintballing, skiing and pushing my car up the snowy hill in Vermont. I thank Maire for proof-reading this dissertation and so much more pieces of writing before. Thank you, Marie, for introducing me to the world of exosomes. Annabelle and Loic have been tremendous co-first-authors.

I thank my committee, Neil, Miguel, Jon and Terry for their continued support on this journey.

Acknowledgement

I met my husband, Jörg, at an RTI tea time. He played a major role in making graduate school bearable for me during difficult times and he shared my joy over science during happy times. I admire his perseverance in getting things done and reaching his goals – a skill I am learning from him every day. I thank Jörg for supporting me emotionally and scientifically through many difficulties and successes of this PhD.

And last, but not least, I thank my family in Hungary. My parents taught me critical thinking and that there were no impossibles. This path led me to UMass for my doctoral thesis work. My sister, Judit, is my best friend with a special ability to always cheer me up no matter how dark things seem. My brother, Peter, has always been my biggest fan. Big thank you for their continued emotional support. I missed them very much.

ABSTRACT

Extracellular vesicles (EVs), exosomes and microvesicles, transfer endogenous RNAs between neurons over short and long distances. We have explored EVs for siRNA delivery to brain. (1) We optimized siRNA chemical modifications and siRNA conjugation to lipids for EV-mediated delivery. (2) We developed a GMP-compatible, scalable method to manufacture active EVs in bulk. (3) We characterized lipid and protein content of EVs in detail. (4) We established how protein and lipid composition relates to siRNA delivering activity of EVs, and we reverse engineered natural exosomes (small EVs) into artificial exosomes based on these data.

We established that cholesterol-conjugated siRNAs passively associate to EV membrane and can be productively delivered to target neurons. We extensively characterized this loading process and optimized exosome-to-siRNA ratios for loading. We found that chemical stabilization of 5'-phosphate with 5'-*E*-vinylphosphonate and chemical stabilization of all nucleotides with 2'-*O*-methyl and 2'-fluoro increases the accumulation of siRNA and the level of mRNA silencing in target cells. Therefore, we recommend using fully modified siRNAs for lipid-mediated loading to EVs. Later, we identified that α-tocopherol-succinate (vitamin E) conjugation to siRNA increases productive loading to exosomes compared to originally described cholesterol.

Low EV yield has been a rate-limiting factor in preclinical development of the EV technology. We developed a scalable EV manufacturing process based on three-dimensional, xenofree culture of mesenchymal stem cells and concentration of EVs from conditioned media using tangential flow filtration. This process yields exosomes more efficient at siRNA delivery than exosomes isolated *via* differential ultracentrifugation from two-dimensional cultures of the same cells.

Abstract

In-depth characterization of EV content is required for quality control of EV preparations as well as understanding composition–activity relationship of EVs. We have generated mass-spectrometry data on more than 3000 proteins and more than 2000 lipid species detected in exosomes (small EVs) and microvesicles (large EVs) isolated from five different producer cells: two cell lines (U87 and Huh7) and three mesenchymal stem cell types (derived from bone marrow, adipose tissue and umbilical cord Wharton's jelly). These data represent an indispensable resource for the community. Furthermore, relating composition change to activity change of EVs isolated from cells upon serum deprivation allowed us to identify essential components of siRNA-delivering exosomes. Based on these data we reverse engineered natural exosomes into artificial exosomes consisting of dioleoyl-phosphatidylcholine, cholesterol, dilysocardiolipin, Rab7, AHSG and Desmoplakin. These artificial exosomes reproduced efficient siRNA delivery of natural exosomes both *in vitro* and *in vivo*. Artificial exosomes may facilitate manufacturing, quality control and cargo loading challenge that currently impede the therapeutic EV field.

TABLE OF CONTENTS

Table of Contents

Table of Contents

LIST OF TABLES

LIST OF FIGURES

List of Figures

List of Figures

LIST OF COPYRIGHTED MATERIALS

- Figure 1.2 is reproduced from
    - Bramsen JB, Kjems J: Development of therapeutic-grade small interfering RNAs by chemical engineering. Frontiers in Genetics. 2012 Aug.20.
- Text and figures in Chapter III are
    - Published in *Nucleic Acid Research* as scientific article
        - MR Hassler*, AA Turanov*, JF Alterman*, **RA Haraszti**, AH Coles, MF Osborn, D Echeverria, M Nikan, WE Salomon, L Roux, BMDC Godinho, DV Morrissey, PD Zamore, SA Karumanchi, MJ Moore, N Aronin, A Khvorova. Comparison of fully and partially chemically-modified siRNA in conjugate-mediated delivery in vivo. Nucl Acid Research. 2018 Febr.8.
    - Published in *Nucleic Acid Research* as scientific article
        - **RA Haraszti***, L Roux*, AH Coles, AA Turanov, JF Alterman, D Echeverria, BM Godinho, N Aronin, A Khvorova. 5′vinylphosphonate improves tissue accumulation and efficacy of conjugated siRNAs *in vivo.* Nucl Acid Research, 2017 June 7.
    - Accepted in *Molecular Therapy* as scientific article
        - A Biscans*, **RA Haraszti***, D Echeverria, R Miller, MC Didiot, M Nikan, L Roux, N Aronin, A Khvorova. Hydrophobicity of lipid-conjugated siRNAs predicts productive loading into small extracellular vesicles.
    - Under Review in *Molecular Therapy Nucleic Acids* as manuscript
        - **RA Haraszti**, R Miller, MC Didiot, A Biscans, JF Alterman, MR Hassler, L Roux, D Echeverria, E Sapp, M DiFiglia, N Aronin, A Khvorova. Optimized cholesterol-siRNA chemistry improves productive loading into small extracellular vesicles.

- Text and figures in Chapter IV are

  - Under Review in *Molecular Therapy* as manuscript

    - **Haraszti RA**, R Miller, M Stoppato, YY Sere, A Coles, MC Didiot, R Wollacot1, E Sapp, J Leszyk, M Dubuke, S Shaffer, M DiFiglia, Y Wang, N Aronin, A Khvorova. Exosomes produced from three-dimensional cultures of mesenchymal stem cells by tangential flow filtration show higher yield and improved activity.

- Text and figures in Chapter V are

  - Published in *Journal of Extracellular Vesicles* as scientific article

    - **Haraszti RA**, Didiot MC, Sapp E, Leszyk J, Shaffer SA, Rockwell HE, Gao F, Narain NR, DiFiglia M, Kiebish MA, Aronin N, Khvorova A. High-resolution proteomic and lipidomic analysis of exosomes and microvesicles from different cell sources. J Extracell Vesicles. 2016 Nov 17.

- Text and figures of Chapter VI are

  - Under Review in *Cell* as manuscript

    - **Haraszti RA**, Miller R, Dubuke ML, Rockwell HE, Coles AH, Sapp E, Didiot MC, Echeverria D, Stoppato M, Sere YY, Leszyk J, Alterman JF, Godinho BMDC, Hassler MR, McDaniel J, Narain NR, Wollacott R, Wang Y, Shaffer SA, Kiebish MA, DiFiglia M, Aronin N, Khvorova A. Exosomes' composition–activity relationship: a path toward the rational design of artificial exosomes for siRNA delivery

PREFACE

The Khvorova laboratory is very collaborative within the lab as well as outside the lab. We work like a theatre troupe that puts on many shows, where each show has a different lead actor and stage director. The troupe is led by the main theater director, Anastasia. Anastasia likes to work with very independent people, who don't always listen to her and often follow their own scientific minds. Data presented in this dissertation is the result of six projects, where I played lead actor and stage director and worked together with the team to put the show on stage. Team work makes us efficient and allows us to conduct experiments that cannot be performed by an individual. Team work is the present and the future of investigative life sciences.

Data, figures and text in Chapters II–VI has been published / submitted in the form of six research articles, where I am either first author or co-first author. In case of co-first author articles (Sections 3.1 and 3.3) I worked together with chemists, who developed and synthesized new siRNAs, whereas I performed biological experiments. Detailed contributions can be found in the chapter–specific prefaces. Chapters I and VII are unpublished original work of mine that I wrote specifically for this dissertation.

CHAPTER I INTRODUCTION

1.1 RNA THERAPEUTICS

The most abundant nucleic acids in nature are ribonucleic acids (RNAs)[1-3], which occur in the form of oligonucleotides or polynucleotides. RNAs are versatile molecules, able to store genetic information, able to form delicate three-dimensional structures, and able to exhibit enzymatic activity[3]. RNAs can interact with DNA, RNA, proteins and lipids[4]. RNAs are involved in all levels of regulation of life[3]. These diverse activities of RNAs are enabled by a diverse landscape of naturally occurring chemical modifications: methylation of the 2'-hydroxy ribose backbone or the nucleotide bases, conjugation of other small molecules to RNA, forming alternative bases *via* isomerization, reduction, replacement of oxygen with sulfur etc[3].

Increasing understanding of the functional and chemical diversity of RNAs in the past decades led to the birth of a new therapeutic concept: if chemically modified natural RNAs can regulate all stages of life, then exogenously synthesized, chemically modified RNAs may regulate health and disease.

1.1.1 Classes of RNA therapeutics

The diversity of RNA therapeutics is comparable to the diversity of natural RNA activities. RNA therapeutics can be classified according to the mode of action (requires exogenous protein, endogenous protein or no protein to act), the location of action (nucleus, cytoplasm or extracellular space), target (DNA, RNA or protein), and secondary structure (single stranded or double stranded). Most RNA therapeutics are synthesized using solid phase synthesis, but some are synthesized using *in vitro* transcription *(i.e.* mRNAs). Most RNA therapeutics inhibit the activity of its target molecule, but some activate it (*i.e.* mRNA, small RNA-mediated transcriptional

activation). A list of major classes of RNA and oligonucleotide therapeutics can be found in Table 1.1

	Mode of action	Location of action	Target	Secondary structure	Reference	Mechanism first identified in (species)
siRNA	Endogenous protein (Ago2)	cytoplasm	mRNA	Double stranded	[5-6]	C. elegans
siRNA	Endogenous protein (Ago2)	cytoplasm	mRNA	Single stranded	[7]	M. musculus
miRNA	Endogenous proteins	cytoplasm	mRNA	Single stranded	[8-9]	C. elegans
Small RNA-mediated transcriptional inhibition / activation	Endogenous proteins	nucleus	Pre-mRNA	Single stranded	[10-12]	N. tabacum H. sapiens
ASO – RnaseH dependent	Endogenous protein (RNaseH)	nucleus	Pre-mRNA	Single stranded	[13]	Rous sarcoma virus
mRNA	Endogenous proteins (ribosome)	cytoplasm	-	Single stranded	[14-15]	E. coli
CRISPR sgRNA	Exogenous protein (Cas)	Nucleus or cytoplasm	DNA or RNA	Single stranded with duplex region	[16-17]	S. pyogenes
aptamer	-	extracellular	protein	Single stranded highly structured	[18]	*In vitro*
ASO – steric blocker antimiR	-	cytoplasm	miRNA	Single stranded	[19-20]	H. sapiens
ASO – steric blocker Splice switching	-	nucleus	Pre-mRNA	Single stranded	[21]	H. sapiens
ASO – steric blocker Triplex forming	-	nucleus	DNA	Single stranded	[22-23]	*In vitro*
ASO – steric blocker Anti-telomerase	-	nucleus	RNA	Single stranded	[24]	H. sapiens
ASO – steric blocker Translation blocking	-	cytoplasm	mRNA	Single stranded	[25]	O. cuniculus
Ribozyme	-	Nucleus/cytoplasm	DNA or RNA	Single stranded	[26-28]	E. coli

Table 1.1 List of RNA and oligonucleotide therapeutic classes.

Beyond diversity of potential therapeutic activity, a major advantage of RNA therapeutics is sequence-specificity. Most RNA therapeutics (except mRNAs and aptamers) use Watson-Crick base pairing to bind their nucleic acid targets. Thus, the alteration of the RNA therapeutic targeting sequence does theoretically enable the targeting of the entire human genome and/or transcriptome. Unlike small molecule drugs or therapeutic proteins, the sequence specificity of RNA therapeutics makes a large array of undruggable targets accessible for therapy.

1.1.2 Chemical modifications of siRNAs

RNA interference, in which short double stranded RNAs (siRNAs) trigger the cleavage of complementary mRNA, was discovered in 1998 in C. elegans[5] and in 2001 in mammalian cells[6]. siRNAs have since become a widely used research tool to silence mRNAs. The promise of siRNAs for a sequence-specific gene silencing therapy was substantial and excitement was amplified by the co-occurring Human Genome Project (1990-2003). The first clinical trial was initiated only 3 years after the discovery of mammalian RNAi[29]. However, early clinical trials of siRNAs either failed to show gene silencing[30] or induced immune stimulation[31-32], dampening initial enthusiasm in RNAi therapeutic development[33-35]. With the failure of these early clinical trials the importance of chemical modifications of therapeutic siRNAs began to emerge.

Natural (unmodified) RNAs are suboptimal as drugs due several reasons: (i) RNAs are substrates of endo- and exonucleases and their half-life in plasma is less than a minute[36]. (ii) Small double stranded RNAs are recognized by the innate immune system and induce an immune response[37-40], and (iii) RNAs are negatively charged large molecules, therefore cannot passively penetrate the cell membrane. The siRNA field tried to overcome these challenges using chemical modifications adopted from early development of antisense oligonucleotides[41].

Rational design of chemically modified siRNAs requires a detailed understanding of how siRNAs interact with proteins outside and inside of the cell. In the extracellular space the siRNA is substrate to 3'-to-5' processive exonucleases[42-43], RNase A type endonucleases[44-46], and recognized by Toll-like receptor 3 of the innate immune system[47-48]. Upon cellular uptake, siRNAs are recognized by endosomal Toll-like receptor TLR7[49-50] as well as intracellular double stranded RNA sensors: interferon-induced, double-stranded RNA-activated protein kinase (PKR)[39, 51] and retinoic acid-inducible gene I (RIG-I)[52]. After overcoming these challenges, siRNAs associate with the RNA-induced silencing complex (RISC) in the cytoplasm[53]. Thermodynamic bias defines a guide strand and a passenger strand in the 21-nucleotide long siRNA duplex: guide strands have less stable base pairs at the 5' terminus [54-55]. Therefore the 5' terminus of the guide strand can tolerate a wide variety of chemical modifications[56]. The guide strand loads in the enzymatically active component of RISC, Ago2[57], whereas the passenger strand is released, typically following cleavage[58-59]. Subsequently, guide strand containing RISC performs multiple rounds of binding and cleaving complementary mRNAs[60]. Events of RNAi in the cytoplasm are depicted in Figure 1.1.

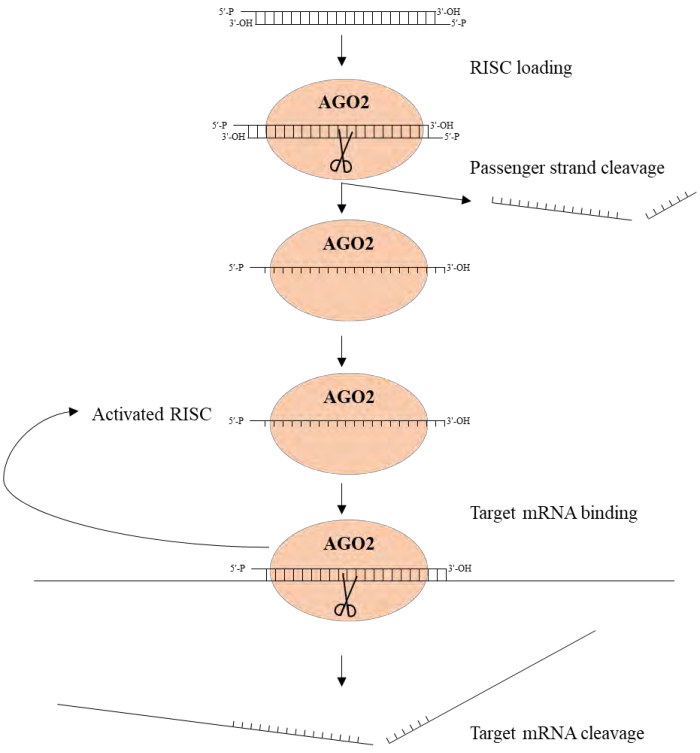

Figure 1.1 Schematic of RNA interference

Chemical modifications introduced into siRNAs are aimed to reduce immunogenicity, increase nuclease resistance, help cellular uptake, and promote correct selection of the guide strand, while preserving interactions with proteins necessary to exhibit silencing activity. The modifications developed to address these needs can be classified as (1) modifications of the phosphodiester backbone, (2) modifications of the ribose 2'-hydroxyl group, and (3) modification of the ribose ring. Generally, positions 2-16 of the guide strand are the least tolerant for chemical modifications, since only this portion of the guide strand base pairs with the target mRNA[61]. A selection of the most frequently used modification is depicted in Figure 1.2.

Among modifications of the phosphorodiester backbone, phosphorothioate[62], phosphorodithioate[63] and boronophosphate[64] have all proved useful to increase siRNA stability. All these backbone modifications decrease the thermostability of the RNA duplex[63, 65-67]. Phosphorothioates also promote non-specific binding to proteins[68]. However, extensive phosphorothioate modification reduces silencing activity[69], may induce toxicity[65-66], and phosphorothioates are only tolerated in certain positions[62, 65-66, 69]. Yet, phosphorothioates are among the most commonly used chemical modifications of siRNA and are incorporated in all current clinical stage compounds[70]. Phosphorothioate modification introduces a chiral phosphorus into the siRNA backbone[71]. Stereopure (R diastereomers only) synthesis of phosphorothioate siRNAs increases both nuclease stability and silencing activity[71].

2'-ribose modifications are more diverse, with 2'-fluoro and the naturally occurring 2'-*O*-methyl being most widely used. 2'-*O*-methyl and 2'-fluoro are tolerated in any individual position of an siRNA[72], but fully modified 2'-*O*-methyl or 2'-fluoro guide strands are either completely inactive or exhibit substantially reduced activity[73]. Therefore, initial patterns included modifications at the terminal nucleotides only[74], at every other nucleotide[75] or at every

pyrimidine[36, 65]. 2'-*O*-methyl and 2'-fluoro modifications modulate duplex thermostability[76], promote nuclease stability[74-75, 77-78] and repress immunogenicity[49, 72, 79-80].

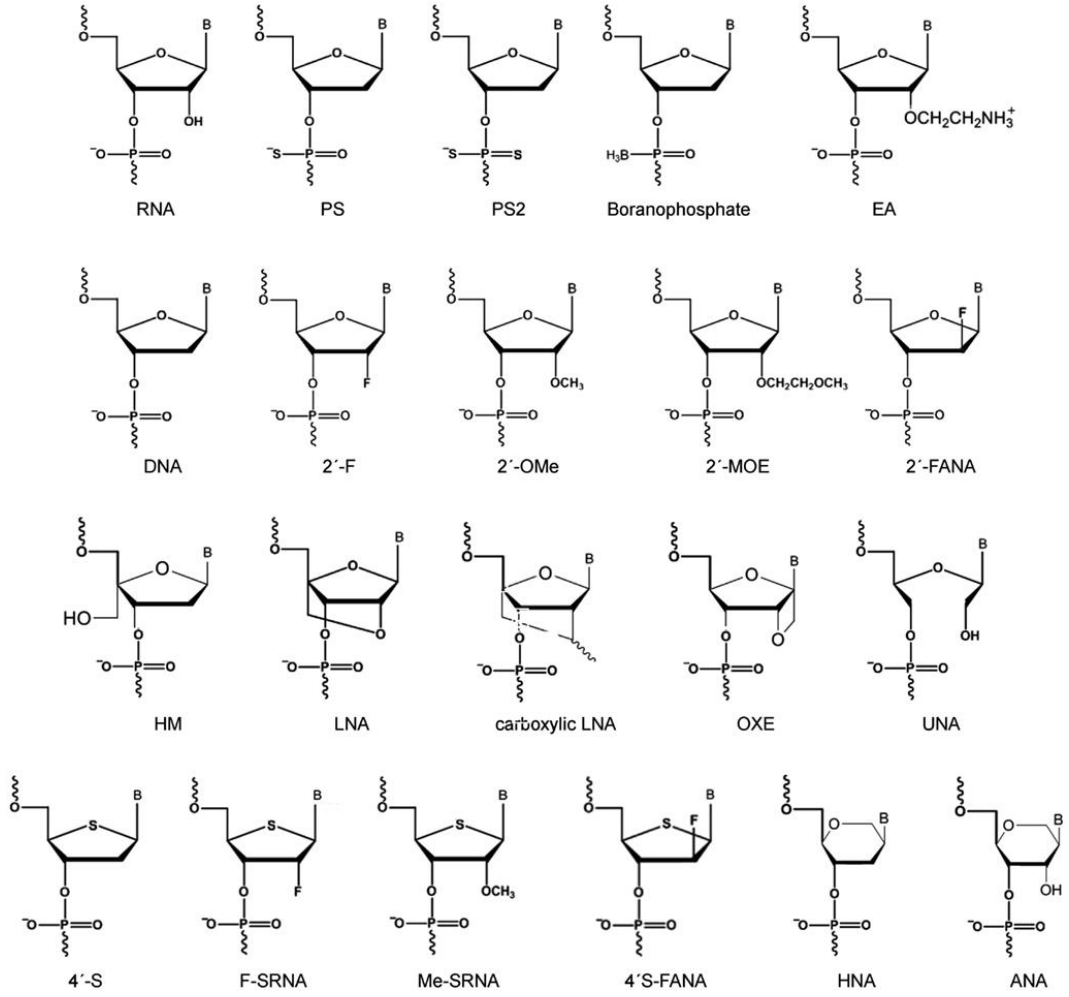

Figure 1.2 Selected modifications used in siRNAs. Adapted from Bramsen and Kjems: Development of therapeutic-grade small interfering RNAs by chemical engineering. Frontiers in Genetics. 2012[81]. RNA: ribonucleic acid, PS: phosphorothioate, PS2: phosphorodithioate, EA: 2'-aminoethyl, DNA: deoxyribonucleic acid, 2'-F: 2'-fluoror, 2'-OMe: 2'-*O*-methyl, 2'-MOE: 2'- *O*-methoxyethyl, 2'-FANA: 2'-deoxy-2'-fluoro-β-D-arabinonucleic acid, HM: 4'-*C*-hydroxymethyl-DNA, LNA: locked nucleic acid, carboxylic LNA: 2',4'-carboxylic-LNA, OXE: oxetane-LNA,UNA: unlocked nucleic acid, 4'-S: 4'-thioribonucleic acid, F-SRNA: 2'-deoxy-2'-fluoro-4'-

thioribonucleic acid, Me-SRNA: 2'-*O*-methyl-4'-thioribonucleic acid, 4'S-FANA: 2'-fluoro-4'-thioarabinoribonucleic acid, HNA: hexitol nucleic acid, ANA: altritol nucleic acid, B: base.

Bulkier 2'-modifications, such as 2'-aminoethyl and 2'- *O*-methoxyethyl (2'-MOE) are best tolerated at the 3'-ends of the strands[82], where they can fine-tune duplex thermostability and asymmetry[83]. Locked nucleic acid (LNA)[84] ,oxetane-LNA[83], and unlocked nucleic acid (UNA)[85] all increase nuclease stability. LNA increases[86], whereas UNA decreases[87] duplex thermostability, which may improve off-target effects[88-89].

Ribose alternatives have also been introduced to siRNAs. 2'-deoxy-2'-fluoro-β-D-arabinonucleic acid (2'-FANA) modification[90] and its thioated version[91] is similar to DNA, decreases thermostability and is mostly tolerated in the passenger strand[90-91]. Other ribose alternatives, such as hexitol nucleic acid (HNA)[92] or altritol nucleic (ANA)[93] can also be incorporated to 3'-ends of the siRNA strands, where they increase nuclease stability and modulate duplex thermostability. Finally, 4'-thio modified riboses have also been successfully incorporated into siRNAs, where they increased nuclease stability, duplex thermostability and silencing acitivity[94-96].

This large chemical toolbox enables the combinatory application of different modifications and fine-tuning of siRNA properties. Yet, 2'-*O*-methyl, 2'-fluoro and phosphorothioate modifications dominate the field[97]. A combinatory screen of these three modifications has been carried out in various industrial and academic laboratories in order to optimize *in vivo* stability, geometry, and thermodynamics, while preserving the silencing activity of siRNAs. Both 2'-*O*-methyl and 2'-fluoro modifications favor C3'-endo ribose conformation and therefore A-form helix

structure of RNA[98-99]. Because fluorine has a higher electronegativity than oxygen, 2'-fluoro ribose slightly overwinds the helix compared to natural 2'-hydroxyl ribose in RNA. Similarly, because carbon has a lower electronegativity than oxygen, 2'- *O*-methyl ribose slightly underwinds the helix compared to natural 2'-hydroxyl ribose in RNA. Thus, a combinatorial pattern of 2'-*O*-methyl and 2'-fluoro modifications can be used for thermodynamic tuning of an siRNA[100]. For example three 2'-*O*-methyls or three 2'-fluoros in a row[101] in the context of alternating 2'-*O*-methyls and 2'-fluoros[77] may improve silencing activity of siRNAs. Generally, an optimized siRNA guide strand should have a flexible 5' end[102], a higher affinity seed region and a lower affinity 3' region[54, 103] to promote correct selection of the guide strand, binding of guide strand to target mRNA and the release of the cleaved target mRNA. Full modification (e.g. modification of every ribose in the duplex) of siRNAs is essential for conjugate-mediated delivery of siRNAs [104], where this modification pattern enables a 10 000-fold increase in tissue accumulation compared to partially modified siRNAs[104]. However, when siRNAs are encapsulated into lipid nanoparticles for delivery, chemical modifications are substantially less beneficial[36, 105]. Optimization of siRNA chemical modification for extracellular vesicle mediated delivery is described in Chapter III.

1.2 EXTRACELLULAR VESICLES

Most cell types in culture or *in vivo* release various types of extracellular vesicles (EVs). The first description of extracellular vesicles from non-neuronal origin dates to 1967: “platelet-dust” comprised of vesicles with coagulation activity that sediment at 134 000 g but not at 18 000 g from plasma and may originate from α-granules (a multivesicular body – related organelle) of platelets[106]. In 1970, EVs were purified from cartilage tissue[107] , in 1971 from erythrocytes[108] and

in 1981 from various cell lines[109]. These initial studies all isolated EVs *via* differential centrifugation and found enzymatic activity associated to the vesicles.

The term "exosome" is often used in this dissertation and generally, in the context of extracellular vesicles. "Exosomes" were initially defined as vesicles sedimenting from conditioned media at 310 000 g but not at 10 000 g and containing 5'-nucleotidease activity[109]. The notion that exosomes originate from the multivesicular body was first posed in 1987[110] in a study about reticulocyte EVs. This speculation was based on the orientation and trafficking properties of transferrin in EV membranes[111]. However, the concept that multivesicular bodies (MVBs) may undergo exocytosis predates the exosome definition by 30 years: in the first report on multivesicular bodies in 1957, Robertis *et al* described a catechol secretion mechanism *via* MVBs in the adrenal gland [112].

Extracellular vesicles encompass several, partially overlapping vesicle subclasses other than exosomes. "Microvesicles", another frequently used term in this dissertation, has been used in the 1970s to refer to erythrocyte and platelet derived EVs playing a role in coagulation[108-109, 113], and formed by plasma membrane budding[114]. However, these initial microvesicles were smaller than 100 nm, sedimented at centrifugation speeds higher than 100 000 g but not at speeds lower than 20 000 g[108-109, 113]. Thus, these initial microvesicles would rather fit the definition of an exosome today. The first microvesicles, which sedimented at centrifugation speeds lower than 100 000 g, were reported in 1982[115].

Other extracellular vesicles types have been named somewhat arbitrarily after either their release mechanism (ectosome[116]), source cell type (oncosome[117]), source organ (prostasome[118]), extracellular space consistency (matrix vesicle[107]), state of source cell (apoptotic body[119-120]) etc.

The two EV terms used in this dissertation, exosomes and microvesicles, may be defined according their intracellular origin or their isolation protocol. Exosomes are traditionally considered to form upon exocytosis of the multivesicular body, while microvesicles are thought to form upon plasma membrane budding[121]. However, the size range, sedimentation properties, and protein markers (see also Chapter V) of these EV subclasses are greatly overlapping. Therefore, no current protocol can sufficiently differentiate vesicles originating in the multivesicular body from vesicles shed from the plasma membrane. Thus, this dissertation uses an EV definition based on isolation protocol: vesicles sedimenting at 10 000 g will be referred to as microvesicles, and vesicles sedimenting at 100 000 g will be referred to as exosomes.

1.2.1 Endogenous activity of EVs

EV release is conserved throughout evolution and occurs in bacteria[122], fungi[123], plants[124], nematodes[125], flies[126] and mammalian cells[109]. Such evolutionary conservation indicates that EVs play a role in both single-cell and multi-cell organisms. The first suggested function of EVs was regulated removal of intracellular and membrane components during reticulocyte maturation[110]. This observation led to a long-lasting but inadequate view of extracellular vesicles as cellular waste[121, 127]. However, a role of EVs in intercellular communication has been showed as early as in 1984[128] and evidence has been growing since then[127]. Intercellular signaling of EVs was discovered in immune presenting cells in the 1990s[129-131] and this discovery marked a shift in the general view of EVs: from cellular waste to intercellular signaling devices. EVs have been shown to exhibit intercellular signaling not only in health, but also in disease, by for example promoting tumor metastasis[132].

Intercellular signaling activity of EVs can be used in clinical applications in three ways: (1) Content of EVs may indicate the state and/or type of producer cell and thus be used as a biomarker[133]. (2) EV activity modulating the immune system[130] or promoting tissue regeneration[134] may be used in disease. (3) EVs may be used to deliver engineered cargo to recipient cells[135-136]. Table 1.2 shows past and present clinical trials involving EVs classified according to the above mechanisms of action. Biomarker trials have clearly been the focus (83 % of trials), whereas regenerative, immunomodulatory and delivery focused trials each represent less than 10% of trials. 30% of EV biomarker trials detects protein(s) and 70% detects RNA(s) as EV cargo of diagnostic relevance.

Clinical Trial ID	Producer Cell	Cargo	Mechanism of Action	Disease
NCT02957279	Blood	-	Biomarker	Sepsis
NCT02393703	Blood, Pancreas	-	Biomarker	Pancreatic Cancer
NCT01779583	Serum, Tumor	-	Biomarker	Gastric Cancer
NCT03109873	Blood	-	Biomarker	Head and Neck Cancer
NCT02226055	Blood	-	Biomarker	Chronic Kidney Disease
NCT02051101	Blood, Skin	-	Biomarker	Port Wine Stain
NCT03392441	Blood	-	Biomarker	Type 1 Diabetes
NCT02977468	Blood	-	Biomarker	Breast Cancer
NCT03228277	Bronchoalveolar Lavage	DNA	Biomarker	Lung Cancer
NCT03267160	Blood, Urine	Protein	Biomarker	Sepsis
NCT02147418	Oropharingeal Rinse	Protein	Biomarker	Oropharyngeal Squamous Cell Carcinoma
NCT03222986	Blood, Urine	Protein	Biomarker	Sepsis
NCT02662621	Blood, Urine	Protein	Biomarker	Cancer

NCT03106246	Blood	Protein	Biomarker	Diabetes mellitus
NCT02921854	Serum	Protein	Biomarker	Cancer
NCT03381482	CSF	Protein	Biomarker	Alzheimer's Disease
NCT03262311	Blood	Protein	Biomarker	Hypoxia
NCT02327403	Urine	Protein	Biomarker	Kidney Transplant
NCT01860118	Blood, Urine	Proteins	Biomarker	Parkinson's Disease
NCT03108677	Blood	RNA	Biomarker	Lung Metastases of Ostersarcoma
NCT02702856	Urine	RNA	Biomarker	Prostate Cancer
NCT03478410	Epicardial Fat	RNA	Biomarker	Cardiac Arrythmias
NCT01344109	Tumor	RNA	Biomarker	Breast Cancer
NCT03102268	Tumor	RNA	Biomarker	Cholangiocarcinoma
NCT02890849	Tumor, Blood	RNA	Biomarker	Lung Cancer
NCT03236675	Blood	RNA	Biomarker	Lung Cancer
NCT03236688	Plasma	RNA	Biomarker	Prostate Cancer
NCT03027726	Blood	RNA	Biomarker	Type 2 Diabetes
NCT03264976	Serum	RNA	Biomarker	Diabetic Retinopathy
NCT03031418	Urine	RNA	Biomarker	Prostate Cancer
NCT03280576	Blood	RNA	Biomarker	Sepsis
NCT02464930	Blood	RNA	Biomarker	Barrett's Esophagus
NCT03227055	Urine	RNA	Biomarker	Chronic Kidney Disease
NCT03384433	Mesenchymal Stem Cell	miR-124	Delivery	Acute Ischaemic Stroke
NCT01294072	Plant	curcumin	Delivery	Colon Cancer
NCT01159288	Dendritic Cells	Tumor Antigens	Delivery	Lung Cancer
NCT02138331	Mesenchymal Stem Cell	-	Immune Modulation	Type 1 Diabetes

NCT01668849	Plant (Grape)	-	Immune Modulation	Oral Mucositis
NCT02565264	Plasma	-	Regenerative	Wound
NCT03437759	Mesenchymal Stem Cell	-	Regenerative	Macular Holes

Table 1.2 List of past and present clinical trials involving extracellular vesicles.

1.2.2 EVs as delivery vesicles

The idea of using EVs as delivery vesicles for RNA therapeutics stems from three key findings: (1) some EVs exhibit cell-type-specific targeting[137]; (2) EVs contain RNA[138]; and (3) the regenerative effect of mesenchymal stem cells can partially be attributed to EV-mediated miRNA delivery[139]. EVs display several further advantages as delivery vesicles: The high membrane rigidity of EVs may enhance stability at neutral pH in circulation[140]. EV membrane proteins may protect from complement activation[141] and phagocytosis[142]. Since EVs occur naturally in all bodily fluids, the exogenous administration of EVs is expected to be safe.

A major challenge in the EV-mediated delivery field is efficient loading of therapeutic cargo into EVs. Loading strategies can be classified according to the timing of intervention, which can occur either before EV isolation (e.g. modifying producer cell), or after EV isolation (e.g. modifying isolated EVs). RNA cargo loading into EVs has been achieved by overexpressing RNA in producer cells with an EV-specific zipcode[132, 143-144] (cis-acting regulatory sequence associated to RNA enrichment in EVs, trans-acting proteins responsible for this enrichment are unknown[143]) or heterogenous nuclear RNP A2B1 binding motif[145], tethering RNA to EV-enriched proteins *via* the MS2 bacteriophage coat protein system[146-147] or *via* the transactivator-of-transcription-trans-activating-response (Tat-TAR) system[148], electroporating RNA into EVs[136, 149-150], transfecting

RNA into EV producer cells[151] or into EVs directly[152], and tethering lipid-conjugated RNAs to the EV membrane[135, 153-155] (see also Chapter III). All these strategies can promote efficient RNA transfer to recipient cells and they are independent of RNA cargo sequence. However, each strategy has its specific caveat. Electroporation of RNAs may induce RNA aggregation[156], transfection of EVs may disrupt EV membrane[152], level of loading cannot be controlled in all expression – based methods. Loading of lipid-conjugated RNAs to EVs is a well-controlled, simple and scalable process (Chapter III and [135]). However, RNAs associated to the EV membrane decrease the surface charge of the vesicles (Chapter III and [135]) and it remains unknown whether this surface charge change interferes with EV trafficking activity. Finally, genes can be productively loaded into EVs in the form of non-enveloped viruses, such as AAV[157-159] or hepatitis A[160], a strategy that promotes better spread and escape from neutralizing antibodies[157-160]. A further iteration of this strategy is Gag-expression-induced virus-like extracellular vesicles, which do not contain a viral genome[161]. These virus-like EVs can efficiently deliver ribonucleoproteins to various cell types *in vivo*[162].

Proteins are traditionally loaded to EVs by expressing proteins in producer cells fused to EV-associated or membrane-associated proteins or protein domains. For example, proteins and peptides can be fused to CD9[163], Lamp2b[149, 164], CD63[165], lactadherin[166] or ARRDC1[148] for EV-targeting. A modification of this approach makes protein-CD9 fusion light-inducible and thus allows an additional level of control over cargo loading into EVs[163]. Fusing proteins to palmitoylation signals[167], myristylation signals[168], phosphatidylinositol-(4,5)-bisphosphate (PIP(2))-binding domain[168], WW-motifs[148] and to transmembrane domain of platelets-derived growth factor receptor (PDGFR)[167] can also drive enrichment of protein cargo in EVs. Another approach is to modify the EV surface after EV isolation. Freeze-thawing, sonicating or extruding

EVs with protein cargo or saponin-mediated permeabilization of EV membrane for the uptake or protein cargo have all been useful for EV loading[169]. Primary amines (present on lysine residues) are prone to amine-specific cross-linking reactions, which has been used to modify EV surface proteins for CLICK-chemistry-based attachment of ligands[170]. Chapter VI describes a strategy, which uses amine-specific cross-linking to load proteins on vesicles surfaces. Cysteines can also be used for orthogonal bioconjugation of ligands to nanoparticles[171]. Surface functionalization of EVs is a very promising intersection between synthetic chemistry and synthetic biology. However, bioconjugation reactions will have to be optimized to (1) maximize conjugation yield, and (2) avoid interference of chemical reaction with the biological activity of EVs and/or conjugated ligands (see Chapter VI).

RNAs or proteins associated to the surface of EVs can serve as cargo as well as targeting ligand. For example, cholesterol-conjugated siRNAs represent surface associated cargo that can be efficiently delivered to recipient cells[153-154, 172], whereas cholesterol-conjugated aptamers can serve as targeting ligands driving therapeutic EVs to tumors[155]. Similarly, proteins or peptides fused to membrane proteins can constitute cargo[148, 166], fluorescent labeling[146], and targeting to certain receptors[149, 164].

Electroporation has been also used to load small molecules, such as curcumin[173], doxorubicin[164], anti-inflammatory Stat3-inhibitor[174] into EVs. Applying a pH gradient between intravesicular and extravesicular space may also drive loading of small molecules[175]. Another strategy to load doxorubicin (or possibly any cargo) into EVs is to re-construct EV-like vesicles from the plasma membrane by serial extrusions[176]. Similar experiments have been conducted to re-form vesicles after disruption of the plasma membrane using nitrogen cavitation[175], extrusion through microfluidic devices[177-178], and centrifugation through a membrane with micro-sized

pores[179]. The versatility and high vesicle yield of this approach is appreciated; however, plasma-membrane derived vesicles may lack the target cell specificity of natural EVs.

1.3 RATIONALE

EV-mediated siRNA delivery is a promising approach to treat diseases of the brain, because (1) abundant EVs transfer RNAs and proteins between neurons and glial cells[180-185]; (2) most neurodegenerative diseases are genetically defined and therefore ideal targets for RNA therapies[186-188185-188]; and (3) brain diseases often involve neuron loss and neuroinflammation, targets of intrinsic neurotrophic and immunomodulatory activity of EVs[139, 189-190]. Drug delivery to brain is very challenging, a fact that justifies the effort invested in EV manufacturing and engineering.

This dissertation focuses on EV-mediated siRNA delivery to silence *Huntingtin* in neurons. Huntington's disease is the third most common neurodegenerative disease, with underlying autosomal dominant trinucleotide repeat expansion in the huntingtin gene [191]. Silencing both the normal and mutant copies of *Huntingtin* represents a therapeutic benefit[192], whereas discrimination between mutant and wild-type copies is also possible *via* either targeting SNPs[187, 193] or the expanded CAG repeat[194]. Currently there are two ongoing clinical trials targeting huntingtin with either a non-allele-selective[188] or an allele-selective antisense oligonucleotide[187]. EVs may play a role in Huntington's disease pathology[185, 195], whereas stem cell-derived EVs can be therapeutic[196]. Thus, EV-mediated siRNA therapy for Huntington's disease would combine the intrinsic therapeutic effects of EVs with gene-specific RNA interference.

Desired characteristics of an ideal delivery vesicle would be minimal toxicity and broad therapeutic window, specific cell-targeting, efficient and controllable loading of EVs with cargo,

and cost-effective and scalable vesicle manufacturing. This dissertation addresses some of the above questions and focuses on (1) chemical optimization of RNA cargo for EV-mediated delivery, (2) developing large-scale manufacturing for active EV production, (3) characterization of EV components, and (4) understanding the EV composition – activity relationship in order to reverse engineer EVs.

CHAPTER II METHODS

2.1 PREPARATION OF OLIGONUCLEOTIDES

Oligonucleotides were synthesized on an Expedite ABI DNA/RNA Synthesizer following standard protocols. For each synthesis the different synthesized lipophilic conjugated CPG[197-198] was used (**Figure 22A-22B compound 4, 8, or 9**) or a commercial C6 amino CPG (*ChemGenes, Wilmington, MA*) (for the post-synthetic conjugation of α-tocopheryl succinate) for the sense strand or at a 10 μmoles scale using a Unylinker® terminus (*ChemGenes, Wilmington, MA*) for the antisense strand. 2′-*O*-methyl phosphoramidites (*ChemGenes, Wilmington, MA*), 2′-fluoro phosphoramidites (*BioAutomation, Irving, Texas*), Cy3 labeled phosphoramidites (*Gene Pharma, Shanghai, China*) and synthesized E-Vinyl Phosphonate phosphoramidites[199] were prepared as 0.15 M solutions in acetonitrile. Phosphoramidite coupling time was 250 s for all amidites using 5-(Benzylthio)-1H-tetrazole (BTT) 0.25 M in acetonitrile as coupling activator. Detritylations were performed using 3% dichloroacetic acid (DCA) in dichloromethane for 80 s and capping was done with a 16% N-methylimidazole in THF (CAP A) and THF:acetic anhydride:2,6-lutidine, (80:10:10, v/v/v) (CAP B) for 15 s. Sulfurizations were carried out with 0.1 M solution of 1,2,4-dithiazole-5-hione (DDTT) in acetonitrile for 3 minutes. Oxidation was performed using 0.02 M iodine in THF:pyridine:water (70:20:10, v/v/v) for 80 s. In the case of 5′-phosphate

compounds, the Chemgenes chemical phosphorylation reagent bis-cyanoethyl-N,N,diisopropyl CED phosphoramidite was used to introduce the 5′-monophosphate. After completion of the automated synthesis, the solid support was washed with 0.1 M piperidine in acetonitrile for 10 min, then washed with anhydrous acetonitrile and dried under argon.

For the coupling of vinylphosphonate phosphoramidite, a 4-fold excess of phosphoramidite was loaded on the solid support, and phosphoramidite condensation was carried out for 20 min. A solution of 3% trichloroacetic acid in dichloromethane was used to remove the dimethoxytrityl group from the 5' hydroxyl group of the nucleotide. A solution of 0.25 M 5-(Ethylthio)-1H-tetrazole in anhydrous acetonitrile was used as an activator for the coupling step. Phosphorothioate linkages were introduced using a 0.05 M solution of 3-((dimethylaminomethylene)amino)-3H-1,2,4-dithiazole-5-thione in pyridine:CH_3CN (1:1) and a 5 min contact. Solid support was washed with anhydrous acetonitrile then anhydrous dichloromethane and flushed with argon.

2.2 Deprotection and purification of oligonucleotides

For vinylphosphonate strands a solution of bromotrimethylsilane and pyridine in dichloromethane (0.75 ml bromotrimethylsilane and 0.53 ml pyridine dissolved in 28.2 ml CH_2Cl_2, 0.5 ml per mmol of solid support) was circulated through the vessel containing the CPG for 30 min at room temperature.

Sense strands were cleaved and deprotected using 1 mL of 40% aq. methylamine at 45 °C for 1h. Antisense strands were first deprotected with a solution of bromotrimethylsilane/pyridine (3:2, v/v) in dichloromethane (5 mL) for the E-Vinyl Phosphonate deprotection and then cleaved and deprotected with 10 mL of 40% aq. methylamine at 45 °C for 1h. For both sense and antisense

strands, the oligonucleotide solutions were frozen in liquid nitrogen for a few minutes and dried under vacuum in a Speedvac overnight. The resulting pellets were suspended in water and purified using an Agilent Prostar System (Agilent, Santa Clara, CA). For the sense strand a Hamilton HxSil C18 column (150 x 21.2) was used (conditions: Buffer A: 50 mM sodium acetate in water with 5% acetonitrile, Buffer B: acetonitrile ; gradient = 90% A, 10% B to 10% A, 90% B in 18 minutes ; Temperature: 70°C ; Flow rate: 5 mL/min) and for the antisense strand, a Dionex NucleoPac PA-100 (9 x 250) was used (conditions = Buffer A: 30% acetonitrile in water, Buffer B: 1 M perchlorate de sodium in water with 30% acetonitrile, Gradient: 100% A to 20% A, 80% B in 30 minutes, Temperature: 65°C, Flow: 10 mL/min). The pure oligonucleotides were collected, desalted by size-exclusion chromatography using a Sephadex G25 column (GE Healthcare Life Sciences, Marlborough, MA) and lyophilized. For the attachment of α-tocopheryl succinate variants, the 3′ end C6 amino or the 3′ PC amino sense strands were dissolved in water and a solution of 1M sodium bicarbonate (pH 8.5) was added to obtain a 0.1M sodium bicarbonate final concentration. Then, a solution of *N*-hydroxysuccinimide-α-tocopheryl succinate (10 to 100 equivalents) (**Figure 22**) in DMF was added to the solutions containing the sense strand. The mixtures were incubated overnight at room temperature. A solution of 3M sodium acetate (pH 5.2) was added to obtain a 0.3M sodium acetate final concentration. Then, 3x of ethanol (95%) of the whole volume were added. The mixtures were vortexed, placed at 80°C for 1h and centrifuged 30 minutes at 5200g. The supernatants were removed and the lipid conjugated sense strands were purified and desalted as described previously.

2.3 ANALYSIS OF OLIGONUCLEOTIDES

The identity of oligonucleotides was established by Liquid Chromatography-Mass Spectrometry (LC-MS) analysis on an Agilent 6530 accurate-mass Q-TOF LC/MS (Agilent technologies, Santa Clara, CA) using the following conditions: buffer A (9mM triethylamine/100mM hexafluoroisopropanol in water), buffer B (9mM triethylamine/100mM hexafluoroisopropanol in MeOH), column: Agilent AdvanceBio oligonucleotides 2.1x50 mm (Agilent technologies, Santa Clara, CA), gradient for sense strand: 0-2 min (1% B - 40% B), 2-10.5 min (40% B - 100% B), gradient for the antisense strand: 0-2 min (1% B - 12% B), 2-10.5 min (12% B - 30% B), 10.5-11 min (30% B - 100% B).

2.4 mRNA QUANTIFICATION FROM CELLS AND TISSUES

HeLa cells (*ATCC, #CCL-2*) were plated in DMEM (*Cellgro, #10-013CV*) supplemented with 6% fetal bovine serum (FBS; *Gibco, #26140*) at 10,000 cells per well in 96-well tissue culture plates. hsiRNA was diluted in OptiMEM (*Gibco, #31985-088*) and added to cells, resulting in 3% FBS. Cells were incubated for 72 hours at 37°C, 5% CO_2. Primary neurons were plated at 100,000 cells per well density in NeuralQ medium (*Sigma-Aldrich, St. Louis, MO, #N3100*). hsiRNA, hsiRNA-loaded exosomes or liposomes were resuspended in NeuralQ medium, added to cells and incubated for 7 days at 37°C, 5% CO_2 post treatment. Cells were then lysed and mRNA quantification was performed using the QuantiGene 2.0 assay kit (*Affymetrix, #QS0011, Thermo Fisher Scientific, Waltham, MA*) according to manufacturer's instruction and as described previously [200].

For *in vivo* experiments, mice were euthanized and organs placed in RNAlater (*Thermo Fisher Scientific, Waltham, MA*, *#AM7021*) at 4°C overnight. Then tissue punches (approximately 10 mg) were taken using 1.5mm disposable biopsy punch with plunger (Integra, Miltex, # 33-31A-

P/25). Brain punches were taken fresh from 300 µm thick brain slices, punches placed in RNAlater (*Thermo Fisher Scientific, Waltham, MA*, *#AM7021*) and incubated at 4°C overnight. Tissue punches were then lysed and mRNA quantification was performed using the QuantiGene 2.0 assay kit (*Affymetrix, #QS0011, Thermo Fisher Scientific, Waltham, MA*) according to manufacturer's instructions and as described previously [200].

Catalog numbers for probes used in QuantiGene 2.0 assay kit were as follows: human *HTT* (*Affymetrix, #SA-50339*), mouse *Htt* (*Affymetrix, #SB-14150*), human *PPIB* (*Affymetrix, #SA-10003*), mouse *Ppib* (*Affymetrix, #SB-10002*), human *HPRT* (*Affymetrix, #SA-10030*), mouse *Hprt* (*Affymetrix, #SB-15463*). Data sets were normalized to housekeeping gene *HPRT.* In Section 3.1, hsiRNA^{PPIB} was used as non-targeting control (NTC) for *HTT* silencing, and hsiRNA^{HTT} was used as non-targeting control (NTC) for *PPIB* silencing.

2.5 PNA (PEPTIDE NUCLEIC ACID) BASED ASSAY FOR QUANTITATION OF SIRNA AND DETECTION OF SIRNA METABOLITES

siRNA guide strands in tissue and cell lysates were quantified using a peptide-nucleic acid (PNA) hybridization assay [28-197, 201-203]. PNAs are oligonucleotides, where the sugar-phosphate backbone is replaced with a charge-neutral polyamide backbone. PNAs have therefore a high hybridization energy to RNA. Tissues punches or cells were either lysed in 100 µl MasterPure™ Tissue Lysis Solution (*EpiCentre*®) in the presence of proteinase K (2mg/ml; *Invitrogen, #25530-049*) or leftover lysates from mRNA level quantitations were used. SDS in lysates was precipitated with 3 M KCl and pelleted at 4,000 × *g* for 15 min. siRNA guide strands in cleared supernatant were annealed to a complementary Cy3-labeled PNA strands (either fully complementary or containing one mismatch) (*PNABio, Thousand Oaks, CA*) by heating to 95°C for 15 min, incubating at 50°C for 15 min, and cooling to room temperature. Tissue lysates containing PNA-

guide strand hybrids were injected into HPLC DNAPac® PA100 anion-exchange column (*Thermo Scientific, Carlsbad, CA*), Cy3 fluorescence was monitored, and peaks were integrated. The mobile phase for HPLC was Buffer A (50% water, 50% acetonitrile, 25 mM Tris-HCl, pH 8.5, 1mM EDTA) and Buffer B (800mM $NaClO_4$ in buffer A). For hsiRNA guide strand quantitation, a steep gradient of Buffer B (10% to 100 % in 2.5 minutes) was used, and for hsiRNA guide strand metabolite detection a shallow gradient of Buffer B (10% to 100 % in 18 minutes) was applied. For calibration curves, known amounts of hsiRNA duplex was spiked into the tissue lysis solution derived from untreated mice before annealing to PNA. Sequences of PNAs used in this dissertation are as follows: hsiRNA^{HTT}: CY3– (OO) –TATATCAGTAAA**T**AGATTAA (mismatch marked in bold), hsiRNA^{PPIB}: Cy3 – (OO)–AACAGCAAATTCCATCGTGA, hsiRNA^{sFLT}: Cy3–(OO) – CTCTCGGATCTCCAAATTTA. Introduction of one mismatch enables the elimination of long purine stretches from the PNA, which promote PNA aggregation. Hence, pyrimidine-rich siRNA guide strands can be detected and quantified using mismatched PNA probes. The PNA hybridization assay has been shared with eight other labs, constitutes a part of thirteen manuscripts (see Appendix A) with currently 84 citations (May 8th, 2018).

2.6 ANIMAL EXPERIMENTS

All animal experiments were performed in accordance with guidelines of University of Massachusetts Medical School Institutional Animal Care and Use Committee (IACUC, protocol number A-2411). Mice were 6- to 10-weeks old at the time of experiments. All animals were kept on a 12-hour light/dark cycle in a pathogen-free facility, with food and water provided *ad libitum*.

For systemic administration of hsiRNA, FVBNj mice were injected with either phosphate buffered saline (PBS) or with different amounts of hsiRNA resuspended in PBS, either through

the tail vein or subcutaneously at the nape of the neck. For administration of compounds into brain, ALZET® osmotic pumps (*ALZET Osmotic Pump, Cupertino, CA;* #1003D) were prefilled with 100 µl of sample following manufacturer instructions and primed overnight at 37°C in a water bath. Osmotic pumps were loaded with either PBS (100 µl per pump), or 6.6 x 10^{10} vesicles loaded with cholesterol-siRNA (3000 copies per vesicle, total dose 0.33 nmol) (100 µl per pump), or equivalent amount of cholesterol-siRNA only (0.33 nmol, 100 µl per pump). Wild-type FVBNj mice were deeply anesthetized with 1.2% Avertin (*Sigma, St Louis, MO;* #T48402). ALZET® osmotic pumps were then placed using a stereotactic device (*World Precision Instruments, Sarasota, FL, #502610*) into the right lateral ventricle (coordinates relative to bregma: 0.2 mm posterior, 0.8 mm lateral, 2.5 mm ventral). Pumps delivered their content for 3 days at 1 µl / hour rate. Mice were administered 4 mg/kg of meloxicam SR subcutaneously for pain management. Osmotic pumps were removed 5 days after infusion ended (8 days after placement) and wound closed with 7mm wound clips.

After a time of incubation— indicated on individual figures—mice were euthanized with 0.1% Avertin or with isoflurane overdose followed by cervical dislocation. Brains were cut in 300 µm thick coronal sections at 4°C on a vibrotome, and 2 mm punches taken from striatum and motor cortex ipsilateral to the infusion. 3 punches were collected for mRNA quantification (immediately placed in RNAlater® (*Thermo Fisher Scientific, Waltham, MA*, *#AM7021*). Other organs were harvested and stored in RNAlater (*Thermo Fisher Scientific, Waltham, MA*, *#AM7021*) for later use.

2.7 *IN VITRO* XRN1 RESISTANCE ASSAY

hsiRNA guide strands (30 pmol) were incubated in water or with 1 µl Terminator™ (EpiCentre) exonuclease for 2 hours at 37°C in buffer A (EpiCentre, provided with Terminator™ enzyme). Then Novex® high-density TBE sample buffer (5x) (Thermo Fisher Scientific) was added to samples and loaded to polyacrylamide gel. Denaturing polyacrylamide gels (24%) were made in house using a mixture of 4 ml 10x TBE (Tris/borate/EDTA buffer), 17 g urea, 14 ml acrylamide:bis-acrylamide (19:1) 40% solution (Bio-Rad), 400 µl of 10% APS (ammonium persulfate) and 30 µl of TEMED (tetramethylethylanediamine). Urea-PAGE was performed in 1x TBE at 500V at room temperature (SE600 system, Hoefer) for approximately 6 hours. Gels were stained with SYBR® Gold Nucelic Acid Gel Stain (Thermo Fisher Scientific) and imaged with ImageQuant LAS 4000 (GE Healthcare).

2.8 CELL CULTURE

Umbilical cord, Wharton's jelly-derived mesenchymal stem cells (PCS -500-010, *ATCC, Manassas, VA*), adipose tissue derived mesenchymal stem cells (PCS-500-011, *ATCC, Manassas, VA*), and bone marrow derived mesenchymal stem cells (Poetics™, PT-2501*, Lonza, Basel, Switzerland*) were cultured in appropriate stem cell medium (PCS-500-030, *ATCC, Manassas, VA,* for umbilical cord and adipose tissue derived cells, and MSCGM™, PT-3238, , *Lonza, Basel, Switzerland* for bone marrow derived cells) in the presence of supplements containing serum and growth factors (PCS-500-040, *ATCC, Manassas, VA* and PT-3001, *Lonza, Basel, Switzerland*) at 37°C, 5% CO_2. Medium was changed every three days, and cells expanded until passage 12, to reach a total of 3000 cm^2 surface in T500 triple flasks. For serum deprivation medium was changed to RPMI (GIBCO™ RPMI 1640, *Thermo Fisher Scientific*) with no FBS or other supplements added for 24 hours. HeLa cells (*ATCC, #CCL-2*), U87

glioblastoma (*ATCC, #HTB-14*) and Huh7 hepatocellular carcinoma cells were cultured in DMEM (*Cellgro, #10-013CV*) supplemented with 10% fetal bovine serum (FBS; *Gibco, #26140*).

For three- dimensional cultures, spinner flasks (250-ml) containing 3.2 g (1150 cm^2 total surface area) of Star-Plus Microcarriers (SoloHill®, *Pall Life Sciences, Port Washington, NY*) were autoclaved. Umbilical cord-derived mesenchymal stem cells were seeded to a density of 8000 cells/cm^2 in umbilical cord-derive stem cell medium, the impeller speed set to 36 rpm, and cells were cultured at 37°C. When cells were homogenously spread on microcarriers, medium was removed, microcarriers washed in PBS twice and 250 ml of serum-free and xenofree StemPro® medium was added (A1067501, *Life Technologies, Carlsbad,CA*), and cells were cultured at 37°C and 36 rpm impeller speed.

2.9 PREPARATION OF EVS

Before EV purifications, medium on cells was changed to exosome-depleted medium (centrifuged at 100 000 g for at least 17 hours) or serum-free medium (GIBCO™ RPMI 1640, *Thermo Fisher Scientific*) (Section 3.3 and Chapter VI) and incubated for 48 hours. Conditioned medium was collected from culture of approximately 80% confluency and EVs prepared by differential ultracentrifugation[204]. Briefly, cell debris was pelleted at 300 g (10 min). Larger vesicles (microvesicles) were pelleted at 10 000 g (30 min), then supernatant filtered through a 0.2 µm membrane (Nalgene® aPES, *Thermo Fisher Scientific, Waltham, MA*) and small vesicles (exosomes) pelleted at 100 000 g (90 min) using 70 ml polycarbonate bottles (*Beckman Coulter, Brea, CA;* #355622) and Type 45 Ti rotor (*Beckman Coulter, Brea, CA;* #339160). Exosome pellet was then washed once in 1 ml sterile PBS and centrifuged again for 90 min at 100 000 g in a tabletop ultracentrifuge using a TLA-110 rotor (*Beckman Coulter*, *Brea, CA;* #366730).

Microvesicle pellets were washed in 1 ml sterile PBS and centrifuged again for 30 min at 10 000 g. EVs were frozen for later use in 0.1M sucrose, 1x protease inhibitor (cOmplete™ Mini, *Sigma-Aldrich*) in PBS.

For tangential flow filtration, 250 ml of conditioned medium (StemPro®,A1067501, *Life Technologies, Carlsbad,CA*) was collected after 48 hours from spinner flasks. Collection was performed four times; conditioned medium was stored at 4°C and subsequently pooled together (final volume 1L). The conditioned medium was filtered through a 0.2 µm polyethersulfone (PES) membrane. Conditioned medium was then subjected to ultrafiltration in a tangential flow filtration system using a 500 kDa cutoff TFF cartridge (MidiKros® mPES 115 cm^2, D02-E500-05-S*, Spectrum Labs, Rancho Dominguez, CA*). A feed flow rate of 120 mL/min, transmembrane pressure of <3.5 psi and a crossflow rate >10:1 were maintained throughout the filtration operation. The conditioned medium was concentrated 9-fold and then buffer exchanged with 6x volume of PBS. The exosomes were 0.2 µm filtered (PES membrane) and stored in 0.1M sucrose in a polyethylene terephthalate glycol (PETG) bottle at -80°C.

2.10 CHARACTERIZATION OF EXOSOMES

Nanoparticle Tracking Analysis (NanoSight NS300, *Malvern, Malvern, UK*) was used to measure concentration and size distribution of EVs. Briefly, samples were diluted in PBS 1:100 – 1:1000, manually injected into the instrument and videos acquired at ambient temperature at camera level 11 for 1 minute per sample, N=3. N depicted in figure legends represents biological replicates (independent EV preparations) and not technical replicates (repeated NTA measurements).

Transmission Electron Microscopy of exosomes was conducted at Mass General Hospital. Samples and grids were prepared at room temperature. An equal volume of 4% paraformaldehyde

was added to the exosome sample and incubated for 2 h. 3 µl aliquots of exosomes were dropped onto grids and incubated in 2% paraformaldehyde for 20 min. The grids were transferred to a wax strip and washed with 100 µl PBS. The grids were incubated in 50 mM glycine/PBS for 5 min and blocked in 5% BSA/PBS for 10 min and washed with 3x PBS followed by incubation in 1% glutaraldehyde for 5 min. Following 8 washes of 2 min with H_20, the grids were incubated for 5 min in uranyl oxalate and in 1% methyl cellulose:4% uranyl acetate (9:1) for 10 min on ice. Excess liquid was removed with a filter paper and the grids were air dried for 5 to 10 min. Exosomes were examined in a JEOL 1100 transmission electron microscope (*JEOL, Peabody, MA*) at 60 kV and images were obtained with an AMT digital camera (*Advanced Microscopy Techniques, Corp., Woburn, MA*).

For Western blot analyses, EVs or cell pellets were suspended in RIPA buffer (Pierce® 899000, *Thermo Fisher Scientific, Waltham, MA*) containing PMSF (36978, *Thermo Fisher Scientific*) and protease inhibitor cocktail (cOmplete Mini, 11836153001, *Roche, Indianapolis, IN*), and samples were sonicated for 15 min. Insoluble material was pelleted by centrifugation for 15 minutes at 10 000 g, 4°C. Proteins (50µg) were loaded onto NuPAGE 4–12% Bis-Tris gels (*Thermo Fisher Scientific, Waltham, MA*). After transfer to PVDF (*BioRad, Hercules, CA*), membranes were incubated with antibodies, washed, and images captured using an Odyssey® system (*Li-Cor, Bad Homburg, Germany*) according to manufacturer's instructions. Primary antibodies used were Calnexin (C5C9, *Cell Signaling, Danvers, MA*), CD63 (H5C6, *BD BioSciences, San Jose, CA*), Tsg101 (4A10, *Abcam, Cambridge, MA*), CD81 (B11, *Santa Cruz Biotechnology, Dallas, TX*), CD9 (C4, *Santa Cruz Biotechnology, Dallas, TX*), Desmoplakin (ab109445, *Abcam, Cambridge, MA)*, AHSG (ab112528, *Abcam, Cambridge, MA)*, Rab7 (ab137029, *Abcam, Cambridge, MA)*.

2.11 LIPOSOME PREPARATION

Conventional liposomes: Dioleoyl-phosphatidylcholine (DOPC) (*#850375, Avanti Polar Lipids, Alabaster, AL*) and cholesterol (, *#700000, Avanti Polar Lipids, Alabaster, AL*) were diluted in chloroform at a concentration of 50 mg/ml. 35 µl of DOPC and 15 µl of cholesterol was transferred into a glass vial and chloroform was evaporated under argon flow. The resulting lipid film was rehydrated in 500 µl of PBS (*#21-031-CV, Dulbecco's Phosphate Buffered Saline, Corning, Manassas, VA*), sonicated for 15 minutes in water bath (*#BB5510, Branson ultrasonic cleaner 40 kHz, Cleanosonic, Richmond VA*), and the extruded using Mini-Extruder (*#610000,Avanti Polar Lipids, Alabaster, AL*) through a 50 nm pore sized polycarbonate membrane (*#WHA800308, Whatman® Nucleopore™, MilliporeSigma, St Louis, MO*). Liposomes were always used fresh, never frozen.

Cardiolipin containing liposomes: Cariolipin (#840012, *Avanti Polar Lipids, Alabaster, AL),* monolysocardiolipin (#850081, *Avanti Polar Lipids, Alabaster, AL)* and dilysocardiolipin (#850082, *Avanti Polar Lipids, Alabaster, AL)* were diluted in chloroform at a concentration of 10 mg/m. 20 µl DOPC, 15 µl cholesterol and 75 µl cardiolipin, or monolyoscariolipin or dilysocardiolipin were mixed together and liposomes prepared as for conventional liposomes. This composition is equivalent to 40:30:30 w/w ratio of DOPC:cholesterol: cardiolipin/monolysocardiolipins/dilysocardiolipin.

Proteoliposomes; Purified proteins were purchased as follows: Rab7 (TP301776, *OriGene, Rockville, MD*), AHSG (TP723089, *OriGene, Rockville, MD*), Rab5 (TP303873, *OriGene, Rockville, MD*), Desmocollin (TP322207, *OriGene, Rockville, MD*), ARRDC1 (TP307160, *OriGene, Rockville, MD*), Dermcidin (TP309352, *OriGene, Rockville, MD*), Histone 1 (TP301249, *OriGene, Rockville, MD*), Desmoplakin (RPU51172, *Biomatik, Wilmington, DE*). Lyophilized proteins (AHSG and Desmoplakin) were dissolved in 0.1M sodium bicarbonate in PBS (pH=8.5). Proteins delivered in Tris-based buffers (Rab5, Desmocollin, ARRDC1,

Dermcidin and Histone 1) underwent buffer exchange using 2K MWCO cutoff membrane dialysis devices (Slide-A-Lyzer™ Mini, #69553, *Thermo Fisher Scientific, Waltham, MA)* 10 µl of sample against 1 l of 0.1M sodium bicarbonate in PBS (pH=8.5) at 4°C overnight. Palmitic acid N-hydroxysuccinimide ester (palmitoyl-NHS) (P1162, *Sigma-Aldrich, St. Louis, MO)* was added to protein samples in a 1:1 molar ratio to the amount of lysines (lysine frequency was estimated to be 7%) and incubated on a rotating wheel at 4°C overnight. Palmitoyl-NHS – protein reaction mixture (equivalent of 1 µg protein) was then incubated with preformed conventional liposomes or dilysocardiolipin liposomes for 1 hour at 37°C and proteoliposome samples centrifuged at 100 000 g for 70 min to remove non-loaded proteins. To prepare artificial exosomes, palmitoylated Rab7, AHSG and Desmoplakin were combined and loaded together to dilysocardiolipin liposomes.

2.12 Loading hsiRNAs into exosomes and liposomes

Known numbers of exosomes or liposomes was co-incubated with 10,000 copies of hsiRNA per vesicle (if not indicated otherwise) at 37°C for one hour in 500 µl PBS (*i.e.* loading mixture). Then the exosome-hsiRNA mixture was centrifuged at 100 000 g for 90 min and supernatant containing unloaded hsiRNA removed (supernatant). Pellet was taken up in 500 µl PBS for fluorescence measurement or in 300 µl Neural Q medium for treatment of primary neurons. To quantify loading of Cy3-labeled hsiRNA a 200 µl aliquot was taken from resuspended exosome pellet or from the supernatant. Fluorescence was assessed at 550 nm excitation, 570 nm emission on TECAN instrument. Percent of loaded hsiRNA was calculated as follows: pellet / (pellet + supernatant). To estimate hsiRNA copy number per exosome, the following formula was used: (percent of loaded hsiRNA) * (amount of hsiRNA initially mixed in with exosomes (mol)) * (Avogadro number) / (number of exosomes initially mixed in).

To quantify loading of not fluorescently labeled hsiRNA, a PNA hybridization-based assay was used[201, 205]. Briefly, a 10 µl aliquot of resuspended exosome pellet loaded with hsiRNA was diluted in 90 µl RIPA buffer (Pierce® 899000, *Thermo Fisher Scientific, Waltham, MA*) and sonicated for 15 min. Then 30 µl of 3M KCl was added to precipitate SDS from the lysate and precipitated SDS was pelleted at 5000 g for 15 min. Supernatant was then removed and a Cy3 labeled PNA oligonucleotide (*PNA Bio, Newbury Park, CA*) fully complementary to hsiRNA guide strand added to the exosome lysate and annealed at 95 ℃ for15 min followed by incubation at 50 ℃ for 15 min and cooling to room temperature. Then PNA-annealed exosome lysate was injected to HPLC anion exchange column (Dionex DNAPac PA100, *Thermo Fisher Scientific, Waltham, MA*) using an autosampler (1260 Infinity system, *Agilent, Santa Clara, CA*). The mobile phase used for HPLC was 50% acetonitrile, 25 mM Tris-HCl (pH 8.5), and 1 mM EDTA in water; and 0-800 mM $NaClO_4$ salt gradient was used to elute the hsiRNA-PNA hybrid. Quantification was performed using a calibration curve of known amounts of hsiRNA.

2.13 MEASUREMENT OF LIVE SIRNA UPTAKE IN NEURONS

For the analysis of siRNA uptake *in vitro*, primary neuron nuclei plated in 35 mm glass bottom dishes (*MatTek, Ashland, MA, #P35G-1.5-10-C*) were stained with NucBlue™ live cell stain (*Thermo Fisher Scientific, Waltham, MA, #R37605*) and neuron were treated with fluorescently labeled siRNA targeting *Ppib* or *Htt* gene. Images were acquired with a Leica DM IRE2 (*Leica Microsystems Inc., Buffalo Grove, IL*) confocal microscope using a 40x oil-immersion objective and Dapi channel (exposure time 50 ms) as well as mCherry channel (exposure time 200 ms). Images were processed using ImageJ software[206] (*NIH, Bethesda, MD*). The relative uptake of siRNA, loaded in UC-exosomes or TFF-exosomes, was estimated based on pixel integrated density of 5 images for each timepoint.

2.14 PREPARATION OF PRIMARY CORTICAL NEURONS

Primary cortical neurons were isolated from E15.5 mouse embryos of wild-type FVBNj mice. Pregnant females were anesthetized by either intraperitoneal injection of Ketamine (100 mg/kg, KETASET®, *Zoetis, Kalamazoo, MI*) - Xylazine (10 mg/kg, AnaSed®, *AKORN, Laker Forest, IL, #NDC59399-111-50*) or isoflurane (Isoflurane, USP, *Piramal Cricital Care, Betlehem, PA, #NDC66794-013-010*) and cervical dislocation followed. Embryos were removed and transferred to ice-cold DMEM/F12 medium (*Invitrogen, Carlsbad, CA;* #11320). Brains were removed from DMEM and meninges were carefully detached under a microscope. Cortices were isolated and transferred into pre-warmed (37˚C) papain-DNase solution for 30 min at 37˚C, 5% CO_2 to dissolve the tissue. Papain (*Worthington, Lakewood, NJ;* #54N15251) was dissolved in 2 ml Hibernate E (*Brainbits, Springfield, IL;* #HE) and supplemented with 0.25 ml of 10 mg/ml DNase1 (*Worthington, Lakewood, NJ;* #54M15168) in Hibernate E. After 30 min incubation, the papain solution was removed and 1 ml NeuralQ (*Sigma-Aldrich, St. Louis, MO, #N3100*) supplemented with 2.5% FBS was added to the tissue. Tissues were then dissociated by trituration through a fire-polished, glass Pasteur pipet. Neurons were counted using Neubauer chamber and diluted at 10^6 cells/ml. 10^5 neurons per well were plated on 96-well plates pre-coated with poly-L-lysine (*BD BIOCOAT, Corning, NY;* #356515). After overnight incubation at 37˚C, 5% CO_2, an equal volume of NeuralQ supplemented with anti-mitotics, 0.484 µl/ml of 5'UtP (*Sigma, St Louis, MO;* #U6625) and 0.2402 µl/ml of 5'FdU (*Sigma, St Louis, MO;* #F3503) was added to prevent the growth of non-neuronal cells. Half of the volume of media was replaced with fresh NeuralQ containing anti-mitotic every 48 hours until the experiments were performed.

2.15 PROTEOMICS

Protein extraction from EVs followed the same protocol as for Western blotting. Total protein (100µg) was applied to an SDS-PAGE gel. Once the entire protein sample entered the stacking gel, electrophoresis was stopped, and the portion of gel containing proteins was excised and stained with Coommassie brilliant blue. The fixed gel fragments were processed by University of Massachusetts Medical School Mass Spectrometry Core. Gel slices were cut into 1 x 1 mm pieces and placed in 1.5-ml microcentrifuge tubes containing 1 ml water and incubated for 30 min. The water was replaced with 200 µl of 250 mM ammonium bicarbonate and 25 µl of 45 mM DTT and the samples were incubated for 30 min at 50°C. Samples were then cooled to room temperature and alkylation was performed by adding 25 µl of 100 mM iodoacetamide and incubating for 30 min. The gel slices were washed twice in water, then incubated in 1ml of a 50:50 solution of 50mM Ammonium Bicarbonate: Acetonitrile for one hour at room temperature. The solution was replaced with 200µl acetonitrile and incubated until the gels slices turned opaque white. The acetonitrile was removed and gel slices were further dried in a Speed Vac. Gel slices were rehydrated in a 100 µl solution of 50mM Ammonium Bicarbonate containing 0.01% ProteaseMAX Surfactant (Promega) and 2ng/µl trypsin (Sigma). Additional bicarbonate buffer was added to ensure complete submersion of the gel slices. Samples were incubated for 21 hours at 37°C. Supernatants were transferred to a fresh 1.5-ml tube. Gel slices were further dehydrated with 200 µl of an 80:20 solution of acetonitrile: 1% formic acid. The extract was combined with the supernatants of each sample. The combined supernatants containing digested proteins were then dried in a Speed Vacc and pellets were redissolved with 25 µl of 5% acetonitrile in 0.1% trifluroacetic acid. A 3.5 µl aliquot was directly injected onto a custom packed 2cm x 100µm C_{18} Magic 5µm particle trap column. Peptides were then eluted and sprayed from a custom packed emitter (75µm x 25cm C_{18} Magic 3µm particle) with a linear gradient from 95% solvent A (0.1%

formic acid in water) to 35% solvent B (0.1% formic acid in acetonitrile) at a flow rate of 300 nanoliters per minute for 120 minutes on a Waters Nano Acquity UPLC system. Data dependent acquisitions were performed on a Q Exactive mass spectrometer (Thermo Scientific) according to an experiment where full MS scans from 300-1750 m/z were acquired at a resolution of 70,000 followed by 10 MS/MS scans acquired under HCD fragmentation at a resolution of 17,500 and an isolation width of 1.6 Da. Raw data files were processed with Proteome Discoverer (version 1.4) before using Mascot Server (version 2.5) to search against the Uniprot_Human protein database. Applied search parameters were fully tryptic with 2 missed cleavages, parent mass tolerances of 10 ppm and fragment mass tolerances of 0.05 Da, and allowed for fixed modification of carbamidomethyl cysteine and variable acetyl-group modifications at the N-termini, e.g. pyroglutamate for N-term glutamine, and oxidation of methionine. Search results were loaded into the Scaffold Viewer (Proteome Software, Inc.) to validate and quantify peptides.

2.16 LIPIDOMICS

MV and exosome samples were pelleted at 10 000 g and 100 000g, respectively. Pellets were frozen at -80°C, and transferred to BERG LLC (Framingham, MA) on dry ice for lipid composition analysis.

Aliquots of each sample were combined with a cocktail of deuterium-labeled and odd chain fatty acid standards. Standards were chosen that represent each lipid class and were at designated concentrations expected to provide the most accurate quantitation of each lipid species. Lipids were extracted with 4 mL of a 1:1 (v/v) solution of chloroform:methanol as previously described[207], using a automated custom sequence routine on a Star Hamilton Robotics system (Hamilton, Reno, NV). Lipid extracts were dried under nitrogen and pellets were dissolved in 300 µl of a 1:1 (v/v) solution of chloroform:methanol per mg of protein. Samples were flushed with

nitrogen and stored at -20°C. For MS analysis, samples were diluted 50-fold in 3:3:3:1 (v/v/v/v) isopropanol:methanol:acetonitrile:water containing 2mM ammonium acetate to enhance ionization efficiency in positive and negative modes. Electrospray ionization-MS was performed on a SCIEX TripleTOF® 5600^{+} (SCIEX) coupled to a customized direct injection loop system on an Ekspert microLC200 system. 50µl of sample was injected at a flowrate of 6µl/min. Lipids were analyzed using a customized data independent analysis strategy on the TripleTOF® 5600^{+} allowing for MS/MS^{ALL} high resolution and high mass accuracy analysis as previously described[208]. Lipids were quantified using an in-house library on MultiQuant™ software.

2.17 STATISTICAL ANALYSIS

siRNA uptake, mRNA silencing, cell viability, and lipidomics data (Chapter VI only) were analyzed using GraphPad Prism 7, version 7.04 (*GraphPad Software Inc., La Jolla, CA*). In *in vitro* siRNA uptake experiments curves were fitted using "exponential growth equation" (PNA hybridization assay data) or "one phase association" (confocal microscopy data). In *in vitro* silencing experiments dose-response curves were fitted using "log(inhibitor) *vs.* response – variable slope (three parameters)" equation. Curves were compared using two-way ANOVA with Tukey multiple comparison for main column effect. In *in vivo* silencing experiments in brain and cell viability assay groups were compared using one-way ANOVA with Tukey multiple comparison test. For *in vivo* systemic silencing, the significance was calculated using Kruskal-Wallis One-Way ANOVA with Dunn′ s multiple comparisons. To compare hsiRNA guide strand concentrations measured by PNA assay upon systemic administration, the data were analyzed by One-Way ANOVA with Tukey′ s multiple comparisons. For *in vivo* duration of effect, the data were analyzed by Two-Way ANOVA with Holm-Sidak correction. When comparing candidate proteins between control and stressed conditions two-way ANOVA with multiple comparison for row effect according to the original FDR method of Benjamini and Hochberg. During lipidomics the amount of lipids were normalized to protein content of

samples. Lipid classes in control versus stressed EVs or cells were compared using two-way ANOVA with Tukey multiple comparison for compare rows within columns. Fatty acid tail properties were correlated with enrichment score using linear regression.

Proteomics and lipidomics data (Chapters IV-VI) were analyzed using Microsoft Excel, Scaffold Viewer (Proteome Software Inc.), R and DAVID version 6.7 [209-210], NIH. Label-free quantification of proteins was performed *via* the iBAQ (intensity-based absolute quantification[211]) method in. Briefly, precursor ion intensities of peptides matching to each particular protein were divided by the theoretical number of peptides that could be derived from each particular protein by trypsin digestion. This method normalizes signal to the number of tryptic sites in a protein. Lipidomic quantitation of molecular species and lipid classes were normalized to protein content of samples. Comparison of total protein profiles (individual iBAQ values), and lipid profiles (nmol of lipid species normalized to total protein content) of exosomes, microvesicles and source cells was performed by pairwise Pearson's correlation in Microsoft Excel. Principal component analysis was performed in R ('prcomp' command) after normalization of protein (individual iBAQ values) and lipid (nmol of lipid species normalized to total protein content) profiles of exosomes and microvesicles to the protein and lipid profile of their source cells. Volcano plots and heatmaps were generated in R using "ggplot2", "pheatmap" and "heatmap3" packages. Gene Ontology analysis to annotate biological function to proteins enriched in EVs was conducted using DAVID, version 6.7 [209-210], NIH).

Differences in all comparisons were considered significant at p-values < 0.05.

CHAPTER III ENGINEERED RNA FOR DELIVERY *VIA* EVS

3.1 5′VINYLPHOSPHONATE IMPROVES TISSUE ACCUMULATION AND EFFICACY OF CONJUGATED SIRNAS *IN VIVO*.

3.1.1 Preface

Text and Figures are reproduced from

- **RA Haraszti***, L Roux*, AH Coles, AA Turanov, JF Alterman, D Echeverria, BM Godinho, N Aronin, A Khvorova. 5′vinylphosphonate improves tissue accumulation and efficacy of conjugated siRNAs *in vivo.* Nucl Acid Research, 2017 June 7.

Anastasia Khvorova conceptualized this project. siRNAs used in this study were synthesized and duplexed by Loic Roux and Dimas Echeverria. I was assisted by Andrew Coles, Bruno Godinho and Anton Turanov with animal injections. Julia Alterman performed experiments in HeLa. I performed all animal harvests and *in vivo* silencing measurements, siRNA level quantification, mass spectrometry and chromatography of siRNA metabolites, *in vitro* exonuclease stability assay and statistical analysis. Anastasia Khvorova and I wrote this manuscript.

3.1.2 Abstract

5′vinylphosphonate modification of siRNAs protects them from phosphatases and improves silencing activity. Here we show that 5′vinylphosphonate confers novel properties to siRNAs. Specifically, 5′vinylphosphonate (1) increases siRNA accumulation in tissues, (2) extends duration of silencing in multiple organs and (3) protects siRNAs from 5′-to-3′ exonucleases. Delivery of conjugated siRNAs requires extensive chemical modifications to achieve stability *in vivo*. Because chemically modified siRNAs are poor substrates for phosphorylation by kinases, and 5′ phosphate is required for loading into RNA-induced silencing complex, the synthetic addition of a 5′ phosphate on a fully modified siRNA guide strand is expected to be beneficial. Here we show that

synthetic phosphorylation of fully modified cholesterol-conjugated siRNAs increases their potency and efficacy *in vitro*, but when delivered systemically to mice, the 5′ phosphate is removed within 2 hours. The 5′-phosphate mimic 5′ -*(E)*-vinylphosphonate stabilizes the 5′ end of the guide strand by protecting it from phosphatases and 5′ -to-3′ exonucleases. The improved stability increases guide strand accumulation and retention in tissues, which significantly enhances the efficacy of cholesterol-conjugated siRNAs and the duration of silencing *in vivo*. Moreover, we show that 5′ -*(E)*-vinylphosphonate stabilizes 5′ phosphate, thereby enabling systemic delivery to and silencing in kidney and heart.

3.1.3 Introduction

Small interfering RNAs (siRNAs) guide the sequence-specific cleavage of targeted mRNAs[5, 212]. The ability to design and chemically synthesize an siRNA against virtually any target gene offers a powerful therapeutic strategy to treat genetic diseases, particularly those for which small molecule drugs do not exist (such as Huntington′ s disease and other neurodegenerative diseases). The sequence of an siRNA determines its target, but the chemical architecture determines its pharmacokinetic behavior [56]. Thus, siRNAs can readily be tailored to fit the needs of personalized medicine.

The clinical utility of siRNA therapeutics has been limited by *in vivo* stability and safe, efficient delivery to tissues. Both challenges are being met by advances in oligonucleotide chemistry [73, 77, 213-214]. Hydrophobic conjugates—e.g., cholesterol—drive efficient cellular uptake of siRNA *via* a general mechanism[213, 215], which may expand the range of tissues that can be targeted. Extensive chemical modification of conjugated siRNAs improves stability and activity

in vivo [213, 216-217]. siRNA compounds currently in clinical studies are modified using a combination of 2′ –fluoro (2′–F) and 2′–*O*–methyl (2′–*O*–Me) modifications [77, 216, 218].

The guide strand of an siRNA duplex must bear a 5′ phosphate to bind the effector protein of the RNA-induced silencing complex Argonaute 2 (AGO2) [219-222]. The *in vivo* phosphorylation state of a synthetic siRNA depends on the balance of kinase and phosphatase activity. A dephosphorylated siRNA must be phosphorylated for effectiveness *in vivo*; however, fully chemically modified siRNAs are poor substrates for intracellular kinases [223]. Therefore, to preserve proper 5′ phosphorylation, phosphonates can be used as metabolically stable phosphate analogs. The stability resides in the carbon-phosphorus bond of phosphonates that resists phosphatases, which hydrolyze oxygen-phosphorus bonds[224]. Among phosphonates tested, 5′ -*(E)*-vinylphosphonate appears to be the most effective phosphate analog [7, 225-227]. Indeed, both single stranded siRNAs and GalNAc-conjugated double stranded siRNAs benefit from 5′ -*(E)*-vinylphosphonate modification [228-231].

Here we evaluate how chemical phosphorylation of hydrophobically modified siRNAs (hsiRNAs) with either phosphate, or the metabolically stable phosphate analog 5′-*(E)*-vinylphosphonate, impacts efficacy and duration of effect *in vitro* and *in vivo*. We show that 5′ phosphate and 5′-*(E)*-vinylphosphonate equally enhance hsiRNA activity *in vitro*. When administered in vivo, 5′ phosphate hsiRNAs are de-phosphorylated within hours, but metabolic stabilization with 5′ -*(E)*-vinylphosphonate significantly increases retention of hsiRNAs in tissues, silencing activity, and duration of effect. The 5′-*(E)*-vinylphosphonate, cholesterol-conjugated hsiRNAs remain active in liver and kidneys for at least 6 weeks after single administration. 5′-*(E)*-vinylphosphonate hsiRNAs silences target genes in the heart, a tissue previously not accessible by conjugated siRNAs. Finally, we show that 5′-*(E)*-vinylphosphonate not only resists phosphatases

in vivo, but also resists 5′-phosphate-dependent exonucleolytic destruction by XRN1, contributing to overall stabilization of the guide strand in tissues.

3.1.4 RESULTS

5′ chemical phosphorylation enhances hsiRNA efficacy *in vitro*

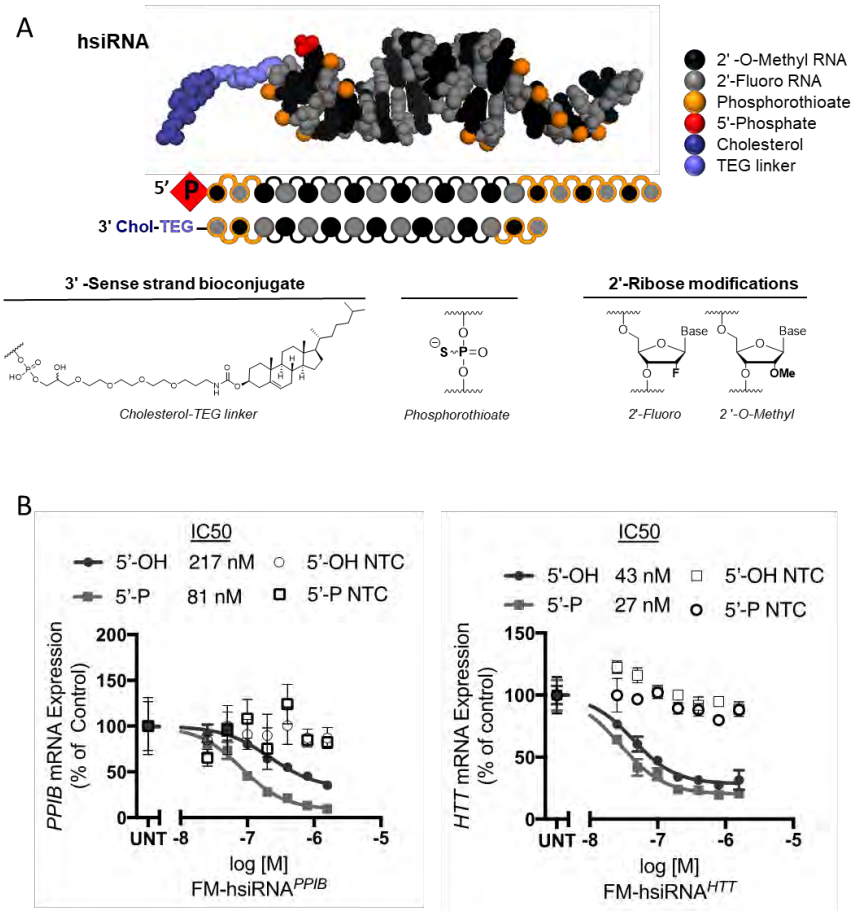

Figure 3.1 5′ phosphorylation of hsiRNAs increases activity *in vitro*. **A.** Cartoon of hsiRNA chemical scaffold. **B.** Graphs showing the levels of *PPIB* (left) or *HTT* mRNA (right) in HeLa cells treated with 5′ hydroxide (5′-OH) or 5′phosphate (5′-P) hsiRNA^{PPIB} (left) or hsiRNA^{HTT} (right) or non-targeting control (NTC) hsiRNAs. mRNA levels measured by QuantiGene® 2.0 assay are normalized to the level of a control *HPRT* mRNA and shown as percent of the untreated (UNT) control. The IC50 for the experimental hsiRNAs are indicated in the legend. N=3 for each datapoint.

Hydrophobically modified hsiRNAs (**Figure 3.1A**) are asymmetric siRNAs with alternating 2′–F and 2′–*O*–Me modification of each ribose to resist endonucleases and avoid innate immune activation. The 2′–F and 2′–*O*–Me modifications offset each other in the short (15 base-pair) double-stranded region. Phosphorothioate linkages at the ends of both strands and throughout the single-stranded 3′ tail of the guide strand enhance cellular uptake of hsiRNAs. A cholesterol group linked to the 3′ end of the passenger strand drives unassisted cellular uptake. hsiRNAs rapidly (within minutes) and efficiently enter cells through an EE1-related endocytosis pathway[232], and they show *in vivo* efficacy after local administration [202, 213, 233].

hsiRNAs targeting *PPIB* (peptidylprolyl isomerare B or cyclophilin B) and *HTT* (huntingtin) were synthesized with 5′-hydroxide and 5′-phosphate on the guide strand (see **Table 3.1** for sequences and chemical modification patterns of hsiRNAs used in this study). Chemical phosphorylation at the 5′ end significantly increased the level of target mRNA silencing and hsiRNA potency (2.7 fold for hiRNA^{PPIB}, $p<0.001$ and 1.6 fold hiRNA^{HTT}, $p=0.01$) compared to 5′hydroxide hsiRNA (**Figure 3.1B**). Thus, chemical phosphorylation significantly contributes to the overall potency of hsiRNAs *in vitro* in passive uptake, with the level of impact showing sequence dependence.

siRNA ID	Gene	Targeting Position	Strand	Sequence and chemical modification pattern	Calculated mass	Observed mass
5'-OH hsiRNA^{HTT}	*HTT*	10150	S	fC#mA#fG.mU.fA.mA.fA.mG.fA.mG.fA.mU.fU#mA#fA	5765.34	5764.22
	HTT	10150	AS	PmU#fU#mA.fA.mU.fC.mU.fC.mU.fU.mU.fA.mC#fU#mG#fA#mU#fA#mU#fA	6540.46	6539.72
5'-P hsiRNA^{HTT}	*HTT*	10150	S	fC#mA#fG.mU.fA.mA.fA.mG.fA.mG.fA.mU.fU#mA#fA	5765.34	5764.22
	HTT	10150	AS	PmU#fU#mA.fA.mU.fC.mU.fC.mU.fU.mU.fA.mC#fU#mG#fA#mU#fA#mU#fA	6620.44	6619.69
5'-VP hsiRNA^{HTT}	*HTT*	10150	S	fC#mA#fG.mU.fA.mA.fA.mG.fA.mG.fA.mU.fU#mA#fA	5765.34	5764.22
	HTT	10150	AS	vPmU#fU#mA.fA.mU.fC.mU.fC.mU.fU.mU.fA.mC#fU#mG#fA#mU#fA#mU#fA	6616.45	6615.70
5'-OH hsiRNA^{PPIB}	*PPIB*	437	S	fC#mA#fA.mA.fU.mU.fC.mC.fA.mU.fC.mG.fU#mG#fA	5654.22	5653.14
	PPIB	437	AS	PmU#fC#mA.fC.mG.fA.mU.fG.mG.fA.mA.fU.mU#fU#mG#fC#mU#fG#mU#fU	6650.55	6649.75
5'-P hsiRNA^{PPIB}	*PPIB*	437	S	fC#mA#fA.mA.fU.mU.fC.mC.fA.mU.fC.mG.fU#mG#fA	5654.22	5653.14
	PPIB	437	AS	PmU#fC#mA.fC.mG.fA.mU.fG.mG.fA.mA.fU.mU#fU#mG#fC#mU#fG#mU#fU	6730.53	6729.72
5'-VP hsiRNA^{PPIB}	*PPIB*	437	S	fC#mA#fA.mA.fU.mU.fC.mC.fA.mU.fC.mG.fU#mG#fA	5654.22	5653.14
	PPIB	437	AS	vPmU#fC#mA.fC.mG.fA.mU.fG.mG.fA.mA.fU.mU#fU#mG#fC#mU#fG#mU#fU	6726.54	6725.71
5'-P hsiRNA^{sFLT1}	*sFLT1*	2283	S	fG#mG#fA.mU.fC.mU.fC.mC.fA.mA.fA.mU.fU#mU#fA	5655.20	5655.11
	sFLT1	2283	AS	PmU#fA#mA.fA.mU.fU.mU.fG.mG.fA.mG.fA.mU#fC#mC#fG#mA#fG#mA#fG	6839.67	6838.80
PNA^{sFLT1}	*sFLT1*	2283	S	Cy3-(OO)-*C*T*C*T*C*T*C*G*G*A*T*C*T*C*C*A*A*A*T*T*T*A	6250.2	6253.4
PNA^{PPIB}	*PPIB*	437	S	Cy3-(OO)–*A*A*C*A*G*C*A*A*A*T*T*C*C*A*T*C*G*T*G*A	6317.3	6320.8
PNA^{HTT}	*HTT*	10150	S	CY3-(OO)-*T*A*T*A*T*C*A*G*T*A*A*A*T*A*G*A*T*T*A*A	6370.3	6373.2

Table 3.1 Sequences and chemical modification patterns of hsiRNAs.

hsiRNAs are quickly dephosphorylated *in vivo* after systemic administration.

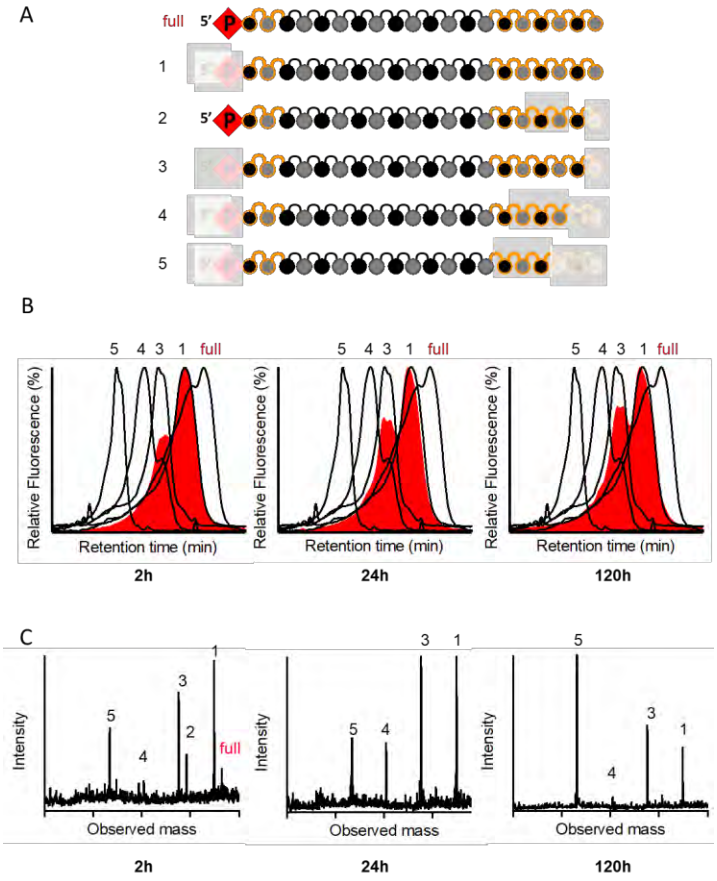

Figure 3.2 5′ phosphorylated hsiRNA is rapidly dephosphorylated upon systemic administration. A. Cartoons of predicted metabolites synthesized. For color code see Figure 1.A. **B.** HPLC traces of Cy3-PNA/hsiRNA hybrids in liver lysates from mice injected with 5′ -P hsiRNA (red-filled traces). Black traces depict traces corresponding to control guide strands: intact guide strand (full) or the synthesized putative metabolites (1 to 5) indicated in panel A. **C.** Mass spectrometry profiles of 5′ -P hsiRNA metabolites in liver lysates of mice injected with 5′ P hsiRNA. Mice were harvested 2, 24, and 120 hours after intravenous injection.

Delivery of conjugated hsiRNA requires chemical modifications that are resistant against metabolic cleavage. To evaluate metabolic stability of chemically introduced 5′-phosphate *in vivo*, we administered 10 mg/kg of 5′-phosphate hsiRNA systemically into mice by tail vein injection. We analyzed the livers of injected mice after 2 hours, 24 hours, or 120 hours for the presence of hsiRNA guide strand metabolites. For comparison, we also analyzed a series of predicted guide strand metabolites (references), which we added into liver lysates from PBS treated animals (**Figure 3.2A and Figure 3.3**). Tissues were lysed and hsiRNA guide strand metabolites were

detected using a peptide nucleic acid (PNA)-based hybridization assay[203] and anion exchange chromatography. Correlation of elution times between the references and metabolites extracted from mouse livers identified major hsiRNA degradation products**.**

We failed to detect intact hsiRNA guide strands in livers harvested 2 hours after injection (**Figure 3.2B**), indicating that systemically administered hsiRNAs, in spite of being fully modified by 2′–F and 2′–*O*–Me, are rapidly metabolized *in vivo*. At each time point, we observed two major chromatography peaks whose elution times correlated with that of a 5′hydroxide full-length (20-nucleotide) guide strand and a 5′hydroxide 19-nucleotide metabolite with one nucleotide removed from the 3′ end (**Figure 3.2B**). Mass spectrometry analysis confirmed the identity of both metabolites (**Figure 3.2C**), and resolved additional products, including a 5′phosphate metabolite trimmed at the 3′ end by 1 nucleotide (product 2, **Figure 3.2A**) and further 5′hydroxide products trimmed at the 3′ end by 2 or 3 nucleotides (products 4 and 5 in **Figure 3.2A**). At 2 hours after injection, most of the hsiRNA guide strand was dephosphorylated at the 5′end, and by 24 hours the levels of full-length 5′phosphate guide strand could not be distinguished from noise. The primary degradation events *in vivo* appear to be eliminating of the 5′ phosphate and trimming the 3′ end. Although RISC should be able to load a phosphorylated guide strand trimmed by one or two 3′ nucleotides[234], dephosphorylated guide strands are expected to be significantly less active, thereby limiting *in vivo* efficacy.

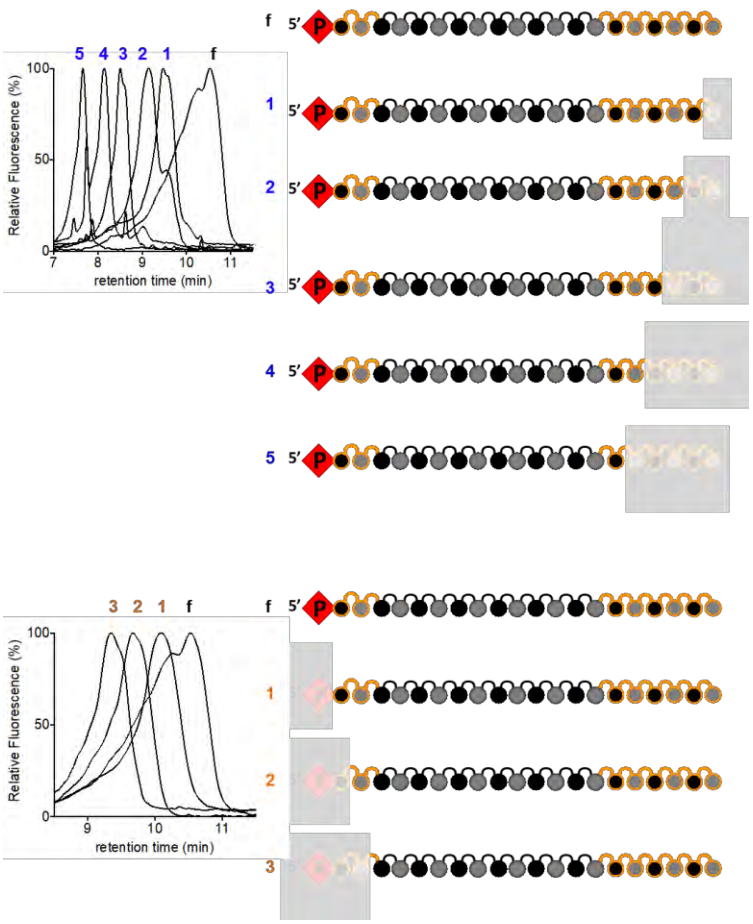

Figure 3.3 Cartoons and HPLC anion exchange chromatograms of synthesized metabolites. For color code, see Figure 3.2

5′ -*(E)*-vinylphosphonate modification could be added to all sequences of hsiRNA and is fully active *in vitro*

We sought to compare the stability and activity of hsiRNAs with 5′–phosphate or a metabolically stabilized 5′–*(E)*–vinylphosphonate. The unsaturated C-C bond of 5′–*(E)*–vinylphosphonate restricts the torsion angle to 180°, and the resulting *trans*—or *E*—configuration mimics the optimal electronic and spatial positioning of 5′ -P phosphate[226] (**Figure 3.4A**). We synthesized the phosphoramidite of 5′ -*(E)*-vinylphosphonate 2′ –*O*–Me-Uridine and incorporated it into the guide strand as a last coupling during the 3′ -5′ oligonucleotide chemical synthesis. Since 5′ terminal base is not involved in RISC-target mRNA interaction [231, 235], the 5′ -*(E)*-

vinylphosphonate 2′–*O*–Me-Uridine phosphoramidite can be used to incorporate 5′-*(E)*-vinylphosphonate in any siRNA independently of target gene and sequence (**Figure 3.4 and 3.5).** When tested *in vitro* by passive uptake, 5′ -*(E)*-vinylphosphonate hsiRNAs were just as effective as 5′-phosphate hsiRNAs, confirming that the 5′ -*(E)*-vinylphosphonate modification is well tolerated by the RNA-induced silencing complex (RISC) assembly (**Figure 3.4B**).

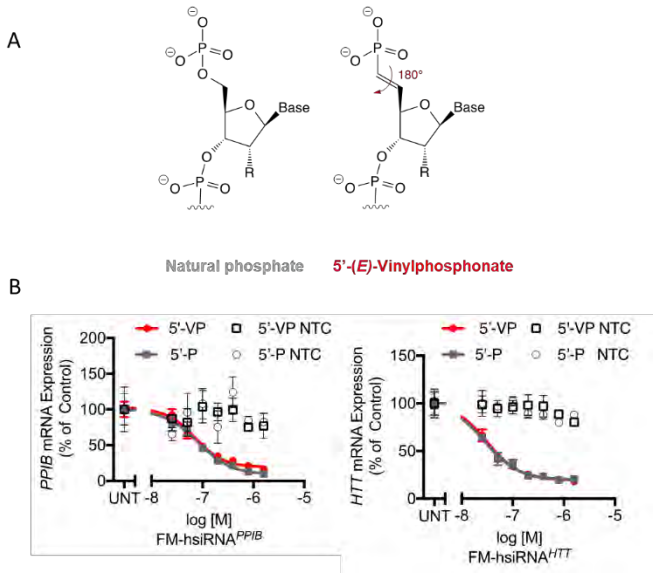

Figure 3.4 Stabilization of the 5′ end by 5′ -*(E)*-vinylphosphonate supports RISC loading and activity.

A. Chemical structures of 5′ -phosphate (5′-P) and 5′ -*(E)*-vinylphosphonate (5′-VP). **B.** As in Figure 1.B., except that HeLa cells treated with 5′ -P or 5′ -VP modified hsiRNAs, as indicated in the legend.

Figure 3.5 Chemical synthesis of the 5' stabilized antisense stand.

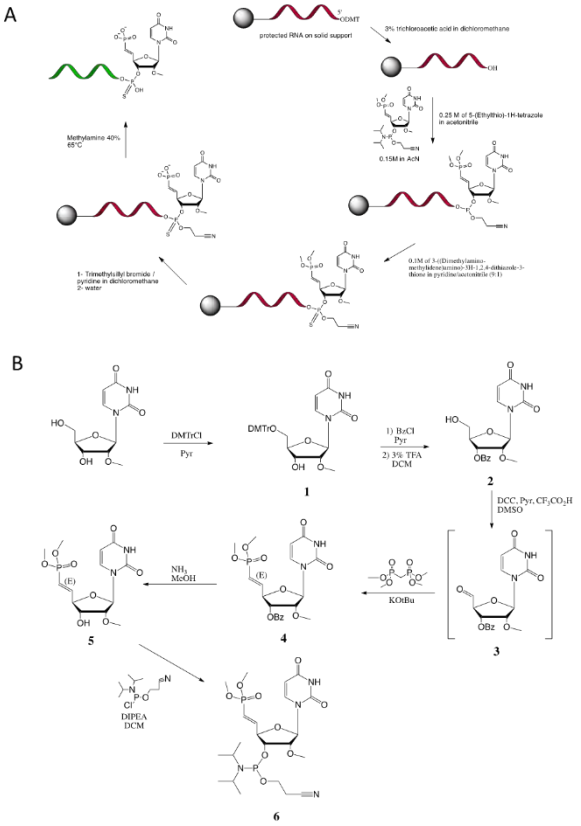

A) (*E*)-vinylphosphonate Uridine phosphoramidite coupling and deprotection procedure of the 5' modified oligonucleotides antisense strand. B) Synthesis pathway of the (*E*)-vinylphosphonate Uridine phosphoramidite.

5′ -*(E)*-vinylphosphonate hsiRNA outperforms 5′phosphate hsiRNA in kidney and heart, and is comparable in liver and spleen

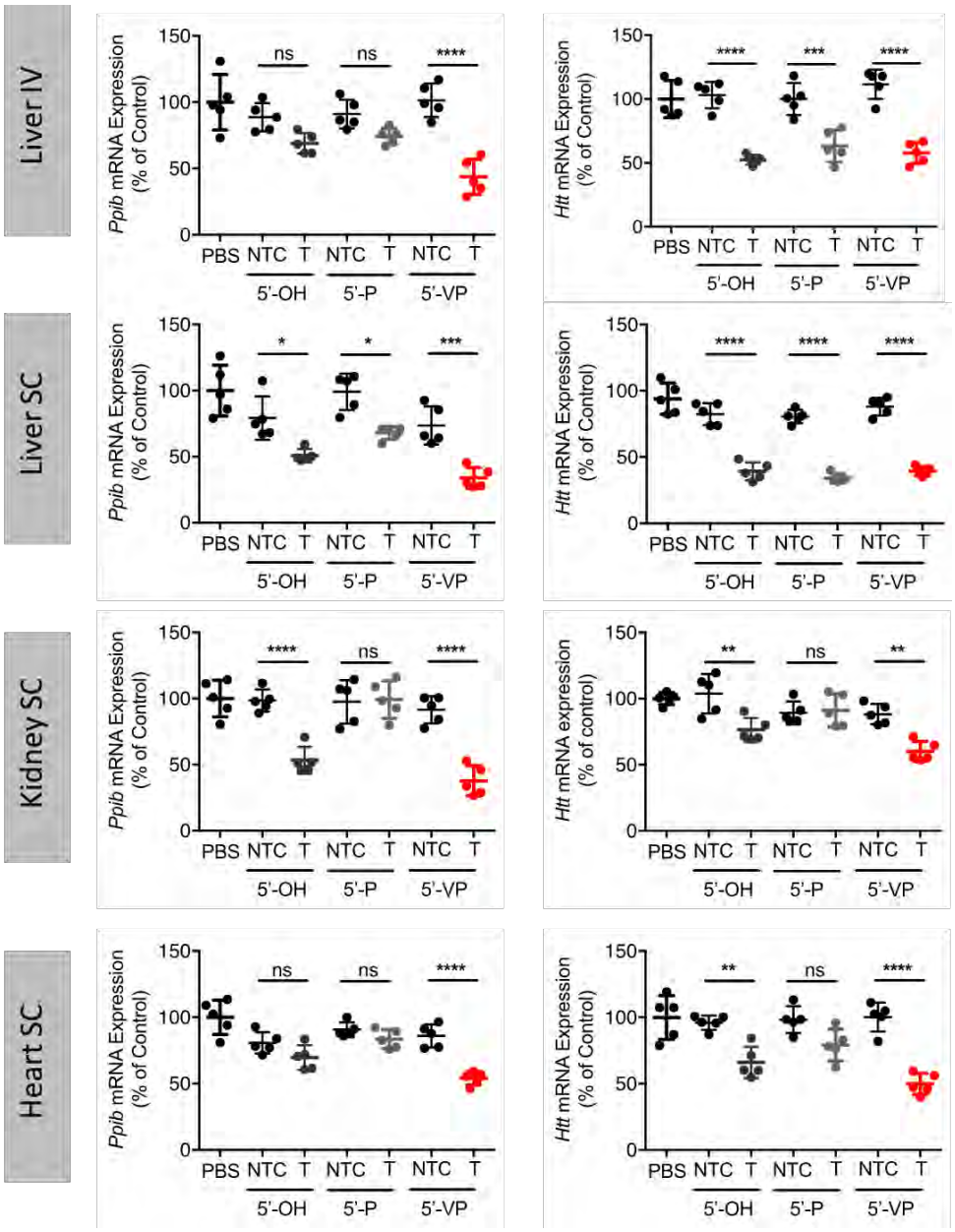

Figure 3.6 5′ -(E)-vinylphosphonate modification enhances hsiRNA efficacy in liver, kidneys and heart. Column scatter plots showing *Ppib* or *Htt* mRNA levels in the livers, kidneys and hearts of mice (n=5 per group) treated with 5′ hydroxide (5′-OH), 5′ phosphate (5′-P), or and 5′ -*(E)*-vinylphosphonate (5′ -VP) hsiRNAs by intravenous (IV) of subcutaneous (SC) injection. mRNA levels measured by QuantiGene® 2.0 assay, were normalized to *Hprt* mRNA and expressed as percent of mRNA levels in PBS-treated animals. NTC, non-targeting control. T, targeting hsiRNA.

Significance calculated by ANOVA with Bonferroni′ s correction: ns, non-significant; *, p≤0.05; **, p≤0.01; ***, p≤0.001; and ****, p≤0.0001.

Current clinical stage siRNAs accumulate in liver [214, 217]. Therefore, we first compared the efficacy of 5′hydroxide-, 5′phosphate, and 5′-*(E)*-vinylphosphonate hsiRNAs in the liver after intravenous or subcutaneous administration. We used previously identified hsiRNA sequences that efficiently silence *Ppib* or *Htt* mRNAs (**Table 3.1**; [213, 233]). All 5′ variants of hsiRNA^{Htt} reduced *Htt* mRNA levels in liver by ~60% when administered subcutaneously and by ~40% when administered intravenously **(Figure 3.6)**. In contrast, 5′-*(E)*-vinylphosphonate modified hsiRNA^{Ppib} silenced *Ppib* mRNA substantially better (66% when administered subcutaneously and 57 % when administered intravenously) than 5′phosphate or 5′hydroxide hsiRNAs (30-50% when administered subcutaneously and 25-30% when administered intravenously) **(Figure 3.6).**

The cholesterol moiety conjugated to hsiRNAs is highly hydrophobic and drives non-specific uptake of hsiRNA by many cell and tissue types such as muscle [215] and eye [213]. We therefore asked whether subcutaneous delivery of hsiRNA could promote silencing in other organs. We specifically looked at kidney as this is prime location for drug clearance, spleen as a major member of the reticuloendothelial system, and heart as a clinically interesting target organ. Since hsiRNA accumulation was expected to be substantially lower in these organs (*i.e.* kidneys, heart and spleen) than in liver, we used a higher dose (20mg/kg) to ensure sufficient hsiRNA accumulation in secondary tissues to support silencing. Subcutaneous administration of 5′phosphate hsiRNA^{PPIB} silenced *Ppib* mRNA by 28% in spleen (**Figure 3.7**) but did not lead to silencing in kidney and heart. 5′ phosphate hsiRNA^{HTT} did not result in silencing *Htt* mRNAs in kidney, spleen or heart (**Figure 3.6**). The 5′ hydroxide hsiRNAs supported 50% silencing of *Ppib*

and 20% silencing of *Htt* in kidney, 15% *Ppib* silencing but no *Htt* silenicing in spleen (**Figure 3.7**) and no *Ppib* silencing but 35% *Htt* silencing in heart (**Figure 3.6**). The metabolically stabilized 5′-*(E)*-vinylphosphonate hsiRNAs showed the highest activity, showing 64% *Ppib* mRNA silencing and 40% *Htt* mRNA silencing in kidney (**Figure 3.6**), 32% *Ppib* silencing and 25% *Htt* silencing (p=0.06) in spleen (**Figure 3.7**), as well as 46% *Ppib* silencing and 51% *Htt* silencing in heart (**Figure 3.6**).

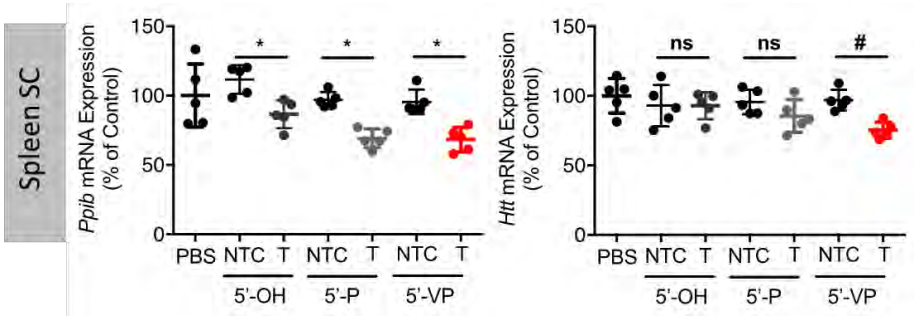

Figure 3.7 5′ -*(E)*-vinylphosphonate hsiRNA is comparable to 5′-phosphate hsiRNA in spleen.

Column scatter plots showing *Ppib* or *Htt* mRNA levels in the spleens of mice (n=5 per group) treated with 5′ hydroxide (5′-OH), 5′ phosphate (5′-P), or and 5′ -*(E)*-vinylphosphonate (5′ -VP) hsiRNAs by intravenous (IV) of subcutaneous (SC) injection. mRNA levels measured by QuantiGene® assay, were normalized to *Hprt* mRNA and expressed as percent of mRNA levels in PBS-treated animals. NTC, non-targeting control. T, targeting hsiRNA. Significance calculated by ANOVA with Bonferroni′ s correction: ns, non-significant; #, p≤0.1; p*, p≤0.05; **, p≤0.01; ***, p≤0.001; and ****, p≤0.0001.

5′ -*(E)*-vinylphosphonate improves hsiRNA accumulation in multiple tissues

Using the PNA-based hybridization assay to quantify hsiRNA levels in tissue lysates, we found that the metabolically stable 5′-*(E)*-vinylphosphonate hsiRNAs accumulated to significantly higher concentrations (up to 22 fold) than 5′ hydroxide hsiRNAs in liver, kidney, heart, and spleen

(**Figure 3.8A and B**). When administered intravenously, the positive impact of 5′-*(E)*-vinylphosphonate modification on hsiRNA concentration was the highest in heart (**Figure 3.8B**). In all tissues examined, 5′-*(E)*-vinylphosphonate hsiRNAs accumulated to higher levels than 5′ phosphate hsiRNAs, regardless of the administration route or hsiRNA sequence (**Figure 3.8A and B**). Hence, the metabolic stabilization of the 5′ phosphate *via* 5′-*(E)*-vinylphosphonate has resulted in overall increase of guide strand tissue accumulation, which could explain improved *in vivo* activity of 5′-*(E)*-vinylphosphonate hsiRNAs.

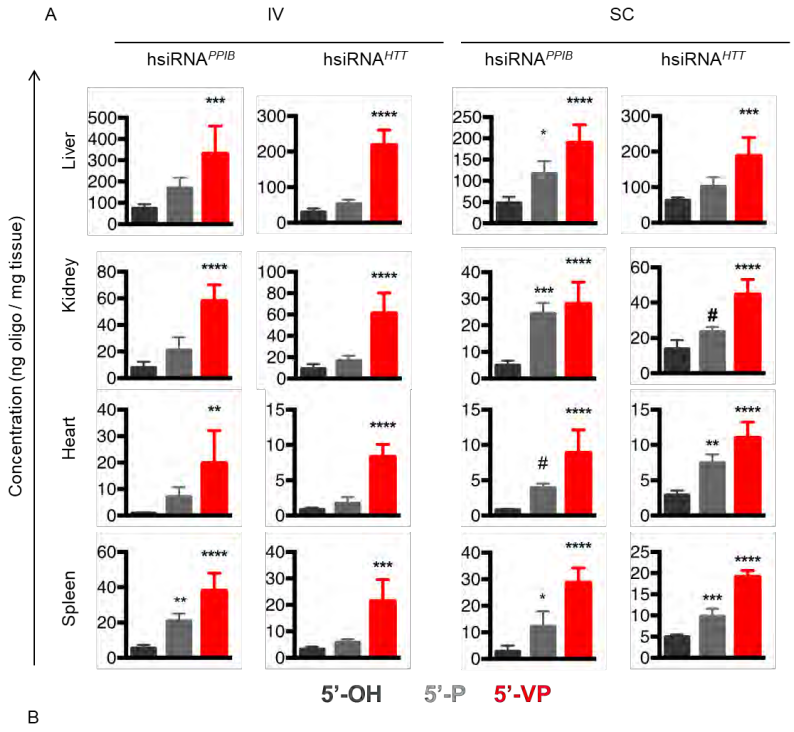

B

	IV				SC			
	hsiRNA^{PPIB}		hsiRNA^{HTT}		hsiRNA^{PPIB}		hsiRNA^{HTT}	
	5′-P	5′-VP	5′-P	5′-VP	5′-P	5′-VP	5′-P	5′-VP
Liver	2.3	4.4	1.7	7.1	2.4	4.0	1.6	3.0
Kidney	2.7	7.2	1.8	6.5	4.9	6.1	1.7	3.2
Heart	7.9	22.0	2.1	10.0	4.9	11.0	2.6	3.8
Spleen	3.8	6.8	1.8	6.5	4.3	10.1	2.0	3.9

Figure 3.8 Metabolic stabilization of the 5′ phosphate increases retention in both primary and secondary tissues.

A. Bar graphs showing the concentrations of 5′ hydroxide (5′-OH), 5′ phosphate (5′-P), or and 5′ -*(E)*-vinylphosphonate (5′ -VP) hsiRNA guide strands and their metabolites in liver (primary tissue), kidneys, heart, and spleen (secondary tissues), one week after intravenous (IV) or subcutaneous (SC) injection. Concentrations measured by PNA hybridization assay. Bar graphs show the mean±SD, n=5 mice per group. **B.** Summary of fold change in concentrations of 5′ -P and 5′ -VP hsiRNA guide strands compared to 5′ -OH hsiRNA

guide strand. Fold changes are color-coded: high fold changes in red and low fold changes in white. Fold changed were calculated by dividing average hsiRNA concentrations in respective organs from n=5 mice per group.

5′ -*(E)*-vinylphosphonate modification of hsiRNA confers resistance to phosphatases and to 5′ -to-3′ exoribonuclease XRN1

The improved retention and silencing activity of 5′-*(E)*-vinylphosphonate hsiRNAs *in vivo* could reflect protection from natural phosphatases and nucleases.

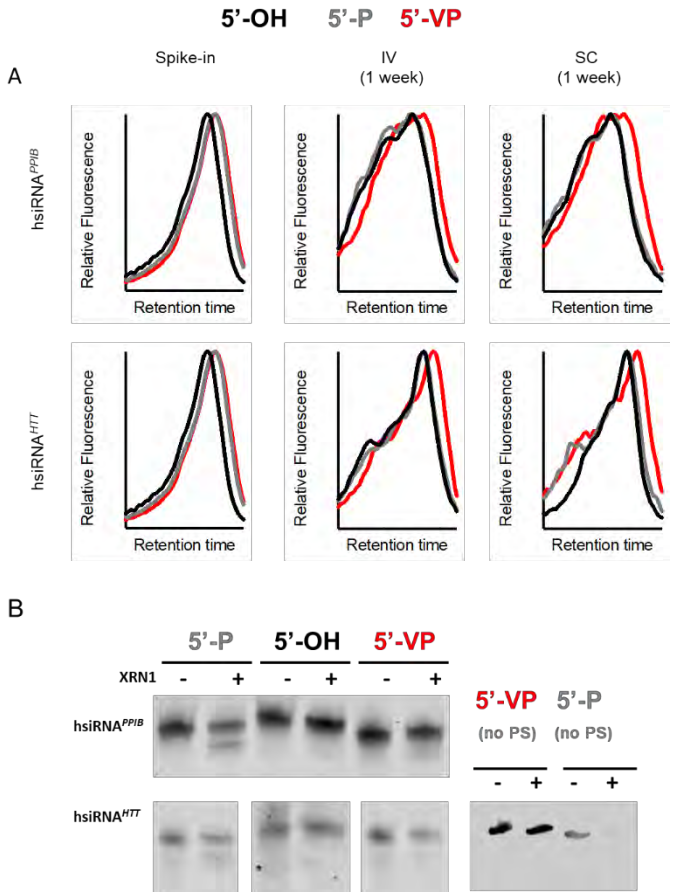

Figure 3.9 5′ -*(E)*-vinylphosphonate infers resistance against phosphatases *in vivo* and 5′ -3′ exonuclease *in vitro*.

A. HPLC traces of Cy3-PNA/hsiRNA hybrids in liver lysates from mice harvested 1 week after intravenous (IV) or subcutaneous (SC) injection with 5′ hydroxide (5′-OH), 5′ phosphate (5′-P), or and 5′ -*(E)*-vinylphosphonate (5′ -VP) hsiRNA. The "spike-in" (left) panels show control traces of Cy3-PNA/hsiRNA hybrids after full-length guide strands were spiked into liver lysates from untreated mice. 5′-P spike-in guide strands elute more slowly than 5′ -OH guide strands, corresponding to the difference of one charge (phosphate). Metabolite profile

in liver lysates clearly show dephosphorylation of 5′ -P hsiRNA but partially intact 5′ end of 5′ -VP hsiRNA. **B.** Urea-PAGE of 5′ hydroxide (5′-OH), 5′ phosphate (5′-P), or and 5′ -*(E)*-vinylphosphonate (5′ -VP) hsiRNAs resolved on an 7 M urea/24% polyacrylamide gel after 12 hours incubation in the absence (–) or presence (+) of Terminator™ enzyme. 5′-P and 5′-VP (no PS) compound had the same nucleotide modification pattern (2′-F, 2′-O-Me) as 5′ -P, 5′ -OH, and 5′ -VP, but did not contain phosphorothioate (PS) internucleotide linkages. 5′ -VP hsiRNA is protecting against degradation by Terminator™ enzyme, whereas 5′ -P hsiRNA is degraded, and phosphorothioate internucleotide linkage interferes with enzyme processivity.

Phosphonate bonds have been shown to resist snake venom phosphatase [224, 226] and 5′-*(E)*-vinylphosphonate siRNAs have performed better *in vivo* than 5′ hydroxide siRNAs (Figure 3., [229-230]) consistent with phosphatase resistance. However, no direct evidence exists to date that 5′-*(E)*-vinylphosphonate resist phosphatases *in vivo* in a mouse. We therefore used a PNA-based hybridization assay [203] to resolve phosphorylated and dephosphorylated hsiRNA metabolites in liver lysates from mice injected with 20mg/kg 5′ hydroxide, 5′ phosphate, or 5′-*(E)*-vinylphosphonate hsiRNAs. As a control, we analyzed untreated liver lysates, into which we added intact hsiRNAs with 5′ hydroxide, 5′ phosphate, or 5′-*(E)*-vinylphosphonate end. The control chromatography shows 5′ phosphate and 5′-*(E)*-vinylphosphonate hsiRNAs elute with overlapping profiles, and 5′ hydroxide hsiRNAs elute earlier, reflecting the difference of one charge (the phosphate) absent in the 5′hydroxide hsiRNA (**Figure 3.9A, left panels**). In livers harvested from mice 1 week after injection, however, we found that chromatography profiles of 5′ phosphate hsiRNA converged with the profile of 5′ hydroxide hsiRNA, whereas 5′-*(E)*-vinylphosphonate hsiRNA guide strand eluted later (**Figure 3.9A, middle and left graphs**), regardless of

administration route or sequence. These findings are consistent with rapid dephosphorylation (and 3′ trimming) of 5′phosphate hsiRNA and protection of 5′-*(E)*-vinylphosphonate hsiRNAs from dephosphorylation.

Nucleic acids with a 5′ phosphate are sensitive to the 5′ -to-3′ exoribonuclease Xrn1 [236]. Furthermore, Xrn1 and Xrn2 play a role in miRNA stability[237-239], especially if miRNA is taken up from the extracellular space [240]. Xrn1 also regulates accumulation of viral dsRNA [241]. Taken together with the observation that 5′-*(E)*-vinylphosphonate hsiRNA showed higher concentrations in several tissues than 5′ phosphate hsiRNA, we hypothesized that 5′-*(E)*-vinylphosphonate hsiRNA may have improved stability due to Xrn1 resistance. To test whether 5′-*(E)*-vinylphosphonate modification protects against 5′-to-3′ exoribonuclease-mediated degradation, we treated 5′ phosphate, 5′ hydroxide, and 5′-*(E)*-vinylphosphonate hsiRNA guide strands with Terminator™ 5′-phosphate-dependent exoribonuclease (i.e., recombinant XRN1) overnight and then resolved potential metabolites by denaturing polyacrylamide gel electrophoresis. Whereas we detected a 5′ phosphate hsiRNA guide strand metabolite shortened by ~1 nt, the 5′ hydroxide and 5′-*(E)*-vinylphosphonate hsiRNA guide strands—regardless of sequence—remained intact (**Figure 3.9B**). This finding indicates that 5′-*(E)*-vinylphosphonate protects against turnover by 5′ phosphate-specific exoribonucleases. We hypothesized that the 19mer metabolite of 5′ phosphate hsiRNA could be a result of interference between phosphorothioate internucleotide linkage with XRN1 processivity. Therefore, we synthesized 5′ phosphate and 5′-*(E)*-vinylphosphonate hsiRNAs fully modified with 2′-O-Me and 2′-F but containing no phosphorothioates. The guide strand of 5′ phosphate hsiRNA lacking phosphorothioates was fully degraded by Terminator™, whereas 5′-*(E)*-vinylphosphonate hsiRNA guide strand containing no phosphorothioates was protected (**Figure 3.9B**). These data suggest that 5′-*(E)*-vinylphosphonate modification is

sufficient to protect hsiRNA guide strand from degradation by 5′ -to-3′ exoribonuclease. Overall, resistance to phosphatases and to the exoribonuclease XRN1 underlie the improved *in vivo* stability of 5′-*(E)*-vinylphosphonate -modified hsiRNAs, leading to improved silencing performance.

5′ -*(E)*-vinylphosphonate modification improves hsiRNA duration of effect *in vivo*

The improved *in vivo* stability and silencing performance of 5′ -VP hsiRNA could translate into improved duration of effect. We tested this hypothesis by subcutaneously injecting a single 20mg/kg dose of 5′ hydroxide or 5′-*(E)*-vinylphosphonate hsiRNA^{Ppib} and monitoring the levels of *Ppib* mRNA and hsiRNA in mouse kidney and liver at different time points. We found that the silencing of *Ppib* mRNA and hsiRNA^{Ppib} concentration in kidney and liver gradually decreased with time, but the level of *Ppib* mRNA silencing and retention of 5′-*(E)*-vinylphosphonate hsiRNA exceeded that of 5′ hydroxide hsiRNA at each time point (**Figure 3.10**). Metabolically stable phosphate containing 5′-*(E)*-vinylphosphonate hsiRNA maintained significant silencing in liver and kidney, from ~70% *Ppib* mRNA silencing in both tissues after 1 week to ~24% (liver) and ~17% (kidney) silencing after 6 weeks. The 5′hydroxide hsiRNA showed ~50% target mRNA silencing after 1 week in both liver and kidney, but lost significant silencing activity within 4 weeks in liver and within 2 weeks in kidney (**Figure 3.10A**). The 5′-*(E)*-vinylphosphonate hsiRNA concentration remained 2 to 4 times higher than the concentration of 5′hydroxide hsiRNA in liver and kidney at each time point (**Figure 3.10B**). Hence, stabilization of 5′ end by 5′ -*(E)*-vinylphosphonate supports increased tissue content, increased silencing activity and increased duration of effect when compared to 5′hydroxide hsiRNA.

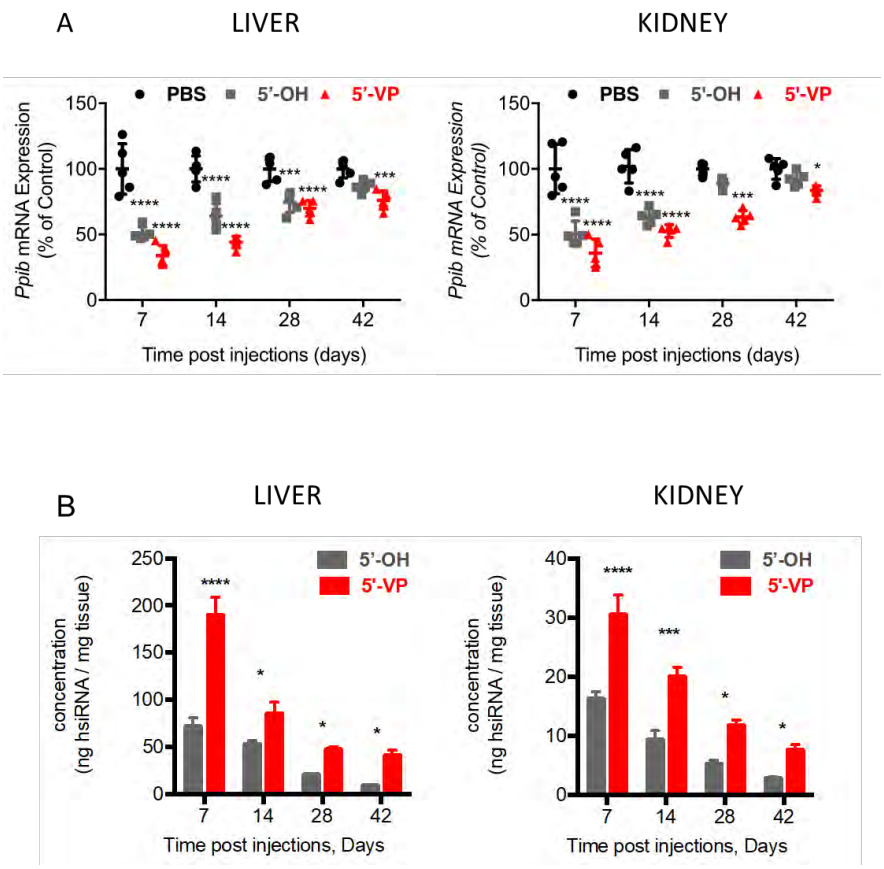

Figure 3.10 Stabilization of 5′ phosphate increases duration of effect and corresponding tissue accumulation of hsiRNA in vivo.

A. Column scatter plots showing *Ppib* mRNA levels in the livers and kidneys of mice (n=5 per group) at the indicated times after subcutaneous injection of PBS or 5′ -OH or 5′ -VP hsiRNAs. mRNA levels measured by QuantiGene® assay were normalized to *Hprt* mRNA and expressed as a percent of mRNA levels in PBS-treated animals. Significance calculated by ANOVA with Bonferroni′ s correction, significance was calculated in comparison to PBS-treated animals: *, p≤0.05; **, p≤0.01; ***, p≤0.001; and ****, p≤0.0001. Mean±SD. **B.** Bar graphs showing the concentration of 5′ -OH and 5′ -VP hsiRNA guide strands in liver and kidney, as measured by the PNA-based hybridization assay at the indicated time points after subcutaneous injection. Mean±SD, N=5

3.1.5 Discussion

Here we have shown that 5′-*(E)*-vinylphosphonate modification confers clinically useful properties to siRNA drugs. These properties include increase in siRNA tissue concentration and duration of silencing, which in turn may allow lowering of dose and frequency of administration. We have identified two underlying mechanisms: resistance to phosphatases and resistance to

5′-to-3′ exonucleases. We and others have shown that 5′-*(E)*-vinylphosphonate is recognized as a phosphate mimic by AGO2 (a nuclease in the RNA-induced silencing complex, RISC) and allows or even facilitates loading of siRNA guide strand into RISC [229, 231]. However, our data suggests that 5′-*(E)*-vinylphosphonate is not recognized as a phosphate mimic by the main cytoplasmic 5′-to-3′ exonuclease, XRN1. Hence, 5′-*(E)*-vinylphosphonate modification improves both the pharmacodynamic (better loading to RISC) and pharmacokinetic (slower degradation) behavior of an siRNA through altering protein binding.

The impact of 5′-*(E)*-vinylphosphonate on siRNA silencing activity showed sequence-dependence in liver but not in kidney and heart. Different hsiRNA-to-target mRNA ratios could explain this observation. In mouse liver, *Ppib* mRNA is expressed at a fifty times higher level than *Htt* mRNA (FPKM ~184 versus FPKM ~4; Proteinatlas.org), whereas hsiRNA^{PPIB} and hsiRNA^{HTT} concentrations were very similar (~200ng/mg). Therefore, the injected dose of 5′phosphate or 5′hydroxide hsiRNA may be above the level needed to fully silence *Htt* in liver, but below the level needed to fully silence *Ppib*. Increased concentration of 5′-*(E)*-vinylphosphonate hsiRNA would therefore improve silencing of *Ppib* but not that of *Htt.* hsiRNA concentrations are approximately six times lower in kidney and twenty times lower in heart than in liver, while mRNA expression levels are within the same range. We propose that 5′-*(E)*-vinylphosphonate only improves silencing activity when hsiRNA-to-target mRNA ratios are below the level of saturation.

We observed that modification of the 5′end of hsiRNAs influenced silencing activity differently *in vitro* and *in vivo*. First, 5′-*(E)*-vinylphosphonate hsiRNA was equally active *in vitro* compared to 5′phosphate hsiRNA, but significantly more active *in vivo.* This is explained by rapid dephosphorylation of 5′phosphate hsiRNA *in vivo* (Figure S1. and [242]) In parallel, 5′hydroxide hsiRNA was less active *in vitro* but more active *in vivo* compared to 5′phosphate hsiRNA. Indeed, unmodified 5′hydroxide siRNA has been found to be more efficacious *in vivo* than unmodified 5′phosphate siRNA[243]. Furthermore, all siRNAs showing efficacy to date in clinical trials have 5′hydroxide ends [218, 244-245]. The mechanism why 5′hydroxide siRNA performs superior to 5′phosphate siRNA *in vivo* is unclear. We propose that the 5′end of the guide strand may influence protein binding profile of the siRNAs in subcutaneous extracellular space or in serum or in lymph. siRNA-bound proteins or peptides can alter the trafficking [246] and phosphorylation [242] of siRNAs. The different impact of 5′end of the guide strand on silencing activity in *in vitro* and *in vivo* experimental settings may be explained by exposure to a different protein environment.

Concentration of 5′-*(E)*-vinylphosphonate hsiRNA was 4-22-fold higher than concentration of 5′hydroxide hsiRNA, while silencing of 5′-*(E)*-vinylphosphonate hsiRNA was only 0.9-3.3-fold higher than silencing of 5′hydroxide hsiRNA. This phenomenon has been observed before [229] and indicates a non-linear relationship between tissue concentration and silencing activity. Resistance to exonucleases shown in this paper is only one contributor to the concentration – silencing activity relationship. Other factors may be proteins or peptides differentially binding to the different 5'ends of hsiRNAs and influence phosphorylation [242] or endosomal release [247].

We found better silencing activity following subcutaneous administration compared to intravenous administration, as has been observed in the case of GalNac-conjugated siRNAs as well

[214]. Subcutaneous administration results in slower release and longer residence time of the hsiRNA compared to intravenous administration. We speculate that certain serum proteins carry hsiRNAs to the organs and the hsiRNA binding capacity of the serum is saturated upon intravenous administration. Binding to the proper carrier protein may enable a productive cellular entry pathway.

In this study we used hsiRNA modified with a combination of 2′-F, 2′-*O*-Me and phosphorothioates. These siRNA modifications can support a duration of silencing up to 6 months *in vivo* [218]. The mechanism may be explained by enhanced nuclease stability and formation of an intracellular depot, which is slowly releasing siRNAs for continuous reloading of Ago2 [248]. However, recent findings suggest that reduction of 2′-F modification of an siRNA could improve safety profiles [218, 249-250]. Thus, carefully fine-tuning the amount of 2′-F modifications in 5′-*(E)*-vinylphosphonate hsiRNA might be crucial to ensure clinical safety and success.

5′-*(E)*-vinylphosphonate hsiRNA leads to long-lasting *Huntingtin* mRNA silencing in liver, heart and kidneys. Lowering *Huntingtin* mRNA could be beneficial in treating peripheral symptoms and improving quality of life of patients with Huntington's disease [251-253].

3.2 Optimized cholesterol-siRNA chemistry improves productive loading into small extracellular vesicles.

3.2.1 Preface

Figure 3.11 is reproduced from

- MR Hassler*, AA Turanov*, JF Alterman*, **RA Haraszti**, AH Coles, MF Osborn, D Echeverria, M Nikan, WE Salomon, L Roux, BMDC Godinho, DV Morrissey, PD Zamore, SA Karumanchi, MJ Moore, N Aronin, A Khvorova. Comparison of fully and partially chemically-modified siRNA in conjugate-mediated delivery in vivo. Nucl Acid Research. 2018 Febr.8.

In Figure 3.11 Julia Alterman and Matthew Hassler designed, Matthew Hassler, Dimas Echeverria, Mehran Nikan and Loic Roux synthesized, Anton Turanov and Andrew Coles injected siRNAs and I measured siRNA levels in all tissues using PNA hybridization assay.

Text and figures 3.12 – 3.17 are reproduced from a submitted manuscript

- **RA Haraszti**, R Miller, MC Didiot, A Biscans, JF Alterman, MR Hassler, L Roux, D Echeverria, E Sapp, M DiFiglia, N Aronin, A Khvorova. Optimized cholesterol-siRNA chemistry improves productive loading into small extracellular vesicles.

Marie Didiot and I conceptualized this project. siRNAs used in this study were synthesized by Loic Roux, Annabelle Biscans, Matthew Hassler and Dimas Echeverria. I duplexed singe strands. I was assisted by Rachael Miller in exosome production. Marie Didiot contributed intellectually to exosome loading with cholesterol-siRNAs and Julia Alterman contributed intellectually in designing siRNAs with cleavable linkers. Ellen Sapp and Marian DiFiglia performed transmission electron microscopy. I performed all vesicle loading experiments, liposome production, primary neurons preparation, silencing measurements, siRNA level quantification, nanoparticle tracking analysis and Western blotting. Anastasia Khvorova and I wrote this manuscript.

3.2.2 Abstract

Exosomes are promising delivery vesicles for therapeutic RNAs. siRNA conjugation to cholesterol enables efficient and reproducible loading of exosomes with the therapeutic cargo. siRNAs are typically chemically modified to fit an application. However, siRNA chemical modification pattern has not been specifically optimized for exosome-mediated delivery. Here we used cholesterol-conjugated, asymmetric siRNAs (hsiRNAs) to evaluate the effect of backbone, 5′-phosphate, and linker chemical modifications on productive hsiRNA loading into exosomes.

hsiRNAs with a combination of 5′-*(E)*-vinylphosphonate and alternating 2′-fluoro and 2′-*O*-methyl backbone modifications outperformed previously used partially modified siRNAs in exosome-mediated *Huntingtin* silencing in neurons. Between two commercially available linkers (TEG and C7) widely used to attach cholesterol to siRNAs, TEG is preferred compared to C7 for productive exosomal loading. Destabilization of the linker completely abolished silencing activity of loaded exosomes. The loading of cholesterol-conjugated siRNAs was saturated at ~3000 siRNA copies per exosome. Overloading impaired the silencing activity of exosomes.

The data reported here provide an optimization scheme for the successful use of hydrophobic modification as a strategy for productive loading of RNA cargo into exosomes.

3.2.3 Introduction

Exosomes are small extracellular vesicles being explored for therapeutic RNA delivery due to (i) their small size (50-150 nm) allowing penetration through some biological barriers [254-255], (ii) their unique protein composition enabling target-cell specificity [137, 256], and (iii) their natural capacity to transfer RNA between cells [132, 138]. Exosomes specifically transfer protein and RNA cargo between neurons and glial cells [180-185]; therefore exosomes are believed to be a promising

approach for therapeutic RNA delivery to brain [135]. Short interfering RNAs (siRNAs), a subclass of therapeutic RNAs, are capable of selective gene silencing [5]. Thus, siRNAs offer a therapeutic option for genetically defined diseases, such as Huntington′s disease. However, delivery to target tissues remains the bottleneck for clinical application of therapeutic RNAs, including siRNAs. Exosomes represent a strategy to overcome the delivery challenge [135-136].

Cholesterol-conjugation mediated loading of siRNAs into exosomes is among the most reproducible and scalable loading strategies [135, 153-154], characterized by efficient transfer of the loaded cholesterol-siRNA to target cells. However, productive gene silencing induced by the transferred cholesterol-siRNA was variable. We speculate that these variations are due to differences in siRNA chemical modification patterns (45-71% of riboses modified), cholesterol placement position (5′ or 3′ of the sense strand), siRNA-to-exosome loading ratio (100s vs 1000s siRNAs/exosome) and siRNA concentrations used in silencing studies (~50-1500 nM) [135 153 154]. All studies used a version of pyrimidine-modified siRNAs, which have been shown to provide stabilization against nucleases *in vitro* in serum [74, 213, 257].

Advances in oligonucleotide chemistry have enabled the expansion of siRNA use from *in vitro* serum-rich environments to systemic delivery *in vivo* [75, 77-78, 213-214]. In particular, siRNAs with modification of all riboses [77, 202, 214, 218, 244, 258] (with 2′-fluoro and 2′-*O*-methyl) were 10,000 fold more active *in vivo* (**Figure 3.11**)[104] than partially modified siRNAs similar to siRNAs originally used for exosomes loading [135, 153-154]. A second type of modification, 5′-*(E)*-vinylphosphonate, also improved the activity of systemically administered conjugated siRNAs [201, 229-230]. However, full chemical modification did not affect the activity of non-conjugated siRNAs delivered in cationic liposomes [78, 259-260]. Exosomal delivery of hsiRNAs combines principles of siRNA conjugation and lipid nanoparticle technology. The impact of siRNA chemical

modifications on efficacy of exosomal delivery is therefore difficult to predict and remains unknown.

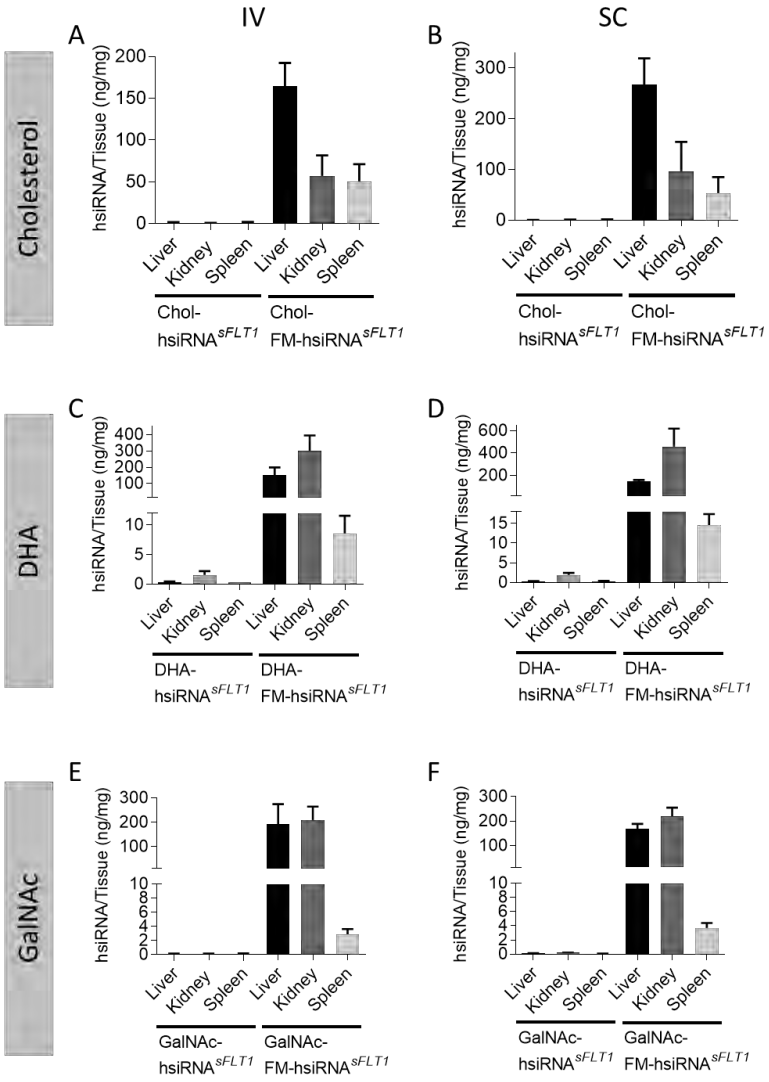

Figure 3.11 Systemic administration of fully modified siRNAs shows enhanced tissue accumulation.

Guide strand tissue quantification by PNA hybridization-based assay in liver, kidney and spleen after 10 mg/kg intravenous (IV) tail vein injection **(A, C and E)** or 10 mg/kg subcutaneous (SC) injection **(B, D and F)**. mean ± SD, N=3 mice. hsiRNA: partially modified siRNA (70% of nucleotides modified), FM-hsiRNA: fully modified siRNA (100% of nucleotides modified), DHA: docosahexaenoic acid GalNAc: N-Acetylgalactoseamine.

Among many synthetic approaches on cholesterol attachment to the siRNA, TEG (triethyl glycol) and C7 (2-aminobutyl-1-3-propanediol) linkers are frequently used and commercially

available. In the amino linker class, the C7 linker was optimal for siRNA passive uptake [261]. Despite the common use of both linkers, no systematic comparison has been published to date.

Here we evaluated the impact of siRNA chemical modification patterns, cholesterol attachment *via* different linkers, and siRNA-to-exosome loading ratio on functional exosome-mediated delivery of siRNAs. We used siRNA concentrations ranging from 23 nM to 1500 nM in all experiments. Furthermore, we used a therapy relevant exosomal cell source (umbilical cord, Wharton-s jelly derived mesenchymal stem cells), siRNA target gene (*Huntingtin*) and exosomal recipient cells (neurons).

3.2.4 Results

Linker chemistry influences efficiency of cholesterol-mediated loading of siRNAs into exosomes.

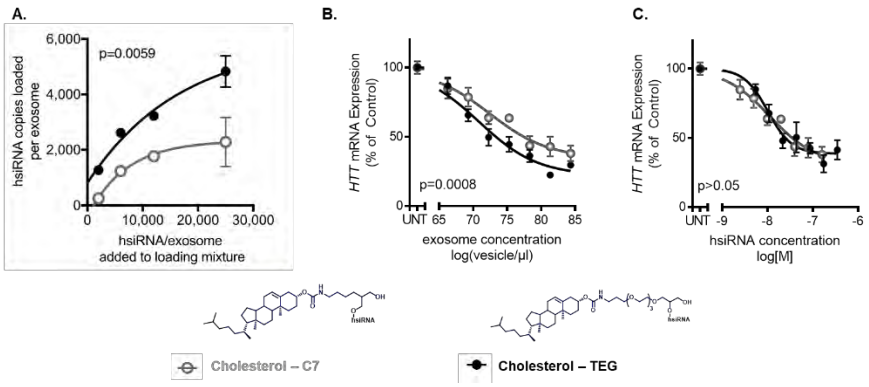

Figure 3.12 Triethyl glycol linker for cholesterol is favorable. Fluorescent, fully modified hsiRNA was loaded into exosomes, primary murine cortical neurons treated for one week and target *Htt* mRNA silencing measured using QuantiGene (Affymetrix). **A.** hsiRNA conjugated to cholesterol with either a TEG (triethyl glycerol) or a C7 (2-aminobutyl-1-3-propanediol) linker was loaded into exosomes at varying hsiRNA-to-exosome ratios. **B.** *Huntingtin* mRNA silencing in primary neurons one week after treatment with varying concentration of hsiRNA-loaded exosomes.

UNT=untreated, N=3 mean ± SEM **C.** Level of silencing from panel B was normalized to hsiRNA content of loaded exosomes.

To compare two commercially available strategies to conjugate cholesterol to siRNAs (TEG and C7 linkers), we used a previously developed asymmetric siRNA scaffold [213, 233], characterized by a short duplex region (15 base pairs) and a fully phosphorothioated tail assisting membrane association [213, 232, 262] (hsiRNAs). hsiRNAs are either partially modified with 2′-fluoro pyrimidines on the antisense strand and 2′-*O*-methyl pyrimidines on the sense strand, or are fully modified using alternating 2′-*O*-methyl and 2′-fluoro pattern providing endonuclease stability and protection from innate immune response [263-265]. We synthesized fully modified cholesterol-hsiRNAs targeting *Huntingtin* mRNA [233] using either TEG or a C7 linkers (**Figure 3.12**). Cholesterol-hsiRNA variants were loaded into exosomes at increasing hsiRNA-to-exosome ratios (**Figure 3.12A**) Both variants showed efficient loading into exosomes with saturation kinetics (**Figure 3.12A**) Cholesterol-TEG-hsiRNAs loaded more efficiently into exosomes than cholesterol-C7-hsiRNA at all ratios tested (**Figure 3.12A**, p=0.0059). More efficient loading led to more potent *Huntingtin* mRNA silencing, when primary neurons were treated with exosomes loaded to saturation (cholesterol-TEG IC50~ $8*10^6$ exosomes, cholesterol-C7 IC50~ $22*10^6$ exosomes, p=0.0008, **Figure 3.12B**). Normalization to hsiRNA content eliminated the observed differences (p>0.05, **Figure 3.12C**). Thus, silencing potency of the two hsiRNA variants were the same. Improved silencing activity upon exosomal delivery could be fully explained by better exosomal loading of cholesterol-TEG-hsiRNA. Therefore, cholesterol-TEG-hsiRNA was used for subsequent experiments.

Optimization of cholesterol-hsiRNA-to-exosome ratio: one to three thousand hsiRNA per exosome is preferred.

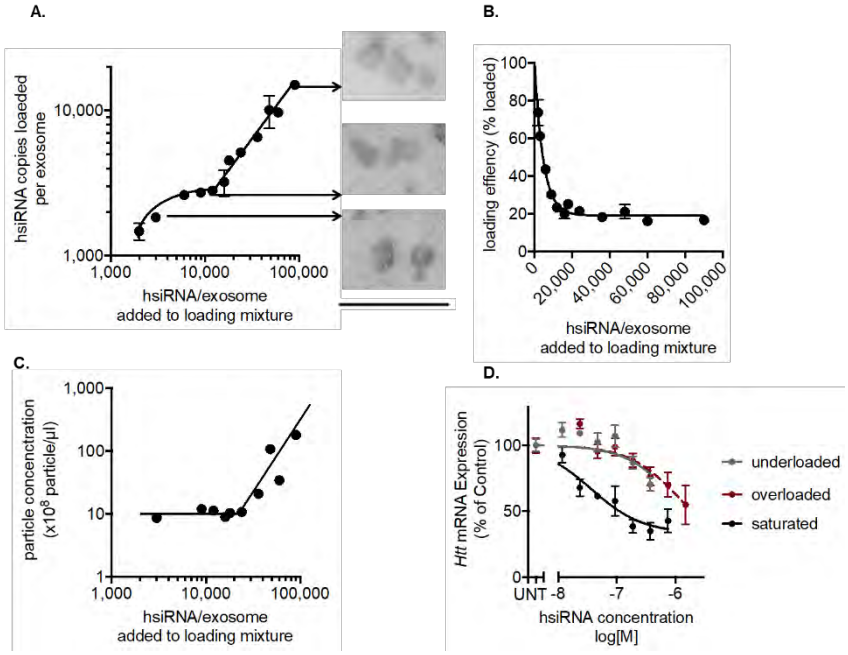

Figure 3.13 Loading of hsiRNA to exosomes is a partially saturatable process.

A. Cholesterol-hsiRNA was loaded into exosomes at different hsiRNA-to-exosomes ratios. The loading curve shows and initial saturation phase followed by a secondary linear phase. Transmission electron microscopy images correspond to hsiRNA loaded exosomes at an hsiRNA-to-exosome ratio of 3000, 10 000 and 100 000. Scale bar represents 500 nm. **B.** Loading efficiency at varying hsiRNA-to-exosome ratios. **C.** Particle concentration as assessed by nanoparticle tracking analysis after loading at varying hsiRNA-to-exosome ratios. **C.** *Huntingtin* mRNA silencing in primary neurons one week after treatment with exosomes loaded with hsiRNA at hsiRNA-to-exosomes ratios of 3000, 10 000 and 100 000. UNT=untreated, N=3 ± SEM

Contrary to conventional siRNA exosomes loading approaches (*i.e.* electroporation or overexpression in parent cells), hydrophobic modifications of siRNA enable association of large number of RNA molecules per exosome. To define an optimal hsiRNA-to-exosome ratio, *i.e.* ratio

supporting productive target mRNA silencing, we evaluated the effect of hsiRNA concentration during the loading process (1,000 to 100,000 hsiRNA copies per exosome added to the loading mixture). Addition of 6,000 hsiRNAs per exosome into the loading mixture resulted in ~ 2,600 hsiRNAs associated per vesicle (**Figure 3.13A**), leading to 43% loading efficiency (**Figure 3.13B**). Further increase in the amount of hsiRNA added to the loading mixture (9,000 and 12, 000 per vesicle) did not support an increase in the amount of exosome-associated hsiRNAs **(Figure 3.13A**), indicating a level of intermediate saturation at ~ 2,500-3000 hsiRNAs per vesicle. As the amount of loaded hsiRNAs stayed constant, the estimated loading efficiency decreased from 43 to 23% (**Figure 3.13B**). Following this initial saturation phase, we observed a linear increase in the amount of hsiRNAs loaded per exosome starting at approximately 20,000 hsiRNA per exosome added to the loading mixture, representing a constant loading efficiency of 18% (**Figure 3.13B**). Transmission electron microscopy showed similar lipid bilayer surrounded vesicles post loading at hsiRNA-to-exosome ratios below the initial saturation phase (3,000), at the initial saturation phase (10,000), and in the linear increase phase (100,000) (**Figure 3.13A**). Increasing hsiRNA-to-exosome loading ratio beyond 20,000 resulted in increased total particle number (**Figure 3.13C**), suggesting hsiRNA aggregation. Formation of extra particles was only observed in the presence of vesicles.

Next, we evaluated how hsiRNA-to-exosome ratio affected the ability of loaded exosomes to silence *Huntingtin* mRNA in primary neurons. 3,000, 10,000 and 100, 000 hsiRNAs (per vesicle) were added to the loading mixture generating exosomes with 1,000, 3,000 and 18,000 RNA molecules per vesicle, respectively. From three hsiRNA-to-exosome ratios tested, exosomes containing 3000 hsiRNA per vesicle performed the best with an IC50 of 37 nM (**Figure 3.13D**). In contrast, exosomes underloaded (1,000 hsiRNA/exosome) or overloaded (18,000

hsiRNA/exosome) were less efficient in *Huntingtin* mRNA silencing (IC50 1330 nM and 1164 nM, respectively) (**Figure 3.13D**). As exosomes loaded with 3000 hsiRNA (saturation level) were 36-fold more potent than underloaded and 31-fold more potent than overloaded exosomes, exosomes loaded with 3000 hsiRNAs were used for subsequent experiments.

Full chemical stabilization of RNA cargo improves productive loading into exosomes.

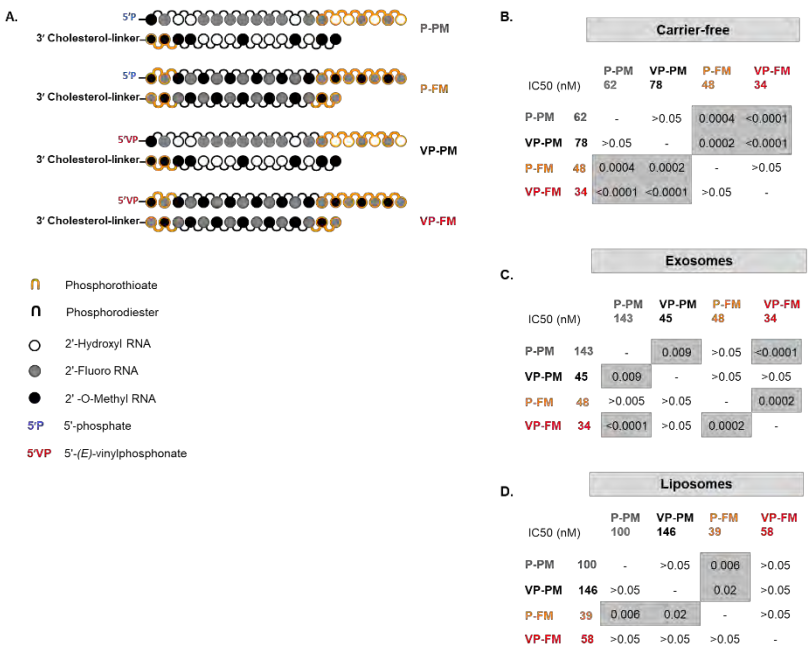

Figure 3.14 Full stabilization of hsiRNA is beneficial for exosome-mediated delivery.

A. Scheme of chemically modified hsiRNAs. P-PM partially modified backbone with 5′-phosphate on guide strand, P-FM fully modified backbone with 5′-phosphate on guide strand, VP-PM partially modified backbone with 5′-*(E)*-vinylphosphonate on guide strand, VP-FM fully modified backbone with 5′-*(E)*-vinylphosphonate on guide strand **B.** Primary murine cortical neurons were incubated for one week with cholesterol-hsiRNA variants with different extent of 2′ ribose and 5′ end modifications either alone (carrier-free), target *Huntingtin* mRNA silencing was measured, and silencing potency calculated (IC50). N=3 Pairwise comparison of curves was conducted using two-way ANOVA with Tukey's post-hoc test. Significance is

depicted in grey. **C.** Experiment from panel B conducted with exosome-mediated delivery. **D.** Experiment from panel B conducted with liposome-mediated delivery.

To evaluate the impact of chemical modifications on exosomal delivery of hsiRNAs, we synthesized four different hsiRNA variants: (1) partially modified (all pyrimidines modified, similar to commercially available siRNAs [213, 257]), (2) partially modified with 5′-*(E)*-vinylphosphonate [201, 229-231], (3) fully modified (100% of riboses modified [77, 202, 214, 218, 244, 258]), and (4) fully modified with 5′-*(E)*-vinylphosphonate (**Figure 3.14A**). In fully modified hsiRNA variants, four additional phosphorothioate modifications were introduced compared to partially modified variants, to provide additional stabilization from exonuclease activity (**Figure** 3**.14A**).

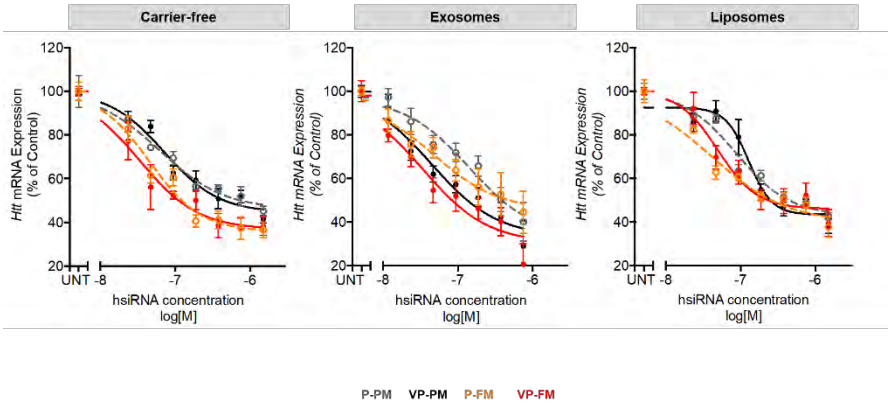

Figure 3.15 Full stabilization of hsiRNA is beneficial for exosome-mediated delivery.

Primary murine cortical neurons were incubated for one week with cholesterol-hsiRNA with different extent of 2’ ribose and 5’ end modifications either alone (carrier-free), or loaded to exosomes or liposomes and target *Huntingtin* mRNA silencing was measured. UNT=untreated, P-PM=5’phosphate with partially modified backbone, VP-PM=5’vinylphosphonate with partially modified backbone, P-FM=5’phosphate with fully modified backbone, VP-FM= 5’vinylphosphonate with fully modified backbone, N=3. mean ± SEM

Surprisingly, only 5′-*(E)*-vinylphosphonate modification improved *Huntingtin* mRNA silencing activity of hsiRNA-loaded exosomes ($p = 0.009$), whereas full modification of hsiRNA backbone alone had no effect ($p > 0.05$) (**Figure 3.14C** and **Figure 3.15** middle panel). However, when combined with 5′-*(E)*-vinylphosphonate, full hsiRNA backbone modification further improved silencing ($p < 0.0001$) compared to 5′-*(E)*-vinylphosphonate alone ($p = 0.009$) (**Figure 3.14C** and **Figure 3.15** middle panel). Thus, phosphatase resistance provided a larger benefit than nuclease resistance during exosome-mediated delivery of hsiRNAs to neurons. An opposite effect was observed with carrier-free (*i.e.* no exosomes, liposomes or transfection reagents used for delivery) hsiRNA uptake, where full modification of hsiRNA backbone improved silencing ($p = 0.0004$), whereas 5′-*(E)*-vinylphosphonate did not ($p > 0.05$) **Figure 3.14C** and **Figure 3.15** left panel). Indeed, previous data showed no effect of 5′-*(E)*-vinylphosphonate modification on silencing activity of siRNAs delivered carrier-free to HeLa cells [201]. As another control we used liposomes with a size range (**Figure 3.16**) and loading technique identical to that of exosomes (*i.e.* hsiRNAs residing predominantly on the surface of liposomes). When hsiRNAs were delivered in neutral liposomes, the effect of chemical modifications resembled carrier-free delivery with full modification of hsiRNA backbone improving silencing activity the most ($p = 0.006$).

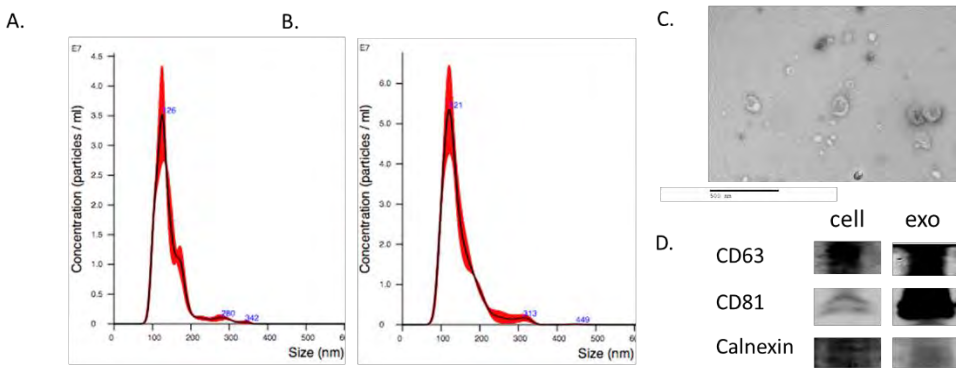

Figure 3.16 Characterization of liposomes and umbilical cord, Wharton-s jelly derived exosomes.

A. Nanoparticle Tracking Analysis shows homogenous exosome size distribution with mean diameter 141± 40 nm, N=3 **B.** Nanoparticle Tracking Analysis of neutral liposomes, mean diameter 144 ± 47 nm, N=3 **C.** Transmission Electron Microscopy image of loaded exosomes, size bar shows 500 nm. **D.** Western blot of positive and negative exosome marker proteins.

Thus, the biological origin and contents of exosomes represent a likely reason for increased relative importance of 5′-*(E)*-vinylphosphonate over chemical modification of siRNA backbone. Indeed, a variety of nucleases, including 5′-nucleotidase, was detected in exosomes purified from umbilical cord derived mesenchymal stem cells using mass spectrometry (**Table 3.2**).

P49184	DNSL1	HUMAN Deoxyribonuclease-1-like 1 OS=Homo sapiens GN=DNASE1L1 PE=1 SV=1	34 kDa
Q7KZF4	SND1	HUMAN Staphylococcal nuclease domain-containing protein 1 OS=Homo sapiens GN=SND1 PE=1 SV=1	102 kDa
O94919	ENDD1	HUMAN Endonuclease domain-containing 1 protein OS=Homo sapiens GN=ENDOD1 PE=1 SV=2	55 kDa
P13489	RINI	HUMAN Ribonuclease inhibitor OS=Homo sapiens GN=RNH1 PE=1 SV=2	50 kDa
P21589	5NTD	HUMAN 5'-nucleotidase OS=Homo sapiens GN=NT5E PE=1 SV=1	63 kDa
P22413	ENPP1	HUMAN Ectonucleotide pyrophosphatase/phosphodiesterase family member 1 OS=Homo sapiens GN=ENPP1 PE=1 SV=2	105 kDa
P09543	CN37	HUMAN Isoform CNPI of 2',3'-cyclic-nucleotide 3'-phosphodiesterase OS=Homo sapiens GN=CNP	45 kDa

Table 3.2 Nucleases detected in exosomes isolated from umbilical cord derived mesenchymal stem cells, *via* mass spectrometry. First column: Uniprot Accession numbers

The stability of the cholesterol linker is essential for productive hsiRNA loading into exosomes.

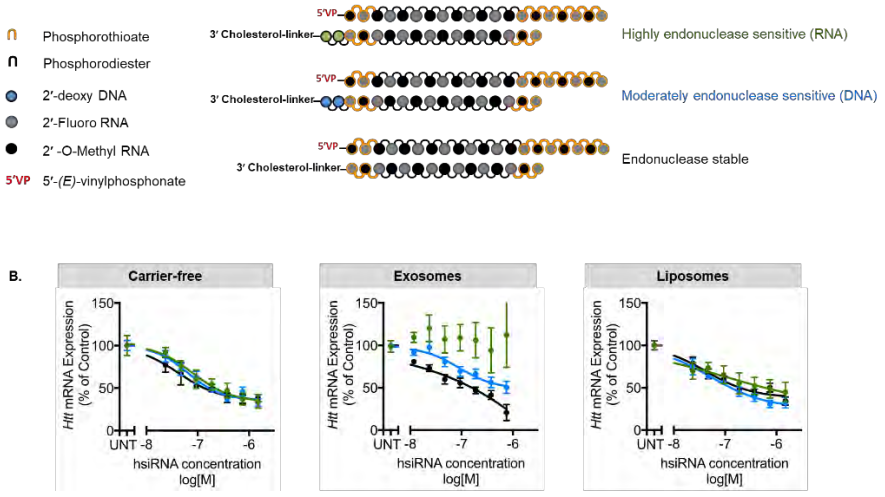

Figure 3.17 Cleavable cholesterol impairs activity of cholesterol-hsiRNA-loaded exosomes.

A. Incorporation of moderately (2′-deoxy-DNA, blue) or highly (2′-hydroxy-RNA, green) endonuclease-sensitive bases into the sense strand is a strategy to facilitate cleavage of cholesterol from cholesterol-conjugated hsiRNA. **B.** *Huntingtin* mRNA silencing in primary neurons one week after treatment with exosomes loaded with hsiRNA variants alone (carrier-free) or loaded into exosomes or liposomes at varying concentrations. UNT=untreated, N=3, mean ± SEM

Loading of hsiRNAs into exosomes is dependent on the presence of the hydrophobic cholesterol conjugate [135], which anchors the hsiRNA into the membrane. Stable association with membranes may potentially trap siRNAs in endosomes and limit loading into cytoplasmic RISC, thus impairing silencing activity [266]. Introduction of cleavable linkers have been used as a successful strategy to enhance silencing activity of conjugated siRNAs [267]. To test whether the use of cleavable linkers is an advantage in exosome-mediated delivery of cholesterol-hsiRNAs, we synthesized three hsiRNA variants with varying stability of the linker connecting cholesterol to the hsiRNA. We used a fully chemically modified hsiRNA variant containing 5′-*(E)*-

vinylphosphonate for these studies. Incorporation of moderately (2′-deoxy-DNA) or highly (2′-hydroxyl-RNA) endonuclease-sensitive bases between the sense strand and the linker was used to modulate rate of cholesterol cleavage (**Figure** 3**.17A**). Destabilization of the linker chemistry greatly impaired of hsiRNA silencing activity when delivered *via* exosomes. *Huntingtin* mRNA silencing was completely abolished ($p < 0.0001$) upon incorporation of two 2′-hydroxyl RNA residues (highly endonuclease sensitive) and significantly reduced ($p = 0.024$) upon incorporation of 2′-deoxy DNA residues (moderately endonuclease sensitive) (**Figure 3.17B** middle panel). On the contrary, chemical stability of the linker had no effect on hsiRNA silencing activity when delivered carrier-free (**Figure 3.17B** right panel) or in neutral liposomes (**Figure 3.17B** left panel). Thus, use of a stable linker is essential for productive loading of exosomes with the RNA cargo.

3.2.5 Discussion

Exosomes are promising delivery vesicles for therapeutic RNAs. Cholesterol conjugation to siRNAs is a simple, scalable and widely used method to load exosomes with RNA cargo that has proven useful in both *in vitro* [153-154] and *in vivo* [135] experiments. However, there is a lack of knowledge on the importance of typical siRNA chemical modifications[75, 77-78, 213-214] on exosome-mediated delivery.

Data presented here the presence of nucleases in exosome preparations bear consideration during the rational design of RNA cargo. This study found that previously used partial modification of siRNA [135, 153-154] is suboptimal for exosome-mediated siRNA delivery. Instead, siRNAs with a combination of 5′-*(E)*-vinylphosphonate [201, 229-230] and alternating 2′-fluoro and 2′-*O*-methyl modifications [77, 202, 214, 218, 244, 258] performed best at exosome-mediated delivery and *Huntingtin* mRNA silencing in neurons. Furthermore, incorporation of nuclease-sensitive bases

into the cholesterol-linker impaired exosome-mediated delivery of hsiRNAs. The benefit of chemical modifications may stem from the localization of hsiRNAs *(i.e.* on the surface of exosomes [135]), altered cellular internalization pathway [135], as well exosomal protein content including a variety of nucleases (Table 3.1) [268] and nuclease activity [269].

Here we showed that the cholesterol conjugation strategy to siRNA plays an important role in exosome-mediated delivery and therefore should be included in optimized RNA cargo design. Between two commercially available strategies to conjugate cholesterol to the 3′ end of the siRNA sense strand, TEG proved to be favorable compared to C7 for productive exosomal loading of cholesterol-siRNA. Both length and hydrophilic character of TEG linker might favor the lipid bilayer geometry and promote more efficient hsiRNA loading.

Our data suggests that hsiRNA loading into exosomes saturates at ~3,000 hsiRNAs molecules per exosome. In addition, overloading (more than 5,000 hsiRNAs per exosomes) may induce aggregation and adversely affect productive gene silencing. Therefore, we suggest ~ 3,000 hsiRNA per exosome as optimal loading capacity. This number might be altered by the nature of the hydrophobic conjugate of hsiRNA (*i.e.* other than cholesterol) and exosomal membrane composition, which varies greatly depending on the source cell [256, 270]. Thus, the maximal hsiRNA copy number per exosome will need to be defined for each hydrophobic conjugate of siRNA and exosomal cell source separately.

The data presented here provide a detailed framework for the successful use of hydrophobic modification as a strategy for productive loading of RNA cargo into exosomes. A similar chemical optimization strategy is likely needed when taking advantage of exosomes to deliver other oligonucleotide species, including CRISPR guide RNAs, artificial miRNAs, small mRNAs, RNA tethers, aptamers or antisense oligonucleotides.

3.3 Hydrophobicity of lipid-conjugated siRNAs predicts productive loading into exosomes.

3.3.1 Preface

Text and figures are reproduced from an accepted manuscript

- A Biscans*, **RA Haraszti***, D Echeverria, R Miller, MC Didiot, M Nikan, L Roux, N Aronin, A Khvorova. Hydrophobicity of lipid-conjugated siRNAs predicts productive loading into small extracellular vesicles. **Molecular Therapy**, Accepted

Annabelle Biscans and I conceptualized this project. Annabelle Biscans designed conjugates, Mehran Nikan developed DHA-conjugated compounds and Loic Roux developed 5′-*E*-vinylphosphonate. Annabelle Biscans and Dimas Echeverria synthesized and duplexed all siRNAs. Annabelle Biscans performed reverse phase chromatography. Marie Didiot intellectually contributed to lipid-conjugate mediated loading of siRNAs to exosomes. I was assisted by Rachael Miller in EV preparations. I prepared primary neurons, loaded all EVs, measured mRNA silencing and siRNA accumulation in neurons, performed Nanoparticle Tracking Analysis and Western blotting, measured zeta potential. Annabelle Biscans, Anastasia Khvorova and I wrote this manuscript. Annabelle Biscans produced Figures 3.19-3.20 with corresponding legends.

3.3.2 Abstract

Exosomes show promise as natural nano-devices for delivery of therapeutic RNA, but efficient loading of therapeutic RNA remains a challenge. We have recently shown that the attachment of cholesterol to siRNAs enables efficient and productive loading into exosomes. Here we systematically explore the ability of lipid conjugates—fatty acids, sterols, and vitamins—to

load siRNAs into exosomes and support gene silencing in primary neurons. Hydrophobicity of the conjugated siRNAs defined loading efficiency and the silencing activity of siRNA-exosomes complexes. Vitamin E-conjugated siRNA supported the best loading into exosomes and productive RNA delivery to neurons.

3.3.3 Introduction

Small extracellular vesicles (exosomes) are produced by most cell types and present in most body fluids (e.g., blood, saliva, urine, cerebrospinal fluid, and milk).[271-273] They possess the ability to transport RNA, including mRNA and microRNA, over short and long intercellular distances, and thus empower sequence-specific, phenotype-modulating RNA types, to act as a messenger.[274-277] The intercellular RNA trafficking mechanism *via* exosomes would make a powerful tool to fight disease when used to deliver therapeutic RNA.

Delivery of small interfering RNAs (siRNAs) to target cells remains an important challenge to their development as therapeutics.[278-279] Nanoparticle carriers have been explored as siRNA delivery vehicles.[280-281] Despite some clinical success, the characteristic toxicity, immunogenicity, and poor trafficking of nanoparticles has hampered further development as therapeutic RNA delivery vehicles.[282-283] By contrast, the natural RNA trafficking properties, low toxicity and immunogenicity, high stability in circulation, and target-cell specificity[137] of exosomes offer a promising alternative for efficient and selective delivery of siRNA to target cells.[153, 284-287]

Loading RNA into exosomes remains a bottleneck for clinical application of exosomes as delivery vesicles for therapeutic RNA. The two most common loading strategies have been direct electroporation into the vesicles[287-289] and transfection into EV source cells.[290-291] However,

electroporation may induce vesicle damage and siRNA aggregation,[292] transfection may disrupt EV integrity,[287] and both methods lack robust batch-to-batch reproducibility and scalability. Recent studies have shown that the covalent conjugation of siRNA to a hydrophobic cholesterol moiety can drive efficient and controllable loading of siRNAs to exosomes, yielding thousands of copies of RNAs per vesicle.[153-154, 286] Conjugation of other hydrophobic moieties (e.g. α-tocopherol or docosahexaenoic acid) to siRNAs have been performed and tested for *in vivo* delivery to liver and brain.[197-198, 293-294] However, hydrophobic moieties other than cholesterol have never been used in EV-mediated delivery of siRNAs.

We have synthesized a panel of lipid-conjugated hydrophobically modified siRNAs (hsiRNAs) to be loaded into exosomes to evaluate how the lipids affect the hsiRNA exosome loading efficiency. We found that hydrophobicity drives loading of lipid-conjugated hsiRNAs into exosomes. Moreover, the ability of exosome-loaded hsiRNAs to silence *Huntingtin* mRNA in primary murine cortical neurons correlates with the amount of lipid-conjugated hsiRNAs loaded into exosomes.

3.3.4 Results

Generation of a library of diverse lipid-conjugated hsiRNAs

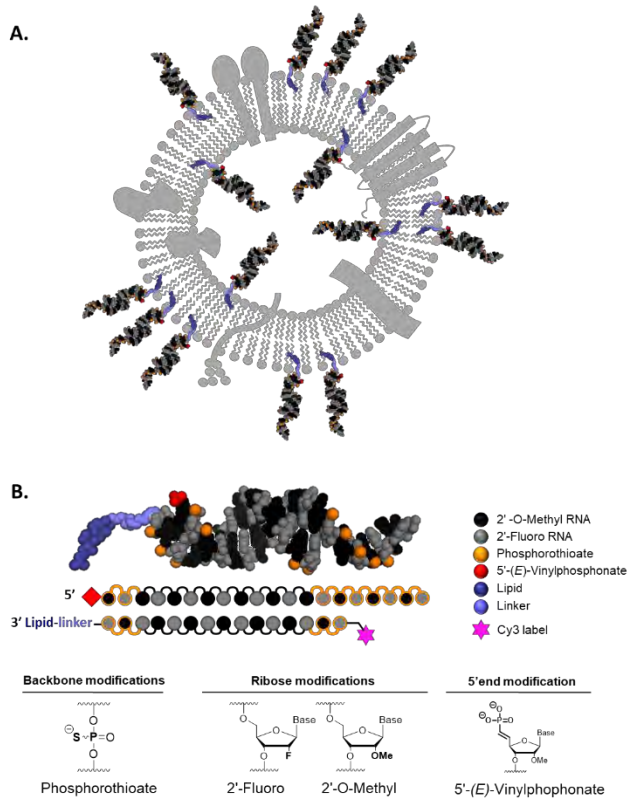

Figure 3.18 Cholesterol-conjugated hsiRNAs load into small extracellular vesicles exosomes. (**A.**) Representation of exosome membrane loaded with cholesterol-conjugated hsiRNAs. Cholesterol is the driving force for efficient loading of siRNA into exosomes. (**B.**) Schematic of hydrophobically modified siRNAs (hsiRNAs).

We have recently shown that cholesterol-conjugated chemically stabilized siRNAs efficiently associate with exosomes.[286] We hypothesized that the hydrophobicity of cholesterol is the driving force behind loading of cholesterol-conjugated siRNAs into membranes (**Figure 3.18A**). To define the structure-function relationship between lipid conjugate and its ability to drive siRNA loading capacity into exosomes, we synthesized a library of lipid-conjugated siRNAs with a broad range of hydrophobicity. In each case, we used the same fully chemically stabilized asymmetric siRNA scaffold (i.e., hydrophobically modified siRNA or hsiRNA).[295] hsiRNAs have a short duplex region (15 base-pairs) and single-stranded fully phosphorothioate-modified tail that assists membrane association.[296-297] All riboses are fully chemically modified using an alternating

2′-*O*-methyl and 2′-fluoro modification pattern, which confers stability and minimizes innate immune activation.[263-265] Moreover, the antisense strand is modified with a 5′-(E)-vinylphosphonate (E-VP) group that mimics the 5′-phosphate of the antisense strand to promote recognition by RISC[298-299] and provides stability against phosphatases and exonucleases.[199, 300-301] Full chemical stabilization of hsiRNAs improves EV-mediated delivery of hsiRNAs (Haraszti *et al.*, 2018, Manuscript in Review, Section 3.2). Compounds were labeled with Cy3 at the 5′-end of the sense strand, which allows visualization and quantification of hsiRNAs loaded into exosomes. The lipid conjugates were attached at the 3′-end of the sense strand (**Figure 3.18B**).

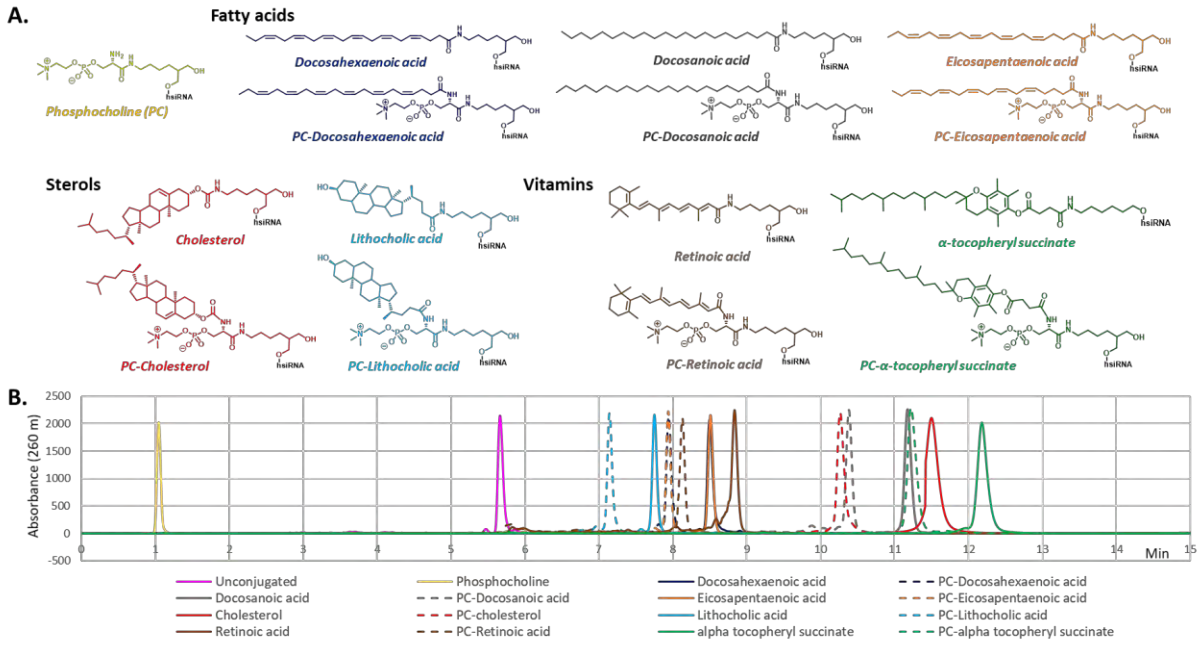

Figure 3.19 The chemical compositions of lipid conjugates significantly affect hsiRNA hydrophobicity. (**A.**) Library of lipophilic moieties attached to hsiRNAs^{Htt}. (**B.**) HPLC retention time of lipid-conjugated Cy3-hsiRNA^{Htt} sense strands. (C18, Buffer A = 0.1 M Triethylammonium acetate in water, Buffer B = Acetonitrile, Gradient = 0-100 % in B in 15 min, Temperature = 60C, Flow = 1 mL/min).

A wide range of natural lipids such as fatty acids, sterols and vitamins were conjugated to the sense strand of hsiRNA^{Htt}, which targets the Huntington's disease gene.[302] In nature, many lipids are esterified (mostly phosphatidyl choline esters), which contributes to the specificity of cellular membrane interactions.[303] To explore how esterification of the lipid conjugate affects hsiRNAs loading into exosomes, all lipid-conjugated hsiRNAs were synthesized with or without a phosphocholine (PC) head group. Because an ester bond is labile and incompatible with solid-phase oligonucleotide synthesis, we have recently developed a synthetic approach that allows a phosphocholine group to be attached to lipid moieties using an amide bond.[197] The chemical compositions of synthesized lipid-conjugated hsiRNAs are depicted in **Figure 3.19A**. All lipid-conjugated hsiRNAs (with the exception of α-tocopheryl succinate hsiRNAs and PC-α-tocopheryl succinate hsiRNAs) were synthesized by using a functionalized solid support (**Figure 3.20A-B**).[197-198] For phosphocholine modified variants, the Fmoc (Fluorenylmethyloxycarbonyl) protected PC group (**Figure 3.20B compound 7**) was first attached to the C7 amino functionalized solid support *via* a peptide bond followed by conjugation of respective lipids (**Figure 3.20B solid supports 9**).[197-198] Both α-tocopheryl succinate variants were synthesized using a post-synthetic conjugation between an amino group present at the 3′-end of the sense strand and the NHS (N-hydroxysuccinimide)-α-tocopheryl-succinate compound (**Figure 3.20C**). For the synthesis of α-tocopheryl succinate sense strands, a commercial C6 amino solid support was used to synthesize the strands. For PC-α-tocopheryl succinate sense strands, the PC amino solid support **8** (**Figure 3.20B**) was used to synthesize the strands.

The relative hydrophobicity of a molecule can be determined by its retention time in reverse-phase high-performance liquid chromatography (HPLC). Hydrophobicity increases with

retention time.[304] **Figure 3.19B** shows HPLC traces for synthesized sense strands, with retention times varying between 1 and 13 minutes, indicating a broad range of hydrophobicity.[305] The structure of the conjugate principally contributed to hsiRNA retention time and hydrophobicity. Compounds with a saturated carbon chain (cholesterol, docosanoic acid and α-tocopheryl succinate) were more hydrophobic than those with an unsaturated carbon chain (docosahexaenoic acid and eicosapentaenoic acid) or cyclic structure (lithocholic acid and retinoic acid). The incorporation of a polar head (phosphocholine group) decreased the hydrophobicity of all lipid-conjugated hsiRNAs. This synthetic library of 15 different lipid-conjugated hsiRNAs, covering a broad range of lipid structures and hydrophobicity allowed us to examine how lipid structure affects efficiency of hsiRNA loading into exosomes.

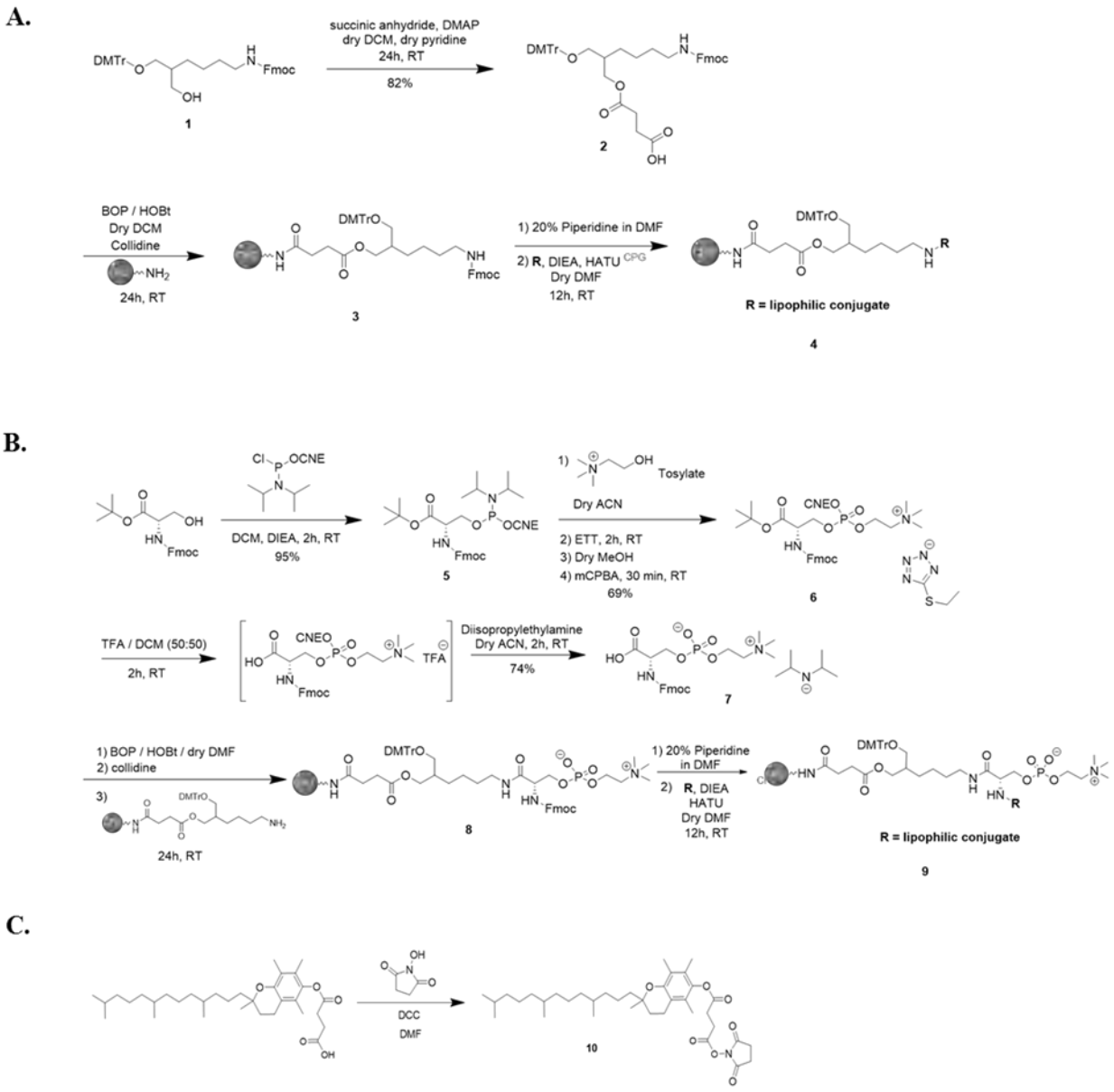

Figure 3.20 Synthetic route of lipophilic compounds used for the synthesis of lipid conjugated siRNAs. (**A**) Synthesis of solid supports conjugated with various lipophilic moieties **(B**) Synthesis of solid supports conjugated with various phosphocholine lipophilic moieties attached though a C7 linker. (**C**) Synthesis of NHS-α-tocopheryl succinate compound for post-synthetic conjugation. (**A**) C7 linker (90% purity) **1** (13.00 g, 19.35 mmol, 1.0 equiv.), 4-dimethylaminopyridine (DMAP) (cat.) and succinic anhydride (2.68 g, 27.09 mmol, 1.4 equiv.) were dissolved in 120 mL of dry

dichloromethane (DCM) and 34 mL of dry pyridine. The mixture was stirred 24h at room temperature and then washed with 300 mL of 10% citric acid. The organic layer was then washed with water and brine and dried over magnesium sulfate. The solvent was evaporated under pressure. A column chromatography on silica gel was performed using a gradient of methanol in a mixture of DCM:pyridine 99:1 from 0 to 10% to obtain **2** (12.24 g, 15.87 mmol, 82%).

Compound **2** (5.72 g, 7.35 mmol, 2.2 equiv.), (Benzotriazol-1-yloxy) tris (dimethylamino) phosphonium hexafluorophosphate (BOP) (4.43 g, 10.02 mmol, 3.0 equiv.) and 1-Hydroxybenzotriazole (HOBt) (1.53 g, 10.02 mmol, 3.0 equiv.) were dissolved in 100 mL of dry DCM. The mixture was stirred few minutes and 2,4,6-collidine (2.61 mL, 20.04 mmol, 6.0 equiv.) was added. The amino controlled pore glass (CPG) (22.00 g, 3.34 mmol, 152 µmol/g) was added after treated with 250 mL of 3% TFA in DCM at room temperature for 4h, filtrated and washed first with TEA:diisopropylethylamine 9:1 (250 mL) and then with DCM and ether. The mixture was stirred mechanically 24h at room temperature. The CPG was washed with DCM, acetonitrile (ACN) and ether and dried under pressure. The CPG was then capped with 16% N-methylimidazole in tetrahydrofuran (THF) (CAP A) and acetic anhydride:pyridine:THF (1:2:2, v/v/v) (CAP B) (1:1, v/v) for 1h and was washed with DCM, ACN and ether and dried under vacuum. **3** is obtained with a loading of 75 µmol/g.

The CPG **3** (1.00 equiv.) was treated with a solution of 20% piperidine in dry dimethylformamide (DMF) (150 mL) two times 15 minutes, washed with DCM, ACN and ether and dried under pressure.

The selected lipid R (6.00 equiv.) was dissolved in 150 mL of dry DMF. 1-[Bis(dimethylamino)methylene]-1H-1,2,3-triazolo[4,5-b]pyridinium 3-oxid hexafluorophosphate (HATU) (2.00 equiv.) and diisopropylethylamine (DIEA) (8.00 equiv.) were added and the

solution was added to the deprotected CPG. The mixture was stirred overnight under mechanical stirring at room temperature. The CPG was washed with DCM, ACN and ether and dried under pressure. The CPG was then capped with 16% N-methylimidazole in THF (CAP A) and acetic anhydride:pyridine:THF (1:2:2, v/v/v) (CAP B) (1:1, v/v) for 1h and was washed with DCM, ACN and ether and dried under vacuum. The lipid functionalized solid supports **4** were obtained with a loading of 55 µmol/g.

(**B**) Fmoc-L-serine-tBu (2.00 g, 5.21 mmol, 1.0 equiv.) was first dried by co-evaporation with toluene. Dry DCM (15 mL) and diisopropylethylamine (DIPEA) (1.54 mL, 8.86 mmol, 1.7 equiv.) were added under argon and 2′-cyanoethyl-N,N-diisopropylchlorophosphoramidite (1.60 g, 6.78 mmol, 1.3 equiv.) was added slowly via a syringe. The reaction mixture was stirred 2h at room temperature. After reaching completion, the reaction mixture was quenched with methanol and was washed with a solution of sodium bicarbonate and brine. The aqueous phase was extracted with DCM. The organic phase was dried on magnesium sulfate, filtrated and evaporated under vacuum. The crude mixture was then purified by column chromatography on silica gel using ethyl acetate/Hexane (8/2) with 1% pyridine as eluent, to afford **5** as a white solid (2.90 g, 4.97 mmol, 95%).

Compound **5** (2.90 g, 5.39 mmol, 1.0 equiv.) was dried with dry toluene and dry ACN. Choline p-toluenesulfonate (1.63 g, 5.93 mmol, 1.1 equiv.) was dried with toluene and dissolved in dry ACN (46 mL). This mixture was added to compound **5** through a cannula. **5**-(Ethylthio)-1H-tetrazole **(**ETT) (0.25 M in ACN) (21.6 mL, 5.39 mmol, 1.0 equiv.) was added slowly with a syringe. The mixture was stirred 2h at room temperature. After reaching completion, the reaction mixture was quenched with methanol. Meta-chloroperoxybenzoic acid (mCPBA) (1.86 g, 10.78 mmol, 2.0 equiv.) was added by portion to the mixture. After 30 min of stirring, the mixture was reduced

under vacuum. The crude was then purified by column chromatography on silica gel using a gradient of Methanol in DCM (0-30%) as eluent, to obtain **6** as a mixture of tetrazolium (major counter anion) and tosylate (less than 5%) salts (2.70 g, 3.69 mmol, yield 69%).

Compound **6** (2.30 g, 3.15 mmol, 1.0 equiv.) was dissolved in 60 mL of (1:1) solution of trifluoroacetic acid (TFA):dry DCM. Triisopropylsilane (2.39 mL, 11.66 mmol, 3.7 equiv.) was added and the mixture was stirred at room temperature for 2h. The solvent and TFA were evaporated and the residue was purified by reverse phase HPLC (C_{18}, Buffer A = Water, Buffer B = ACN, Gradient = 5-65% of B in 12 min, T = 45°C). The ACN was removed under vacuum and the aqueous solution was freeze-dried. The lyophilized powder was dissolved in 10% diisopropylamine (14 mL) in ACN (140 mL) and the mixture was stirred at room temperature for 2h. The solvent was evaporated under vacuum and the crude was purified by reverse phase HPLC (C_{18}, Buffer A = Water, Buffer B = ACN, Gradient = 5-65% of B in 12 min, T = 45°C). The ACN was removed under vacuum and the aqueous solution was freeze-dried to afford **7** as diisopropylammonium salt (1.38 g, 2.32 mmol, yield 74% over two steps).

Compound **7** (1.00 g, 1.69 mmol, 4.75 equiv.) was dissolved in dry DMF (100 mL). (Benzotriazol-1-yloxy)tris(dimethylamino)phosphonium hexafluorophosphate (BOP) (0.59 g, 1.34 mmol, 3.76 equiv.) and hydroxybenzotriazol (HOBt) (0.21 g, 1.34 mmol, 3.76 equiv.) were added and stirred until the solution went clear. 2,4,6-collidine (560 µL, 4.32 mmol, 12.42 equiv.) was added followed by **3** deprotected with 20% piperidine in DMF (6.55 g, loading of 55 µmol/g, 360 µmol, 1.00 equiv.) and the suspension was mixed overnight on a rotary mixer. The CPG was filtered off and washed with DCM, ACN and ether and dried under vacuum. The CPG was capped with 16% N-methylimidazole in THF (CAP A) and acetic anhydride:pyridine:THF (1:2:2, v/v/v) (CAP B) (1:1, v/v) for 1h and was washed with DCM, ACN and ether and dried under vacuum.

CPG **8** (6.00 g, 330 µmol, 1.0 equiv.) was first treated with 20% piperidine in dry DMF for 15 minutes. This procedure was repeated twice to ensure complete deprotection of the Fmoc group. The amine-bearing CPG was filtered off and washed successively with DCM, ACN and ether and dried under vacuum. Then the CPG was mixed with a mixture of the selected lipid R (6.0 equiv.), HATU (2.0 equiv.) and DIEA (8.0 equiv.) in dry DMF. The suspension was mixed on a rotary mixer for 24h. The CPG was then filtered off and washed with DCM, ACN and ether and dried under vacuum. The CPG was capped with 16% N-methylimidazole in THF (CAP A) and acetic anhydride:pyridine:THF (1:2:2, v/v/v) (CAP B) (1:1, v/v) during 15 min and was washed with DCM, ACN and ether and dried under vacuum. The PC lipid functionalized solid supports **9** were obtained with a loading of 55 µmol/g.

(**C**) α-tocopheryl succinate (0.5 g, 0.94 mmol, 1.0 equiv.), N-hydroxysuccinimide (0.21 g, 1.88 mmol, 2.0 equiv.) and dicyclohexylcarbodiimide (DCC) (0.39 g, 1.88 mmo, 2.0 equiv.) were dissolved in 25 mL of anhydrous DMF. The mixture was stirred overnight at room temperature. The dicyclohexyl urea was filtrated and the filtrate was evaporated under pressure. The product **10** was isolated by precipitation with methanol (0.47 g, 0.75 mmol, 80%).

Loading efficiency of conjugated-hsiRNAs into exosomes correlates with hsiRNA hydrophobicity

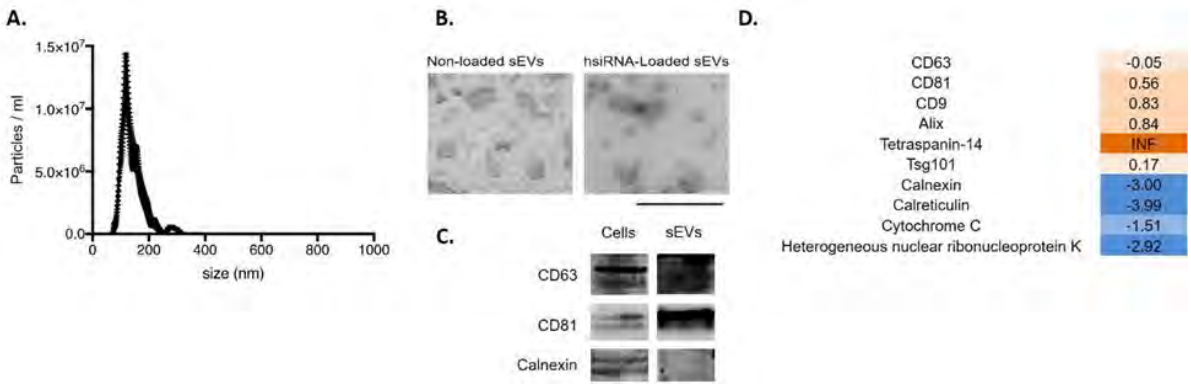

Figure 3.21 Characterization of umbilical cord, Wharton's jelly derived exosomes.

Umbilical cord, Wharton's jelly derived mesenchymal stem cells were expanded to passage 9 at 3600 cm^2, medium changed to serum-free RPMI for 24 hours, and exosomes purified from conditioned media via differential ultracentrifugation. (A**)** Nanoparticle Tracking Analysis of 100,000 g fraction from differential ultracentrifugation protocol (e.g. small EVs). N=11, mean ± SEM (B) Transmission Electron Microscopy image of unloaded and loaded exosomes, size bar shows 500 nm. (C) Western blot of positive and negative exosome marker proteins. (D) Protein enrichment (logarithmic) in exosomes *versus* cells as detected by LC-MS/MS. INF=infinite (detected in exosome fraction but not detected in cells)

Exosomes were isolated by differential ultracentrifugation from Wharton's jelly-derived (umbilical cord) mesenchymal stem cells.[204] They displayed uniform size distribution (mean, 140 nm; **Figure 3.21A**). Small EVs appeared as lipid bilayer surrounded vesicles on transmission electron microscopy (**Figure 23B**). Western-blot (**Figure 3.21C**) and LC-MS/MS (**Figure 3.21D**) showed enrichment in positive EV marker proteins (CD63, CD81, CD9, Alix, Tetraspanin-14 and Tsg101) and depletion in negative EV marker proteins (Calnexin, Calreticulin, Cytochrome C and

HNRPK). Thus, small EVs used in this study are *bona fide* extracellular vesicles according to the guidelines established by International Society of Extracellular Vesicles.[306]

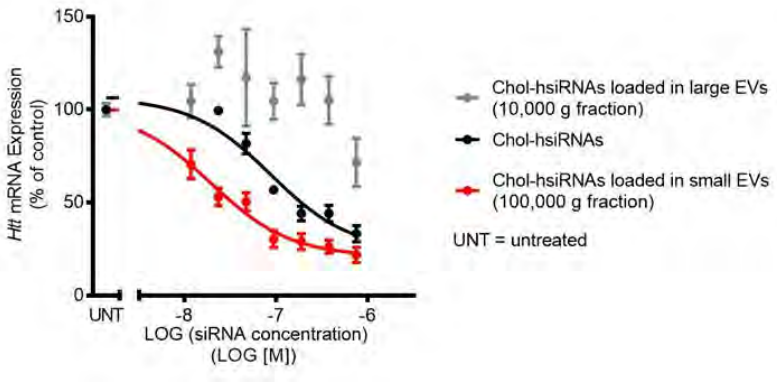

Figure 3.22 Silencing activities of cholesterol conjugated hsiRNA-loaded exosomes using 10,000 and 100,000 g pellet fractions and cholesterol conjugated hsiRNA.

Htt mRNA levels in primary mouse neurons incubated with increasing concentrations of cholesterol conjugated hsiRNA^{Htt}-loaded small EVs (100,000 g fraction), large EVs (10,000 g fraction) or cholesterol conjugated hsiRNA^{Htt} for one week. *Htt* mRNA levels were normalized to Hprt (Hypoxanthine-guanine phosphoribosyl transferase), and presented as percent of untreated control (n=3, mean ± SEM). UNT, untreated

Cholesterol-conjugated hsiRNAs were more efficient at inducing *Huntingtin* mRNA silencing in neurons when they were delivered *via* small EVs (e.g. 100,000 g fraction of differential ultracentrifugation protocol) compared to cholesterol-hsiRNA alone (**Figure 3.22**). Cholesterol-hsiRNAs did not silence target mRNA when delivered *via* large EVs (e.g. 10,000 g fraction) (**Figure 3.22**). Therefore, we used small EVs (e.g. 100,000 g fraction) to test delivery of all conjugated hsiRNA to neurons. exosomes were co-incubated with increasing concentrations of Cy3-hsiRNA^{Htt} conjugated to the above described lipids (1:2000, 1:6000, 1:12000, and 1:25000 exosome-to-hsiRNA ratios). Ultracentrifugation of Cy3-hsiRNA-exosome mixture resulted in a fluorescent pink pellet, revealing the association of labeled hsiRNA with exosomes (**Figure 3.23**).

Ultracentrifugation of hsiRNAs^{Htt} without exosome did not generate a pellet, indicating the absence of hsiRNA aggregation (**Figure 3.24A**). The integrity of the exosome membrane after hsiRNA loading was confirmed by using transmission electron microscopy (**Figure 3.22B**).

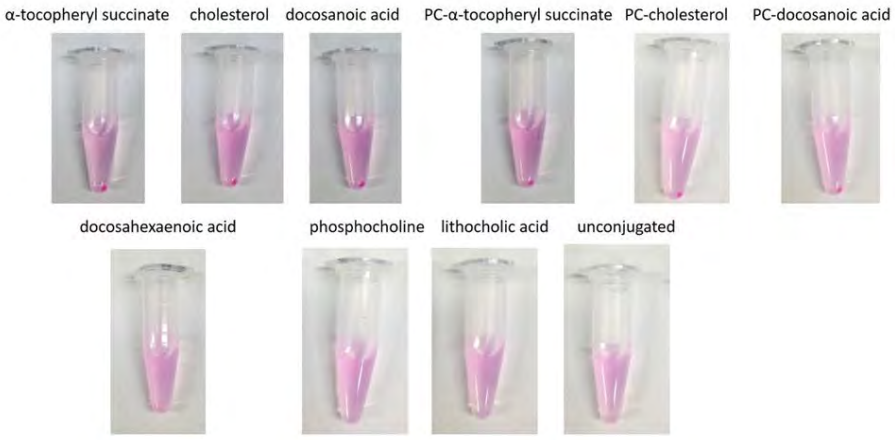

Figure 3.23 Pictures of exosomes loaded with lipid-conjugated hsiRNAs after ultracentrifugation.

The efficiency of Cy3-hsiRNA loading into exosomes was quantified by spectrophotometry (**Figure 3.24B**). Increasing hsiRNA-to-exosome ratios yielded higher loading efficiencies with saturation kinetics: at a 1:25000 exosome-to-hsiRNA ratio, loading was nearly saturated for each lipid-conjugated hsiRNA. The loading efficiency depended on the structure of the lipid conjugate attached to the hsiRNA. A strong exponential correlation was observed between the hydrophobicity of the lipid-conjugated hsiRNA and the exosome loading efficiency (**Figure 3.24C**). Thus, hydrophobicity of an hsiRNA directly predicts the number of molecules that can that can be loaded into exosomes. Efficient loading (at least 1700 hsiRNAs per vesicle for a 1:25000 ratio) required the presence of a highly hydrophobic conjugate (Cholesterol, PC-cholesterol, Docosanoic acid, PC-docosanoic acid, α-tocopheryl succinate and PC-α-tocopheryl

succinate) attached to the hsiRNA. Unsaturated fatty acid chains (docosahexaenoic acid and eicosapentaenoic acid) conferred less hydrophobicity and therefore less vesicle loading efficiency to hsiRNAs. Conjugation of α-tocopheryl succinate (vitamin E) to hsiRNA yielded the best exosome loading efficiency, outperforming cholesterol. Docosanoic acid was as effective as cholesterol at loading hsiRNAs into exosomes. Despite being structurally similar to cholesterol, the reverse sterol conjugate formed by lithocholic acid is not as efficient as the cholesterol conjugate, indicating that the saturated carbon tail of cholesterol is important for exosome loading. These data suggest the model that anchoring of hsiRNA to the surface of EV is mediated by the insertion of the saturated carbon chain into the vesicular membrane.

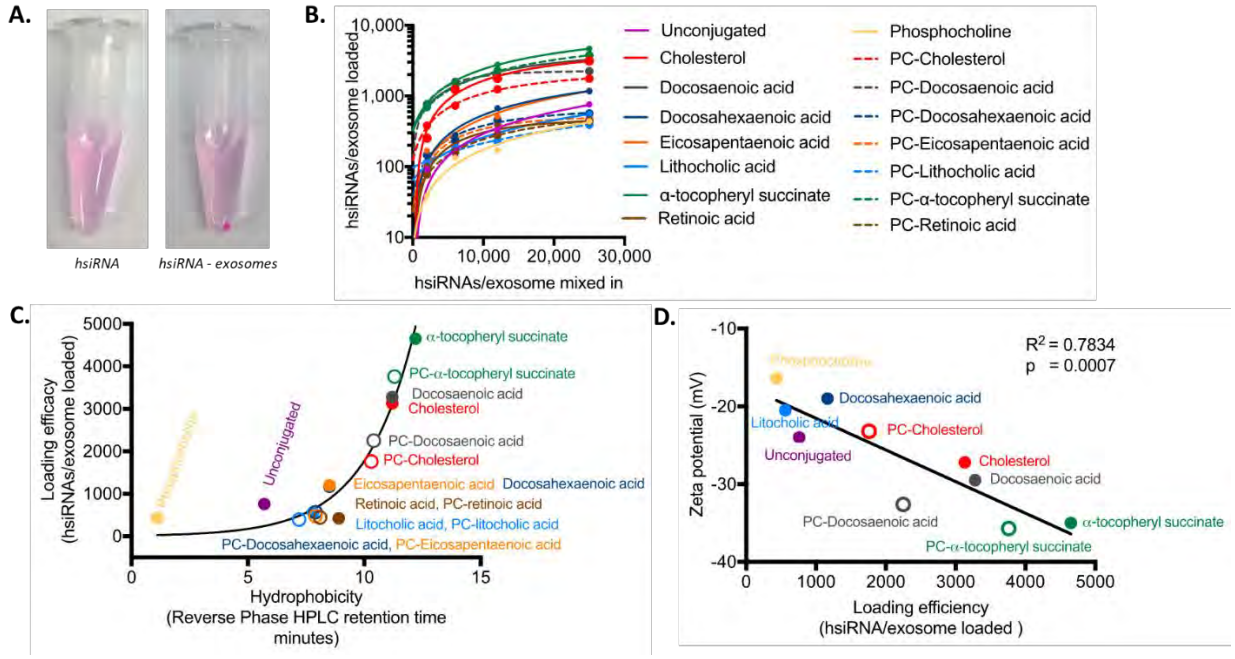

Figure 3.24 The number of hsiRNAs loaded into exosomes depends on the hydrophobicity of the conjugate.

(**A.**) Ultracentrifugation of conjugated Cy3-hsiRNAs incubated without exosome (left) showing absence of pellet and after co-incubation of Cy3-hsiRNAs and exosomes (right) showing formation of pellet. Representative pictures are shown. (**B.**) Cy3-hsiRNA accumulation in pellet

following co-incubation of hsiRNAs and exosomes with varying hsiRNA:exosome ratio (n=3, mean ± SEM for the last point). (**C.**) Exponential relationship between loading efficiency and hydrophobicity of conjugated hsiRNA (n=3, mean ± SEM). (**D.**) Linear correlation between the surface charge of hsiRNA-loaded exosomes and hsiRNA loading efficiency (n=2, mean ± SEM).

Consistent with our previous studies,[286] the loading of lipid-conjugated hsiRNAs reduced the zeta potential of exosomes (**Figure 3.24D**), indicating the presence of negatively charged hsiRNAs on the surfaces of vesicles. We observed a linear correlation between zeta potential and hsiRNA loading efficiency: the lower the surface charge the higher the loading efficiency. α-tocopheryl succinate (vitamin E) conjugated hsiRNA-loaded exosomes had the highest hsiRNA-to-exosome ratio and displayed a zeta potential of –35mV, a significant change relative to unloaded exosomes (–13mV). We have shown previously that the majority of hsiRNAs are bound to the outside of the exosomes.[286] However, since the hsiRNAs are stable against RNases *in vitro* and *in vivo*,[199, 263] the presence of hsiRNAs on the surface of exosomes should not reduce siRNA activity.

Of 15 lipid-conjugated hsiRNA variants evaluated, we identified five additional lipid-conjugated hsiRNAs that associate with exosomes as well as or better than cholesterol-conjugated hsiRNA: PC-cholesterol, Docosanoic acid, PC-docosanoic acid, α-tocopheryl succinate and PC-α-tocopheryl succinate hsiRNAs. The degree of hydrophobicity of the lipid-conjugated hsiRNA seems to defines the efficiency of loading into exosomes. Loading efficiency of lipid-conjugated hsiRNAs correlates with a decrease in exosome surface charge, which indicates of the amount of hsiRNAs bound to the surface of the exosome.

Lipid-conjugated hsiRNA-loaded exosomes induce gene silencing in primary mouse neurons

We next asked whether the change in the charge and perhaps other properties of exosome membranes loaded with hsiRNA affect the trafficking of exosomes to target cells. We incubated primary mouse neurons with increasing concentrations of exosomes loaded with lipid-conjugated hsiRNA^{Htt} for one week and measured *Htt* mRNA levels (**Figure 3.25A**). We assigned lipid-conjugated hsiRNAs to groups based on their hydrophobicity and chose to test only a subset of representative hsiRNAs: (i) low hydrophobicity: phosphocholine, lithocholic acid, and unconjugated hsiRNAs; (ii) medium hydrophobicity: docosahexaenoic acid; and (iii) high hydrophobicity: docosanoic acid, PC-docosanoic acid, cholesterol, PC-cholesterol, α-tocopheryl succinate, and PC-tocopheryl succinate. Only lipid-conjugated hsiRNAs with high hydrophobicity resulted in a visible pink pellet upon loading (**Figure 3.23**). Dose-dependent silencing of *Htt* mRNA was observed for medium and high hydrophobicity lipid-conjugated hsiRNAs loaded into exosomes (**Figure 3.25A**). Non-conjugated hsiRNAs or lipid-conjugated hsiRNAs with low hydrophobicity did not induce silencing when loaded into exosomes. These results are consistent with hsiRNAs levels detected in neurons (**Figure 3.26**). Medium and high hydrophobic enabled the accumulation of 2-6 folds more hsiRNA in neurons than low hydrophobic compounds when delivered *via* exosomes.

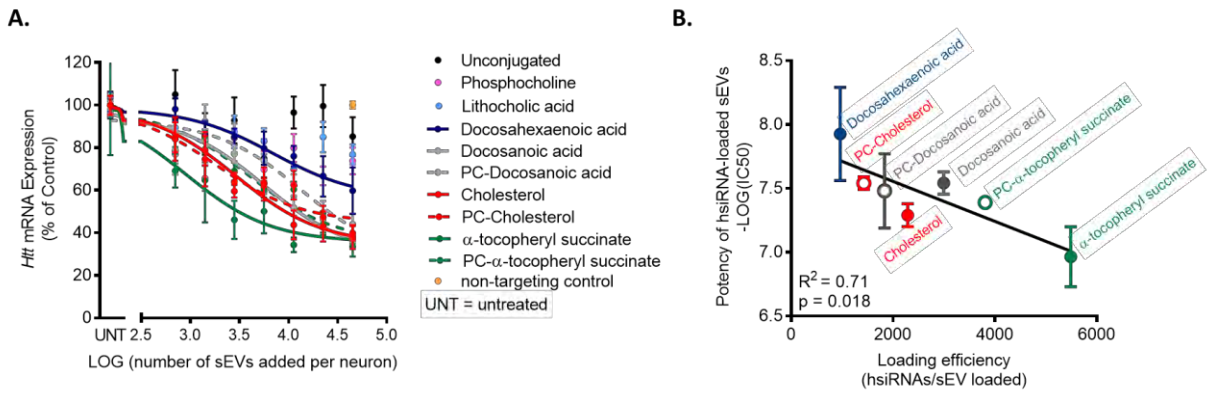

Figure 3.25 Silencing activity of hsiRNA-loaded exosomes correlates with the loading efficiency of hsiRNAs. (**A.**) *Htt* mRNA levels in primary mouse neurons incubated with increasing concentrations of hsiRNA^{Htt}-loaded exosomes (exosome:hsiRNA ratio = 1:25000) for one week. *Htt* mRNA levels were normalized to *Hprt* (Hypoxanthine-guanine phosphoribosyl transferase), and presented as percent of untreated control (n=3, mean ± SEM). UNT, untreated (**B.**) Correlation between IC50 of hsiRNA-loaded exosomes and loading efficiency of hsiRNAs (n=2).

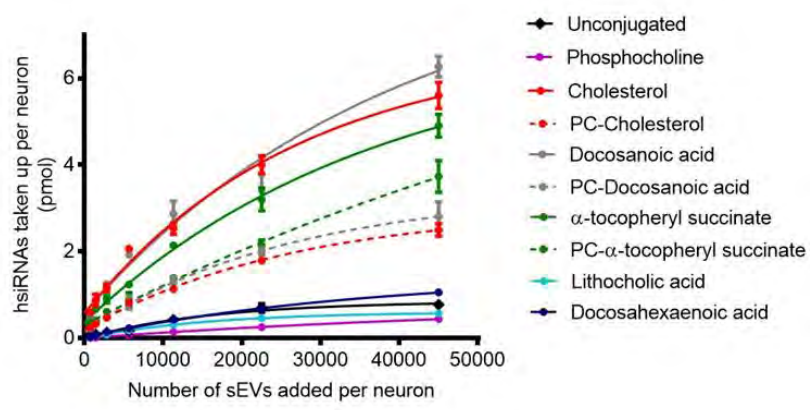

Figure 3.26 Uptake efficiency of hsiRNA loaded exosomes by neurons. hsiRNAs levels in neurons were quantified using PNA hybridization assay after incubation of neurons with increasing amounts of loaded exosomes for one week. (n=3, mean ± SEM).

In general, only hydrophobic conjugates that support loading of more than 1000 hsiRNAs per vesicle enabled productive silencing (**Figure 3.24B**). exosomes loaded with lipid-conjugated hsiRNAs induced sequence-specific silencing, since exosomes loaded with non-targeting control hsiRNAs of similar chemical composition were ineffective (**Figure 3.25A**). We observed a linear correlation between the half-maximal inhibitory concentration (IC50) of hsiRNA-loaded exosomes and the amount of loaded hsiRNAs, which defines the activity of hsiRNA-loaded exosomes (**Figure 3.25B**). Thus, hydrophobic conjugates that efficiently load hsiRNAs into exosomes induce productive silencing of *Htt* mRNA in primary neurons. The direct correlation between efficiency of loading and silencing indicates that, independent of the structure of the conjugate, loaded hsiRNA can induce functional silencing.

3.3.5 Discussion

The simple and scalable loading of cholesterol-conjugated siRNAs provides an attractive strategy for loading RNA cargo into exosomes.[153-154, 286] We used the principle to expand the range of lipid conjugates that can drive efficient loading of therapeutic RNA into exosomes. Notably, docosanoic acid and α-tocopheryl succinate, and their PC-derivatives supported siRNA loading into exosomes as well as or better than cholesterol.

Because loading into exosomes is proportional to hydrophobicity, a range of available lipid conjugates enables dynamic modulation of RNA cargo levels in exosomes for a range of applications. Particle charge may influence pharmacokinetic behavior *in vivo* or interfere with the natural trafficking pathways of exosomes. Titrating the amount of RNA cargo in exosomes will therefore be essential to accurately set the charge and function of the vesicle.

We expect that exosomes purified from various sources will be loaded by lipid-conjugated siRNAs. Indeed, in addition to Wharton's jelly-derived mesenchymal stem cells (umbilical cord) used in this study, we have successfully used cholesterol-conjugated siRNAs to load exosomes from U87 glioblastoma cells,[286] bEND3 endothelial polyoma cells, bone marrow-derived and adipose-derived mesenchymal stem cells. Nevertheless, because hsiRNA loading is driven by lipid-conjugate hydrophobicity, the exact level of loading may depend on the specific membrane composition and therefore cell source[270, 307] of the exosomes. Future work is needed to identify the optimal hsiRNA for a given exosome source.

The structure-activity relationship between lipid conjugates and exosome loading of siRNA creates a framework for the rational design of RNA cargo for exosome delivery. The covalent lipid-conjugation strategy could be used to load exosomes with other types of therapeutic oligonucleotides, including CRISPR guide RNAs or miRNAs. Using lipid-conjugated small RNA tethers, the loading of larger oligonucleotide species might also be possible.

Finally, we observed a correlation between the exosome loading efficiency of hsiRNAs and target gene silencing in neurons. We believe that exosomes loaded with lipid-conjugated siRNA could be used to deliver therapeutic nucleic acids to recipient cells other than neurons. Indeed, exosomes administered by injection efficiently distribute in the brain[182, 185, 286, 308] and other tissues.[134, 136-137, 309] Thus, a simple and scalable method of efficiently loading therapeutic oligonucleotides into exosomes is a significant advance toward the treatment of neurodegenerative disorders,[310] inflammatory diseases,[311-312] and cancer.[136]

CHAPTER IV DEVELOPMENT OF A LARGE SCALE EV ISOLATION STRATEGY

4.1 PREFACE

Text and figures are reproduced from a submitted manuscript

- **Haraszti RA**, R Miller, M Stoppato, YY Sere, A Coles, MC Didiot, R Wollacott, E Sapp, J Leszyk, M Dubuke, S Shaffer, M DiFiglia, Y Wang, N Aronin, A Khvorova. Exosomes produced from three-dimensional cultures of mesenchymal stem cells by tangential flow filtration show higher yield and improved activity.

This project was conceptualized by Neil Aronin, Anastasia Khvorova, Yang Wang and me. I conducted two-dimensional cultures and EV isolation by differential ultracentrifugation with the assistance of Rachael Miller. Matteo Stoppato conducted three-dimensional cell culture and Yves Sere isolated EVs *via* tangential flow filtration with my intellectual guidance. siRNAs were synthesized by Dimas Echeverria and duplexed by me. Ellen Sapp and Marian DiFiglia conducted transmission electron microscopy. Michelle Dubuke, John Leszyk and Scott Shaffer conducted mass-spectrometry for proteomics. Marie Didiot intellectually contributed to establishing loading of cholesterol-siRNAs to EVs. Andrew Coles assisted in primary neuron preparations. I performed Nanoparticle Tracking Analysis, Western blotting, Bredford assays, siRNA loading to EVs, silencing and live uptake in primary neurons and all data analysis. I wrote this manuscript with the assistance of Anastasia Khvorova and Neil Aronin.

4.2 ABSTRACT

Exosomes can deliver therapeutic RNAs to neurons. The composition and the safety profile of exosomes depends on the type of the exosome-producing cell. Mesenchymal stem cells are considered to be an attractive cell type for therapeutic exosome production. However, scalable methods to isolate and manufacture exosomes from mesenchymal stem cells are lacking, a limitation to the clinical translation of exosome technology. We evaluate mesenchymal stem cells

from different sources and find that umbilical cord-derived mesenchymal stem cells produce the highest exosome yield. To optimize exosome production, we cultivate umbilical cord-derived mesenchymal stem cells in scalable microcarrier-based three-dimensional cultures. In combination with tangential flow filtration, three-dimensional mesenchymal stem cell cultures yield fifty-fold more exosomes (TFF-exosomes) than the conventional methodology of differential ultracentrifugation and two-dimensional culture (UC-exosomes). TFF-exosomes are fifteen times more potent in siRNA transfer to neurons compared to UC-exosomes. Microcarrier-based three-dimensional culture and tangential flow filtration allow scalable production of biologically active exosomes from mesenchymal stem cells. These findings lift a major roadblock for the clinical utility of mesenchymal stem cell exosomes.

4.3 INTRODUCTION

Exosomes are nano-sized (40 to 150 nm) extracellular vesicles are surrounded by a lipid bilayer, and are derived from internal cellular compartments[313]. Exosomes are released by most cell types and are considered to be part of the intercellular communication system, carrying RNAs and proteins locally and systemically [132, 138, 180, 182, 314-316]. Information transferred *via* exosomes influences the phenotype of recipient cells [134-136, 155, 309, 317]. Stem cell-derived exosomes are believed to mediate cellular restorative function [134, 318-319] and to modulate the inflammatory state [320-326]. Due to their unique trafficking characteristics, exosomes are being explored as therapeutic RNA delivery vehicles [135-136, 153-155].

The preclinical and clinical development of exosome technology as a delivery platform requires large quantities of exosomes. The isolation method of exosomes is required to be easily expandable to support large-scale manufacturing (*e.g.* scalable)[327-328]. Current methods generate low yields of exosomes and are not scalable, a situation that so far has impeded studies to evaluate preclinical efficacy of exosomes in animals. A dose of 10^9 to 10^{11} exosomes administered per

mouse is typically used to achieve biological outcomes [134-136, 155]. Isolation of this exosome quantity requires the processing of liters of conditioned media to treat one animal. Therefore, exosome production to support a well-powered animal study can take several months. Exosomes are usually purified by size exclusion [329-330] or affinity chromatography [331], or by density gradient [332-333] or differential ultracentrifugation [204]. The gold standard for exosome retrieval, differential centrifugation, requires 4 to 5 sequential centrifugation steps. None of these methods is scalable. Unlike immortal tumor cells lines, the expansion of mesenchymal stem cells is limited in culture. Low yields is exosomes impede the use of mesenchymal stem cells for exosome production,

We combined the strengths of three production strategies to develop a robust and scalable strategy compatible with good manufacturing practices (GMP) for exosome production from mesenchymal stem cells. (1) Microcarrier-based three-dimensional cell culture is commonly used to grow adherent cells in bioreactors[334]. (2) Tangential flow filtration is a method to concentrate proteins or viruses from large amount of cell culture media[335-337]. (3) Xenofree (*i.e.* not containing animal-derived material) medium is typically used to manufacture cell therapies[338]. The physicochemical characteristics of exosomes produced by three-dimensional cultures in xenofree medium and tangential flow filtration were compared to those of exosomes produced by traditional two-dimensional cultures and differential ultracentrifugation. Compared to standard methods, we show that three-dimensional culture, xenofree medium and tangential flow filtration yielded 50-fold more exosomes and that these exosomes were 15-fold more active in their ability to transfer therapeutic siRNAs to primary neurons. Thus, the method reported here advances the yield of mesenchymal stem cell exosomes and enables their preclinical exploration.

4.4 RESULTS

Wharton's jelly-derived mesenchymal stem cells produce the most exosomes

To develop a scalable method for exosome production suitable for manufacturing, we compared exosome yields and doubling times of mesenchymal stem cells derived from common sources: bone marrow, adipose tissue, and umbilical cord Wharton's jelly (i.e., connective tissue of umbilical cord). Umbilical cord mesenchymal stem cells are distinct from cord blood hematopoietic stem cells. In traditional plastic flask-based cultures, umbilical cord mesenchymal stem cells grew faster (~3 day doubling time) than mesenchymal stem cells from bone marrow or adipose tissue (~7 day doubling time). Umbilical cord mesenchymal stem cells yielded four times as many exosomes per cell than did mesenchymal stem cells from bone marrow (p=0.0063) or adipose tissue (p=0.006) (**Figure 4.1A**). Exosomes derived from umbilical cord mesenchymal stem cells were also larger (140±18 nm) than exosomes from bone marrow (116±9 nm, p=0.01) and adipose tissue (105±12 nm, p=0.0004) mesenchymal stem cells (**Figure 4.1B**). Based on their availability, favorable doubling time, and high yield of exosomes per cell, we used umbilical cord mesenchymal stem cells for the development of a scalable exosome isolation method.

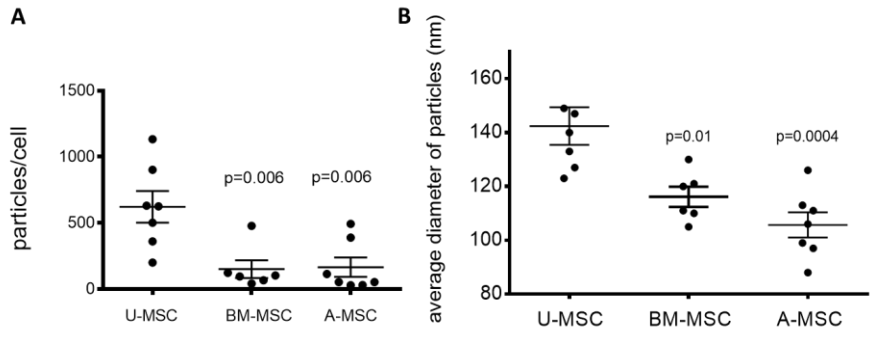

Figure 4.1 Umbilical cord mesenchymal stem cells yield the most exosomes.

(**A**) Yield of exosomes isolated by differential ultracentrifugation from mesenchymal stem cells derived from umbilical cord (U-MSC), bone marrow (BM-MSC), or adipose (A-MSC). Yield calculated as the number of exosomes in the isolated sample measured by Nanoparticle Tracking Analysis divided by the

number of cells in the source cultures. Results of 7 experiments shown, with mean ± SD, one-way ANOVA. (**B**) Average sizes of U-MSC, BM-MSC, or A-MSC exosomes purified in (A).

Three-dimensional culture and tangential flow filtration enhances exosome yield

Large-scale cell culture is a prerequisite for exosome production on a manufacturing scale. Exosomes are standardly concentrated by differential centrifugation of conditioned media from two-dimensional adherent cell cultures in plastic flasks (**Figure 4.2A**). From two-dimensional cultures of adherent umbilical cord mesenchymal stem cells grown in three-layer plastic culture flasks, we typically obtain a density of 20,000 cells/cm^2 at confluence. To increase the expansion of umbilical cord mesenchymal stem cells, we used microcarrier-based three-dimensional culture—a strategy commonly used for large-scale culture of adherent cells[334]. Cells are grown on the surfaces of spherical support matrix beads and distributed in medium by stirring in a spinner flask (**Figure 4.2B**). In this three-dimensional culture system, umbilical cord mesenchymal stem cells reached 40,000 cells/cm^2, double the density obtained in two-dimensional cultures.

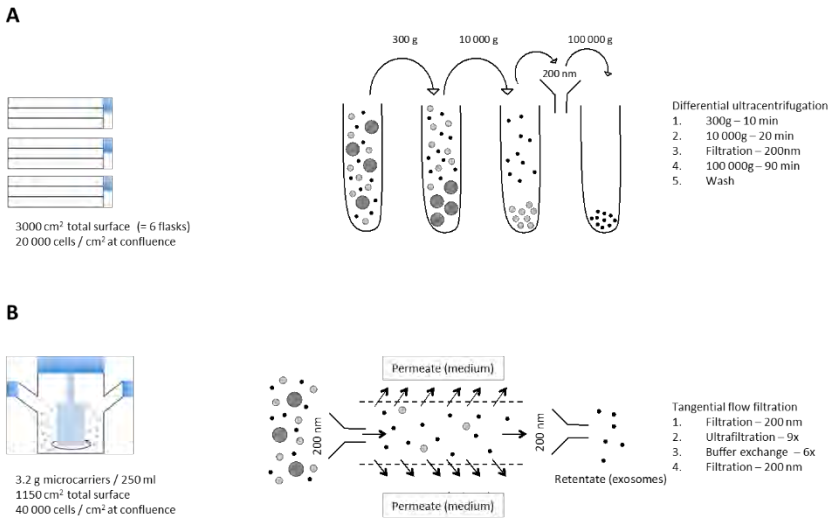

Figure 4.2 Scheme of mesenchymal stem cell culturing methods and exosome isolation methods.

(**A**) Schematic of flask-based (two-dimensional) mesenchymal stem cell culture and isolation of exosomes by differential ultracentrifugation. (left) Cells are cultured in triple-layer flasks in mesenchymal basal medium to a density of 20,000 cells/cm^2. (right) Exosomes are enriched from

culture supernatants by sequential ultracentrifugation, with filtration and wash steps, as indicated. (**B**) Schematic of microcarrier-based (three-dimensional) MSC cultures and isolation of exosomes by tangential flow filtration. (left) Cells are cultured on microcarriers in serum-free/GMP-compatible medium in 250-ml spinner flasks to ~40,000 cells/cm^2. (right) Exosomes are enriched from culture supernatants by tangential flow filtration using a 500-kDa cutoff cartridge, as indicated.

Differential ultracentrifugation of exosomes relies on their vesicle size and sedimentation properties. Sequential centrifugation steps with increasing force of centrifugation deplete the conditioned medium from large particles and/or vesicles with high sedimentation rates. A final ultracentrifugation step sediments small vesicles or exosomes, leaving the smaller proteins in the supernatant[204]. We adapted this method to include 300 × g, 10,000 × g and 100,000 × g centrifugation steps (**Figure 4.2A**), a filtration step through a 200-nm pore size membrane, and a wash step[135].

Tangential flow filtration is a concentration and buffer exchange strategy used during large-scale manufacturing of biologics [335-336] and viruses [337]. In this method, a pump circulates the conditioned culture medium through membranes or filters with pores that are sized for a specific application. Particles that are smaller than the pore size pass through and are removed from the system (*e.g.* permeate). Larger particles than the pore size are withheld in the lumen of the fibers (*e.g.* retentate) and circulated back into the product. Multiple rounds of the ultrafiltration step lead to efficient particle concentration. In particular, we first passed the conditioned cell culture supernatant through a 200-nm pore size membrane to remove large vesicles and particles (**Figure 4.2B**). The filtered conditioned medium was subjected to tangential flow filtration using a hollow fiber filter with a 500-kDa molecular weight cutoff (MWCO) and concentrated 9-fold (volume reduced 9-fold). In the next step the cell culture medium was exchanged with phosphate-buffered saline (PBS), by continuously feeding the system with PBS to replace the loss of permeate. The

final product was sterile filtered using 200 nm filter, resulting in a filtrate that contains exosomes in PBS (**Figure 4.2B**).

We compared exosomes produced in microcarrier-based three-dimensional cultures in xenofree medium and isolated by tangential flow filtration (TFF-exosomes) and exosomes produced in conventional two-dimensional culture and isolated by differential ultracentrifugation (UC-exosomes). TFF-exosomes and UC-exosomes were similar in size (100 to 200 nm), with the same mean size, though TFF-exosomes were more heterogenous in size than UC-exosomes (**Figure 4.3A-B**). TFF-exosomes and UC-exosomes were structurally similar by electron microscopy (**Figure 4.3C**), and both contained exosomal marker proteins (**Figure 4.3D**). The main difference between TFF- and UC-exosomes was yield and protein-to-vesicle ratio. Tangential flow filtration yielded ~50-fold more exosomes than differential ultracentrifugation (**Figure 4.3E**). In addition, TFF-exosomes had a 10-fold higher protein-to-vesicle ratio than UC-exosomes (**Figure 4.3F**).

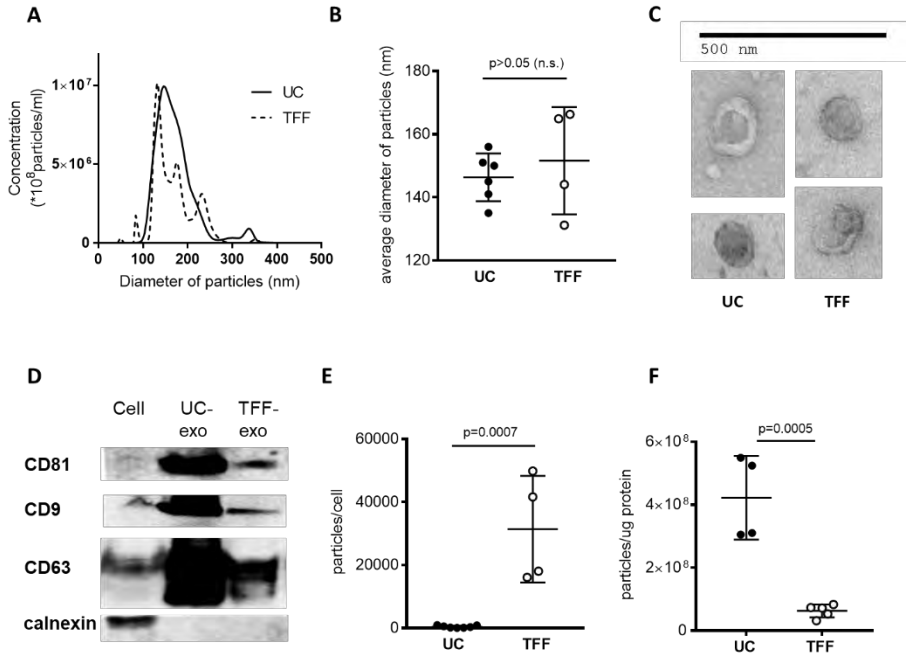

Figure 4.3 Characterization of exosomes.

(**A**) Size distribution of exosomes isolated by differential ultracentrifugation (UC, solid) or tangential flow filtration (TFF, dashed). Concentration and size of exosomes were measured by Nanoparticle Tracking Analysis. UC exosomes purified from two-dimensional

cultures, and TFF exosomes purified from three-dimensional cultures. (**B**) Average size of exosomes isolated by UC (N=6) or TFF (N=4) plotted, showing the mean ± SD of all measurements, Student's t-test. (**C**) Transmission electron microscopy images of exosomes isolated by UC or TFF.

Proteomics analyses showed that 66% of TFF-exosome proteins were present in UC-exosomes, and 82% of UC exosome proteins were present in TFF exosomes (**Figure 4.4A**). In addition, TFF-exosomes contained 62 high-abundance proteins (34% of all TFF-exosome proteins) not present in UC-exosomes, and UC-exosomes contained 484 low-abundance proteins (18% of UC exosomes proteins) (**Figure 4.4A**). Proteins unique to TFF-exosomes were smaller (48±27 kDa) than proteins present in both (73±75 kDa, p=0.049) or proteins unique to UC-exosomes (80±80 kDa, p=0.0048) (**Figure 4.4B**). Gene ontology analysis revealed that proteins unique to TFF-exosomes were enriched in secreted proteins (in particular albumin), lipoproteins, immunoglobulins, and complement (**Figure 4.4C**). Proteins present in both TFF- and UC-exosome types were enriched in integrin binding, heparin binding, ribosomal, and generally extracellular exosomal proteins (**Figure 4.4C**). These findings suggest (i) that TFF- and UC-exosomes have a similar protein composition, and (ii) that high levels of secreted proteins are responsible for higher protein-to-vesicle ratio in TFF-exosome samples.

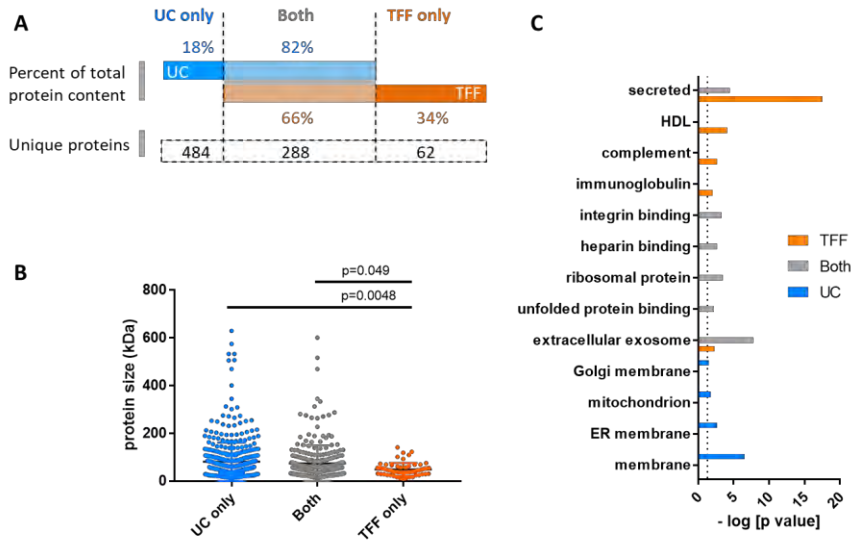

Figure 4.4 Proteomic content of exosomes.

(**A**) Schematic summary of proteomic studies showing percent of total protein content specific (solid) or common (opaque gray overlay between vertical dashed lines) to UC (blue) and TFF (orange) exosome preparations. The number of unique proteins in each category charted below. Protein content was determined by intensity-based absolute quantification (iBAQ) analysis [256]. (**B**) Size distribution of proteins specific to or unique to UC-exosomes and TFF-exosomes, from panel (A), one-way ANOVA. (**C**) Gene ontology analysis of proteins shared or unique to UC-exosomes and TFF-exosomes, from panel (A).

TFF-exosomes deliver siRNA to neurons better than UC-exosomes

Exosome integrity is essential for biological activity and is therefore a major requirement for the development of large-scale isolation methods. We have previously shown that UC-exosomes can efficiently deliver therapeutic siRNAs to primary neurons [135]. Loading of cholesterol-conjugated, fully chemically modified siRNAs into exosomes is efficient, fast, easily scalable, and supports potent mRNA silencing in recipient cells (Haraszti et al, in review). We therefore compared the ability of TFF-exosomes and UC-exosomes to deliver *Huntingtin* siRNA to neurons, using *Huntingtin* silencing as a readout for efficient neuronal delivery.

Seven days after treatment, we found that TFF-exosomes were ~15-fold more efficient at siRNA transfer and *Huntingtin* silencing in neurons compared to UC-exosomes (TFF IC50, ~8

nM; UC IC50 ~122 nM; p<0.0001) (**Figure 4.5A**). To address whether the increased potency reflects better vesicle uptake or increased biological availability of internalized siRNAs, neurons were treated with both types of exosomes loaded with equal amounts of fluorescently labeled siRNAs. Neurons internalized TFF-exosomes faster (9 minutes half-life) than UC-exosomes (2 hours half-life) (p<0.0001) (**Figure 4.5B**). In addition, total fluorescence was higher in primary neurons treated with TFF-exosomes (**Figure 4.5B**). These findings suggest that enhanced trafficking of TFF-exosomes into neurons likely underlies their ability to support more efficient silencing.

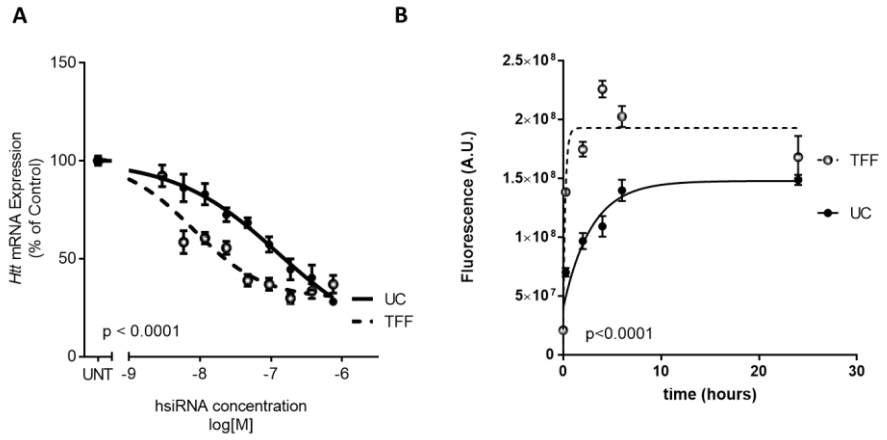

Figure 4.5 TFF-exosomes are more efficient at delivering siRNAs to neurons.

(**A**) Dose response analysis showing *Huntingtin* (*Htt*) mRNA levels in mouse primary neurons treated with UC (solid) or TFF (dashed) exosomes containing the indicated doses of siRNA. Each data point represents the mean ± SEM of N=3 experiments, each experiment was run in duplicates. UNT= untreated, two-way ANOVA. (B) Time course of fluorescence in primary neurons treated with UC (solid) or TFF (dashed) exosomes containing Cy3-labeled siRNA. Each data point represents the mean ± SEM of 5 images per timepoint, two-way ANOVA.

4.5 DISCUSSION

The development of exosomes as therapeutic delivery vehicles requires production and purification methods compatible with good manufacturing practices (GMP). Three-dimensional culture systems, xenofree medium and tangential flow filtration are suitable for GMP-grade biologics[335-337, 339]. Here we show that three-dimensional xenofree cultures of umbilical cord mesenchymal stem cells and tangential flow filtration of the conditioned supernatants produced substantially higher yields of exosomes than standard two-dimensional culture and ultracentrifugation. Whereas TFF- and UC-prepared exosomes have similar size distributions and protein contents, TFF-exosomes are more efficient at siRNA delivery to neurons and at inducing mRNA silencing.

The differences in protein-to-vesicle ratios as well as in activity between TFF- and UC-exosomes probably reflect differences in their production and preparation methods. The high protein-to-vesicle ratio in TFF-exosome preparations might result from protein aggregates that form in GMP-compatible xenofree medium used for three-dimensional cultures. Optimization of xenofree culture and purification conditions will undoubtedly be required to identify and generate exosomes with desired protein content and protein-to-vesicle ratios. Thus, the functional difference between exosomes prepared by tangential flow filtration and differential ultracentrifugation likely reflects physical differences in the preparation methods. The high centrifugal forces applied to exosomes may damage the integrity of exosomal membranes [330] and thus compromise cellular uptake [137]. The gentler tangential flow filtration is widely used to purify biologics and viruses, which are highly sensitive to structural alterations.

Cell culture conditions and exosome isolation methods should be developed together to advance exosome technology. Therapeutic virus production might serve as an example for exosome technology development[340]. Though we use umbilical-cord derived mesenchymal stem cells, the cell culture and exosome isolation methods described here should work for other cell

sources. Quality control steps for large scale exosome production need to be worked out in detail based on published recommendations for small-scale exosome isolation methods [306, 341]. Protein-to-exosome ratio should be considered as part of the quality control protocols[327].

Genetic interference strategies are being developed into promising therapeutic drugs to treat genetically defined diseases. Here we used delivery of *Huntingtin* siRNAs and silencing as a readout for exosome activity produced at a large scale. We speculate that exosomes produced from microcarrier-based three-dimensional xenofree cultures by tangential flow filtration will prove useful as delivery vehicles for other therapeutic oligonucleotides that target numerous diseases: siRNAs, antisense oligonucleotides, and CRISPR guide RNAs. The effective, scalable exosome isolation method described here will facilitate the successful transition of the exosome technology to clinical applications.

CHAPTER V EV CHARACTERIZATION

5.1 PREFACE

Figures and text are reproduced from a scientific article

- **Haraszti RA**, Didiot MC, Sapp E, Leszyk J, Shaffer SA, Rockwell HE, Gao F, Narain NR, DiFiglia M, Kiebish MA, Aronin N, Khvorova A. High-resolution proteomic and lipidomic analysis of exosomes and microvesicles from different cell sources. J Extracell Vesicles. 2016 Nov 17.

Anastasia Khvorova and I conceptualized this project. Ellen Sapp and Marian DiFiglia performed transmission electron microscopy. John Leszyk and Scott Shaffer performed mass spectrometry for proteomics. Hannah Rockwell and Michael Kiebish performed mass spectrometry for lipidomics. Marie Didiot established EV isolation protocols. I isolated all EVs, prepared short gels for proteomics, transported samples for mass spectrometry analysis, analyzed all data and performed Western blotting. Anastasia Khvorova and I wrote this manuscript.

5.2 ABSTRACT

Extracellular vesicles (EVs), including exosomes and microvesicles, are explored for use in diagnostics, therapeutics and drug delivery. However, little is known about the relationship of protein and lipid composition of EVs and their source cells. Here, we report high-resolution lipidomic and proteomic analyses of exosomes and microvesicles derived by differential ultracentrifugation from three different cell types: U87 glioblastoma cells, Huh7 hepatocellular carcinoma cells, and human bone marrow-derived mesenchymal stem cells (MSC). We identified 3532 proteins and 1961 lipid species in the screen. Exosomes differed from microvesicles in several different areas: (i) The protein patterns of exosomes were more likely different from their cells of origin than were the protein patterns of microvesicles; (ii) The proteomes of U87 and Huh7

exosomes were similar to each other but different from the proteome of MSC exosomes, whereas the lipidomes of Huh7 and MSC exosomes were similar to each other but different from the lipidome of U87 exosomes; (iii) Exosomes exhibited proteins of extracellular matrix, heparin binding, receptors, immune response, and cell adhesion functions, whereas microvesicles were enriched in endoplasmic reticulum, proteasome and mitochondrial proteins. Exosomes and microvesicles also differed in their types of lipid contents. Enrichment in glycolipids and free fatty acids characterized exosomes, whereas enrichment in ceramides and sphingomyelins characterized microvesicles. Furthermore, Huh7 and MSC exosomes were specifically enriched in cardiolipins; U87 exosomes were enriched in sphingomyelins. This study comprehensively analyzes the protein and lipid composition of exosomes, microvesicles and source cells in three different cell types.

5.3 INTRODUCTION

Extracellular vesicles occur in most bodily fluids and cell culture supernatants. With the advent of parallel sequencing technologies, the RNA content of EVs is being heavily investigated as a new type of diagnostic biomarker [342]. The RNA contents of EVs from a variety of bodily fluids, including urine, saliva, blood, and cerebrospinal fluid, have been explored as biomarkers for indications throughout the body [343-349]. EVs as tumor biomarkers are especially valuable, since bodily fluid EVs provide an alternative to repeated biopsies for continuous monitoring and an option for tumors inaccessible to biopsies (*i.e.* brain tumors). Extracellular vesicles are also being explored as natural carriers of therapeutic RNAs [350-351]. EVs for therapeutic applications are typically derived from mesenchymal stem cells, a cell type well characterized for cell-based therapies [341, 351].

Two EV subgroups in particular, exosomes and microvesicles (MVs), have the ability to carry biomarkers or therapeutic RNA. Exosomes are small vesicles (traditionally considered 50-150 nm) that originate from endocytic compartments within the cell. During endosome maturation,

intraluminal vesicles are formed by endosomal membrane budding inside multivesicular bodies, and intraluminal vesicles become exosomes upon the exocytosis of multivesicular bodies [313]. Compared to exosomes, microvesicles are larger vesicles (traditionally considered 200-1000 nm) and are formed by budding directly from the plasma membrane [352]. Available purification methods include separation based on size (differential ultracentrifugation [204] and ultrafiltration [353]), density (OptiPrep™ [332], sucrose [333]), floatation velocity [354], immunoaffinity [331] and PEG-based precipitation [353]. These strategies enrich EVs within certain size ranges but are not able to fully separate EV subgroups, resulting in mixed EV populations in the isolates [355]. The purification strategy defines the nature of EV subgroup mixture in the isolate, which in turn will determine its biological function and biochemical properties. Furthermore, EV purification strategies can co-isolate non-vesicular extracellular proteins and lipoprotein particles with EVs.

The protein and lipid composition of EVs from various sources have been studied *via* biochemical assays and mass spectrometry [356-369] and provide a robust basis for protein biomarker identification in EVs for research quality control purposes. Exosomal isolates commonly contain membrane proteins, specifically tetraspanins, as well as various amounts of extracellular matrix proteins; they are devoid of nuclear proteins[332]. Microvesicular isolates may contain proteins of mitochondrial or endoplasmic reticulum origin[332]. A detailed understanding of the biochemical (protein and lipid) composition of EV subgroups and the extent to which EV composition reflects source cell composition is necessary for further development into diagnostics and therapeutics. To address this question, we performed a comparative analysis of the protein and lipid composition of two EV subgroups and their source cells. We chose a glioblastoma (U87) and a hepatocellular carcinoma (Huh7) cell line, since the EVs of these tumor types are in the focus of interest for diagnostic biomarker development[347, 370]. We further chose bone marrow-derived mesenchymal stem cells (MSC), since this cell type is frequently used for therapeutic vesicle production[351]. For EV purification, we sought a strategy that would not introduce bias into the composition of EV isolates (unlike immunoaffinity-based purification), would not co-enrich non-vesicular

extracellular proteins (unlike PEG-precipitation) [353] and would provide sufficient yield for mass spectrometric measurement. Differential ultracentrifugation is considered the gold standard of EV purification and met the above requirements.

5.4 RESULTS

We sought to characterize the protein and lipid composition of exosomes and microvesicles and to determine whether protein and lipid content depends on source cell type. Although it does not provide full separation of microvesicles and exosomes, differential ultracentrifugation is currently the gold standard method of EV purification [204]. Hence, for the purposes of this publication, we will refer to the 10 000 g pellet as microvesicles, and to the 100 000 g pellet as exosomes (**Figure 5.1**). We purified exosomes and microvesicles from the conditioned cell media of U87, Huh7 and MSC cells (**Figure 5.1**). As expected, exosomes were relatively homogenous with an average diameter of approximately 135 nm (50 to 200 nm; **Figure 5.1A**). Microvesicles, however, were more heterogeneous in size (50 to 600 nm). We then analyzed the protein content of EVs and source cells by liquid chromatography followed by tandem mass spectrometry (LC-MS/MS) and the lipid content using an information-independent acquisition method known as MS/MS^{ALL} [208]. Protein and lipid contents of EVs from each cell type were compared to the total protein and lipid contents of the respective source cell type in downstream analyses (**Figure 5.1**).

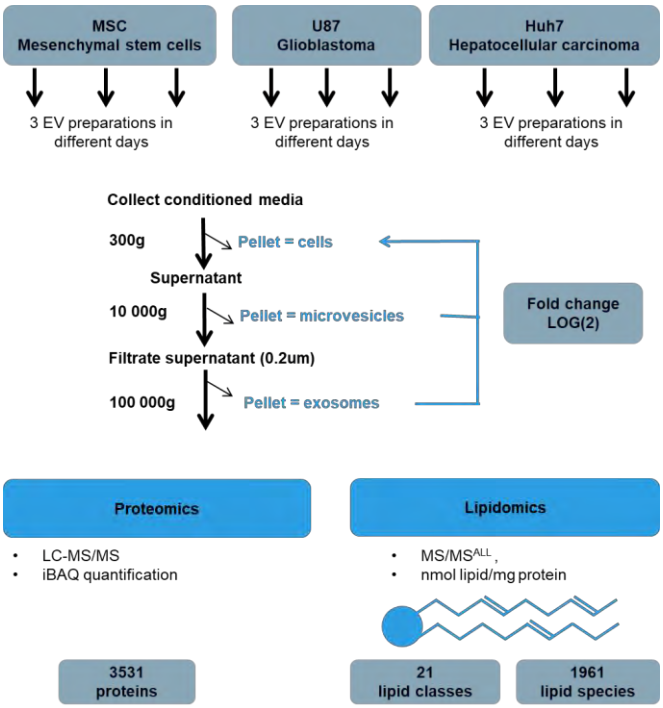

Figure 5.1 Workflow of EV preparation and Mass Spectrometry. Mesenchymal Stem Cells (MSC), glioblastoma cells (U87) and hepatocellular carcinoma cells (Huh7) were cultured and EVs prepared on six different days by differential ultracentrifugation. Resulting samples (cells, microvesicles and exosomes, altogether 54 samples) were subjected to proteomic (27 samples, LC-MS/MS) and lipidomic (27 samples, MS/MS^{ALL}) analysis. Proteins were quantified by the label-free quantification method iBAQ (intensity-based absolute quantification, see details in Methods). Analysis detected 3531 proteins and 1961 lipid species (defined by headgroup identity, length, saturation and number of fatty acid tails) in 22 lipid classes (defined by headgroup identity). Level of proteins and lipids in exosomes and microvesicles were later normalized to their respective source cells and expressed on a log(2) scale.

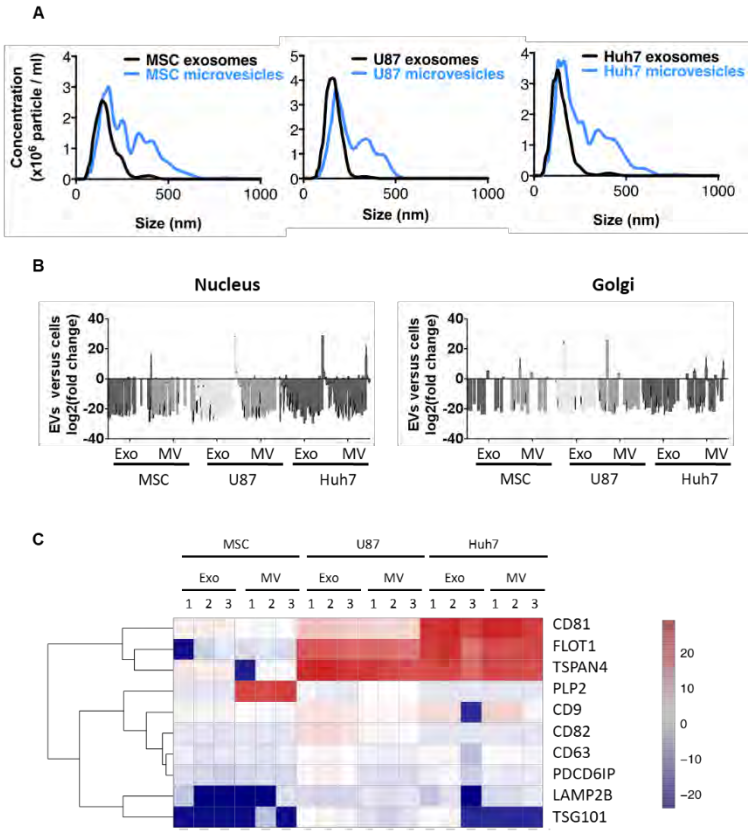

Figure 5.2 Quality control of EV preparations. (A) Representative size distribution profiles of EVs from three different cell sources as obtained by Nanoparticle Tracking Analysis (NanoSight NS300, Malvern). Microvesicles were more heterogenous in size independently of cell source. **(B)** EVs are depleted in proteins of nuclear or Golgi origin. Origin of proteins identified by Scaffold Proteome Software. **(C)** Enrichment of exosomal marker proteins in EVs. Fold change of proteins in EVs *versus* source cells is color-coded on a log(2) scale. Enrichment of established protein markers in exosomes was source cell type dependent and most exosomal markers were, although to a lower extent, also enriched in microvesicles.

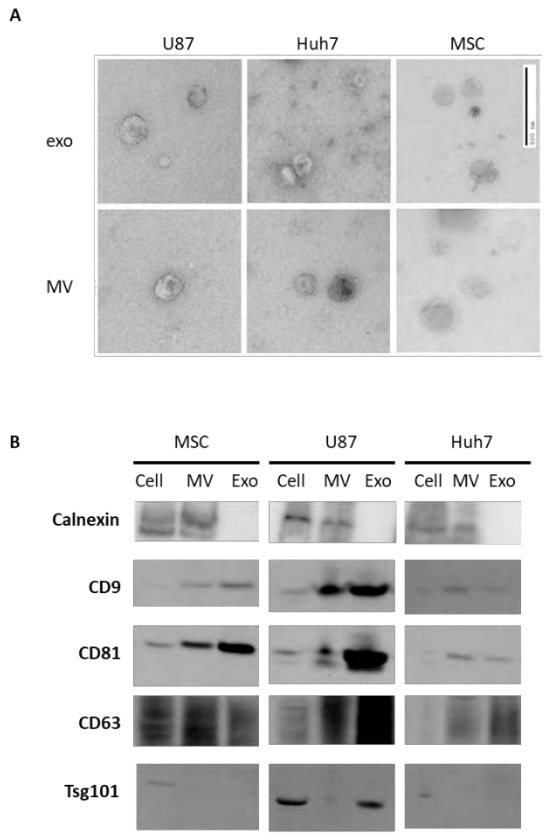

Figure 5.3 Isolates purified by differential ultracentrifugation are bona fide extracellular vesicles. (**A**) Transmission electron microscopy images show that all isolates consisted of vesicles surrounded by bilayer membranes. Scale bar represents 500 nm. (**B**) Western blot analysis of EV isolates. Calnexin is present in cells and microvesicles but absent from exosomes. CD9 and CD81 are enriched in all EVs but enrichment level is higher in exosomes. CD63 is present in all EVs, but only enriched in U87 and Huh7 vesicles, where it maintains a higher enrichment level in exosomes than in microvesicles. Tsg101 was only detected in U87, where it was enriched in exosomes.

Exosomes differ from microvesicles in protein composition

To assure that we purified bona fide extracellular vesicles, we confirmed membrane-surrounded vesicular structures in all the EV isolates on EM (**Figure 5.3**) and investigated the presence of known exosomal marker proteins and absence of non-vesicular proteins in our EV preparations. As expected, nuclear and Golgi-resident proteins were few or absent from microvesicles and exosomes (**Figure 5.2B**), while the ER marker calnexin was absent from exosomes but present in microvesicles (**Figure 5.3B**). Enrichment of EV marker proteins showed significant source cell type dependence. Traditional exosome markers CD81 and CD9 [268] were enriched in both exosomes and microvesicles, with level of enrichment being higher in exosomes (**Figure 5.2C** and **Figure 5.3B**). CD63 enrichment was specific to U87 and Huh7 exosomes, while Tsg101, PDCD6IP (Alix) and CD82 were only enriched in U87 exosomes (**Figure 5.2C** and

Figure 5.3B). Flotilin 1 and Tetraspanin 4 were highly enriched in all U87 and Huh7 EVs, while PLP2 enrichment was unique to MSC MVs **(Figure 5.2C**). The immunoblot of individual protein markers corresponded well with label free quantification of proteomics. Generally, 91% of top EV marker proteins (n = 100; ExoCarta [371]) were present in our EV samples (Table 5.1).

Gene Symbol	Number of times identified (ExoCarta)	Present in EV samples of current study
CD9	98	all samples
PDCD6IP	96	all samples
HSPA8	96	all samples
GAPDH	95	all samples
ACTB	93	all samples
ANXA2	83	all samples
CD63	82	all samples
SDCBP	78	all EV samples
ENO1	78	all samples
HSP90AA1	77	all samples
TSG101	75	yes, except Huh7 MV and MSC exo
PKM	72	all samples
LDHA	72	all samples
EEF1A1	71	all samples
YWHAZ	69	all samples
PGK1	69	all samples
EEF2	69	all samples
ALDOA	69	all samples
HSP90AB1	67	all samples
ANXA5	67	all samples
FASN	66	all samples
YWHAE	65	all samples
CLTC	64	all samples
CD81	64	all samples
ALB	63	all samples
VCP	62	all samples
TPI1	62	all samples
PPIA	62	all samples
MSN	62	all samples
CFL1	62	all samples
PRDX1	61	all samples
PFN1	61	all samples

RAP1B	60	all samples
ITGB1	60	all samples
HSPA5	58	all samples
SLC3A2	57	all samples
HIST1H4A	57	all samples
GNB2	57	yes, except MSC exo
ATP1A1	57	all samples
YWHAQ	56	all samples
FLOT1	56	all EV samples
FLNA	56	all samples
CLIC1	56	all samples
CCT2	56	all samples
CDC42	55	all samples
YWHAG	54	all samples
A2M	54	all EV samples
TUBA1B	53	none, instead TUBA4A is present in all samples
RAC1	53	all samples
LGALS3BP	53	only in MSC exo, U87 exo and U87 MV
HSPA1A	53	all samples
GNAI2	53	all EV samples
ANXA1	53	all samples
RHOA	52	all samples
MFGE8	52	all EV samples
PRDX2	51	all samples
GDI2	51	all samples
EHD4	51	all samples
ACTN4	51	all samples
YWHAB	50	only in Huh7 MV, MSC MV, U87 exo and U87 MV
RAB7A	50	all samples
LDHB	50	all EV samples
GNAS	50	all samples
RAB5C	49	all samples
ARF1	49	all samples
ANXA6	49	all samples
ANXA11	49	all samples
ACTG1	49	none
KPNB1	48	yes, except MSC exo
EZR	48	all samples
ANXA4	48	all samples
ACLY	48	all samples

TUBA1C	47	none
TFRC	47	all samples
RAB14	47	all samples
HIST2H4A	47	none
GNB1	47	all samples
THBS1	46	yes, except U87 MV
RAN	46	none
RAB5A	46	all samples
PTGFRN	46	yes, except MSC MV
CCT5	46	all samples
CCT3	46	all samples
AHCY	46	all samples
UBA1	45	all samples
RAB5B	45	all samples
RAB1A	45	none
LAMP2	45	all samples
ITGA6	45	all EV samples
HIST1H4B	45	none
BSG	45	all samples
YWHAH	44	all samples
TUBA1A	44	none
TKT	44	all samples
TCP1	44	all samples
STOM	44	all EV samples
SLC16A1	44	all samples
RAB8A	44	none
MYH9	44	all samples
MVP	44	yes, except Huh7 MV

Table 5.1 List of EV-enriched proteins.

Pairwise Pearson's correlation of protein levels (iBAQ scores) revealed that exosomes were more different from source cells ($R^2 < 0.1$) than microvesicles were ($R^2 = 0.28$ to 0.66). Exosomes also differed from microvesicles ($R^2 < 0.2$) (**Figure 5.4A**). Hence, exosomes and microvesicles displayed a very different protein profile, despite overlap in their size range (**Figure 5.4A**).

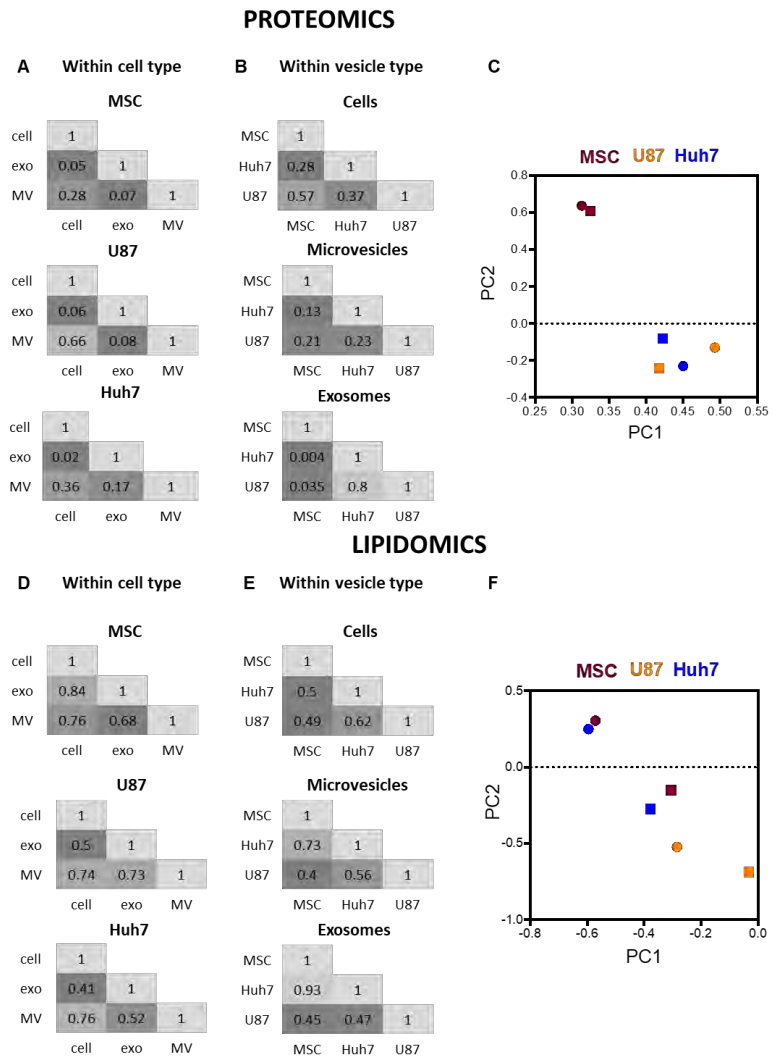

Figure 5.4 Protein and lipid sorting into EVs are not linked. Pairwise Pearson's correlations of protein and lipid levels in cells, microvesicles and exosomes derived form three source cell types. Numbers represent R^2. **(A)** Microvesicular proteome was more similar to the source cell than the exosomal proteome was in all three cell types investigated. **(B)** Cancer cell derived proteomes (U87 and Huh7) were increasingly similar to each other and increasingly different form stem cell proteome (MSC) while moving from cells towards microvesicles and exosomes. **(C)** Principal component analysis of protein levels in exosomes (round) and microvesicles (square) normalized to their respective source cell. MSC derived exosomes and microvesicles segregate from cancer cell EVs. **(D)** Lipidomes of exosomes, microvesicles and source cells are more similar to each other than their proteomes are. **(E)** Huh7 and MSC lipidomes showed increasing level of similarity moving from source cells to microvesicles to exosomes. **(F)** Principal component analysis of lipid levels in exosomes (round) and microvesicles (square) normalized to their respective source cell. MSC and Huh7 derived EVs increasingly cluster together and segregate from U87 moving from microvesicles to exosomes.

Exosomal proteomes effectively distinguish between cancer origin and mesenchymal stem cell origin

Huh7 and U87 exosomes had similar protein compositions (R^2=0.8), despite poor correlations between MV (R^2=0.23) and source cell (R^2=0.37) protein levels (**Figure 5.4B**). These data suggested that exosomal proteome was similar between source cell types, whereas microvesicle proteome differed between source cell types. However, MSC exosomes markedly differed from U87 and Huh7 exosomes (R^2=0.035 and 0.004). Furthermore, this contrast could not be explained by the difference in source cell protein compositions (MSC to U87 R^2=0.57 and MSC to Huh7 R^2=0.28). To look at cell type specific protein enrichment in EVs, we normalized EV protein levels (iBAQ scores) to their respective source cell type's protein levels. Then we used principal component analysis to determine whether source cell type affected which proteins were enriched in EVs. Indeed, MSC-derived exosomes and microvesicles clustered very close together and clearly segregated from U87 and Huh7 vesicles (**Figure 5.4C**).

Overrepresented protein pathways depend on vesicle type

To compare functional content of exosomes and microvesicles, we conducted Gene Ontology (GO) analysis on the list 719 proteins present in exosomes from all three cell types (n=719) and the 1357 proteins present in microvesicles from all three cell types using DAVID version 6.7 [209-210] (NIH) (**Figure 5.5A**). Gene Ontology is a knowledgebase where genes are assigned to molecular functions, cellular components or biological processes (GO terms). GO analysis tests, whether the representation of GO terms in a specific set of genes could be explained by random chance or does it enrich for certain GO terms. We found that exosomes and microvesicles were both enriched in vesicle proteins, membrane-associated proteins, and GTPases [355] **(Figure 5.5B**). Both exosomes and microvesicles also enriched for translation and glycolysis pathways.

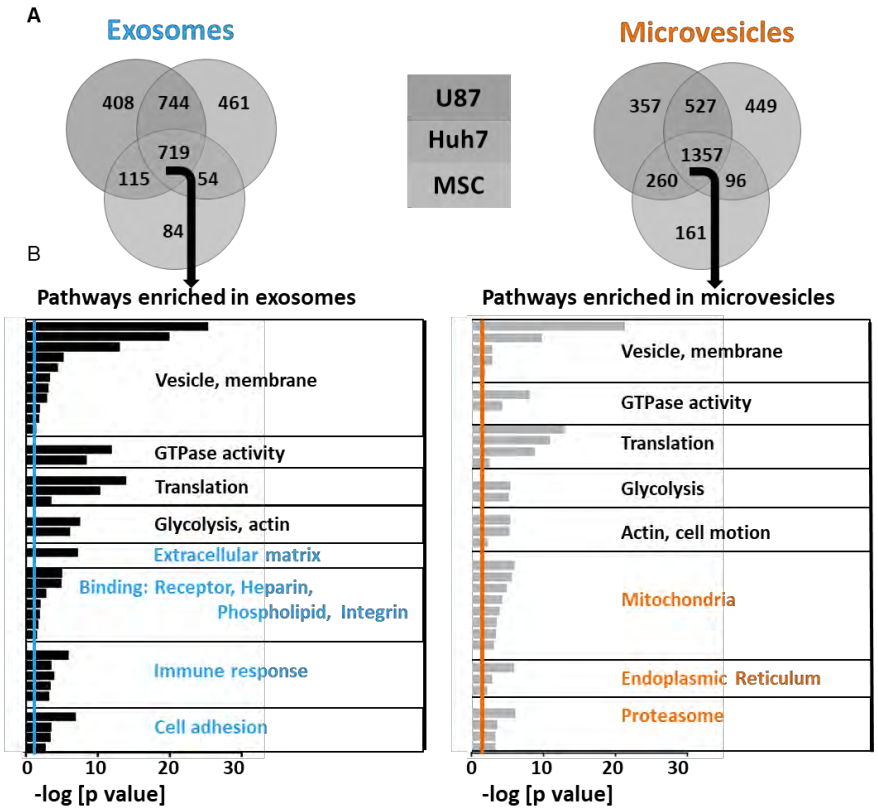

Figure 5.5 Overrepresented protein pathways depend on vesicle type. **(A)** Venn diagrams of detected proteins in exosomes and microvesicles of three different source cell types. MSC EVs had a lower diversity of proteins. **(B)** Proteins shared among exosomes or microvesicles derived from all three source cell types (middle section in the Venn diagrams) underwent Gene Ontology analysis. The negative logarithm of p values is shown for each GO term, colorful lines represent significance threshold (p=0.05). Common (depicted in black), as well as distinct (depicted in color) pathways emerged in exosomes *versus* microvesicles.

Meanwhile, certain GO terms were differentially enriched in exosomes and microvesicles. Extracellular matrix, receptors, heparin-binding, phospholipid-binding, integrin, immune response, and cell adhesion functions were characteristic for exosomes, whereas mitochondrial, endoplasmic reticulum, and proteasomal functions were exclusive to microvesicles **(Figure 5.5B)**.

To examine how cell type influences protein enrichment in EVs, we normalized EV protein content (iBAQ values) to the respective source cell protein content and performed unsupervised cluster analysis, which revealed nine clusters described below (**Figure 5.6**).

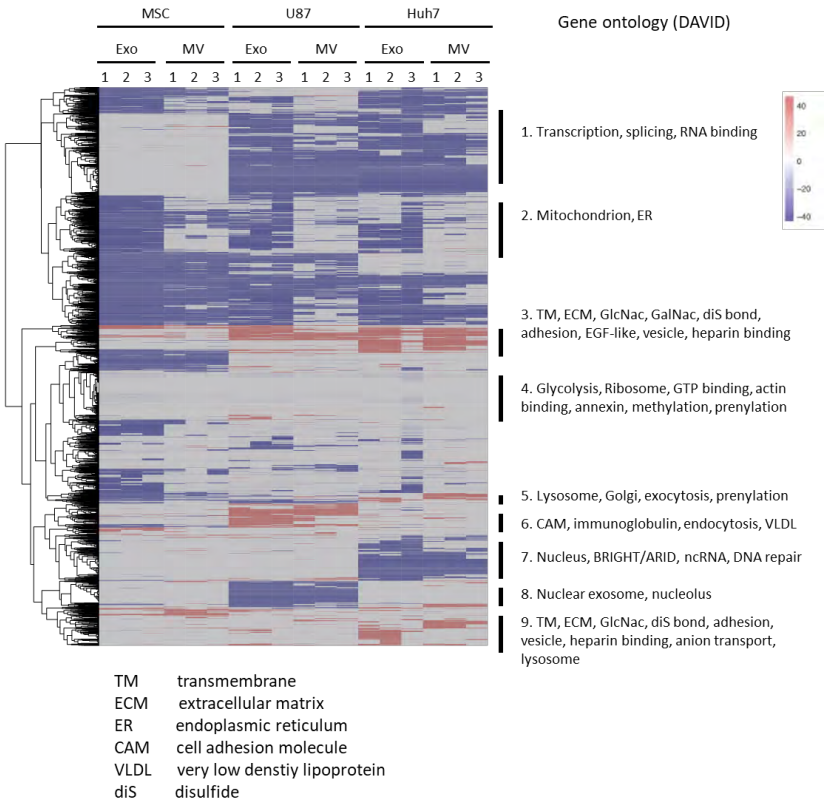

Figure 5.6 Heatmap of all protein levels in EVs normalized to their respective source cells. iBAQ values of proteins in EVs were normalized to the corresponding protein levels in source cells, expressed on a log(2) scale and color-coded. Depletion is depicted in blue and enrichment in red. Clusters from heatmap underwent Gene Ontology analysis, and terms significantly enriched are shown on the right.

Clusters 1, 7, and 8: Proteins in clusters 1, 7, and 8 were depleted from vesicles of U87 cells, Huh7 cells, or both, and absent of all MSC samples. These clusters comprised nuclear proteins, consistent with quality control experiments showing the depletion of nuclear proteins (**Figure 5.2B**).

Cluster 2: Proteins in cluster 2 were depleted from exosomes but not from microvesicles. This cluster consisted of proteins that function in mitochondria or endoplasmic reticulum, consistent with the microvesicle-specific GO terms we identified above (**Figure 5.5**) and with an analysis of the relative abundance of endoplasmic reticulum and mitochondrial marker proteins (**Figure 5.7**).

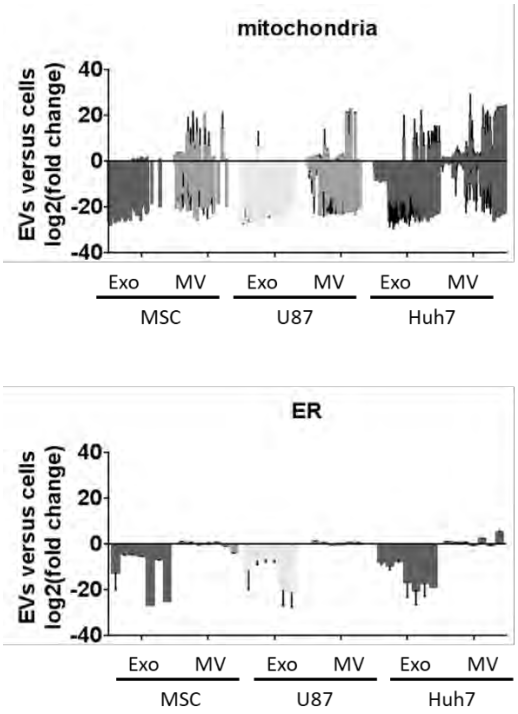

Figure 5.7 Exosomes are depleted in mitochondrial and endoplasmic reticulum marker proteins, whereas microvesicles are not. Mitochondrial and ER marker protein levels in EVs were normalized to the respective source cell. Origin of proteins identified by Scaffold Proteome Software.

Clusters 3 and 9: Proteins in clusters 3 and 9 were enriched or unchanged in EVs regardless of cell type or vesicle type. These clusters consisted of membrane proteins, vesicular proteins, extracellular matrix, heparin-binding, cell adhesion and blood coagulation pathways. Furthermore, Gene Ontology analysis detected enrichment in certain protein motifs (e.g., EGF-like domain) and post-translational modifications (e.g., disulfide bonds and glycosylation), consistent with the enrichment of membrane proteins. We did not observe an enrichment of proteins known to be palmitoylated, a posttranscriptional modification that has been shown to direct protein accumulation in exosomes [146].

Clusters 5 and 6: Proteins in clusters 5 and 6 were enriched in vesicles of Huh7 (cluster 5) or U87 (cluster 6) cells. Huh7-specific cluster 5 consisted of proteins involved in exocytosis, whereas U87-specific cluster 6 included endocytosis pathway proteins. These observations show source cell-dependent EV content, which may suggest source cell-dependent exosome production and maturation mechanisms. When focusing on two protein classes, vesicular trafficking regulator Rabs (**Figure 5.8**) and EV organotropism regulator integrins[137] (**Figure 5.9**), source cell influence

on EV content is particularly clear. Endocytotic Rab34 and Rab23 were highly enriched in U87 exosomes, retrograde transport Rab9 and Rab6 were enriched in Huh7 exosomes, and exocytotic Rab27 was enriched in MSC exosomes (**Figure 5.8**). While integrin β3 was enriched in all EVs except Huh7 microvesicles, integrins α2b (indicated in lung-tropism[137]) and α6 were specific to MSC EVs, integrins α1, α2 and α5 were characteristic to Huh7 EVs, and integrins α3, α7, αV (liver-tropic[137]), β1 (lung-tropic[137]) and β5 (liver-tropic[137]) were characteristic to U87 EVs (**Figure 5.9**).

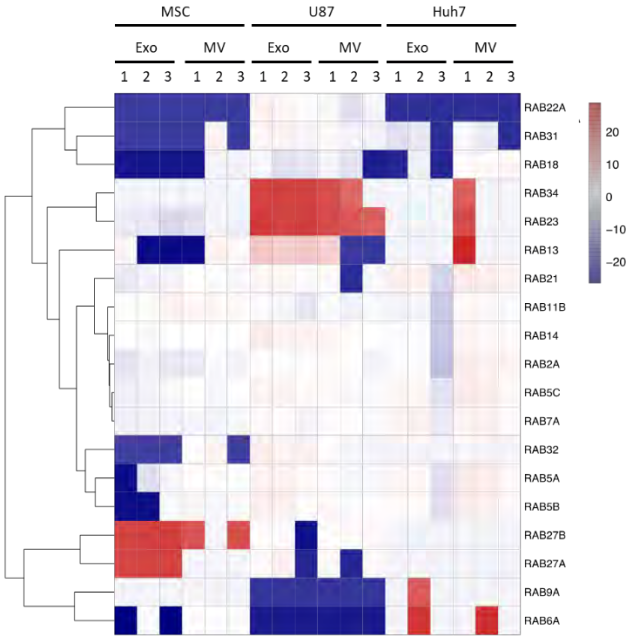

Figure 5.8 Rab protein enrichment in EVs depends on source cell type. Heatmap shows enrichment (red) or depletion (blue) of Rab proteins in EVs relative to source cells (log(2) scale). Rab proteins are involved in vesicle trafficking and their enrichment in EVs clearly depends on source cell type.

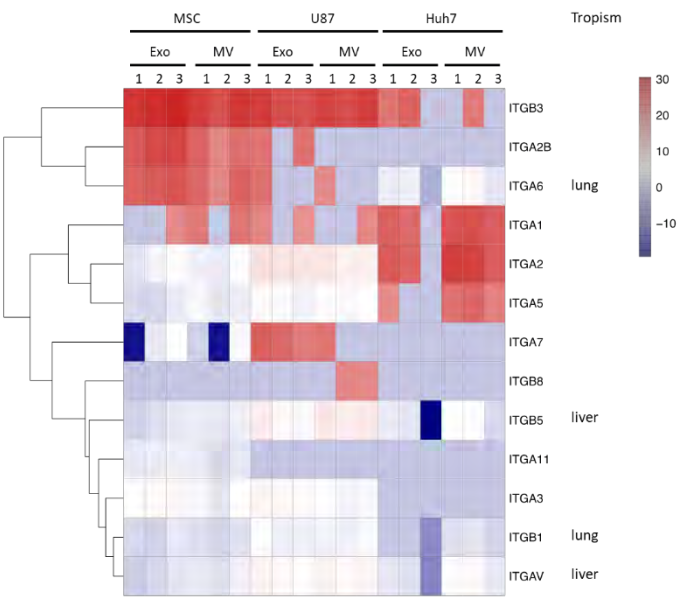

Figure 5.9 Integrin enrichment in EVs depends on source cell type. Heatmap shows enrichment (red) or depletion (blue) of integrins in EVs relative to source cells (log(2) scale). On the left organotropism associated so some of the integrins[137] are depicted.

Lipid and protein enrichment in EVs are not linked

MS/MS^{ALL} analysis identified 22 lipid classes (defined by headgroup) and almost 2000 lipid species (defined by headgroup, fatty acid tail length and saturation) across all samples. Lipid content was more similar between samples (R^2 = 0.41 to 0.93) than was protein content (R^2 = 0.004 to 0.66) (**Figure 5.4D-E**). Surprisingly, lipid enrichment in EVs did not follow the pattern of protein enrichment we observed earlier (**Figure 5.4A-C**): lipid content of U87 and Huh7 exosomes was different (R^2=0.47), despite their protein content being very similar (R^2=0.8) (**Figure 5.4B and 5.4E**). Instead, lipid composition of Huh7 and MSC exosomes showed striking similarity (R^2=0.93). This similarity was present, although less pronounced, between Huh7 and MSC microvesicles as well (R^2=0.73; **Figure 5.4E**). Again, similarity in lipid profiles did not correlate with difference in protein profiles of Huh7 and MSC exosomes (R^2=0.004), or microvesicles (R^2=0.13) (**Figure 5.4B**). High degree of similarity between Huh7 and MSC exosomes could not be explained by source cell lipid profiles either (**Figure 5.4E**, R^2=0.5). When lipid levels in EVs were normalized to their respective source cells and underwent principal component analysis, Huh7 and MSC exosomes clustered very close to each other and segregated from U87 vesicles

(**Figure 5.4F**). Huh7 and MSC microvesicles showed a less clear segregation from U87 EVs. Taken together, certain source cells differing in protein and lipid composition enriched the same proteins but not the same lipids (U87 and Huh7), and yet other source cells enriched the same lipids but not the same proteins (Huh7 and MSC) in their EVs. This data suggested that protein and lipid enrichment mechanisms were not linked.

Next we asked, whether Huh7 and MSC cells shared characteristics that could possibly relate to their similar exosomal lipid composition. We observed that Huh7 and MSC cells yielded significantly fewer and smaller exosomes (73 /cell and 36 /cell, 129±14 nm and 131±12 nm, respectively) than U87 cells (1382 /cell, 148±8 nm).

Lipid enrichment in EVs correlates with headgroup charge, tail length and saturation

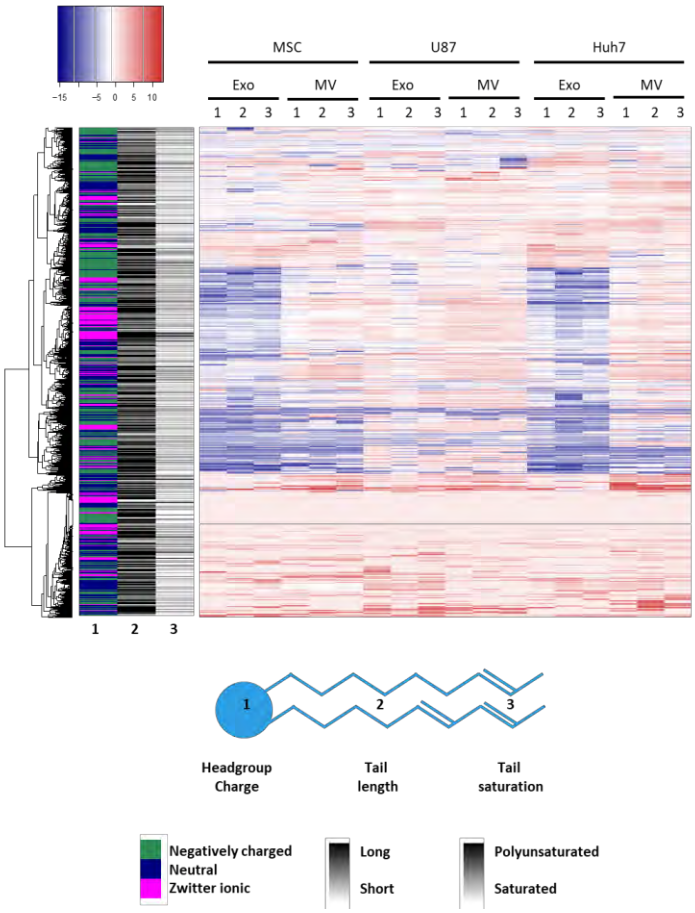

Figure 5.10 Lipid enrichment in EVs correlates with headgroup charge and fatty acid tail length and saturation. Lipid species levels in EVs were normalized to the corresponding lipid levels in source cells, expressed on a log(2) scale and color-coded. Depletion is depicted in blue and enrichment in red. Sidebar on the left encodes 3 characteristics of a lipid species: headgoup charge (in color), average length of fatty acid tails (greyscale) and average level of saturation of fatty acid tails (greyscale). Lipid

species clustered not only according to headgroup charge but also according to length and saturation of tails.

Concentration of the 1961 detected lipid species (defined by headgroup, number, length and saturation of fatty acid tails) in EVs were normalized to respective source cell lipidome. Color-coding of enrichment (red) and depletion (blue) of lipids (**Figure 5.10**) in EVs *versus* source cells showed a good concordance between triplicate measurements and confirmed that MSC and Huh7 exosomes displayed a very similar lipid composition. Next, we were interested whether enrichment or depletion in EVs *versus* source cells depended on headgroup or fatty acid tail characteristics. Hence, we created a sidebar on the left, which color-coded three characteristics of each lipid species: charge of its headgroup (negative (green), neutral (navy) or zwitterionic (magenta)), average length (the darker, the longer) and average saturation (the darker, the more double bonds) of its fatty acid tails. The colors and gray shades partially followed unsupervised clustering of lipids indicating that headgroup charge as well as tail length and saturation correlated lipid enrichment in EVs. Specifically, MSC microvesicles ($p=0.007$), U87 exosomes ($p=0.004$) and U87 microvesicles ($p=0.006$) were enriched in zwitterionic lipid headgroups (phosphatidylcholines and/or phosphatidylethanolamines) and depleted in other headgroups. MSC exosomes, MSC microvesicles and Huh7 exosomes were enriched in long lipid species (more than 60 carbons, $p\leq0.001$, $p=0.041$ and $p\leq0.001$, respectively) and polyunsaturated lipid species (more than 10 double bonds, $p=0.006$, 0.038 and 0.001, respectively).

Lipid class enrichment in EVs depends on vesicle type and source cell type

The 22 lipid classes detected could be sorted into groups marking enrichment in microvesicles or exosomes, depletion in most EVs or no change in EVs relative to source cells (**Figure 5.11**)

Ceramides and sphingomyelins were consistently enriched in all microvesicles, whereas cholesterol esters showed enrichment only in MSC and Huh7 MVs and acyl carnitines and lysophosphatidylcholines only in MSC MVs (**Figure 5.11** upper panel). These lipid classes were depleted from or unchanged in exosomes, with the exception of marked sphingomyelin enrichment in U87 exosomes.

Glycolipid, free fatty acid and phosphatidylserine enrichment characterized all exosomes and were depleted from or unchanged in MVs, except for phosphatidylserine enrichment in U87 MVs (**Figure 5.11** upper middle panel). The free fatty acids most enriched in MSC and Huh7 exosomes were fully saturated (data not shown). Cardiolipins were markedly enriched in MSC and Huh7 exosomes only. Lyso derivatives (where one fatty acid tail is removed by hydrolysis) of phosphatidylserines, phosphatidylglycerols and phosphatidylinositols showed enrichment in MSC and Huh7 exosomes, whereas lyso-phosphatidylethanolamines were rather enriched in U87 exosomes. These lysoderivatives were also enriched in MSC MVs but depleted from U87 and Huh7 MVs.

Structural membrane lipids, including phosphatidylglycerols, phosphatidylinositols, and phosphatidylethanolamines showed depletion from all exosomes and most microvesicles (**Figure 5.11** lower middle panel). Phosphatidylcholines were depleted in exosomes but unchanged or enriched in microvesicles. Depletion in diacyl and triacylglycerols in EVs was most pronounced in Huh7 cells, which had a high baseline level of these lipid classes.

Concentration of phosphatidic acids and their lysophosphatidyl derivatives did not differ between source cells and EVs (**Figure 5.11** lower panel).

Taken together, both vesicle type and source cell type affected the lipid composition of EVs.

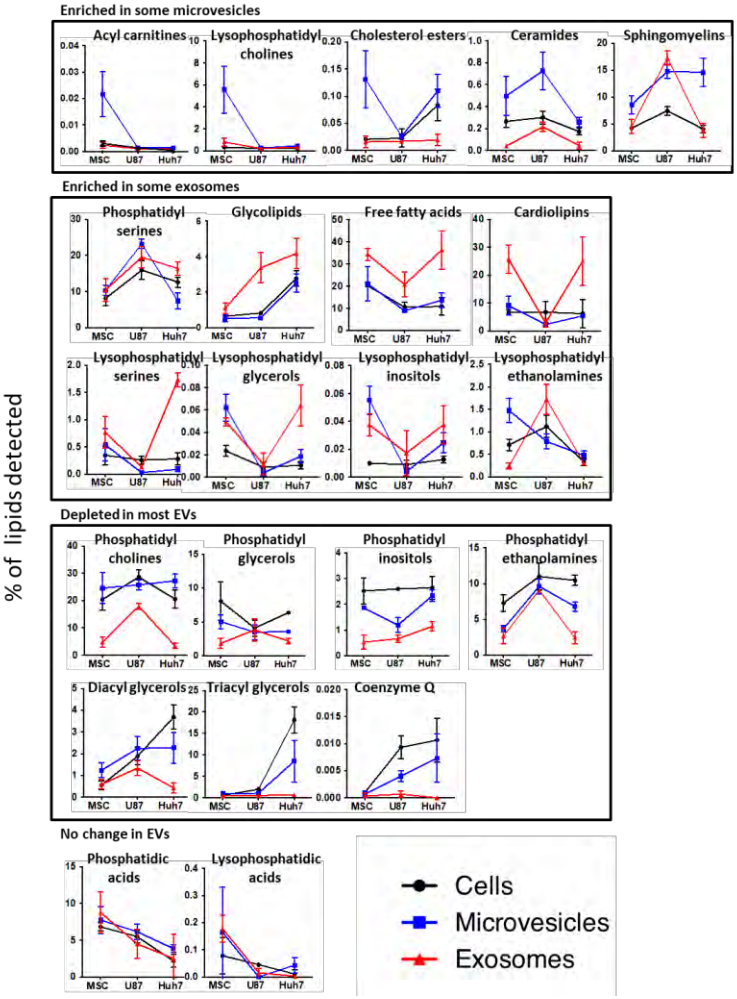

Figure 5.11 Lipid class enrichment in EVs depends on vesicle type and source cell type. Percentage of each lipid class within a sample is depicted on slope charts and lipid class grouped according to their enrichment in microvesicles (upper panel), enrichment in exosomes (upper middle panel), depletion in most EVs (lower middle panel) or no difference between EVs and source cells (lower panel). Source cells are depicted in black, exosomes in red and microvesicles in blue. Since different lipid classes represent vastly different percentage of cells' or vesicles' lipid composition, the scale of the y axes shows a corresponding variability.

5.5 Discussion

Extracellular vesicles consist of heterogeneous subgroups, which are difficult to fully distinguish by current purification methods. Here we showed that (i) exosomes and microvesicles could be well distinguished on the proteome level but did not display source cell-independent, vesicle type-specific protein markers, (ii) proteome but not lipidome of EVs distinguished cancerous source cells from stem source cells, (iii) protein and lipid enrichment in EVs compared

to source cells were not linked. Furthermore, the current study provides the largest dataset of EV lipid content to date.

We observed cell-type-specific enrichment of proteins and lipids in EVs. The clear difference between composition of source cells and EVs indicated that lipids and proteins are likely actively sorted into EVs. However, the enrichment of commonly used exosome markers was source cell type dependent, and although to a different extent, all exosomal markers were enriched in microvesicles as well. Enrichment of Rab proteins in EVs, a protein family indicated in exosomal biogenesis[372], showed marked source cell dependency, suggesting that protein sorting mechanisms into EVs may depend on source cell type. Commonly enriched pathways in EVs correlated well with previously described behaviors of EVs (such as heparin binding[373], immune response stimulation[325, 367], integrin content[137] and antiphagocytic CD47[374] of exosomes and mitochondrial, proteasomal and ER content of microvesicles[332, 375]). Gene ontology analysis found enrichment of certain posttranslational modification motifs (e.g., glycosylation and prenylation) common to all EVs, although the exosome targeting palmytoil modification[146] was not detected. We were not able to detect any protein biomarkers that were enriched in exosomes of all source cells and at the same time depleted in microvesicles of all source cells. Nevertheless, we showed that exosomal content and microvesicle content on the proteome level differed significantly from each other independent of source cell type. Therefore, we suggest that the correlation between exosome and microvesicle content could be explored as an additional biomarker for "vesiculome" (mass spectrometry and RNASeq) studies.

Protein enrichment in exosomes distinguished cancer cells from the stem cells used in this study. If further studies on EVs derived from multiple malignant and benign cell types will confirm this observation, then protein enrichment in exosomes might become a particularly useful general

cancer marker. Furthermore, this phenomenon suggests that stem cells and cancer cells may use different mechanisms to sort proteins into EVs. Hence, the biomarker value of exosomes might lie in indicating sorting dysregulation in their source cells, whereas microvesicles are valuable for reflecting the content of their source cells.

Protein and lipid sorting into EVs did not appear to be linked: U87 and Huh7 (cancerous) cells enriched similar proteins but different lipids in their EVs, while Huh7 and MSC (yielding few and smaller exosomes) cells enriched similar lipids but different proteins in their EVs. Hence protein sorting into EVs associated best with stem or cancer cell origin in this study, whereas lipid sorting associated best with yield and size of exosomes. Further studies are needed to confirm whether these associations explain EV biogenesis mechanisms.

The current study mapped EV lipidome to a great depth, identifying almost 2000 lipid species. Since lipids are not coded in the genetic code and biological functions of most lipids detectable by mass spectrometry are unknown, data interpretation may follow biochemical/structural principles. Here we showed that not only headgroup identity, but also headgroup charge, fatty acid tail length and saturation contributed to lipid enrichment in EVs. These parameters modify the headgroup-to-tail size ratio, which, in turn, defines the spontaneous curvature of a lipid monolayer. Since EVs are small vesicles, their limiting bilayer membranes are highly curved. We found exosomes to be enriched in positive curvature promoting (free fatty acids and lysophosphatidyl derivatives, both having one tail only and favoring outer membranes) as well as negative curvature promoting (cardiolipins having four tails and favoring inner membranes) lipids. While cardiolipin is believed to exclusively reside in the inner mitochondrial membrane (a highly curved membrane itself), other mitochondrial contents (proteins) were specifically depleted from the same Huh7 and MSC exosomes. This data suggest that cardiolipin must be actively sorted

into exosomes of Huh7 cells and MSCs and it might function to stabilize these unusually small vesicles. However, a wider screen of source cell types is necessary to establish a firm correlation between cardiolipin content and exosome size. Furthermore, it is intriguing to speculate that anti-cardiolipin antibodies present in several autoimmune diseases[376] might partially be generated due to the presence of cardiolipin on circulating exosomes.

Sphingomyelins and ceramides have been implicated in exosomal biogenesis in brain cells (oligodendrocytes[377],neurons[184], neuroblastoma [310]) but not in in PC-3 cells[378]. We found enrichment of sphingomyelins in U87 glioblastoma (a brain cell type) exosomes only, whereas both sphingomyelins and ceramides were characteristically enriched in all microvesicles. Ceramide-triggered exosome formation pathway is thought to be independent of the ESCRT-mediated exosome formation pathway[377] and controls the packaging of only a subset of proteins into exosomes[184]. Hence, source cell type may influence which pathway is predominantly involved in exosome formation and which lipid sorting mechanism is applied. Different exosome formation pathways may overlap with microvesicle formation pathways in a source cell type dependent manner.

We found that structural plasma membrane lipids, including phosphatidylcholines, phosphatidylinositols, phosphatidylglycols and phosphatidylethanolamines, were depleted, whereas phosphatidylserines showed a mild enrichment in exosomes but not in microvesicles. These data are consistent with previous findings showing depletion of phosphatidylcholines and enrichment of phosphatidylserines in exosomes[363]. These lipids comprise the majority of membranes and their levels in microvesicles were more similar to source cells than their levels in exosomes.

CHAPTER VI EXOSOMES' COMPOSITION–ACTIVITY RELATIONSHIP: A PATH TOWARD THE RATIONAL DESIGN OF ARTIFICIAL EXOSOMES

6.1 PREFACE

Text and figures are reproduced from a submitted manuscript

- **Haraszti RA**, Miller R, Dubuke ML, Rockwell HE, Coles AH, Sapp E, Didiot MC, Echeverria D, Stoppato M, Sere YY, Leszyk J, Alterman JF, Godinho BMDC, Hassler MR, McDaniel J, Narain NR, Wollacott R, Wang Y, Shaffer SA, Kiebish MA, DiFiglia M, Aronin N, Khvorova A. Exosomes' composition–activity relationship: a path toward the rational design of artificial exosomes for siRNA delivery

Anastasia Khvorova, Neil Aronin and I conceptualized this project. siRNAs were synthesized by Dimas Echeverria and duplexed by me. Matthew Hassler maintained oligonucleotide synthesizers and HPLCs. I was assisted in EV preparations by Rachael Miller and Marie Didiot. Michelle Dubuke, John Leszyk and Scott Shaffer performed mass spectrometry for proteomics. Hannah Rockwell and Michael Kiebish performed mass spectrometry for lipidomics. Matteo Stoppato, Yves Sere, Rachael Wollacott and Yang Wang prepared large-scale exosomes following three-dimensional cultures. Ellen Sapp and Marian DiFiglia performed transmission electron microscopy. Andrew Coles implanted Alzet pumps to mouse brain. I was assisted by Julia Alterman and Bruno Godinho at animal harvests. I prepared liposomes, performed Western blotting, Nanoparticle Tracking Analysis, Bredford assays, loaded all vesicles, prepared primary neurons, measured all mRNA silencing and all siRNA levels in cells or tissues, performed confocal microscopy, analyzed data including proteomics and lipidomics, palmitoylated proteins and constructed artificial exosomes. I wrote this manuscript with the assistance of Anastasia Khvorova and Neil Aronin.

6.2 ABSTRACT

Exosomes can serve as delivery vehicles for advanced therapeutics. The components necessary and sufficient to support exosomal delivery properties has not been established. Here, we connect exosomal biochemical composition and activity to optimize artificial exosome-mediated delivery of small interfering RNAs (siRNAs). This information is used to create effective artificial exosomes. We show that serum-deprived mesenchymal stem cells produce exosomes up to-twenty-two-fold more effective at delivering siRNAs to neurons than exosomes derived from control cells. Proteinase treatment of exosomes stops siRNA transfer, indicating that surface proteins on exosomes are essential for trafficking. Proteomic and lipidomic analyses show that exosomes derived in serum-deprived conditions are enriched in six protein pathways and one lipid class, dilysocardiolipin. Based on this information, we engineer an "artificial exosome," in which the incorporation of one lipid (dilysocardiolipin) and three proteins (Rab7, Desmoplakin, and AHSG) into conventional neutral liposomes produces vesicles that replicate cargo delivering activity of natural exosomes. Data presented here lay out a path toward the capacity to rationally design and produce artificial exosomes in bulk for the delivery of advanced therapeutics.

6.3 INTRODUCTION

Extracellular vesicles (EVs), including exosomes (small EVs) and microvesicles (large EVs), transfer molecules, such as therapeutic RNAs[136, 308, 341], to induce phenotype change in recipient cells [132, 138, 182, 323, 379]. Critical questions impede the use of exosomes for clinical applications: (1) production of exosomes from cells is a tedious, low yield and difficult to control; (2) the essential components of active exosomes are not established; and (3) the fundamental mechanisms of exosomal delivery need to be clarified to produce artificial exosomes in bulk. We

optimized conditions to improve the delivery of exosomal cargo (siRNA), and used these optimized exosomes to find the necessary and sufficient molecules that affect exosome activity. Finally, we constructed artificial exosomes based on these findings. Our strategy aims to (1) substitute natural exosomes with reverse engineered artificial exosomes appropriate for large-scale production; (2) establish exosome composition – activity relationship *via* comparing exosomes from stressed and control cells; and (3) identify proteins and lipids mediating exosome trafficking.

Cellular stress of EV producer cells can alter the activity[380-382] as well as the protein[382-385] and RNA composition[386-387] of EVs. Therefore, relating the change in composition of EVs to the change in their activity under stressed and control conditions can establish their composition–activity relationship. Serum deprivation is a common means of inducing cellular stress[388] , is widely used in extracellular vesicle production, and has been found to alter EV number[384, 389-390], activity[384, 388, 390], and composition[332, 385]. Surface proteins[384] as well as intravesicular proteins[390] have been linked to improved EV activity upon serum deprivation. We speculate that the membrane composition (proteins and lipids) of EVs is responsible for EV intercellular trafficking activity. We show that upon serum deprivation, producer cells release exosomes, but not microvesicles, that are more efficient at delivering siRNAs to neurons (a model for intercellular trafficking). This activity change is accompanied by substantial protein and lipid composition changes. We then screen several proteins and lipids, which ae enriched in stressed exosomes, for enhancement in vesicle-mediated siRNA delivery to neurons. Subsequently we combine a candidate lipid (dilysocardiolipin) and three candidate proteins (Rab7, AHSG and Desmoplakin) from the screen into liposomes in order to construct "artificial exosomes." These artificial exosomes replicate the siRNA delivery activity of natural stressed exosomes both *in vitro* and *in vivo*.

6.4 RESULTS

Characterization of extracellular vesicles produced from control and serum-deprived mesenchymal stem cells

We incubated mesenchymal stem cells derived from umbilical cord, adipose tissue, and bone marrow in either the recommended stem cell medium depleted of EVs (*Control*) or serum-free RPMI medium for 24 hours (*Stressed*). We used differential ultracentrifugation to generate two EV populations, small and large EVs, enriched based on their sedimentation properties[204]. We refer to the EVs from a 10,000 g pellet as microvesicles, and EVs from the 100,000 g pellet as exosomes. Throughout this study we compare stressed conditions with control conditions within the same sample type: stressed cells *versus* control cells, microvesicles from stressed *versus* from control cells, and exosomes from stressed *versus* from control cells.

Mesenchymal stem cells tolerated serum deprivation for up to 4 days (**Figure 6.1A**) without loss of viability. EVs showed homogenous size distribution (**Figure 6.1B**). Exosomes and microvesicles isolated from both the control or stressed (serum deprived for 24 hours) conditions displayed positive and were devoid of negative protein markers of EVs (**Figure 6.1C**) and appeared as lipid bilayer-surrounded vesicles on transmission electron microscopy (**Figure 6.1D**). Serum deprivation did not affect the exosome yield from umbilical cord-derived cells ($p=0.3$) but significantly decreased the exosome yield from both adipose= and bone marrow-derived cells (6-fold, $p=0.04$ and 10-fold, $p=0.002$ respectively, **Figure 6.2A**). Serum deprivation did not alter the amount of microvesicles (**Figure 6.2B**). Exosomes derived from umbilical cord mesenchymal stem cells were slightly larger than exosomes from either adipose tissue and bone marrow cells (142±14 nm, 110±19 nm, and 117±10 nm, respectively). Serum deprivation did not affect EV size (**Figure 6.2C-D**). Protein-to-particle ratio varied substantially between vesicles from different

sources and was affected by serum deprivation for some EV populations (**Figure 6.2E-F**). Umbilical cord-derived exosomes had the lowest protein-to-particle ratio, which remained unchanged upon serum deprivation (**Figure 6.2E-F**).

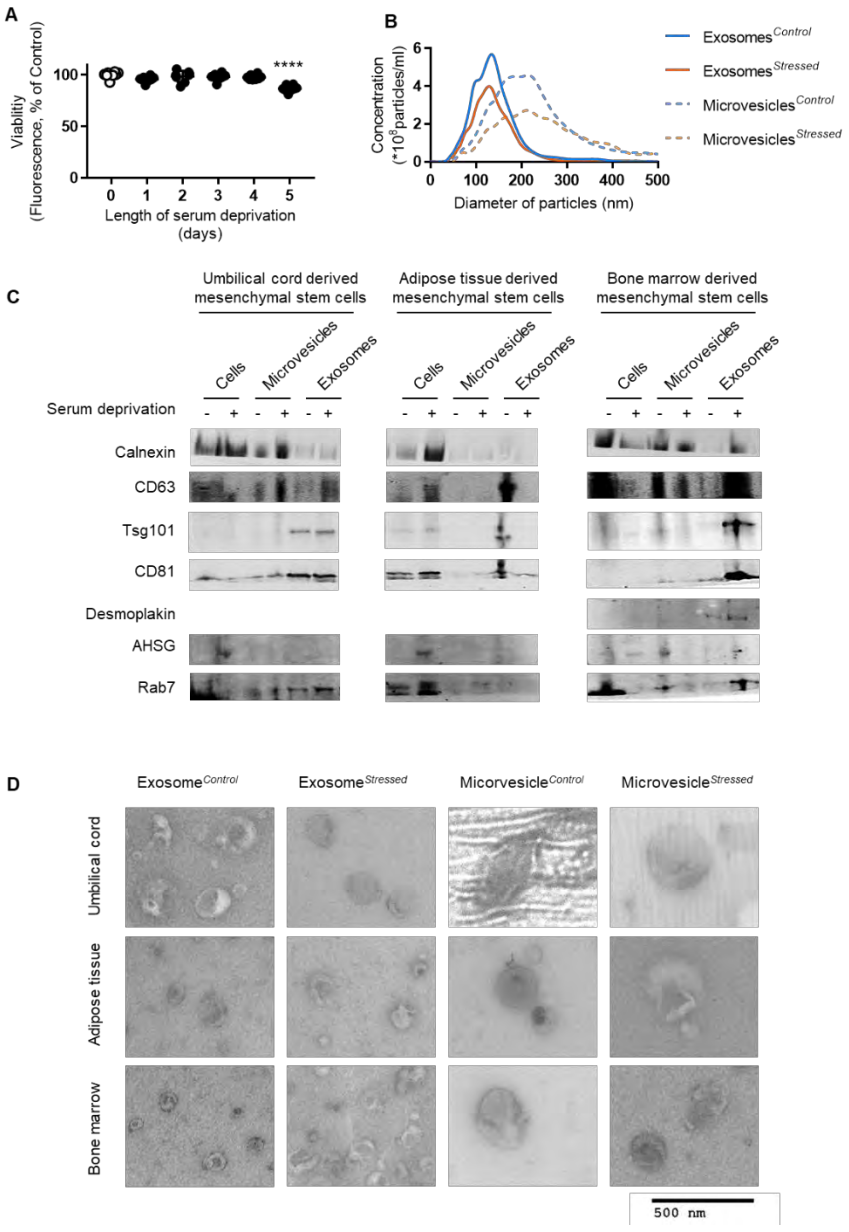

Figure 6.1 Characterization of cell culture conditions and extracellular vesicles.

A. Umbilical cord derived mesenchymal stem cells were cultured in either the recommended stem cell medium or in RPMI for differing times. Alamar Blue® was added an incubated at 37°C for 12 hours, and fluorescence measured at 570 nm excitation, 585 nm emission. Signal is normalized to not serum deprived samples. N = 8, mean ± SD, one-way ANOVA. **B.** Representative size distribution curves of EVs enriched from umbilical cord derived mesenchymal stem cells, N=3, mean, Nanoparticle Tracking Analysis. **C.** Western blots of cells, microvesicles and exosomes derived under control

or serum deprived conditions from umbilical cord, adipose tissue or bone marrow derived mesenchymal stem cells. Negative marker: calnexin. Positive markers: CD63, Tsg101, CD81. Proteins shown to be enriched in Exosomes^{Stressed} or Cell^{Stressed}: Desmoplakin, AHSG, Rab7. **D.** Representative transmission electron microscopy images of EVs derived under control or serum deprived conditions from umbilical cord, adipose tissue or bone marrow derived mesenchymal stem cells.

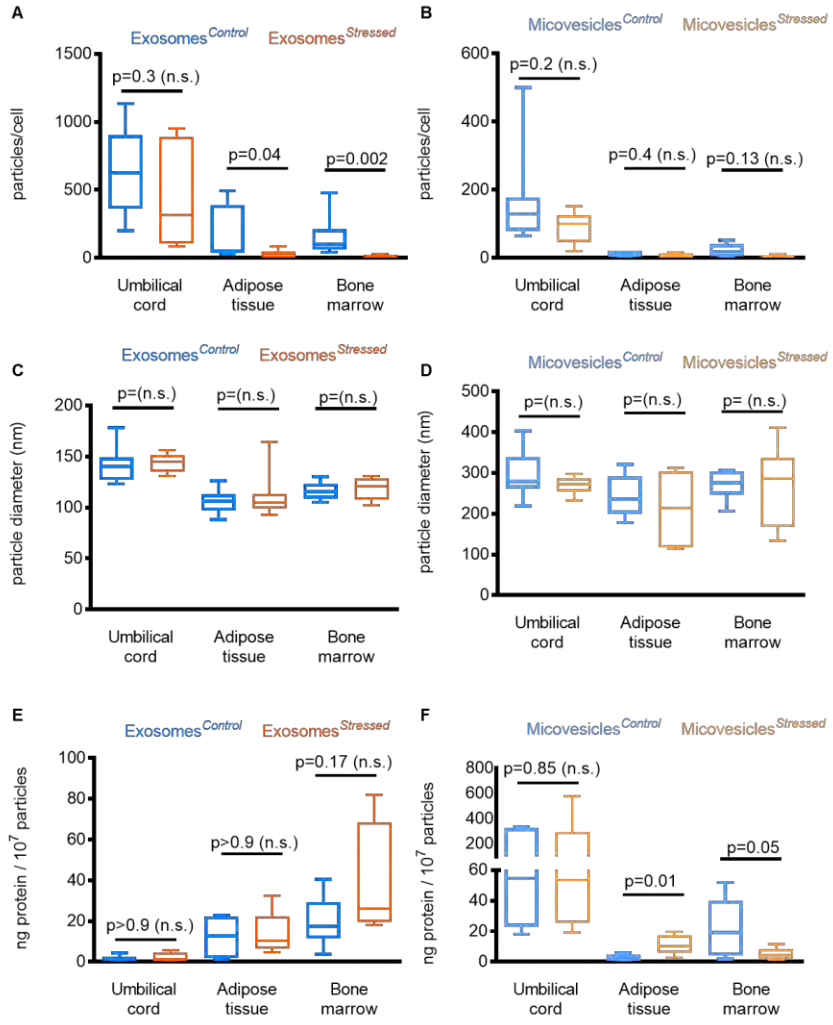

Figure 6.2 Serum deprivation of source cells alters yield and protein-to-vesicle ratio of extracellular vesicles. Extracellular vesicles (EVs) were purified from umbilical cord, adipose tissue or bone marrow derived mesenchymal stem cells *via* differential ultracentrifugation. Cells were cultured under control condition or serum deprived for 24 hours. N=7, lines represent mean, boxes represent 25-75 percentile range and whiskers represent the minimum and maximum value in each group. n.s. = non-significant (p>0.05), Mann-Whitney test **A.** Yield, **C.** Size, and **E.** Protein-to-particle ratio of exosomes enriched from

conditioned media of control or stressed mesenchymal stem cells *via* differential ultracentrifugation (100 000 g fraction). **B.** Yield, **D.** Size, and **F.** Protein-to-particle ratio of microvesicles enriched from conditioned media of control or stressed mesenchymal stem cells *via* differential ultracentrifugation (10 000 g fraction).

Upon serum deprivation, mesenchymal stem cells release exosomes (but not microvesicles), which are more efficient in delivery of siRNA

Extracellular vesicles transport RNA between cells[132, 138, 190]. We previously have shown that exosomes can productively transfer loaded cholesterol-conjugated siRNAs to neurons[135]. Here we loaded *Huntingtin*-targeting, cholesterol-conjugated siRNA[233] to exosomes and treated primary neurons as a model for exosome trafficking. We evaluated the rates of exosome uptake to neurons using confocal microscopy and quantified the level of guide strand accumulation and target mRNA silencing in neurons.

First, exosomes isolated from serum-deprived cells ($Exosomes^{Stressed}$) delivered more siRNA to target neurons compared to $Exosomes^{Control}$ across all mesenchymal stem cell origins tested (**Figure 6.3A-C**). Second, when loaded with fluorescently labeled siRNA, $Exosomes^{Stressed}$ showed an approximately two-fold faster neuronal uptake kinetic (half-time 1.7 *versus* 3.8 hours, $p<0.0001$) (**Figure 6.4A-B**). Finally, siRNA-containing $Exosomes^{Stressed}$ were five-to-twenty-two-fold more efficient at inducing *Huntingtin* mRNA silencing than $Exosomes^{Control}$ (**Figure 6.3D-F**).

Stress-dependent enhancement in activity was characteristic of exosomes and not of microvesicles, where serum deprivation impaired activity (**Figure 6.3G-I**). These data indicated that activity enhancement upon stress depended on an exosome-specific characteristic. Protein

composition is one characteristic that differs between exosomes and microvesicles[332, 391], therefore worth investigating in this context.

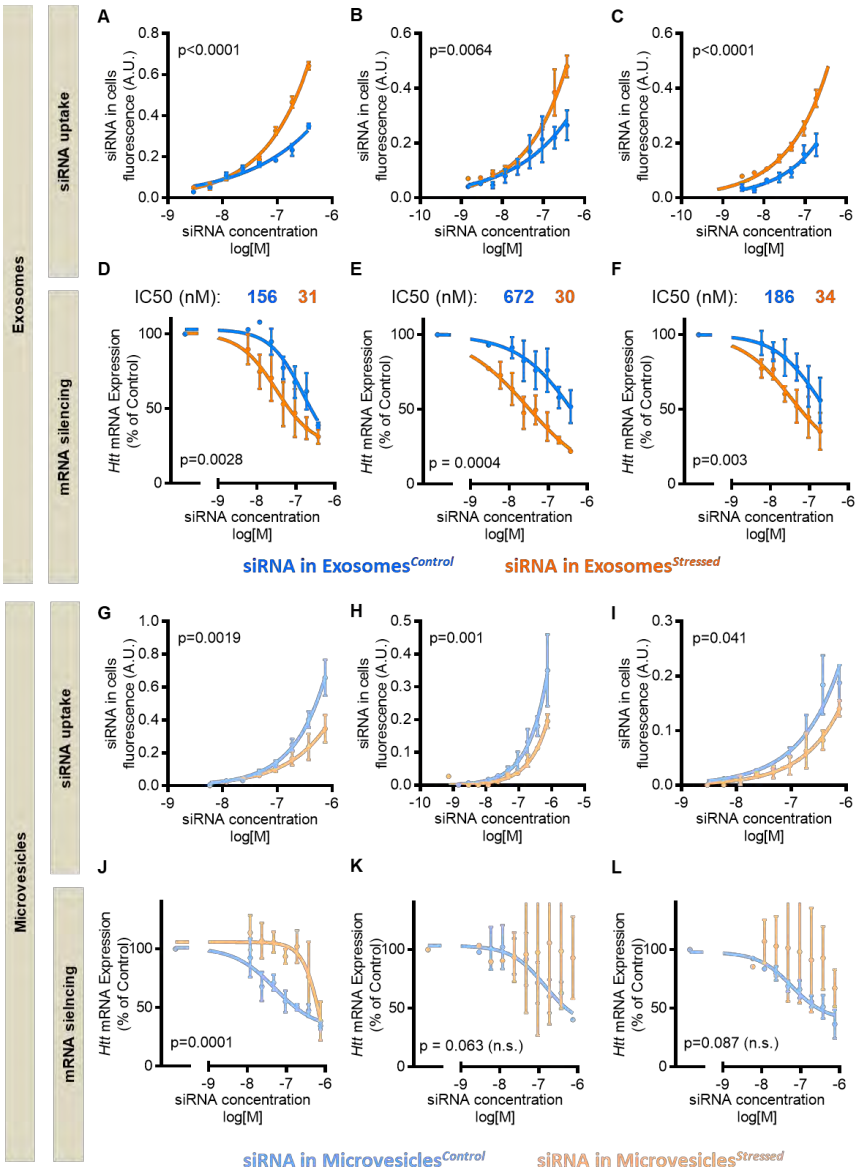

Figure 6.3 Serum deprivation of mesenchymal stem cells improves exosome activity but impairs microvesicle activity. Primary neurons were treated with fluorescent siRNA-containing exosomes or microvesicles derived from control or stressed (serum deprived) cells. After 7 days of incubation, siRNA levels and target mRNA levels were quantified in neurons. mRNA levels were normalized to housekeeping gene and to untreated control. N=3, mean ± SEM, curves were compared using two-way ANOVA. **A-C.** uptake of siRNA into neurons delivered *via* exosomes. **D-F.** mRNA silencing induced by treatment of siRNA-containing exosomes. **G-I.** uptake of siRNA into neurons delivered *via* microvesicles. **J-L.** mRNA silencing induced by treatment of siRNA-containing microvesicles. **A., D., G., J.** EVs

enriched from umbilical cord derived mesenchymal stem cells. **B., E., H., K.** EVs enriched from adipose tissue derived mesenchymal stem cells. **C., F., I., L.** EVs enriched from bone marrow derived mesenchymal stem cells.

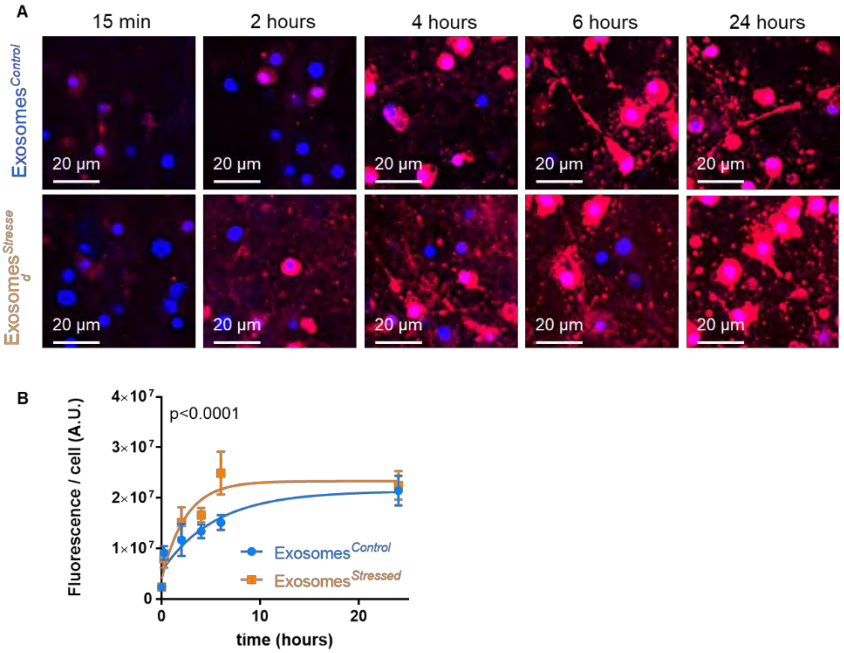

Figure 6.4 Neuronal uptake of control and stressed exosomes. Primary cortical neurons were cultures on glass bottom plates and treated with fluorescent siRNA containing Exosomes^{Control} or Exosomes^{Stressed}. **A.** Fluorescence was monitored over time using confocal microscopy. Red: siRNA, Blue: nuclei. **B.** Red signal in images were quantified in ImageJ software, N= 39-50 cells per timepoint and kinetic curves compared using two-way ANOVA.

Serum deprivation of mesenchymal stem cells substantially alters protein composition of exosomes

To evaluate serum deprivation-induced changes in the protein composition of exosomes, we performed LC-MS/MS proteomic analysis. We collected data from three independent repeats of (1) control or serum-deprived mesenchymal stem cells (derived from umbilical cord, adipose

tissue, or bone marrow); (2) microvesicles from control or serum-deprived cells; and (3) exosomes from control or serum-deprived cells.

As expected, serum deprivation had a profound effect on the proteome of cells, microvesicles, and exosomes, consistent in biological replicates (**Figure 6.5A-C., Figure 6.6-6.8**). Protein composition differed substantially between exosomes and microvesicles (**Figure 6.6-6.8**). Proteins enriched in stressed exosomes were either unchanged or depleted in corresponding microvesicles and source cells (**Figure 6.6-6.8**, **Figure 6.5D-F**).

Gene Ontology analysis showed enrichment of extracellular exosome, proteasome, membrane, desmosome, cell-cell adhesion, ribosome, and Golgi proteins in Exosomes^{Stressed} fractions throughout all cell sources tested (**Figure 6.5G-I**). We speculated that membrane, desmosome and cell-cell adhesion proteins may play a role in enhanced cellular uptake of stressed exosomes. In addition, categories often described in exosomes (multivesicular body, endosome, histone, tetraspanin) and categories not yet endoplasmic reticulum, ER-to-Golgi transport, and chaperone proteins were enriched in Exosomes^{Stressed} derived from at least two of three cell sources tested (**Figure 6.5G-I**).

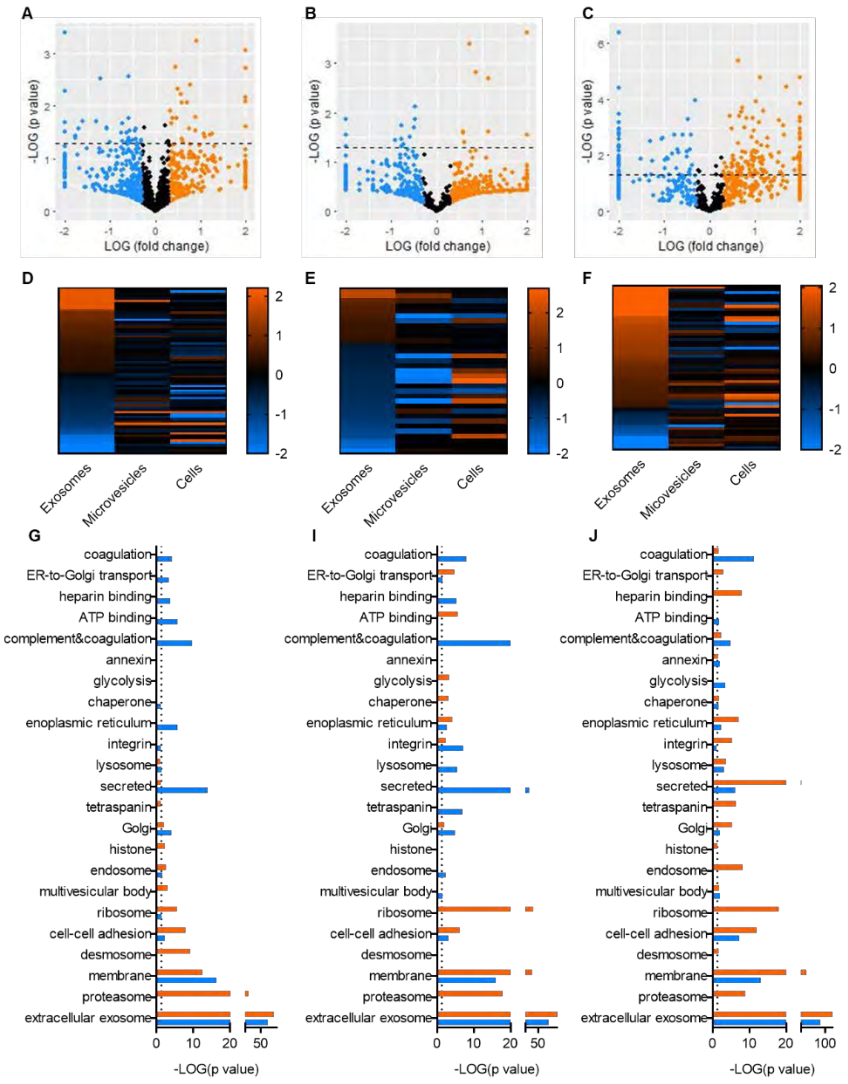

Figure 6.5 Serum deprivation of source cells alters protein content of released exosomes. Exosomes, microvesicles and cells derived from control conditions or stress conditions (serum deprivation) underwent LC-MS/MS proteomics analysis. N=3 biological replicates were analyzed and label-free quantification carried out using intensity-based absolute quantification method. **A-C.** volcano plots of proteins detected in exosome. Orange dots represent proteins enriched at least 2-fold in Exosomes^{Stressed} and blue dots represent proteins enriched at least 2-fold in Exosomes^{Control}. Dashed line marks the threshold of significance (p=0.05, t-test with Benjamini-Hochberg correction for multiple comparison). Proteins above the dashed line significantly differ between Exosomes^{Stressed} and Exosomes^{Control}. Proteins detected in one group and absent in the other group were arbitrarily assigned the fold change of 20 or -20. **D-F.** Heatmaps of proteins different (p<0.1) in Exosomes^{Stressed} *versus* Exosomes^{Control}. Orange represents enrichment in stressed conditions

versus control conditions (Exosomes^{Stressed} *versus* Exosomes^{Control}, Microvesicles^{Stressed} *versus* Microvesicles^{Control}, and Cells^{Stressed} *versus* Cells^{Control}), whereas blue represents enrichment in control conditions *versus* stress conditions. **G-I.** Gene Ontology analysis of proteins at least 2-fold enriched in Exosomes^{Stressed} or Exosomes^{Control} (e.g. proteins labeled orange or blue in panels A-C.). **A., D. and G.** Umbilical cord derived mesenchymal stem cells. **B., E. and I.** Adipose tissue derived mesenchymal stem cells. **C., F. and J.** Bone marrow derived mesenchymal stem cells.

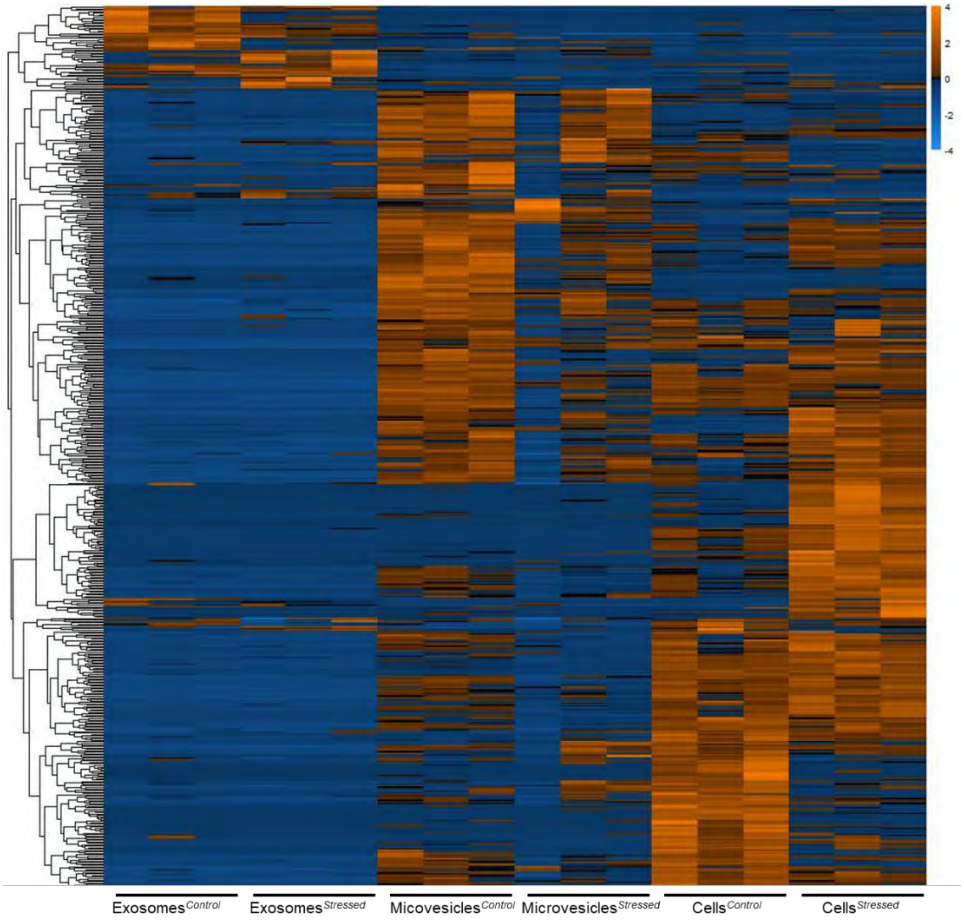

Figure 6.6 Proteomics analysis of umbilical cord derived mesenchymal cells and EVs under control or stressed conditions. Label-free quantification was carried out using the intensity-base absolute quantification method. Heatmap was then generated in R, using "pheatmap" package, hierarchical clustering of rows, scaling method: "row".

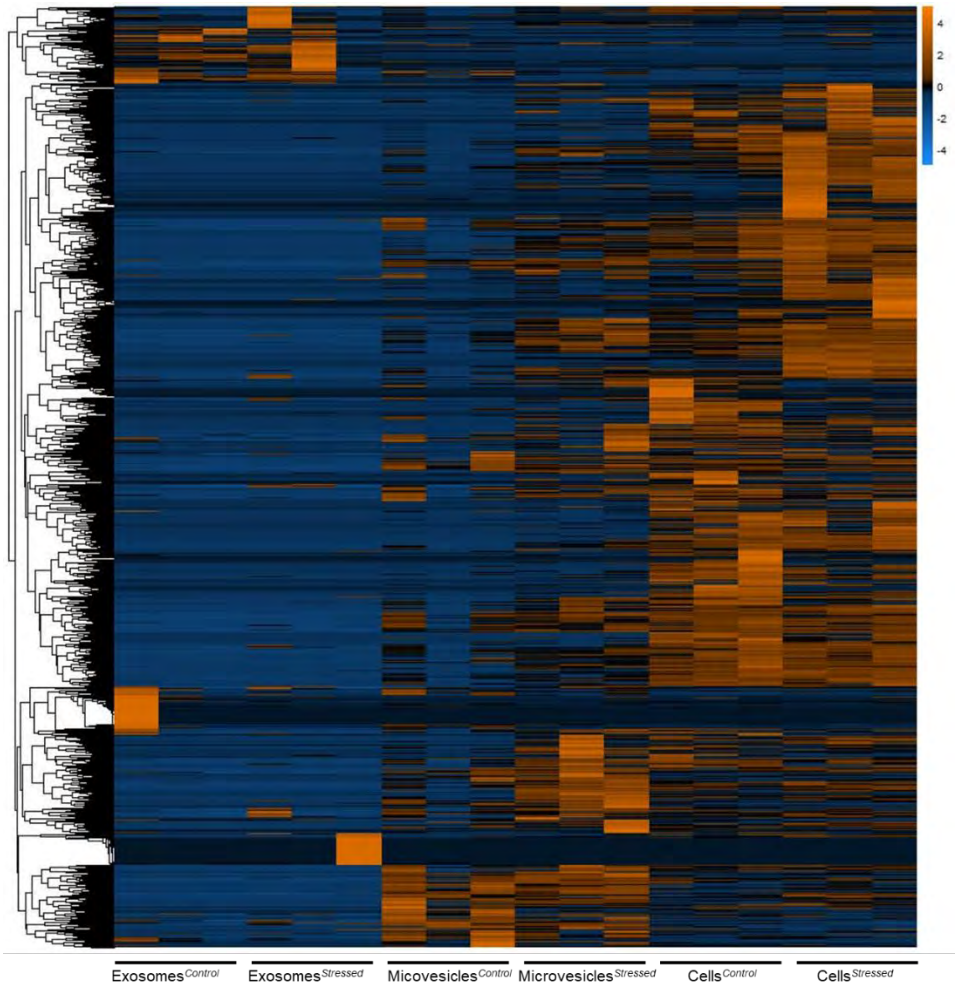

Figure 6.7 Proteomics analysis of adipose tissue derived mesenchymal cells and EVs under control or stressed conditions. Label-free quantification was carried out using the intensity-base absolute quantification method. Heatmap was then generated in R, using "pheatmap" package, hierarchical clustering of rows, scaling method: "row".

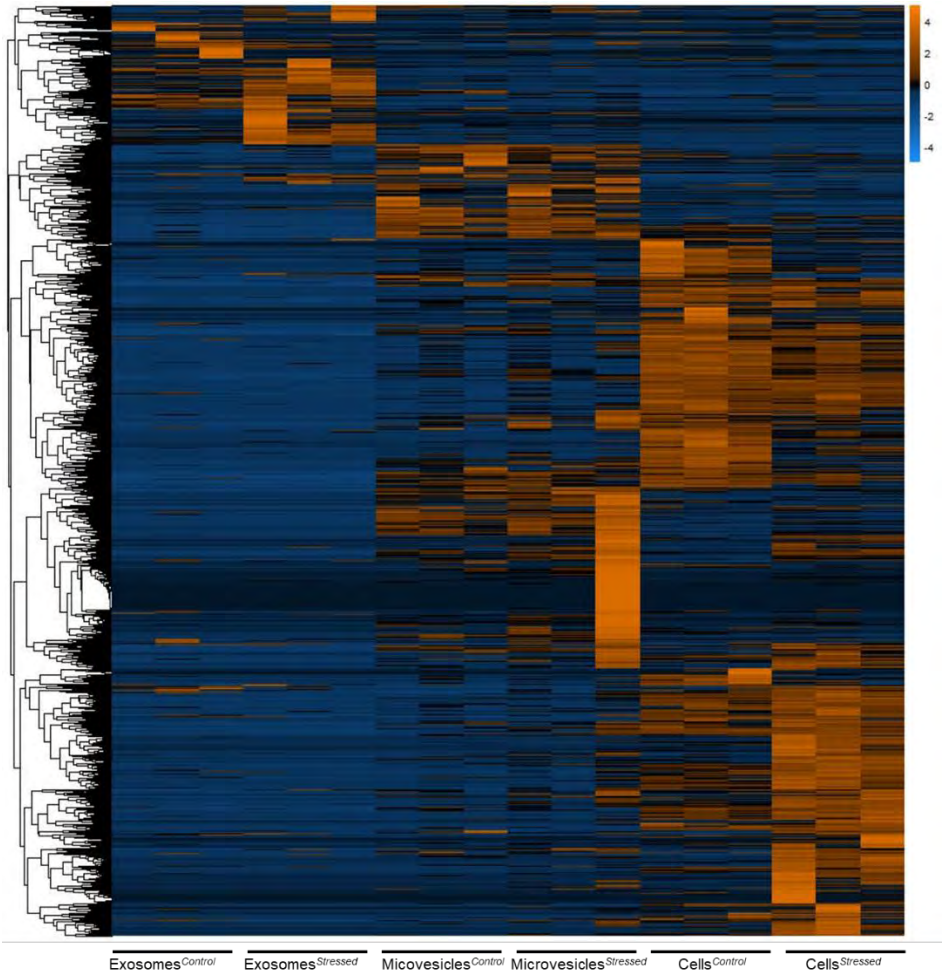

Figure 6.8 Proteomics analysis of bone marrow derived mesenchymal cells and EVs under control or stressed conditions. Label-free quantification was carried out using the intensity-base absolute quantification method. Heatmap was then generated in R, using "pheatmap" package, hierarchical clustering of rows, scaling method: "row".

Several proteins enriched in stressed exosomes contribute to improved siRNA transfer to neurons

Altered surface protein composition may explain the enhanced activity of Exosomes^{Stressed}. Proteinase K treatment (degrades surface proteins) impaired the exosome-mediated siRNA transfer and resulted in *Huntingtin* silencing (**Figure 6.9A-B**), confirming that exosomes' surface proteins are essential for the delivery of cargo into neurons. The difference in the activity of Exosomes^{Stressed} over Exosomes^{Control} is not related to potential inhibition by serum proteins present, as incubation with serum-containing (EV-depleted) media had no effect on Exosomes^{Stressed} activity (**Figure 6.9A**).

To establish a protein composition–activity relationship in exosomes, we selected proteins that (1) have an established role in vesicle trafficking or membrane adhesion, and (2) were enriched in stressed exosomes derived from at least two of three mesenchymal stem cell sources. Based on these criteria, the shortlist included proteins from endosomal pathways (Rab5 and Rab7[392]), plasmamembrane budding (ARRDC1[393]), secreted proteins interacting with membranes (dermcidin[394]), desmosome (Desmocollin, Desmoplakin[395]), and nucleo-extracellular shuttles (AHSG and Histone 1[396]) (**Figure 6.9C**). AHSG has been reported to shuttle histones from the nucleus to exosomes[396] and was consistently enriched in stressed cells (not present in EVs) (**Figure 6.9C**), whereas histones were specifically enriched in stressed exosomes (**Figure 6.5G-I, Figure 6.9C**). The enrichment of Desmoplakin and Rab7 in stressed exosomes and AHSG in stressed cells has been independently confirmed on Western blots (**Figure 6.1D**).

Purified proteins were chemically palmitoylated and co-incubated with neutral liposomes (dioleoyl-phosphatidylcholine: cholesterol, 7:3) in order associate to the liposome surface. Palmitoylation has been reported as a strategy to enrich proteins associated to exosomal

memrbanes[146]. Incorporation of Rab7, Desmoplakin, and AHSG improved liposome-mediated siRNA transfer to neurons and improved *Huntingtin* mRNA silencing ($p<0.0001$ two-way ANOVA, **Figure 6.9D**). Incorporation of Rab5, Desmocollin, ARRDC1, Dermcidin, and Histone 1 had no effect (**Figure 6.9D**). Thus, incorporation of at least three candidate proteins from the proteomic analysis to the liposome surface affected the efficiency of vesicle transfer to neurons.

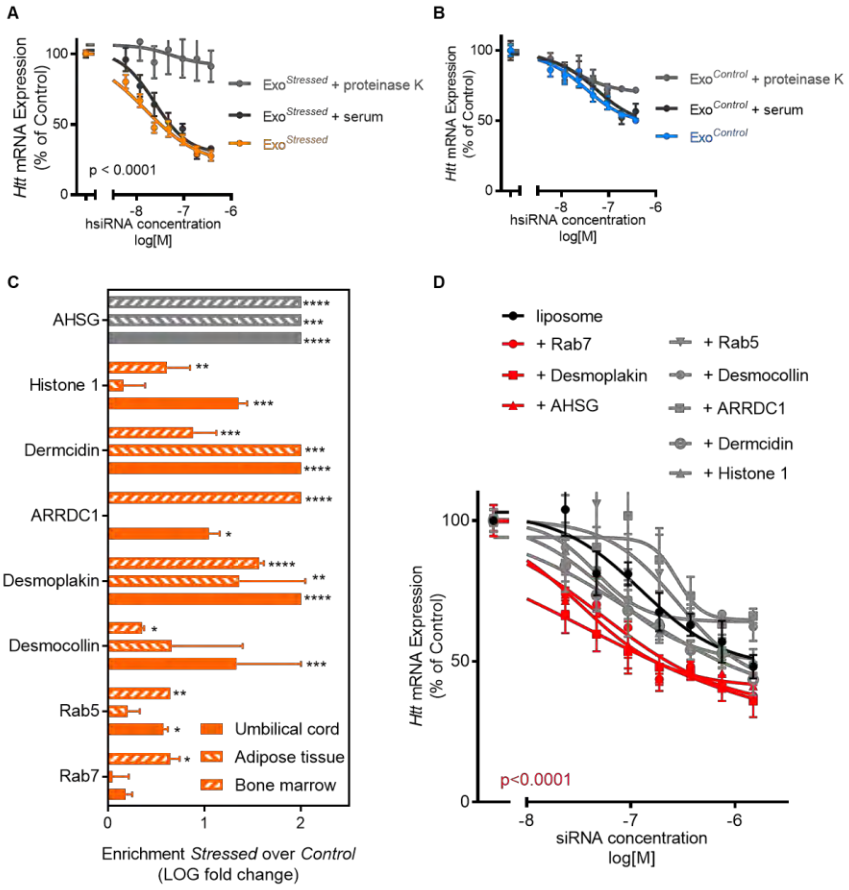

Figure 6.9 Proteins enriched in stressed exosomes contribute to improved siRNA transfer to neurons.

A-B. Exosomes were enriched from serum starved (**A.**) or control (**B.**) umbilical cord derived mesenchymal stem cells and either not further treated or treated with proteinase K or EV-depleted serum containing medium (serum). Primary neurons were then treated with the above exosome variants containing siRNAs and mRNA levels in neurons quantified after seven days of incubation. N=5, mean ± SEM, curves compared using two-way ANOVA. **C.** Enrichment of selected proteins in Exosomes^{Stressed} *versus* Exosomes^{Control} (orange) or in Cells^{Stressed} *versus* Cells^{Control} (grey). Proteins detected in stressed conditions but absent in

control conditions were arbitrarily assigned the fold change of 20. N=3, mean ± SEM. Two-way ANOVA, **** $p<0.0001$, *** $p<0.001$, ** $p<0.01$, * $p<0.05$. **E.** Primary neurons were treated with siRNA containing liposomes alone or liposomes incorporating purified proteins from panel C. and target mRNA levels in neurons quantified after 7 days of incubation. N=4, mean ± SEM, two-way ANOVA.

Dilysocardiolipin enrichment in stressed exosomes contributes to improved trafficking to neurons

Membrane composition is a likely contributor to the enhanced trafficking activity of stressed exosomes. Membrane trafficking is regulated by both proteins and lipids[397-398]. To evaluate the effect of serum deprivation on the lipid composition of exosomes, we performed MS/MS^{ALL} lipidomic analysis. Among all lipid classes detected, only cardiolipins showed significant enrichment in exosomes derived from serum-deprived cells ($p=0.004$, two-way ANOVA) (**Figure 6.10A** and **Figure 6.11A**). Similar to protein enrichment, cardiolipin enrichment was specific to stressed exosomes and did not occur in corresponding cells and microvesicles (**Figure 6.10A**). In addition, we have observed a modest but statistically significant enrichment in unsaturated and long-tailed cardiolipins in stressed exosomes (**Figure 6.11B-C**).

Cardiolipin is a diphosphatidylglycerol lipid with four fatty acid tails (**Figure 6.10B**). Hydrolytic removal of one or two fatty acid tails results in the formation of monolysocardiolipin (**Figure 6.10C**) or dilysocardiolipin (**Figure 6.10D**), known intermediates in cardiolipin remodeling[399]. Cardiolipin remodeling has been associated with highly curved membranes[400].

Among different cardiolipin subclasses, dilysocardiolipins showed the highest enrichment in stressed exosomes (sixteen-fold, $p<0.0001$), followed by intact cardiolipins (nine-fold, $p<0.0001$), and monolysocardiolipins (six-fold, $p<0.0001$) (**Figure 6.10E**), compared to control exosomes. Cardiolipin subclass enrichment was specific to stressed exosomes and was not observed in corresponding microvesicles and cells (**Figure 6.10E**).

To test whether cardiolipins play a role in vesicle trafficking to neurons, we incorporated intact cardiolipin, monolysocardiolipin, or dilysocardiolipin (30% of total lipid amount) in conventional liposomes (dioleoyl-phosphatidylcholine, cholesterol). Incorporation of dilysocardiolipin but not other variants into liposomes improved siRNA transfer to neurons and resulted in *Huntingtin* silencing ($p=0.007$, two-way ANOVA) (**Figure 6.10F**). Thus, dilysocardiolipin enrichment in stressed exosomes might be a contributing factor to enhanced neuronal uptake.

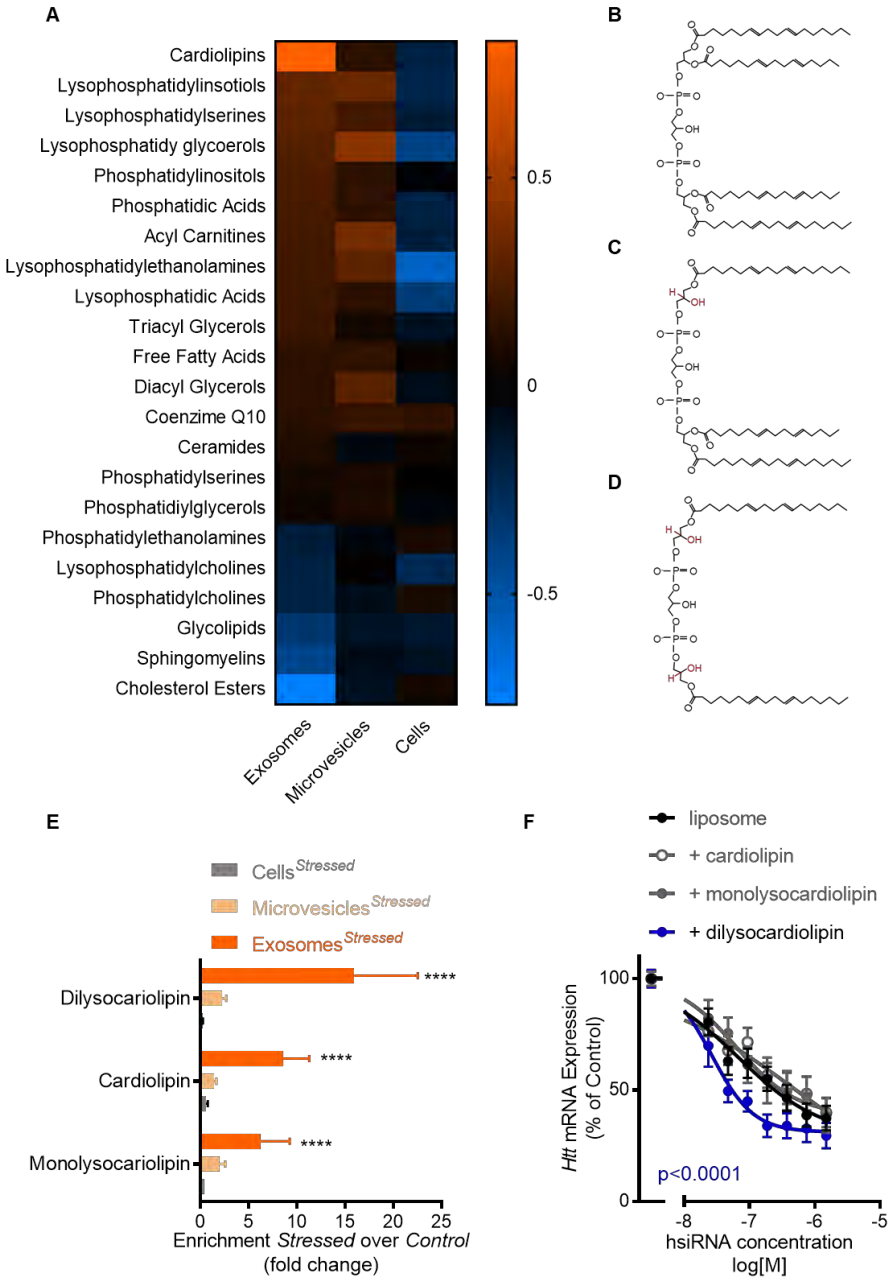

Figure 6.10 Dilysocardiolipin enrichment in stressed exosomes contributes to improved trafficking to neurons.

Exosomes purified from umbilical cord derived mesenchymal stem cells under control conditions or stress conditions (serum deprivation) underwent MS/MS^{ALL} lipidomics analysis. N=2-5 biological replicates were analyzed per group. **A.** Heatmap of lipid classes in stressed conditions *versus* control conditions. Orange represents enrichment in Exosomes^{Stressed} *versus* Exosomes^{Control}, Microvesicles^{Stressed} *versus* Microvesicles^{Control}, and Cells^{Stressed} *versus* Cells^{Control}, whereas blue represents enrichment in control conditions *versus* stress conditions. **B.** Scheme of cardiolipin. Length and saturation of fatty acid tails depicted is representative only and varies

between natural cardiolipin species. **C.** Scheme of monolysocardiolipin. Differences to cardiolipin is shown in red. Length and saturation of fatty acid tails depicted is representative only and varies between natural monolysocardiolipin species. **D.** Scheme of dilysocardiolipin. Differences to cardiolipin is shown in red. Length and saturation of fatty acid tails depicted is representative only and varies between natural dilysocardiolipin species. **E.** Enrichment of cardiolipin subclasses from panels B-D. in Exosomes^{Stressed} *versus* Exosomes^{Control} (dark orange), Microvesicles^{Stressed} *versus* Microvesicles^{Control} (light orange), and in Cells^{Stressed} *versus* Cells^{Control} (grey). Two-way ANOVA, **** $p<0.0001$. **F.** Primary neurons were treated with siRNA containing liposomes alone or liposomes incorporating lipids from panel E. and target mRNA levels in neurons quantified after seven days of incubation. N=4, mean ± SEM, two-way ANOVA.

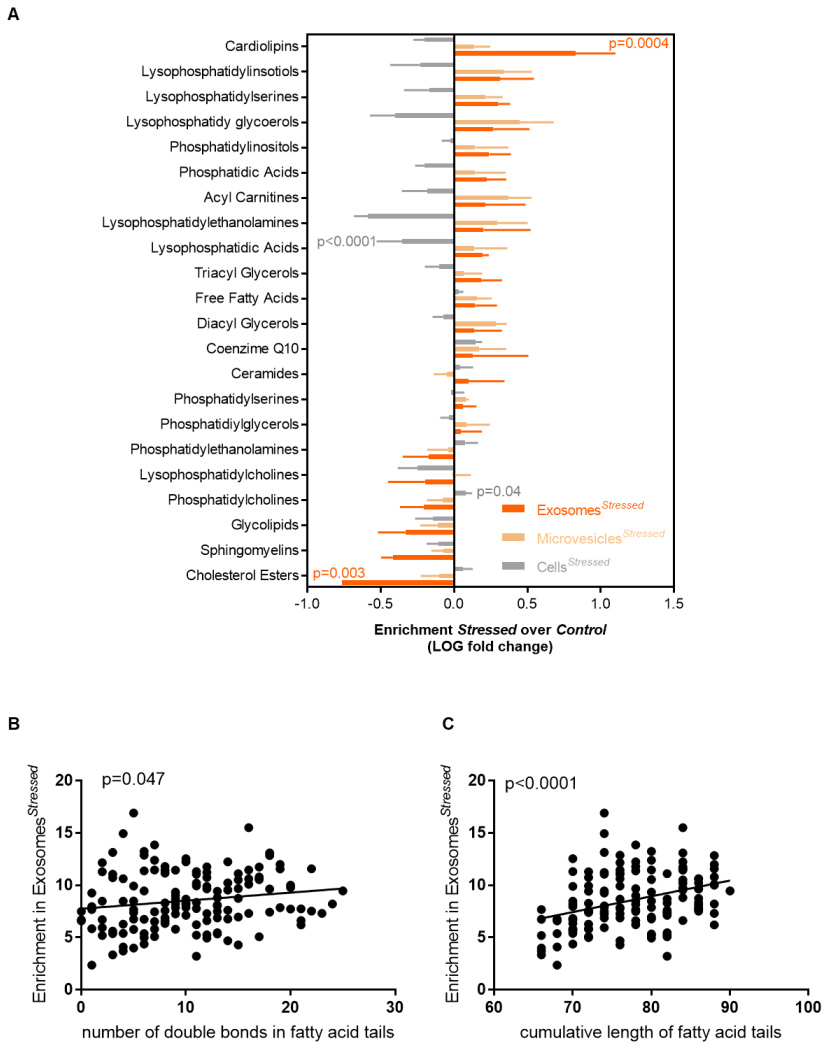

Figure 6.11 Serum deprivation of umbilical cord derived mesenchymal stem cells alters lipid composition of exosomes.

Umbilical cord derived mesenchymal stem cells and EVs from control or stress conditions (serum deprivation) underwent MS/MS^{ALL} lipidomics analysis. **A.** Bar graph shows of lipid classes in stressed conditions *versus* control conditions. Exosomes^{Stressed} *versus* Exosomes^{Control} (dark orange), Microvesicles^{Stressed} *versus* Microvesicles^{Control} (light orange), and Cells^{Stressed} *versus* Cells^{Control} (grey). N = 2-5, mean ± SD, two-way ANOVA. **B.** Correlation of enrichment in Exosomes^{Stressed} *versus* Exosomes^{Control} with the cumulative number of double bonds in the fatty acid tails of a cardiolipin species (N = 149). Each dot represents a cardiolipin species. **C.** Correlation of enrichment in Exosomes^{Stressed} *versus* Exosomes^{Control} with the cumulative length of the fatty acid tails of a cardiolipin species (N = 149). Each dot represents a cardiolipin species.

Artificial exosomes are equally active at siRNA delivery as natural exosomes *in vitro* and *in vivo*

Having identified three proteins and one lipid class to be enriched in Exosomes^{Stressed} and thereby improve vesicle uptake into neurons, we decided to explore whether we can engineer an artificial exosome displaying similar activity to that of Exosomes^{Stressed}. We combined common liposome components (dioleoylphosphatidylcholine and cholesterol) with dilysocardiolipin and palmitoylated Rab7, Desmoplakin, and AHSG in a proteoliposome (Exosome^{Artificial}). Incorporation of three proteins and one lipid to liposomes significantly improved liposome-mediated siRNA transfer to neurons ($p<0.0001$, two-way ANOVA) (**Figure 6.12A**). The efficiency of siRNA-containing artificial exosomes in *Huntingtin* silencing was indistinguishable from that of stressed exosomes (**Figure 6.12A**)

To evaluate if siRNA-containing artificial exosomes will support *Huntingtin* silencing *in vivo,* we compared siRNA-containing natural exosomes and artificial exosomes infused into mouse brain. For the *in vivo* study, natural exosomes were produced using a combination of three-dimensional xenofree mesenchymal stem cell culture and tangential flow filtration-based exosome isolation (Exosomes$^{Large\text{-}Scale}$) (Haraszti *et al*. in review). This method enabled us to collect a sufficient number of exosomes necessary to power the *in vivo* studies. Natural exosomes (Exosomes$^{Large\text{-}Scale}$**)** showed an activity indistinguishable from that of Exosomes^{Stressed} and Exosomes^{Artificial} *in vitro* in primary neurons (**Figure 6.12A**). When infused to the lateral ventricle of the mouse brain, both siRNA containing Exosomes$^{Large\text{-}Scale}$ and Exosome^{Artifical} induced *Huntingtin* mRNA (**Figure 6.12B-C**) silencing, whereas control liposomes, non-targeting-control siRNA containing vesicles, and non-formulated siRNA were inactive (**Figure 6.12B-C**).

This study introduces the concept of reverse engineering exosomes using mass spectrometry data of exosome composition with different activities (**Figure 6.12D**). First, the introduction of a stress factor (*i.e.*, serum deprivation) into exosome-producing cells improves exosome activity by altering protein and lipid composition. Second, proteins and lipids enriched in stressed exosomes are validated for contribution to enhanced vesicle trafficking to target cells. Finally, purified versions of the proteins and lipids identified in the second step are associated with neutral liposomes. This proof-of-concept study introduces a reverse engineering approach to building protein and lipid components into artificial exosomes, which then exhibit the essential biological activity of natural exosomes, similar to the construction of minimal artificial cells[401].

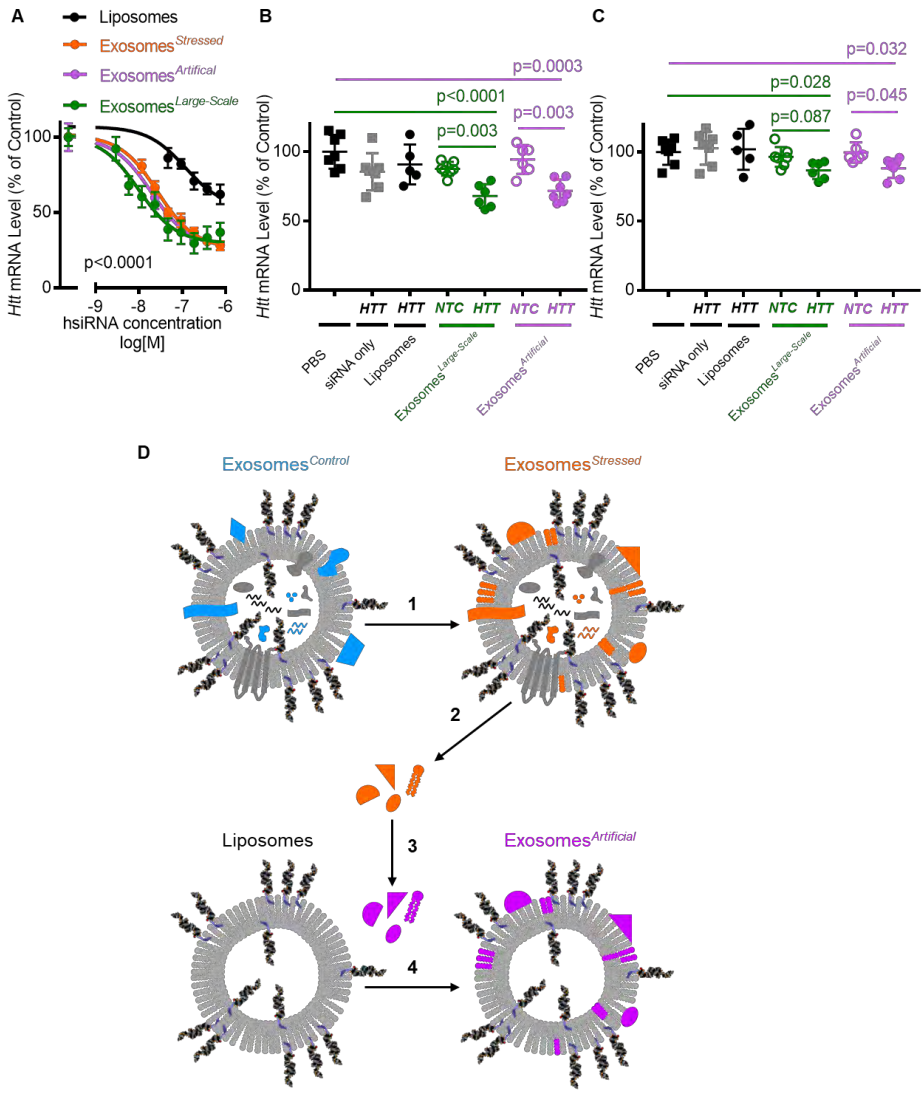

Figure 6.12 Artificial exosomes recapitulate the activity of stressed exosomes.

A. Primary neurons were treated with siRNA containing Exosomes^{Stressed}, Exosome$^{Large\text{-}Scale}$ or Exosomes^{Articial} and target mRNA levels in neurons quantified after seven days of incubation. Exosomes^{Stressed} and Exosome$^{Large\text{-}Scale}$ were enriched from umbilical cord derived mesenchymal stem cells *via* differential ultracentrifugation or tangential flow filtration, respectively. Exosomes^{Articial} consisted of dioleoylphosphatidylcholine, cholesterol, dilysocardiolipin, Rab7, Desmoplakin and AHSG. N=5, mean ± SEM, two-way ANOVA. **B-C.** *Huntingtin* (*HTT*) – targeting or non-targeting control (*NTC*) siRNAs were infused into the lateral ventricle of mice either alone, or in liposomes, Exosome$^{Large\text{-}Scale}$ or Exosomes^{Articial} . *Huntingtin* mRNA were quantified four weeks after infusion in striatum (**B.**) and motor cortex (**C.**). N = 5-7, mean ± SD, one-way ANOVA. **D.** Exosomes enriched from cells in control conditions contain a lipid bilayer,

specific (blue) proteins (shapes) and nucleic acids (lines) as well as universal (grey) lipids, proteins and nucleic acids. Cholesterol-siRNA associates to the membrane of vesicles (cholesterol: dark blue, siRNA: black). Upon serum deprivation (Step 1), exosomes contain a lipid bilayer with specific (orange) lipids, proteins and nucleic acids as well as universal (grey) lipids, proteins and nucleic acids. Proteins and lipids enriched in Exosomes^{Stressed} (orange) are identified and validated (Step 2) for enhancing vesicle trafficking to target cells based on Figures 4. and 5. Then, purified versions of above lipids and proteins are obtained (magenta, Step 3) and incorporated into lipid bilayer liposomes (Exosomes^{Artificial}, Step 4).

6.5 DISCUSSION

Extracellular vesicles (EVs) exhibit specific and efficient intercellular trafficking activity[132, 138, 182, 323, 379] and therefore are promising delivery vehicles of various classes of therapeutic proteins and RNAs[136, 308, 341]. However, the mechanisms imparting specific trafficking activity to EVs are unknown. The identification of components necessary and sufficient to make a vesicle behave like an EV would open a new chapter to overcome the delivery challenge of protein- and nucleic acid-based advanced therapeutics.

Serum deprivation is often used to enhance EV activity [384, 388-390] and induces an integrated cellular stress response[402-404] supporting a considerable change in the cellular[403-405] and secreted proteome[406-407]. Here we relate serum deprivation-induced changes in EV membrane composition to EV-mediated siRNA delivery with the aim of identifying EV components capable of replicating EV activity.

Serum deprivation of source cells may differentially influence the yield and activity of released EVs. Here we find that serum deprivation of mesenchymal stem cells increases the

activity but decreases the yield of exosomes. In contrast, serum deprivation decreases the activity but does not alter the yield of microvesicles. The concept that serum deprivation may alter the yield of different EV subclasses into different directions has been raised before[332]. However, the notion that serum deprivation may increase the activity of one EV subclass but decrease the activity of another EV subclass produced from the same cells is novel. This observation indicates that exosome and microvesicle production pathways are differentially regulated in stress conditions.

Exosomes released from stressed cells exhibit a specific enhancement in activity and a specific protein composition. Therefore, stressed exosomes are ideally suited for composition–activity relationship studies. The protein content of EVs from serum-deprived and control cells has been shown to differ[332, 385]. The functional 20S proteasome, all subunits of which we find specifically enriched in stressed exosomes, has been detected in EVs before[332, 408] and has been proposed to be of therapeutic value[409]. We also observe enrichment in desmosomal proteins, ribosomal proteins, histones, and endosomal proteins, all of which have been reported in EVs and are proposed to play a role in an EV release mechanism[396, 410-415]. Several strategies have been successfully applied to modulate the surface of EVs: expressing proteins fused to palmitoylation signals[167], to transmembrane domains[167], or to exosomal marker proteins[149, 163] in source cells; CLICK chemistry-based conjugation[170]; fusing EVs with liposomes[416-417]; and loading cholesterol-conjugated aptamers onto the surface of EVs[155]. Here we show that three out of eight proteins (Desmoplakin, AHSG, and Rab7) enhance vesicle trafficking to neurons. We used the chemical palmitoylation to enable protein loading into the vesicle membrane. Different proteins may have different sensitivity to this treatment (*i.e.*, high pH and palmitoylation on lysine residues instead of the naturally occurring cysteine, serine, and threonine residues). Thus, the lack of enhancement in liposome neuronal uptake may not indicate a lack of contribution to vesicle trafficking. Further

advancement of the technology presented here will require combinatorial optimization of protein loading-to-membrane as well as lipid-to-protein ratios.

A pioneering finding of this study is showing a functionally relevant difference in the lipid content of EVs derived from serum-deprived cells and control cells. We previously have reported on cardiolipin enrichment in exosomes compared to cells and microvesicles[256]. Here we show that dilysocardiolipins are enriched in stressed exosomes and that this enrichment is functionally relevant. Lysocardiolipins are substrates of a cardiolipin remodeling enzyme residing in the endoplasmic reticulum (acyl-coA:lysocardiolipin acyltransferase 1)[399]. We find proteins of ER-to-Golgi transport also are enriched in stressed exosomes. Thus, dilysocardiolipin may use the ER-Golgi secretory pathway to enter exosomes under stress conditions. The ER-Golgi secretory pathway may overlap with the release of exosomes from the multivesicular body[418-420].

Artificial exosomes constructed from purified lipid and protein components would have several advantages over natural exosomes. First, the manufacture of proteoliposomes is an easily scalable process and may be more cost-effective than manufacturing cell-derived exosomes. Second, the quality control of cell-free artificial exosomes could follow established guidelines from the liposome field, whereas the quality control requirements of natural therapeutic exosomes remain unclear[327, 341]. Third, loading therapeutic cargo (proteins or RNA) into or onto artificial exosomes could be a simple step added to the manufacturing process, whereas efficient loading of therapeutic cargo to natural exosomes still is challenging. The activity of artificial exosome composition identified here might be limited to neuronal uptake, and alteration or optimization of this composition likely is necessary to tune artificial exosomes for delivery to other cell types.

CHAPTER VII DISCUSSION

This dissertation lays out a path for the rational design of either natural or artificial exosomes for the delivery of advanced therapeutics. Exosome technology can combine RNA therapeutics (Chapter III), stem cell therapeutics (Chapter IV) and gene therapies[148, 157-158] in one particle. This combinatorial potential represents a leap forward in the development of advanced therapeutics.

When I started my thesis work, the RNA therapeutics field was in the need of diversifying delivery strategies in order to successfully treat organs other than the liver. At the same time, the extracellular vesicle field wished to enhance intrinsic therapeutic effects of exosomes by enriching therapeutic RNA content. Work in this dissertation fills those gaps by developing siRNAs with increased stability and activity *in vivo* (Section 3.1) and optimizing productive loading of these siRNA compounds to exosomes (Sections 3.2 and 3.3).

Extracellular vesicles encompass a very heterogenous group of vesicles. At the beginning of my thesis work the EV field dogma defined proteins specific to certain EV subclasses, such as exosomes and microvesicles, and absent from other EV subclasses. The work described in Chapters V and VI contributed to the change of this dogma. The current view is that no protein and no isolation method can fully differeniate between EV subclasses and EV content is largely dependent on the producer cell. The work in Chapters V and VI coincided with other proteomic studies comparing different classes of EVs[332] and different EV isolation methods[332] that also contributed to the change of the EV dogma. However, Chapter V was crucial in showing the high producer cell dependence in EV content. The term “extracellular vesicle” became similar to the term “cancer”, where both terms mark highly heterogenous entities with high source-cell-

dependence, diversity on the benign/therapeutic – malignant axis, lack of specific markers, and need for characterization at the omics level (e.g. genome, transcriptome, proteome, lipidome). Just like there is no single marker of a malignant tumor, there is no single marker of therapeutic EVs. However, similar to how the growing resolution of cancer characterization has enabled effective target-therapies, growing resolution of EV characterization will enable further EV classification into specific, maybe even personalized therapeutic vesicles.

The lack of specific markers impedes our understanding on composition – activity relationship of different EV classes. At the beginning of my thesis work there were speculations about the RNA content of EVs being responsible for their therapeutic effect[351]. Antiphagocytotic molecules have also been described on EV surface[374]. However, the components making EVs good delivery vesicles were unknown. The work in Chapter VI identified four molecules, dilysocardiolipin, Rab7, AHSG and Desmoplakin, that contribute the EV-mediated delivery to neurons. The mechanism, how these molecules enhance vesicle uptake remains to be elucidated. Independent of the mechanism, however, the strategy described in Chapter VI enables the large-scale development of reverse engineered exosomes for targeting specific cells. Furthermore, the four molecules identified can be considered as components or coating for a variety of delivery vehicles, including not only artificial exosomes, but also liposomes, lipid nanoparticles and polymer-based nanoparticles. Cardiolipins and its lyso-derivatives, monolysocardiolipins and dilysocardiolipins, are known regulators of membrane organization and membrane curvature[400] and therefore may be used to fine-tune vesicle membrane structure and size as well as to enhance delivery. Immunogenicity of such new delivery vesicles needs to be elucidated.

When I joined my thesis laboratory, a new mechanism of siRNA loading to exosomes just have been developed: cholesterol-conjugated siRNAs passively associated to the EV membrane[135].

Beyond contributing to this work, this dissertation further optimized the lipid conjugate and the scheme for chemical modifications of RNA cargo for EV-mediated delivery (Chapter III). These strategies can be extended to load mRNAs *via* lipid-conjugated tethers (collaboration with Alexis Forterre and AC Matin), miRNAs (collaboration with Sicheng Wen and Peter Quesenberry), aptamers[155] and presumably antimiRs, antisense oligonucleotides and sgRNAs for CRISPR. Furthermore, Chapter VI showed that there is a functional difference between two EV subclasses, exosomes and microvesicles, in their siRNA delivering capacity.

During my thesis work I adopted chemical palmitoylation for the loading of protein cargo on vesicle membranes (Chapter VI). This method requires the presence of lysines in the protein and stability of the protein at pH 8. All proteins with these characteristics can be loaded onto vesicles using chemical palmitoylation. Thus, chemical palmitoylation may enable exosomes to deliver therapeutic antibodies, Cas proteins for CRISPR or proteins for enzyme replacement.

Most of RNA and protein therapeutics can be delivered to target tissues without the use of exosomes or EVs. The advantage of using exosomes for delivery lies in better spread (Chapter VI and [135]), lower doses needed (Chapter VI and [135]), and in the combinatorial potential: combining different classes of RNA therapeutics in one exosome (e.g. targeting different pathways *via* different mechanisms in the same target cell), or combining RNA therapeutics with proteins or viruses. CRISPR is a classic example of such combinatorial therapeutic: it requires the delivery of an sgRNA and a protein or an sgRNA and an mRNA. Exosomes, therefore, represent an ideal delivery platform for CRISPR[148, 162]. Another advantageous combination is AAV and siRNA in exosomes: both exosomes and siRNAs can provide temporary immune modulation to overcome the largest impediment of AAV therapeutics today: pre-existing antibodies[157]. Immune modulation may be advantageous for antibody therapies and protein replacement therapies as well. Yet,

another combination could be that of therapeutic cargo with targeting moiety, such as a protein or an aptamer.

Chapter VI describes a first proof-of-concept experiment for artificial exosomes. Artificial exosomes stand at the crossroad of cell-derived therapeutics (extracellular vesicles) and drug-delivering synthetic nanoparticles. Therefore, artificial exosomes may combine the advantages of both approaches: minimal toxicity and high delivering efficiency of EVs with scalable manufacturing and straightforward quality control procedures of synthetic nanoparticles.

Quality control of natural exosomes remains challenging[327]. As shown in Chapters V and VI, EV contents are very complex. Single-vesicle resolution of EV content characterization would therefore be desirable. FACS-based technology is being currently developed for single-vesicle characterization of EVs[421]. FACS may enable further classification of EVs and sorting of EVs according to their contents. This will allow more accurate understanding of composition-activity relationship of EVs and to better purify EVs for therapeutic use.

Low yield of EVs is the major rate-limiting factor in advancing the EV technology towards preclinical animal experiments and clinical trials[327]. Work in Chapter IV fills this gap by developing a high yield, scalable and GMP-compatible mesenchymal stem cell culture and EV isolation strategy. This method allowed us to power mouse experiments (Chapter VI) using mesenchymal stem cell derived EVs. However, cost of EV production remains high. Thus, we suggest to use natural EVs only to treat diseases that are inaccessible to other therapeutics or other delivery vehicles. In organs accessible to various therapeutic classes, artificial exosomes are a good and cost-effective alternative to natural exosomes.

When I started my thesis work, quantification of chemically modified siRNAs, especially cholesterol-conjugated siRNAs, in cells and tissues was challenging. During my thesis work I adopted a PNA hybridization assay (originally developed by AxoLabs Gmbh[203], see Section 2.5) to measure siRNA levels in cells and tissues. I further optimized this assay to be able to detect purine-rich sequences: I established that a mismatch in the sequence can prevent aggregation of PNAs caused by long purine stretches and does not compromise the accuracy and sensitivity of the assay. Using this strategy, I enabled the measurement of *Huntingtin*-targeting siRNAs used throughout this dissertation together with seven other siRNA sequences. My measurements of siRNA levels in cells and tissues were used in five first-author publications and thirteen co-author publications (see Appendix A). Alnylam, a leading siRNA company, later adopted this assay in a modified form[422].

In conclusion, this dissertation enables high-throughput measurement of siRNA levels in tissues (Section 2.5), optimizes chemistry of RNA cargo for EV-mediated delivery (Chapter III), develops a large-scale EV isolation method (Chapter IV), extensively characterizes EV content (Chapter V), establishes composition – activity relationship in EVs (Chapter VI) and describes proof-of-concept artificial exosomes (Chapter VI). These findings will accelerate the transition of EV technology into therapeutic applications.

APPENDICES

APPENDIX A: CO-AUTHOR MANUSCRIPTS – PNA HYBRIDIZATION ASSAY

1. MC Didiot, LM Hall, AH Coles, **RA Haraszti**, BM Goindho, K Chase, E Sapp, S Ly, JF Alterman, MR Hassler, L Raj DV Morrissey, M DiFiglia, N Aronin, A Khvorova. Exosome-mediated delivery of hydrophobically modified siRNA for Huntingtin mRNA silencing. **Molecular Therapy**, 2016 Aug. 9.
2. M Nikan, MF Osborn, AH Coles, BM Godinho, LM Hall, **RA Haraszti**, MR Hassler, D Echeverria, N Aronin, A Khvorova. Docosahexaenoic Acid Conjugation Enhances Distribution and Safety of siRNA upon Local Administration in Mouse Brain. **Mol Ther Nucleic Acids**. 2016 Aug 9.
3. M Nikan, MF Osborn, AH Coles, A Biscans, BM Godinho, **RA Haraszti**, E Sapp, D Echverria, M DiFiglia, N Aronin, A Khvorova. Synthesis and Evaluation of Parenchymal Retention and Efficacy of a Metabolically Stable, *O*-phosphocholine-*N*-docosahexaenoyl-L-serine siRNA Conjugate in Mouse Brain. **Bioconjug Chem.** 2017 May 10.
4. MC Didiot, **RA Haraszti**, N Aronin, A Khvorova. Loading of Extracellular Vesicles With Hydrophobically Modified siRNAs. In: Patel T. (eds) Extracellular RNA. **Methods in Molecular Biology**, vol 1740. Humana Press, New York, NY
5. BMDC Godinho, JW Gilbert, **RA Haraszti**, AH Coles, A Biscans, L Roux, M Nikan, D Echeverria, M Hassler, A Khvorova. Pharmacokinetic profiling of conjugated therapeutic oligonucleotide: a high-throughput method based upon serial blood microsapling coupled to peptide nucleic acid hybridization assay. **Nucleic Acid Ther**. 2017. Dec. 27.
6. J Sancheez-Ramos, S Song, X Kong, P Foroutan, G Martinez, W Dominguez-Viqueria, A Mohapatra, **RA Haraszti**, A Khvorova, N Aronin, V Sava. Chitosan-mangafodipir nanoparticles designed for intranasal delivery of siRNA and DNA to brain. **J Drug Delivery Sci and Tech**. 2018. Febr. 2.
7. MR Hassler*, AA Turanov*, JF Alterman*, **RA Haraszti**, AH Coles, MF Osborn, D Echeverria, M Nikan, WE Salomon, L Roux, BMDC Godinho, SM Davis, DV Morrissey, PD Zamore, SA Karumanchi, MJ Moore, N Aronin, A Khvorova. Comparison of fully and partially chemically-modified siRNA in conjugate-mediated delivery in vivo. **Nucl Acid Research**. 2018. March 6.
8. MF Osborn, AH Coles, A Biscans, **RA Haraszti**, L Roux, SM Davis, S Ly, D Echeverria, MR Hassler, A Khvorova. Hydrophobicity drives the systemic distribution of lipid-conjugated siRNAs via lipid transport pathways. **In Review**, bioRxriv, 2018. March 23.
9. A Biscans, AH Coles, **RA Haraszti**, D Echeverria, MR Hassler, MF Osborn, A Khvorova. Diverse lipid conjugates for functional extra-hepatic siRNA delivery in vivo. **In Review**, bioRxriv, 2018. March 26.

10. AA Turanov, MR Hassler, A Ashar-Patel, A Makris, A Lo, JF Alterman, AH Coles, **RA Haraszti**, BMDC Godinho, D Echeverria, A Hennessy, SA Karumanchi, MJ Moore, A Khvorova. Development of therapeutic anti-sFLT1 siRNA for the treatment of preeclampsia. **In Review**
11. BMDC Godinho, J Bouley, JF Alterman, **RA Haraszti**, J Gilbert, AH Coles, A Biscans, M Nikan, D Echeverria, N Henninger, A Khvorova. Transvascular Delivery of Hydrophobically Modified siRNAs to the Rat Brain. **In Review**
12. BMDC Godinho, J Gilbert, **RA Haraszti**, AH Coles, JF Alterman, D Echeverria, MR Hassler, A Khvorova. Triple-strand duplex: a novel PEGylation strategy for hydrophobically modified siRNAs. **In Preparation**
13. JF Alterman*, MR Hassler*, BMDC Godinho, **RA Haraszti**, AH Coles, L Roux, D Echeverria, K Chase, R Miller, N Aronin, A Khvorova. Dimeric fully modified siRNA for therapy of Huntington's disease. **In Preparation**

APPENDIX B: CO-AUTHOR MANUSCRIPTS – EV PROTEOMICS ANALYSIS

1. B Shaha, F Momen-Heravi, K Kodys, D Catalano, A Gangopadhyay, I Furi, **RA Haraszti**, A Shatishchandran, A Iracheta-Vellve, A Adejumo, S Shaffer, G Szabo. Extracellular vesicles from mice with alcoholic liver disease carry a distinct protein cargo and induce macrophage activation via Hsp90. **Hepatology,** 2017 Dec.18.

APPENDIX C: CO-AUTHOR MANUSCRIPTS – EXONUCLEASE STABILITY ASSAY

1. VK Sharma, SK Singh, PM Krishnamurthy, JF Alterman, **RA Haraszti**, A Khvorova, AK Prasad, JK Watts. Synthesis and biological properties of triazole-linked locked nucleic acid. **Chem Commun** 2017 Aug.3.

APPENDIX D: PATENT APPLICATIONS

1. A Khvorova, M Nikan, MR Hassler, MF Osborn, **RA Haraszti**, AH Coles, AA Turanov, N Aronin: Bioactive conjugates for oligonucleotide delivery. US15236051, 2017. Febr. 16.

BIBLIOGRAPHY

1. Mourant, J. R.; Yamada, Y. R.; Carpenter, S.; Dominique, L. R.; Freyer, J. P., FTIR spectroscopy demonstrates biochemical differences in mammalian cell cultures at different growth stages. *Biophys J* **2003,** *85* (3), 1938-47.
2. Short, K. W.; Carpenter, S.; Freyer, J. P.; Mourant, J. R., Raman spectroscopy detects biochemical changes due to proliferation in mammalian cell cultures. *Biophys J* **2005,** *88* (6), 4274-88.
3. Alberts B, J. A., Lewis J, et al., The RNA World and the Origins of Life. In *Molecular Biology of the Cell. 4th edition.*, Garland Science: New York, 2002.
4. Vlassov, A.; Khvorova, A.; Yarus, M., Binding and disruption of phospholipid bilayers by supramolecular RNA complexes. *Proc Natl Acad Sci U S A* **2001,** *98* (14), 7706-11.
5. Fire, A.; Xu, S.; Montgomery, M. K.; Kostas, S. A.; Driver, S. E.; Mello, C. C., Potent and specific genetic interference by double-stranded RNA in Caenorhabditis elegans. *Nature* **1998,** *391* (6669), 806-11.
6. Elbashir, S. M.; Harborth, J.; Lendeckel, W.; Yalcin, A.; Weber, K.; Tuschl, T., Duplexes of 21-nucleotide RNAs mediate RNA interference in cultured mammalian cells. *Nature* **2001,** *411* (6836), 494-8.
7. Lima, W. F.; Prakash, T. P.; Murray, H. M.; Kinberger, G. A.; Li, W.; Chappell, A. E.; Li, C. S.; Murray, S. F.; Gaus, H.; Seth, P. P.; Swayze, E. E.; Crooke, S. T., Single-stranded siRNAs activate RNAi in animals. *Cell* **2012,** *150* (5), 883-94.
8. Lee, R. C.; Feinbaum, R. L.; Ambros, V., The C. elegans heterochronic gene lin-4 encodes small RNAs with antisense complementarity to lin-14. *Cell* **1993,** *75* (5), 843-54.
9. Lagos-Quintana, M.; Rauhut, R.; Lendeckel, W.; Tuschl, T., Identification of novel genes coding for small expressed RNAs. *Science* **2001,** *294* (5543), 853-8.
10. Matzke, M. A.; Primig, M.; Trnovsky, J.; Matzke, A. J., Reversible methylation and inactivation of marker genes in sequentially transformed tobacco plants. *Embo J* **1989,** *8* (3), 643-9.
11. Morris, K. V.; Chan, S. W.; Jacobsen, S. E.; Looney, D. J., Small interfering RNA-induced transcriptional gene silencing in human cells. *Science* **2004,** *305* (5688), 1289-92.
12. Janowski, B. A.; Younger, S. T.; Hardy, D. B.; Ram, R.; Huffman, K. E.; Corey, D. R., Activating gene expression in mammalian cells with promoter-targeted duplex RNAs. *Nat Chem Biol* **2007,** *3* (3), 166-73.
13. Zamecnik, P. C.; Stephenson, M. L., Inhibition of Rous sarcoma virus replication and cell transformation by a specific oligodeoxynucleotide. *Proc Natl Acad Sci U S A* **1978,** *75* (1), 280-4.
14. Wolff, J. A.; Malone, R. W.; Williams, P.; Chong, W.; Acsadi, G.; Jani, A.; Felgner, P. L., Direct gene transfer into mouse muscle in vivo. *Science* **1990,** *247* (4949 Pt 1), 1465-8.
15. Brenner, S.; Jacob, F.; Meselson, M., An unstable intermediate carrying information from genes to ribosomes for protein synthesis. *Nature* **1961,** *190*, 576-581.
16. Jinek, M.; Chylinski, K.; Fonfara, I.; Hauer, M.; Doudna, J. A.; Charpentier, E., A programmable dual-RNA-guided DNA endonuclease in adaptive bacterial immunity. *Science* **2012,** *337* (6096), 816-21.
17. Cong, L.; Ran, F. A.; Cox, D.; Lin, S.; Barretto, R.; Habib, N.; Hsu, P. D.; Wu, X.; Jiang, W.; Marraffini, L. A.; Zhang, F., Multiplex genome engineering using CRISPR/Cas systems. *Science* **2013,** *339* (6121), 819-23.

18. Tuerk, C.; Gold, L., Systematic evolution of ligands by exponential enrichment: RNA ligands to bacteriophage T4 DNA polymerase. *Science* **1990,** *249* (4968), 505-10.
19. Meister, G.; Landthaler, M.; Dorsett, Y.; Tuschl, T., Sequence-specific inhibition of microRNA- and siRNA-induced RNA silencing. *Rna* **2004,** *10* (3), 544-50.
20. Hutvagner, G.; Simard, M. J.; Mello, C. C.; Zamore, P. D., Sequence-specific inhibition of small RNA function. *PLoS Biol* **2004,** *2* (4), E98.
21. Dominski, Z.; Kole, R., Restoration of correct splicing in thalassemic pre-mRNA by antisense oligonucleotides. *Proc Natl Acad Sci U S A* **1993,** *90* (18), 8673-7.
22. Hanvey, J. C.; Shimizu, M.; Wells, R. D., Site-specific inhibition of EcoRI restriction/modification enzymes by a DNA triple helix. *Nucleic Acids Res* **1990,** *18* (1), 157-61.
23. Orson, F. M.; Thomas, D. W.; McShan, W. M.; Kessler, D. J.; Hogan, M. E., Oligonucleotide inhibition of IL2R alpha mRNA transcription by promoter region collinear triplex formation in lymphocytes. *Nucleic Acids Res* **1991,** *19* (12), 3435-41.
24. Feng, J.; Funk, W. D.; Wang, S. S.; Weinrich, S. L.; Avilion, A. A.; Chiu, C. P.; Adams, R. R.; Chang, E.; Allsopp, R. C.; Yu, J.; et al., The RNA component of human telomerase. *Science* **1995,** *269* (5228), 1236-41.
25. Blake, K. R.; Murakami, A.; Miller, P. S., Inhibition of rabbit globin mRNA translation by sequence-specific oligodeoxyribonucleotides. *Biochemistry* **1985,** *24* (22), 6132-8.
26. Cech, T. R.; Zaug, A. J.; Grabowski, P. J., In vitro splicing of the ribosomal RNA precursor of Tetrahymena: involvement of a guanosine nucleotide in the excision of the intervening sequence. *Cell* **1981,** *27* (3 Pt 2), 487-96.
27. Stark, B. C.; Kole, R.; Bowman, E. J.; Altman, S., Ribonuclease P: an enzyme with an essential RNA component. *Proc Natl Acad Sci U S A* **1978,** *75* (8), 3717-21.
28. Sioud, M.; Natvig, J. B.; Forre, O., Preformed ribozyme destroys tumour necrosis factor mRNA in human cells. *J Mol Biol* **1992,** *223* (4), 831-5.
29. Open Label Study for the Evaluation of Tolerability of Five Dose Levels of Cand5. https://ClinicalTrials.gov/show/NCT00722384.
30. Study of PF-04523655 (REDD14NP) In Subjects With Choroidal Neovascularization (CNV) Secondary to Age-Related Macular Degeneration (Wet AMD). https://ClinicalTrials.gov/show/NCT00725686.
31. Dejneka, N. S.; Wan, S.; Bond, O. S.; Kornbrust, D. J.; Reich, S. J., Ocular biodistribution of bevasiranib following a single intravitreal injection to rabbit eyes. *Mol Vis* **2008,** *14*, 997-1005.
32. Singerman, L., Combination therapy using the small interfering RNA bevasiranib. *Retina* **2009,** *29* (6 Suppl), S49-50.
33. Ledford, H., Drug giants turn their backs on RNA interference. *Nature* **2010,** *468* (7323), 487.
34. Krieg, A. M., Is RNAi dead? *Mol Ther* **2011,** *19* (6), 1001-2.
35. Schmidt, C., RNAi momentum fizzles as pharma shifts priorities. *Nat Biotechnol* **2011,** *29* (2), 93-4.
36. Layzer, J. M.; McCaffrey, A. P.; Tanner, A. K.; Huang, Z.; Kay, M. A.; Sullenger, B. A., In vivo activity of nuclease-resistant siRNAs. *Rna* **2004,** *10* (5), 766-71.
37. Kleischmidt, W. J.; Ellis, L. F.; Van Frank, R. M.; Murphy, E. B., Interferon stimulation by a double stranded RNA of a mycophage in statolon preparations. *Nature* **1968,** *220* (5163), 167-8.

38. Bridge, A. J.; Pebernard, S.; Ducraux, A.; Nicoulaz, A. L.; Iggo, R., Induction of an interferon response by RNAi vectors in mammalian cells. *Nat Genet* **2003,** *34* (3), 263-4.
39. Sledz, C. A.; Holko, M.; de Veer, M. J.; Silverman, R. H.; Williams, B. R., Activation of the interferon system by short-interfering RNAs. *Nat Cell Biol* **2003,** *5* (9), 834-9.
40. Judge, A. D.; Sood, V.; Shaw, J. R.; Fang, D.; McClintock, K.; MacLachlan, I., Sequence-dependent stimulation of the mammalian innate immune response by synthetic siRNA. *Nat Biotechnol* **2005,** *23* (4), 457-62.
41. Corey, D. R., RNA learns from antisense. *Nat Chem Biol* **2007,** *3* (1), 8-11.
42. Kennedy, S.; Wang, D.; Ruvkun, G., A conserved siRNA-degrading RNase negatively regulates RNA interference in C. elegans. *Nature* **2004,** *427* (6975), 645-9.
43. Zou, Y.; Tiller, P.; Chen, I. W.; Beverly, M.; Hochman, J., Metabolite identification of small interfering RNA duplex by high-resolution accurate mass spectrometry. *Rapid Commun Mass Spectrom* **2008,** *22* (12), 1871-81.
44. Haupenthal, J.; Baehr, C.; Kiermayer, S.; Zeuzem, S.; Piiper, A., Inhibition of RNAse A family enzymes prevents degradation and loss of silencing activity of siRNAs in serum. *Biochem Pharmacol* **2006,** *71* (5), 702-10.
45. Haupenthal, J.; Baehr, C.; Zeuzem, S.; Piiper, A., RNAse A-like enzymes in serum inhibit the anti-neoplastic activity of siRNA targeting polo-like kinase 1. *Int J Cancer* **2007,** *121* (1), 206-10.
46. Turner, J. J.; Jones, S. W.; Moschos, S. A.; Lindsay, M. A.; Gait, M. J., MALDI-TOF mass spectral analysis of siRNA degradation in serum confirms an RNAse A-like activity. *Mol Biosyst* **2007,** *3* (1), 43-50.
47. Kariko, K.; Bhuyan, P.; Capodici, J.; Weissman, D., Small interfering RNAs mediate sequence-independent gene suppression and induce immune activation by signaling through toll-like receptor 3. *J Immunol* **2004,** *172* (11), 6545-9.
48. Alexopoulou, L.; Holt, A. C.; Medzhitov, R.; Flavell, R. A., Recognition of double-stranded RNA and activation of NF-kappaB by Toll-like receptor 3. *Nature* **2001,** *413* (6857), 732-8.
49. Diebold, S. S.; Kaisho, T.; Hemmi, H.; Akira, S.; Reis e Sousa, C., Innate antiviral responses by means of TLR7-mediated recognition of single-stranded RNA. *Science* **2004,** *303* (5663), 1529-31.
50. Hornung, V.; Guenthner-Biller, M.; Bourquin, C.; Ablasser, A.; Schlee, M.; Uematsu, S.; Noronha, A.; Manoharan, M.; Akira, S.; de Fougerolles, A.; Endres, S.; Hartmann, G., Sequence-specific potent induction of IFN-alpha by short interfering RNA in plasmacytoid dendritic cells through TLR7. *Nat Med* **2005,** *11* (3), 263-70.
51. Puthenveetil, S.; Whitby, L.; Ren, J.; Kelnar, K.; Krebs, J. F.; Beal, P. A., Controlling activation of the RNA-dependent protein kinase by siRNAs using site-specific chemical modification. *Nucleic Acids Res* **2006,** *34* (17), 4900-11.
52. Marques, J. T.; Devosse, T.; Wang, D.; Zamanian-Daryoush, M.; Serbinowski, P.; Hartmann, R.; Fujita, T.; Behlke, M. A.; Williams, B. R., A structural basis for discriminating between self and nonself double-stranded RNAs in mammalian cells. *Nat Biotechnol* **2006,** *24* (5), 559-65.
53. Hammond, S. M.; Boettcher, S.; Caudy, A. A.; Kobayashi, R.; Hannon, G. J., Argonaute2, a link between genetic and biochemical analyses of RNAi. *Science* **2001,** *293* (5532), 1146-50.

54. Khvorova, A.; Reynolds, A.; Jayasena, S. D., Functional siRNAs and miRNAs exhibit strand bias. *Cell* **2003,** *115* (2), 209-16.
55. Schwarz, D. S.; Hutvagner, G.; Du, T.; Xu, Z.; Aronin, N.; Zamore, P. D., Asymmetry in the assembly of the RNAi enzyme complex. *Cell* **2003,** *115* (2), 199-208.
56. Khvorova, A.; Watts, J. K., The chemical evolution of oligonucleotide therapies of clinical utility. *Nat Biotechnol* **2017,** *35* (3), 238-248.
57. Martinez, J.; Tuschl, T., RISC is a 5' phosphomonoester-producing RNA endonuclease. *Genes Dev* **2004,** *18* (9), 975-80.
58. Matranga, C.; Tomari, Y.; Shin, C.; Bartel, D. P.; Zamore, P. D., Passenger-strand cleavage facilitates assembly of siRNA into Ago2-containing RNAi enzyme complexes. *Cell* **2005,** *123* (4), 607-20.
59. Leuschner, P. J.; Ameres, S. L.; Kueng, S.; Martinez, J., Cleavage of the siRNA passenger strand during RISC assembly in human cells. *EMBO Rep* **2006,** *7* (3), 314-20.
60. Hutvagner, G.; Zamore, P. D., A microRNA in a multiple-turnover RNAi enzyme complex. *Science* **2002,** *297* (5589), 2056-60.
61. Wang, Y.; Juranek, S.; Li, H.; Sheng, G.; Wardle, G. S.; Tuschl, T.; Patel, D. J., Nucleation, propagation and cleavage of target RNAs in Ago silencing complexes. *Nature* **2009,** *461* (7265), 754-61.
62. Braasch, D. A.; Paroo, Z.; Constantinescu, A.; Ren, G.; Oz, O. K.; Mason, R. P.; Corey, D. R., Biodistribution of phosphodiester and phosphorothioate siRNA. *Bioorg Med Chem Lett* **2004,** *14* (5), 1139-43.
63. Yang, X.; Sierant, M.; Janicka, M.; Peczek, L.; Martinez, C.; Hassell, T.; Li, N.; Li, X.; Wang, T.; Nawrot, B., Gene silencing activity of siRNA molecules containing phosphorodithioate substitutions. *ACS Chem Biol* **2012,** *7* (7), 1214-20.
64. Hall, A. H.; Wan, J.; Shaughnessy, E. E.; Ramsay Shaw, B.; Alexander, K. A., RNA interference using boranophosphate siRNAs: structure-activity relationships. *Nucleic Acids Res* **2004,** *32* (20), 5991-6000.
65. Harborth, J.; Elbashir, S. M.; Vandenburgh, K.; Manninga, H.; Scaringe, S. A.; Weber, K.; Tuschl, T., Sequence, chemical, and structural variation of small interfering RNAs and short hairpin RNAs and the effect on mammalian gene silencing. *Antisense Nucleic Acid Drug Dev* **2003,** *13* (2), 83-105.
66. Amarzguioui, M.; Holen, T.; Babaie, E.; Prydz, H., Tolerance for mutations and chemical modifications in a siRNA. *Nucleic Acids Res* **2003,** *31* (2), 589-95.
67. Li, P.; Sergueeva, Z. A.; Dobrikov, M.; Shaw, B. R., Nucleoside and oligonucleoside boranophosphates: chemistry and properties. *Chem Rev* **2007,** *107* (11), 4746-96.
68. Brown, D. A.; Kang, S. H.; Gryaznov, S. M.; DeDionisio, L.; Heidenreich, O.; Sullivan, S.; Xu, X.; Nerenberg, M. I., Effect of phosphorothioate modification of oligodeoxynucleotides on specific protein binding. *J Biol Chem* **1994,** *269* (43), 26801-5.
69. Chiu, Y. L.; Rana, T. M., siRNA function in RNAi: a chemical modification analysis. *Rna* **2003,** *9* (9), 1034-48.
70. Shen, X.; Corey, D. R., Chemistry, mechanism and clinical status of antisense oligonucleotides and duplex RNAs. *Nucleic Acids Res* **2018,** *46* (4), 1584-1600.
71. Jahns, H.; Roos, M.; Imig, J.; Baumann, F.; Wang, Y.; Gilmour, R.; Hall, J., Stereochemical bias introduced during RNA synthesis modulates the activity of phosphorothioate siRNAs. *Nat Commun* **2015,** *6* (6317), 6317.

72. Prakash, T. P.; Allerson, C. R.; Dande, P.; Vickers, T. A.; Sioufi, N.; Jarres, R.; Baker, B. F.; Swayze, E. E.; Griffey, R. H.; Bhat, B., Positional effect of chemical modifications on short interference RNA activity in mammalian cells. *J Med Chem* **2005,** *48* (13), 4247-53.
73. Deleavey, G. F.; Watts, J. K.; Alain, T.; Robert, F.; Kalota, A.; Aishwarya, V.; Pelletier, J.; Gewirtz, A. M.; Sonenberg, N.; Damha, M. J., Synergistic effects between analogs of DNA and RNA improve the potency of siRNA-mediated gene silencing. *Nucleic Acids Res* **2010,** *38* (13), 4547-57.
74. Soutschek, J.; Akinc, A.; Bramlage, B.; Charisse, K.; Constien, R.; Donoghue, M.; Elbashir, S.; Geick, A.; Hadwiger, P.; Harborth, J.; John, M.; Kesavan, V.; Lavine, G.; Pandey, R. K.; Racie, T.; Rajeev, K. G.; Rohl, I.; Toudjarska, I.; Wang, G.; Wuschko, S.; Bumcrot, D.; Koteliansky, V.; Limmer, S.; Manoharan, M.; Vornlocher, H. P., Therapeutic silencing of an endogenous gene by systemic administration of modified siRNAs. *Nature* **2004,** *432* (7014), 173-8.
75. Czauderna, F.; Fechtner, M.; Dames, S.; Aygun, H.; Klippel, A.; Pronk, G. J.; Giese, K.; Kaufmann, J., Structural variations and stabilising modifications of synthetic siRNAs in mammalian cells. *Nucleic Acids Res* **2003,** *31* (11), 2705-16.
76. Freier, S. M.; Altmann, K. H., The ups and downs of nucleic acid duplex stability: structure-stability studies on chemically-modified DNA:RNA duplexes. *Nucleic Acids Res* **1997,** *25* (22), 4429-43.
77. Allerson, C. R.; Sioufi, N.; Jarres, R.; Prakash, T. P.; Naik, N.; Berdeja, A.; Wanders, L.; Griffey, R. H.; Swayze, E. E.; Bhat, B., Fully 2'-modified oligonucleotide duplexes with improved in vitro potency and stability compared to unmodified small interfering RNA. *J Med Chem* **2005,** *48* (4), 901-4.
78. Choung, S.; Kim, Y. J.; Kim, S.; Park, H. O.; Choi, Y. C., Chemical modification of siRNAs to improve serum stability without loss of efficacy. *Biochem Biophys Res Commun* **2006,** *342* (3), 919-27.
79. Heil, F.; Hemmi, H.; Hochrein, H.; Ampenberger, F.; Kirschning, C.; Akira, S.; Lipford, G.; Wagner, H.; Bauer, S., Species-specific recognition of single-stranded RNA via toll-like receptor 7 and 8. *Science* **2004,** *303* (5663), 1526-9.
80. Cekaite, L.; Furset, G.; Hovig, E.; Sioud, M., Gene expression analysis in blood cells in response to unmodified and 2'-modified siRNAs reveals TLR-dependent and independent effects. *J Mol Biol* **2007,** *365* (1), 90-108.
81. Bramsen, J. B.; Kjems, J., Development of Therapeutic-Grade Small Interfering RNAs by Chemical Engineering. *Front Genet* **2012,** *3* (154), 154.
82. Odadzic, D.; Bramsen, J. B.; Smicius, R.; Bus, C.; Kjems, J.; Engels, J. W., Synthesis of 2'-O-modified adenosine building blocks and application for RNA interference. *Bioorg Med Chem* **2008,** *16* (1), 518-29.
83. Bramsen, J. B.; Laursen, M. B.; Nielsen, A. F.; Hansen, T. B.; Bus, C.; Langkjaer, N.; Babu, B. R.; Hojland, T.; Abramov, M.; Van Aerschot, A.; Odadzic, D.; Smicius, R.; Haas, J.; Andree, C.; Barman, J.; Wenska, M.; Srivastava, P.; Zhou, C.; Honcharenko, D.; Hess, S.; Muller, E.; Bobkov, G. V.; Mikhailov, S. N.; Fava, E.; Meyer, T. F.; Chattopadhyaya, J.; Zerial, M.; Engels, J. W.; Herdewijn, P.; Wengel, J.; Kjems, J., A large-scale chemical modification screen identifies design rules to generate siRNAs with high activity, high stability and low toxicity. *Nucleic Acids Res* **2009,** *37* (9), 2867-81.

84. Braasch, D. A.; Jensen, S.; Liu, Y.; Kaur, K.; Arar, K.; White, M. A.; Corey, D. R., RNA interference in mammalian cells by chemically-modified RNA. *Biochemistry* **2003,** *42* (26), 7967-75.
85. Snead, N. M.; Escamilla-Powers, J. R.; Rossi, J. J.; McCaffrey, A. P., 5' Unlocked Nucleic Acid Modification Improves siRNA Targeting. *Mol Ther Nucleic Acids* **2013,** *2* (2), e103.
86. Shen, L.; Johnson, T. L.; Clugston, S.; Huang, H.; Butenhof, K. J.; Stanton, R. V., Molecular dynamics simulation and binding energy calculation for estimation of oligonucleotide duplex thermostability in RNA-based therapeutics. *J Chem Inf Model* **2011,** *51* (8), 1957-65.
87. Langkjaer, N.; Pasternak, A.; Wengel, J., UNA (unlocked nucleic acid): a flexible RNA mimic that allows engineering of nucleic acid duplex stability. *Bioorg Med Chem* **2009,** *17* (15), 5420-5.
88. Bramsen, J. B.; Pakula, M. M.; Hansen, T. B.; Bus, C.; Langkjaer, N.; Odadzic, D.; Smicius, R.; Wengel, S. L.; Chattopadhyaya, J.; Engels, J. W.; Herdewijn, P.; Wengel, J.; Kjems, J., A screen of chemical modifications identifies position-specific modification by UNA to most potently reduce siRNA off-target effects. *Nucleic Acids Res* **2010,** *38* (17), 5761-73.
89. Vaish, N.; Chen, F.; Seth, S.; Fosnaugh, K.; Liu, Y.; Adami, R.; Brown, T.; Chen, Y.; Harvie, P.; Johns, R.; Severson, G.; Granger, B.; Charmley, P.; Houston, M.; Templin, M. V.; Polisky, B., Improved specificity of gene silencing by siRNAs containing unlocked nucleobase analogs. *Nucleic Acids Res* **2011,** *39* (5), 1823-32.
90. Dowler, T.; Bergeron, D.; Tedeschi, A. L.; Paquet, L.; Ferrari, N.; Damha, M. J., Improvements in siRNA properties mediated by 2'-deoxy-2'-fluoro-beta-D-arabinonucleic acid (FANA). *Nucleic Acids Res* **2006,** *34* (6), 1669-75.
91. Watts, J. K.; Choubdar, N.; Sadalapure, K.; Robert, F.; Wahba, A. S.; Pelletier, J.; Pinto, B. M.; Damha, M. J., 2'-fluoro-4'-thioarabino-modified oligonucleotides: conformational switches linked to siRNA activity. *Nucleic Acids Res* **2007,** *35* (5), 1441-51.
92. Fisher, M.; Abramov, M.; Van Aerschot, A.; Rozenski, J.; Dixit, V.; Juliano, R. L.; Herdewijn, P., Biological effects of hexitol and altritol-modified siRNAs targeting B-Raf. *Eur J Pharmacol* **2009,** *606* (1-3), 38-44.
93. Fisher, M.; Abramov, M.; Van Aerschot, A.; Xu, D.; Juliano, R. L.; Herdewijn, P., Inhibition of MDR1 expression with altritol-modified siRNAs. *Nucleic Acids Res* **2007,** *35* (4), 1064-74.
94. Hoshika, S.; Minakawa, N.; Kamiya, H.; Harashima, H.; Matsuda, A., RNA interference induced by siRNAs modified with 4'-thioribonucleosides in cultured mammalian cells. *FEBS Lett* **2005,** *579* (14), 3115-8.
95. Hoshika, S.; Minakawa, N.; Shionoya, A.; Imada, K.; Ogawa, N.; Matsuda, A., Study of modification pattern-RNAi activity relationships by using siRNAs modified with 4'-thioribonucleosides. *Chembiochem* **2007,** *8* (17), 2133-8.
96. Dande, P.; Prakash, T. P.; Sioufi, N.; Gaus, H.; Jarres, R.; Berdeja, A.; Swayze, E. E.; Griffey, R. H.; Bhat, B., Improving RNA interference in mammalian cells by 4'-thio-modified small interfering RNA (siRNA): effect on siRNA activity and nuclease stability when used in combination with 2'-O-alkyl modifications. *J Med Chem* **2006,** *49* (5), 1624-34.
97. Khvorova, A.; Watts, J. K., Oligonucleotide Therapeutics: From Chemistry Advances to Clinical Utility. *Nature Biotechnology* **2017,** *In Press*.

98. Williams, D. M.; Benseler, F.; Eckstein, F., Properties of 2'-fluorothymidine-containing oligonucleotides: interaction with restriction endonuclease EcoRV. *Biochemistry* **1991,** *30* (16), 4001-9.
99. Pieken, W. A.; Olsen, D. B.; Benseler, F.; Aurup, H.; Eckstein, F., Kinetic characterization of ribonuclease-resistant 2'-modified hammerhead ribozymes. *Science* **1991,** *253* (5017), 314-7.
100. Addepalli, H.; Meena; Peng, C. G.; Wang, G.; Fan, Y.; Charisse, K.; Jayaprakash, K. N.; Rajeev, K. G.; Pandey, R. K.; Lavine, G.; Zhang, L.; Jahn-Hofmann, K.; Hadwiger, P.; Manoharan, M.; Maier, M. A., Modulation of thermal stability can enhance the potency of siRNA. *Nucleic Acids Res* **2010,** *38* (20), 7320-31.
101. Charisse, K. G. R. T. Z. M. M. M. M. S. K. K. RNAi agents, compositions and methods of use thereof for treating transthyretin (TTR) associated diseases. 2016.
102. Jackson, A. L.; Burchard, J.; Leake, D.; Reynolds, A.; Schelter, J.; Guo, J.; Johnson, J. M.; Lim, L.; Karpilow, J.; Nichols, K.; Marshall, W.; Khvorova, A.; Linsley, P. S., Position-specific chemical modification of siRNAs reduces "off-target" transcript silencing. *Rna* **2006,** *12* (7), 1197-205.
103. Salomon, W. E.; Jolly, S. M.; Moore, M. J.; Zamore, P. D.; Serebrov, V., Single-Molecule Imaging Reveals that Argonaute Reshapes the Binding Properties of Its Nucleic Acid Guides. *Cell* **2015,** *162* (1), 84-95.
104. Hassler, M. R.; Turanov, A. A.; Alterman, J. F.; Haraszti, R. A.; Coles, A. H.; Osborn, M. F.; Echeverria, D.; Nikan, M.; Salomon, W. E.; Roux, L.; Godinho, Bruno M D C.; Davis, S. M.; Morrissey, D. V.; Zamore, P. D.; Karumanchi, S. A.; Moore, M. J.; Aronin, N.; Khvorova, A., Comparison of partially and fully chemically-modified siRNA in conjugate-mediated delivery in vivo. *Nucleic Acids Research* **2018**, gky037-gky037.
105. Bartlett, D. W.; Davis, M. E., Effect of siRNA nuclease stability on the in vitro and in vivo kinetics of siRNA-mediated gene silencing. *Biotechnol Bioeng* **2007,** *97* (4), 909-21.
106. Wolf, P., The nature and significance of platelet products in human plasma. *Br J Haematol* **1967,** *13* (3), 269-88.
107. Ali, S. Y.; Sajdera, S. W.; Anderson, H. C., Isolation and characterization of calcifying matrix vesicles from epiphyseal cartilage. *Proc Natl Acad Sci U S A* **1970,** *67* (3), 1513-20.
108. Schrier, S. L.; Godin, D.; Gould, R. G.; Swyryd, B.; Junga, I.; Seeger, M., Characterization of microvesicles produced by shearing of human erythrocyte membranes. *Biochim Biophys Acta* **1971,** *233* (1), 26-36.
109. Trams, E. G.; Lauter, C. J.; Salem, N., Jr.; Heine, U., Exfoliation of membrane ecto-enzymes in the form of micro-vesicles. *Biochim Biophys Acta* **1981,** *645* (1), 63-70.
110. Johnstone, R. M.; Adam, M.; Hammond, J. R.; Orr, L.; Turbide, C., Vesicle formation during reticulocyte maturation. Association of plasma membrane activities with released vesicles (exosomes). *J Biol Chem* **1987,** *262* (19), 9412-20.
111. Johnstone, R. M.; Adam, M.; Pan, B. T., The fate of the transferrin receptor during maturation of sheep reticulocytes in vitro. *Can J Biochem Cell Biol* **1984,** *62* (11), 1246-54.
112. De Robertis, E.; Vaz Ferreira, A., A multivesicular cathecol-containing body of the adrenal medulla of the rabbit. *Exp Cell Res* **1957,** *12* (3), 575-81.
113. Billington, D.; Coleman, R., Effects of bile salts of human erythrocytes. Plasma membrane vesiculation, phospholipid solubilization and their possible relationships to bile secretion. *Biochim Biophys Acta* **1978,** *509* (1), 33-47.

114. Crawford, N., The presence of contractile proteins in platelet microparticles isolated from human and animal platelet-free plasma. *Br J Haematol* **1971,** *21* (1), 53-69.
115. George, J. N.; Thoi, L. L.; McManus, L. M.; Reimann, T. A., Isolation of human platelet membrane microparticles from plasma and serum. *Blood* **1982,** *60* (4), 834-40.
116. Stein, J. M.; Luzio, J. P., Ectocytosis caused by sublytic autologous complement attack on human neutrophils. The sorting of endogenous plasma-membrane proteins and lipids into shed vesicles. *Biochem J* **1991,** *274 (Pt 2)* (Pt 2), 381-6.
117. Al-Nedawi, K.; Meehan, B.; Micallef, J.; Lhotak, V.; May, L.; Guha, A.; Rak, J., Intercellular transfer of the oncogenic receptor EGFRvIII by microvesicles derived from tumour cells. *Nat Cell Biol* **2008,** *10* (5), 619-24.
118. Stegmayr, B.; Ronquist, G., Promotive effect on human sperm progressive motility by prostasomes. *Urol Res* **1982,** *10* (5), 253-7.
119. Klion, F. M.; Schaffner, F., The ultrastructure of acidophilic "Councilman-like" bodies in the liver. *Am J Pathol* **1966,** *48* (5), 755-67.
120. Kerr, J. F.; Wyllie, A. H.; Currie, A. R., Apoptosis: a basic biological phenomenon with wide-ranging implications in tissue kinetics. *Br J Cancer* **1972,** *26* (4), 239-57.
121. Tkach, M.; Kowal, J.; Thery, C., Why the need and how to approach the functional diversity of extracellular vesicles. *Philos Trans R Soc Lond B Biol Sci* **2018,** *373* (1737).
122. Kim, J. H.; Lee, J.; Park, J.; Gho, Y. S., Gram-negative and Gram-positive bacterial extracellular vesicles. *Semin Cell Dev Biol* **2015,** *40*, 97-104.
123. Rodrigues, M. L.; Nakayasu, E. S.; Almeida, I. C.; Nimrichter, L., The impact of proteomics on the understanding of functions and biogenesis of fungal extracellular vesicles. *J Proteomics* **2014,** *97*, 177-86.
124. Rutter, B. D.; Innes, R. W., Extracellular Vesicles Isolated from the Leaf Apoplast Carry Stress-Response Proteins. *Plant Physiol* **2017,** *173* (1), 728-741.
125. Wehman, A. M.; Poggioli, C.; Schweinsberg, P.; Grant, B. D.; Nance, J., The P4-ATPase TAT-5 inhibits the budding of extracellular vesicles in C. elegans embryos. *Curr Biol* **2011,** *21* (23), 1951-9.
126. Korkut, C.; Ataman, B.; Ramachandran, P.; Ashley, J.; Barria, R.; Gherbesi, N.; Budnik, V., Trans-synaptic transmission of vesicular Wnt signals through Evi/Wntless. *Cell* **2009,** *139* (2), 393-404.
127. Cocucci, E.; Racchetti, G.; Meldolesi, J., Shedding microvesicles: artefacts no more. *Trends Cell Biol* **2009,** *19* (2), 43-51.
128. Bastida, E.; Ordinas, A.; Escolar, G.; Jamieson, G. A., Tissue factor in microvesicles shed from U87MG human glioblastoma cells induces coagulation, platelet aggregation, and thrombogenesis. *Blood* **1984,** *64* (1), 177-84.
129. Raposo, G.; Tenza, D.; Mecheri, S.; Peronet, R.; Bonnerot, C.; Desaymard, C., Accumulation of major histocompatibility complex class II molecules in mast cell secretory granules and their release upon degranulation. *Mol Biol Cell* **1997,** *8* (12), 2631-45.
130. Zitvogel, L.; Regnault, A.; Lozier, A.; Wolfers, J.; Flament, C.; Tenza, D.; Ricciardi-Castagnoli, P.; Raposo, G.; Amigorena, S., Eradication of established murine tumors using a novel cell-free vaccine: dendritic cell-derived exosomes. *Nat Med* **1998,** *4* (5), 594-600.
131. Denzer, K.; van Eijk, M.; Kleijmeer, M. J.; Jakobson, E.; de Groot, C.; Geuze, H. J., Follicular dendritic cells carry MHC class II-expressing microvesicles at their surface. *J Immunol* **2000,** *165* (3), 1259-65.

132. Zomer, A.; Maynard, C.; Verweij, F. J.; Kamermans, A.; Schafer, R.; Beerling, E.; Schiffelers, R. M.; de Wit, E.; Berenguer, J.; Ellenbroek, S. I.; Wurdinger, T.; Pegtel, D. M.; van Rheenen, J., In Vivo imaging reveals extracellular vesicle-mediated phenocopying of metastatic behavior. *Cell* **2015,** *161* (5), 1046-57.
133. Krug, A. K.; Enderle, D.; Karlovich, C.; Priewasser, T.; Bentink, S.; Spiel, A.; Brinkmann, K.; Emenegger, J.; Grimm, D. G.; Castellanos-Rizaldos, E.; Goldman, J. W.; Sequist, L. V.; Soria, J. C.; Camidge, D. R.; Gadgeel, S. M.; Wakelee, H. A.; Raponi, M.; Noerholm, M.; Skog, J., Improved EGFR mutation detection using combined exosomal RNA and circulating tumor DNA in NSCLC patient plasma. *Ann Oncol* **2017,** *5* (4693822).
134. Wen, S.; Dooner, M.; Cheng, Y.; Papa, E.; Del Tatto, M.; Pereira, M.; Deng, Y.; Goldberg, L.; Aliotta, J.; Chatterjee, D.; Stewart, C.; Carpanetto, A.; Collino, F.; Bruno, S.; Camussi, G.; Quesenberry, P., Mesenchymal stromal cell-derived extracellular vesicles rescue radiation damage to murine marrow hematopoietic cells. *Leukemia* **2016**, 107.
135. Didiot, M.-C.; Hall, L. M.; Coles, A. H.; Haraszti, R. A.; Godinho, B. M. D. C.; Chase, K.; Sapp, E.; Ly, S.; Alterman, J. F.; Hassler, M. R.; Echeverria, D.; Raj, L.; Morrissey, D. V.; DiFiglia, M.; Aronin, N.; Khvorova, A., Exosome-mediated Delivery of Hydrophobically Modified siRNA for Huntingtin mRNA Silencing. *Molecular Therapy* **2016**.
136. Kamerkar, S.; LeBleu, V. S.; Sugimoto, H.; Yang, S.; Ruivo, C. F.; Melo, S. A.; Lee, J. J.; Kalluri, R., Exosomes facilitate therapeutic targeting of oncogenic KRAS in pancreatic cancer. *Nature* **2017,** *546* (7659), 498-503.
137. Hoshino, A.; Costa-Silva, B.; Shen, T. L.; Rodrigues, G.; Hashimoto, A.; Tesic Mark, M.; Molina, H.; Kohsaka, S.; Di Giannatale, A.; Ceder, S.; Singh, S.; Williams, C.; Soplop, N.; Uryu, K.; Pharmer, L.; King, T.; Bojmar, L.; Davies, A. E.; Ararso, Y.; Zhang, T.; Zhang, H.; Hernandez, J.; Weiss, J. M.; Dumont-Cole, V. D.; Kramer, K.; Wexler, L. H.; Narendran, A.; Schwartz, G. K.; Healey, J. H.; Sandstrom, P.; Labori, K. J.; Kure, E. H.; Grandgenett, P. M.; Hollingsworth, M. A.; de Sousa, M.; Kaur, S.; Jain, M.; Mallya, K.; Batra, S. K.; Jarnagin, W. R.; Brady, M. S.; Fodstad, O.; Muller, V.; Pantel, K.; Minn, A. J.; Bissell, M. J.; Garcia, B. A.; Kang, Y.; Rajasekhar, V. K.; Ghajar, C. M.; Matei, I.; Peinado, H.; Bromberg, J.; Lyden, D., Tumour exosome integrins determine organotropic metastasis. *Nature* **2015,** *527* (7578), 329-35.
138. Valadi, H.; Ekstrom, K.; Bossios, A.; Sjostrand, M.; Lee, J. J.; Lotvall, J. O., Exosome-mediated transfer of mRNAs and microRNAs is a novel mechanism of genetic exchange between cells. *Nat Cell Biol* **2007,** *9* (6), 654-9.
139. Xin, H.; Li, Y.; Buller, B.; Katakowski, M.; Zhang, Y.; Wang, X.; Shang, X.; Zhang, Z. G.; Chopp, M., Exosome-mediated transfer of miR-133b from multipotent mesenchymal stromal cells to neural cells contributes to neurite outgrowth. *Stem Cells* **2012,** *30* (7), 1556-64.
140. Laulagnier, K.; Motta, C.; Hamdi, S.; Roy, S.; Fauvelle, F.; Pageaux, J. F.; Kobayashi, T.; Salles, J. P.; Perret, B.; Bonnerot, C.; Record, M., Mast cell- and dendritic cell-derived exosomes display a specific lipid composition and an unusual membrane organization. *Biochem J* **2004,** *380* (Pt 1), 161-71.
141. Clayton, A.; Harris, C. L.; Court, J.; Mason, M. D.; Morgan, B. P., Antigen-presenting cell exosomes are protected from complement-mediated lysis by expression of CD55 and CD59. *Eur J Immunol* **2003,** *33* (2), 522-31.
142. Kim, H. S.; Choi, D. Y.; Yun, S. J.; Choi, S. M.; Kang, J. W.; Jung, J. W.; Hwang, D.; Kim, K. P.; Kim, D. W., Proteomic analysis of microvesicles derived from human mesenchymal stem cells. *J Proteome Res* **2012,** *11* (2), 839-49.

143. Bolukbasi, M. F.; Mizrak, A.; Ozdener, G. B.; Madlener, S.; Strobel, T.; Erkan, E. P.; Fan, J. B.; Breakefield, X. O.; Saydam, O., miR-1289 and "Zipcode"-like Sequence Enrich mRNAs in Microvesicles. *Mol Ther Nucleic Acids* **2012,** *1* (1), e10.
144. Wang, J. H.; Forterre, A. V.; Zhao, J.; Frimannsson, D. O.; Delcayre, A.; Antes, T. J.; Efron, B.; Jeffrey, S. S.; Pegram, M. D.; Matin, A. C., Anti-HER2 scFv-directed extracellular vesicle-mediated mRNA-based gene delivery inhibits growth of HER2-positive human breast tumor xenografts by prodrug activation. *Mol Cancer Ther* **2018,** *26*, 1535-7163.
145. Villarroya-Beltri, C.; Gutierrez-Vazquez, C.; Sanchez-Cabo, F.; Perez-Hernandez, D.; Vazquez, J.; Martin-Cofreces, N.; Martinez-Herrera, D. J.; Pascual-Montano, A.; Mittelbrunn, M.; Sanchez-Madrid, F., Sumoylated hnRNPA2B1 controls the sorting of miRNAs into exosomes through binding to specific motifs. *Nat Commun* **2013,** *4* (2980), 2980.
146. Lai, C. P.; Kim, E. Y.; Badr, C. E.; Weissleder, R.; Mempel, T. R.; Tannous, B. A.; Breakefield, X. O., Visualization and tracking of tumour extracellular vesicle delivery and RNA translation using multiplexed reporters. *Nat Commun* **2015,** *6* (7029), 7029.
147. Hung, M. E.; Leonard, J. N., A platform for actively loading cargo RNA to elucidate limiting steps in EV-mediated delivery. *J Extracell Vesicles* **2016,** *5* (31027), 31027.
148. Wang, Q.; Yu, J.; Kadungure, T.; Beyene, J.; Zhang, H.; Lu, Q., ARMMs as a versatile platform for intracellular delivery of macromolecules. *Nat Commun* **2018,** *9* (1), 960.
149. Alvarez-Erviti, L.; Seow, Y.; Yin, H.; Betts, C.; Lakhal, S.; Wood, M. J., Delivery of siRNA to the mouse brain by systemic injection of targeted exosomes. *Nat Biotechnol* **2011,** *29* (4), 341-5.
150. Momen-Heravi, F.; Bala, S.; Kodys, K.; Szabo, G., Exosomes derived from alcohol-treated hepatocytes horizontally transfer liver specific miRNA-122 and sensitize monocytes to LPS. *Sci Rep* **2015,** *5* (9991), 9991.
151. Mathiyalagan, P.; Sahoo, S., Exosomes-Based Gene Therapy for MicroRNA Delivery. *Methods Mol Biol* **2017,** *1521*, 139-152.
152. Zhu, Z.; Zhang, D.; Lee, H.; Menon, A. A.; Wu, J.; Hu, K.; Jin, Y., Macrophage-derived apoptotic bodies promote the proliferation of the recipient cells via shuttling microRNA-221/222. *J Leukoc Biol* **2017,** *101* (6), 1349-1359.
153. O'Loughlin, A. J.; Mager, I.; de Jong, O. G.; Varela, M. A.; Schiffelers, R. M.; El Andaloussi, S.; Wood, M. J. A.; Vader, P., Functional Delivery of Lipid-Conjugated siRNA by Extracellular Vesicles. *Mol Ther* **2017,** *25* (7), 1580-1587.
154. Stremersch, S.; Vandenbroucke, R. E.; Van Wonterghem, E.; Hendrix, A.; De Smedt, S. C.; Raemdonck, K., Comparing exosome-like vesicles with liposomes for the functional cellular delivery of small RNAs. *J Control Release* **2016,** *232*, 51-61.
155. Pi, F.; Binzel, D. W.; Lee, T. J.; Li, Z.; Sun, M.; Rychahou, P.; Li, H.; Haque, F.; Wang, S.; Croce, C. M.; Guo, B.; Evers, B. M.; Guo, P., Nanoparticle orientation to control RNA loading and ligand display on extracellular vesicles for cancer regression. *Nat Nanotechnol* **2018,** *13* (1), 82-89.
156. Kooijmans, S. A.; Stremersch, S.; Braeckmans, K.; de Smedt, S. C.; Hendrix, A.; Wood, M. J.; Schiffelers, R. M.; Raemdonck, K.; Vader, P., Electroporation-induced siRNA precipitation obscures the efficiency of siRNA loading into extracellular vesicles. *J Control Release* **2013,** *172* (1), 229-38.
157. Gyorgy, B.; Fitzpatrick, Z.; Crommentuijn, M. H.; Mu, D.; Maguire, C. A., Naturally enveloped AAV vectors for shielding neutralizing antibodies and robust gene delivery in vivo. *Biomaterials* **2014,** *35* (26), 7598-609.

158. Gyorgy, B.; Sage, C.; Indzhykulian, A. A.; Scheffer, D. I.; Brisson, A. R.; Tan, S.; Wu, X.; Volak, A.; Mu, D.; Tamvakologos, P. I.; Li, Y.; Fitzpatrick, Z.; Ericsson, M.; Breakefield, X. O.; Corey, D. P.; Maguire, C. A., Rescue of Hearing by Gene Delivery to Inner-Ear Hair Cells Using Exosome-Associated AAV. *Mol Ther* **2017,** *25* (2), 379-391.
159. Wassmer, S. J.; Carvalho, L. S.; Gyorgy, B.; Vandenberghe, L. H.; Maguire, C. A., Exosome-associated AAV2 vector mediates robust gene delivery into the murine retina upon intravitreal injection. *Sci Rep* **2017,** *7* (45329), 45329.
160. Feng, Z.; Hensley, L.; McKnight, K. L.; Hu, F.; Madden, V.; Ping, L.; Jeong, S. H.; Walker, C.; Lanford, R. E.; Lemon, S. M., A pathogenic picornavirus acquires an envelope by hijacking cellular membranes. *Nature* **2013,** *496* (7445), 367-71.
161. Gheysen, D.; Jacobs, E.; de Foresta, F.; Thiriart, C.; Francotte, M.; Thines, D.; De Wilde, M., Assembly and release of HIV-1 precursor Pr55gag virus-like particles from recombinant baculovirus-infected insect cells. *Cell* **1989,** *59* (1), 103-12.
162. Mangeot, P. E.; Rissons, V.; Fusil, F.; Marnef, A.; Laurent, E.; Blin, J.; Mournetas, V.; Massourides, E.; Sohier, T. J. M.; Corbin, A.; Aube, F.; Pinset, C.; Schaeffer, L.; Legube, G.; Cosset, F.-L.; Verhoeyen, E.; Ohlmann, T.; Ricci, E. P., Efficient genome editing in primary cells and in vivo using viral-derived "Nanoblades" loaded with Cas9/sgRNA ribonucleoproteins. *bioRxiv* **2017**.
163. Yim, N.; Ryu, S. W.; Choi, K.; Lee, K. R.; Lee, S.; Choi, H.; Kim, J.; Shaker, M. R.; Sun, W.; Park, J. H.; Kim, D.; Heo, W. D.; Choi, C., Exosome engineering for efficient intracellular delivery of soluble proteins using optically reversible protein-protein interaction module. *Nat Commun* **2016,** *7* (12277), 12277.
164. Tian, Y.; Li, S.; Song, J.; Ji, T.; Zhu, M.; Anderson, G. J.; Wei, J.; Nie, G., A doxorubicin delivery platform using engineered natural membrane vesicle exosomes for targeted tumor therapy. *Biomaterials* **2014,** *35* (7), 2383-90.
165. Amano, T.; Furuno, T.; Hirashima, N.; Ohyama, N.; Nakanishi, M., Dynamics of intracellular granules with CD63-GFP in rat basophilic leukemia cells. *J Biochem* **2001,** *129* (5), 739-44.
166. Hartman, Z. C.; Wei, J.; Glass, O. K.; Guo, H.; Lei, G.; Yang, X. Y.; Osada, T.; Hobeika, A.; Delcayre, A.; Le Pecq, J. B.; Morse, M. A.; Clay, T. M.; Lyerly, H. K., Increasing vaccine potency through exosome antigen targeting. *Vaccine* **2011,** *29* (50), 9361-7.
167. Lai, C. P.; Mardini, O.; Ericsson, M.; Prabhakar, S.; Maguire, C. A.; Chen, J. W.; Tannous, B. A.; Breakefield, X. O., Dynamic biodistribution of extracellular vesicles in vivo using a multimodal imaging reporter. *ACS Nano* **2014,** *8* (1), 483-94.
168. Shen, B.; Wu, N.; Yang, J. M.; Gould, S. J., Protein targeting to exosomes/microvesicles by plasma membrane anchors. *J Biol Chem* **2011,** *286* (16), 14383-95.
169. Haney, M. J.; Klyachko, N. L.; Zhao, Y.; Gupta, R.; Plotnikova, E. G.; He, Z.; Patel, T.; Piroyan, A.; Sokolsky, M.; Kabanov, A. V.; Batrakova, E. V., Exosomes as drug delivery vehicles for Parkinson's disease therapy. *J Control Release* **2015,** *207*, 18-30.
170. Smyth, T.; Petrova, K.; Payton, N. M.; Persaud, I.; Redzic, J. S.; Graner, M. W.; Smith-Jones, P.; Anchordoquy, T. J., Surface functionalization of exosomes using click chemistry. *Bioconjug Chem* **2014,** *25* (10), 1777-84.
171. Liu, Y.; Hou, W.; Sun, H.; Cui, C.; Zhang, L.; Jiang, Y.; Wu, Y.; Wang, Y.; Li, J.; Sumerlin, B. S.; Liu, Q.; Tan, W., Thiol-ene click chemistry: a biocompatible way for orthogonal bioconjugation of colloidal nanoparticles. *Chem Sci* **2017,** *8* (9), 6182-6187.

172. Didiot, M. C.; Hall, L. M.; Coles, A. H.; Haraszti, R. A.; Godinho, B. M.; Chase, K.; Sapp, E.; Ly, S.; Alterman, J. F.; Hassler, M. R.; Echeverria, D.; Raj, L.; Morrissey, D. V.; DiFiglia, M.; Aronin, N.; Khvorova, A., Exosome-mediated Delivery of Hydrophobically Modified siRNA for Huntingtin mRNA Silencing. *Mol Ther* **2016**.
173. Sun, D.; Zhuang, X.; Xiang, X.; Liu, Y.; Zhang, S.; Liu, C.; Barnes, S.; Grizzle, W.; Miller, D.; Zhang, H. G., A novel nanoparticle drug delivery system: the anti-inflammatory activity of curcumin is enhanced when encapsulated in exosomes. *Mol Ther* **2010,** *18* (9), 1606-14.
174. Zhuang, X.; Xiang, X.; Grizzle, W.; Sun, D.; Zhang, S.; Axtell, R. C.; Ju, S.; Mu, J.; Zhang, L.; Steinman, L.; Miller, D.; Zhang, H. G., Treatment of brain inflammatory diseases by delivering exosome encapsulated anti-inflammatory drugs from the nasal region to the brain. *Mol Ther* **2011,** *19* (10), 1769-79.
175. Gao, J.; Wang, S.; Wang, Z., High yield, scalable and remotely drug-loaded neutrophil-derived extracellular vesicles (EVs) for anti-inflammation therapy. *Biomaterials* **2017,** *135*, 62-73.
176. Jang, S. C.; Kim, O. Y.; Yoon, C. M.; Choi, D. S.; Roh, T. Y.; Park, J.; Nilsson, J.; Lotvall, J.; Kim, Y. K.; Gho, Y. S., Bioinspired exosome-mimetic nanovesicles for targeted delivery of chemotherapeutics to malignant tumors. *ACS Nano* **2013,** *7* (9), 7698-710.
177. Jo, W.; Jeong, D.; Kim, J.; Cho, S.; Jang, S. C.; Han, C.; Kang, J. Y.; Gho, Y. S.; Park, J., Microfluidic fabrication of cell-derived nanovesicles as endogenous RNA carriers. *Lab Chip* **2014,** *14* (7), 1261-9.
178. Yoon, J.; Jo, W.; Jeong, D.; Kim, J.; Jeong, H.; Park, J., Generation of nanovesicles with sliced cellular membrane fragments for exogenous material delivery. *Biomaterials* **2015,** *59*, 12-20.
179. Jo, W.; Kim, J.; Yoon, J.; Jeong, D.; Cho, S.; Jeong, H.; Yoon, Y. J.; Kim, S. C.; Gho, Y. S.; Park, J., Large-scale generation of cell-derived nanovesicles. *Nanoscale* **2014,** *6* (20), 12056-64.
180. Westergard, T.; Jensen, B. K.; Wen, X.; Cai, J.; Kropf, E.; Iacovitti, L.; Pasinelli, P.; Trotti, D., Cell-to-Cell Transmission of Dipeptide Repeat Proteins Linked to C9orf72-ALS/FTD. *Cell Rep* **2016,** *17* (3), 645-652.
181. Grad, L. I.; Pokrishevsky, E.; Silverman, J. M.; Cashman, N. R., Exosome-dependent and independent mechanisms are involved in prion-like transmission of propagated Cu/Zn superoxide dismutase misfolding. *Prion* **2014,** *8* (5), 331-5.
182. Fruhbeis, C.; Frohlich, D.; Kuo, W. P.; Amphornrat, J.; Thilemann, S.; Saab, A. S.; Kirchhoff, F.; Mobius, W.; Goebbels, S.; Nave, K. A.; Schneider, A.; Simons, M.; Klugmann, M.; Trotter, J.; Kramer-Albers, E. M., Neurotransmitter-triggered transfer of exosomes mediates oligodendrocyte-neuron communication. *PLoS Biol* **2013,** *11* (7), e1001604.
183. Bahrini, I.; Song, J. H.; Diez, D.; Hanayama, R., Neuronal exosomes facilitate synaptic pruning by up-regulating complement factors in microglia. *Sci Rep* **2015,** *5* (7989), 7989.
184. Guo, B. B.; Bellingham, S. A.; Hill, A. F., The neutral sphingomyelinase pathway regulates packaging of the prion protein into exosomes. *J Biol Chem* **2015,** *290* (6), 3455-67.
185. Zhang, X.; Abels, E. R.; Redzic, J. S.; Margulis, J.; Finkbeiner, S.; Breakefield, X. O., Potential Transfer of Polyglutamine and CAG-Repeat RNA in Extracellular Vesicles in Huntington's Disease: Background and Evaluation in Cell Culture. *Cell Mol Neurobiol* **2016,** *36* (3), 459-70.

186. Mercuri, E.; Darras, B. T.; Chiriboga, C. A.; Day, J. W.; Campbell, C.; Connolly, A. M.; Iannaccone, S. T.; Kirschner, J.; Kuntz, N. L.; Saito, K.; Shieh, P. B.; Tulinius, M.; Mazzone, E. S.; Montes, J.; Bishop, K. M.; Yang, Q.; Foster, R.; Gheuens, S.; Bennett, C. F.; Farwell, W.; Schneider, E.; De Vivo, D. C.; Finkel, R. S., Nusinersen versus Sham Control in Later-Onset Spinal Muscular Atrophy. *N Engl J Med* **2018,** *378* (7), 625-635.
187. Safety and Tolerability of WVE-120102 in Patients With Huntington's Disease. https://ClinicalTrials.gov/show/NCT03225846.
188. Safety, Tolerability, Pharmacokinetics, and Pharmacodynamics of IONIS-HTTRx in Patients With Early Manifest Huntington's Disease. https://ClinicalTrials.gov/show/NCT02519036.
189. Doeppner, T. R.; Herz, J.; Gorgens, A.; Schlechter, J.; Ludwig, A. K.; Radtke, S.; de Miroschedji, K.; Horn, P. A.; Giebel, B.; Hermann, D. M., Extracellular Vesicles Improve Post-Stroke Neuroregeneration and Prevent Postischemic Immunosuppression. *Stem Cells Transl Med* **2015,** *4* (10), 1131-43.
190. Yang, J.; Zhang, X.; Chen, X.; Wang, L.; Yang, G., Exosome Mediated Delivery of miR-124 Promotes Neurogenesis after Ischemia. *Mol Ther Nucleic Acids* **2017,** *7*, 278-287.
191. Norremolle, A.; Riess, O.; Epplen, J. T.; Fenger, K.; Hasholt, L.; Sorensen, S. A., Trinucleotide repeat elongation in the Huntingtin gene in Huntington disease patients from 71 Danish families. *Hum Mol Genet* **1993,** *2* (9), 1475-6.
192. Kay, C.; Skotte, N. H.; Southwell, A. L.; Hayden, M. R., Personalized gene silencing therapeutics for Huntington disease. *Clin Genet* **2014,** *86* (1), 29-36.
193. Drouet, V.; Ruiz, M.; Zala, D.; Feyeux, M.; Auregan, G.; Cambon, K.; Troquier, L.; Carpentier, J.; Aubert, S.; Merienne, N.; Bourgois-Rocha, F.; Hassig, R.; Rey, M.; Dufour, N.; Saudou, F.; Perrier, A. L.; Hantraye, P.; Deglon, N., Allele-specific silencing of mutant huntingtin in rodent brain and human stem cells. *PLoS One* **2014,** *9* (6), e99341.
194. Hu, J.; Matsui, M.; Gagnon, K. T.; Schwartz, J. C.; Gabillet, S.; Arar, K.; Wu, J.; Bezprozvanny, I.; Corey, D. R., Allele-specific silencing of mutant huntingtin and ataxin-3 genes by targeting expanded CAG repeats in mRNAs. *Nat Biotechnol* **2009,** *27* (5), 478-84.
195. Strehlow, A. N.; Li, J. Z.; Myers, R. M., Wild-type huntingtin participates in protein trafficking between the Golgi and the extracellular space. *Hum Mol Genet* **2007,** *16* (4), 391-409.
196. Lee, M.; Liu, T.; Im, W.; Kim, M., Exosomes from adipose-derived stem cells ameliorate phenotype of Huntington's disease in vitro model. *Eur J Neurosci* **2016,** *44* (4), 2114-9.
197. Nikan, M.; Osborn, M. F.; Coles, A. H.; Biscans, A.; Godinho, B. M.; Haraszti, R. A.; Sapp, E.; Echeverria, D.; DiFiglia, M.; Aronin, N.; Khvorova, A., Synthesis and evaluation of parenchymal retention and efficacy of a metabolically stable O-Phosphocholine-N-docosahexaenoyl-l-serine siRNA conjugate in mouse brain. *Bioconjugate Chem.* **2017,** *28*, 1758-1766.
198. Nikan, M.; Osborn, M. F.; Coles, A. H.; Godinho, B. M.; Hall, L. M.; Haraszti, R. A.; Hassler, M. R.; Echeverria, D.; Aronin, N.; Khvorova, A., Docosahexaenoic acid conjugation enhances distribution and safety of siRNA upon local administration in mouse brain. *Mol. Ther. Nucleic acids* **2016,** *5*, e344.
199. Haraszti, R. A.; Roux, L.; Coles, A. H.; Turanov, A. A.; Alterman, J. F.; Echeverria, D.; Godinho, B. M.; Aronin, N.; Khvorova, A., 5′-Vinylphosphonate improves tissue

accumulation and efficacy of conjugated siRNAs in vivo. *Nucleic Acids Res.* **2017,** *45*, 7581-7592.
200. Coles, A. H.; Osborn, M. F.; Alterman, J. F.; Turanov, A. A.; Godinho, B. M.; Kennington, L.; Chase, K.; Aronin, N.; Khvorova, A., A High-Throughput Method for Direct Detection of Therapeutic Oligonucleotide-Induced Gene Silencing In Vivo. *Nucleic Acid Ther* **2016,** *26* (2), 86-92.
201. Haraszti, R. A.; Roux, L.; Coles, A. H.; Turanov, A. A.; Alterman, J. F.; Echeverria, D.; Godinho, B.; Aronin, N.; Khvorova, A., 5-Vinylphosphonate improves tissue accumulation and efficacy of conjugated siRNAs in vivo. *Nucleic Acids Res* **2017,** *45* (13), 7581-7592.
202. Nikan, M.; Osborn, M. F.; Coles, A. H.; Godinho, B. M.; Hall, L. M.; Haraszti, R. A.; Hassler, M. R.; Echeverria, D.; Aronin, N.; Khvorova, A., Docosahexaenoic Acid Conjugation Enhances Distribution and Safety of siRNA upon Local Administration in Mouse Brain. *Mol Ther Nucleic Acids* **2016,** *5* (8), e344.
203. Roehl, I.; Schuster, M.; Seiffert, S., Oligonucleotide detection method. 2011; Vol. US20110201006 A1.
204. Thery, C.; Amigorena, S.; Raposo, G.; Clayton, A., Isolation and characterization of exosomes from cell culture supernatants and biological fluids. *Curr Protoc Cell Biol* **2006,** *Chapter 3*, Unit 3 22.
205. Roehl, I.; Schuster, M.; Seiffert, S. Oligonucleotide detection method. 2011.
206. Schneider, C. A.; Rasband, W. S.; Eliceiri, K. W., NIH Image to ImageJ: 25 years of image analysis. *Nat Methods* **2012,** *9* (7), 671-5.
207. Kiebish, M. A.; Bell, R.; Yang, K.; Phan, T.; Zhao, Z.; Ames, W.; Seyfried, T. N.; Gross, R. W.; Chuang, J. H.; Han, X., Dynamic simulation of cardiolipin remodeling: greasing the wheels for an interpretative approach to lipidomics. *J Lipid Res* **2010,** *51* (8), 2153-70.
208. Simons, B.; Kauhanen, D.; Sylvanne, T.; Tarasov, K.; Duchoslav, E.; Ekroos, K., Shotgun Lipidomics by Sequential Precursor Ion Fragmentation on a Hybrid Quadrupole Time-of-Flight Mass Spectrometer. *Metabolites* **2012,** *2* (1), 195-213.
209. Huang da, W.; Sherman, B. T.; Lempicki, R. A., Bioinformatics enrichment tools: paths toward the comprehensive functional analysis of large gene lists. *Nucleic Acids Res* **2009,** *37* (1), 1-13.
210. Huang da, W.; Sherman, B. T.; Lempicki, R. A., Systematic and integrative analysis of large gene lists using DAVID bioinformatics resources. *Nat Protoc* **2009,** *4* (1), 44-57.
211. Wilhelm, M.; Schlegl, J.; Hahne, H.; Moghaddas Gholami, A.; Lieberenz, M.; Savitski, M. M.; Ziegler, E.; Butzmann, L.; Gessulat, S.; Marx, H.; Mathieson, T.; Lemeer, S.; Schnatbaum, K.; Reimer, U.; Wenschuh, H.; Mollenhauer, M.; Slotta-Huspenina, J.; Boese, J. H.; Bantscheff, M.; Gerstmair, A.; Faerber, F.; Kuster, B., Mass-spectrometry-based draft of the human proteome. *Nature* **2014,** *509* (7502), 582-7.
212. Zamore, P. D., RNA interference: listening to the sound of silence. *Nat Struct Biol* **2001,** *8* (9), 746-50.
213. Byrne, M.; Tzekov, R.; Wang, Y.; Rodgers, A.; Cardia, J.; Ford, G.; Holton, K.; Pandarinathan, L.; Lapierre, J.; Stanney, W.; Bulock, K.; Shaw, S.; Libertine, L.; Fettes, K.; Khvorova, A.; Kaushal, S.; Pavco, P., Novel hydrophobically modified asymmetric RNAi compounds (sd-rxRNA) demonstrate robust efficacy in the eye. *J Ocul Pharmacol Ther* **2013,** *29* (10), 855-64.
214. Nair, J. K.; Willoughby, J. L.; Chan, A.; Charisse, K.; Alam, M. R.; Wang, Q.; Hoekstra, M.; Kandasamy, P.; Kel'in, A. V.; Milstein, S.; Taneja, N.; O'Shea, J.; Shaikh, S.; Zhang, L.; van der

Sluis, R. J.; Jung, M. E.; Akinc, A.; Hutabarat, R.; Kuchimanchi, S.; Fitzgerald, K.; Zimmermann, T.; van Berkel, T. J.; Maier, M. A.; Rajeev, K. G.; Manoharan, M., Multivalent N-acetylgalactosamine-conjugated siRNA localizes in hepatocytes and elicits robust RNAi-mediated gene silencing. *J Am Chem Soc* **2014,** *136* (49), 16958-61.
215. Khan, T.; Weber, H.; DiMuzio, J.; Matter, A.; Dogdas, B.; Shah, T.; Thankappan, A.; Disa, J.; Jadhav, V.; Lubbers, L.; Sepp-Lorenzino, L.; Strapps, W. R.; Tadin-Strapps, M., Silencing Myostatin Using Cholesterol-conjugated siRNAs Induces Muscle Growth. *Mol Ther Nucleic Acids* **2016,** *5* (8), e342.
216. Matsuda, S.; Keiser, K.; Nair, J. K.; Charisse, K.; Manoharan, R. M.; Kretschmer, P.; Peng, C. G.; A, V. K. i.; Kandasamy, P.; Willoughby, J. L.; Liebow, A.; Querbes, W.; Yucius, K.; Nguyen, T.; Milstein, S.; Maier, M. A.; Rajeev, K. G.; Manoharan, M., siRNA conjugates carrying sequentially assembled trivalent N-acetylgalactosamine linked through nucleosides elicit robust gene silencing in vivo in hepatocytes. *ACS chemical biology* **2015,** *10* (5), 1181-7.
217. Sehgal, A.; Vaishnaw, A.; Fitzgerald, K., Liver as a target for oligonucleotide therapeutics. *J Hepatol* **2013,** *59* (6), 1354-9.
218. Fitzgerald, K.; White, S.; Borodovsky, A.; Bettencourt, B. R.; Strahs, A.; Clausen, V.; Wijngaard, P.; Horton, J. D.; Taubel, J.; Brooks, A.; Fernando, C.; Kauffman, R. S.; Kallend, D.; Vaishnaw, A.; Simon, A., A Highly Durable RNAi Therapeutic Inhibitor of PCSK9. *New England Journal of Medicine* **2016**.
219. Martinez, J.; Patkaniowska, A.; Urlaub, H.; Luhrmann, R.; Tuschl, T., Single-stranded antisense siRNAs guide target RNA cleavage in RNAi. *Cell* **2002,** *110* (5), 563-74.
220. Ma, J. B.; Yuan, Y. R.; Meister, G.; Pei, Y.; Tuschl, T.; Patel, D. J., Structural basis for 5'-end-specific recognition of guide RNA by the A. fulgidus Piwi protein. *Nature* **2005,** *434* (7033), 666-70.
221. Frank, F.; Sonenberg, N.; Nagar, B., Structural basis for 5[prime]-nucleotide base-specific recognition of guide RNA by human AGO2. *Nature* **2010,** *465* (7299), 818-822.
222. Weitzer, S.; Martinez, J., The human RNA kinase hClp1 is active on 3' transfer RNA exons and short interfering RNAs. *Nature* **2007,** *447* (7141), 222-6.
223. Kenski, D. M.; Cooper, A. J.; Li, J. J.; Willingham, A. T.; Haringsma, H. J.; Young, T. A.; Kuklin, N. A.; Jones, J. J.; Cancilla, M. T.; McMasters, D. R.; Mathur, M.; Sachs, A. B.; Flanagan, W. M., Analysis of acyclic nucleoside modifications in siRNAs finds sensitivity at position 1 that is restored by 5'-terminal phosphorylation both in vitro and in vivo. *Nucleic Acids Res* **2010,** *38* (2), 660-71.
224. Engel, R., Phosphonates as analogues of natural phosphates. *Chemical Reviews* **1977,** *77* (3), 349-367.
225. Yu, D.; Pendergraff, H.; Liu, J.; Kordasiewicz, H. B.; Cleveland, Don W.; Swayze, Eric E.; Lima, Walt F.; Crooke, Stanley T.; Prakash, Thazha P.; Corey, David R., Single-Stranded RNAs Use RNAi to Potently and Allele-Selectively Inhibit Mutant Huntingtin Expression. *Cell* **2012,** *150* (5), 895-908.
226. Hampton, A.; Kappler, F.; Perini, F., Evidence for the conformation about the C(5′)-O(5′) bond of AMP complexed to AMP kinase: Substrate properties of a vinyl phosphonate analog of AMP. *Bioorganic Chemistry* **1976,** *5* (1), 31-35.

227. Kappler, F.; Hai, T. T.; Hampton, A., Use of a vinyl phosphonate analog of ATP as a rotationally constrained probe of the C5′ · O5′ torsion angle in ATP complexed to methionine adenosyl transferase. *Bioorganic Chemistry* **1985,** *13* (4), 289-295.
228. Prakash, T. P.; Lima, W. F.; Murray, H. M.; Elbashir, S.; Cantley, W.; Foster, D.; Jayaraman, M.; Chappell, A. E.; Manoharan, M.; Swayze, E. E.; Crooke, S. T., Lipid nanoparticles improve activity of single-stranded siRNA and gapmer antisense oligonucleotides in animals. *ACS Chem Biol* **2013,** *8* (7), 1402-6.
229. Parmar, R.; Willoughby, J. L.; Liu, J.; Foster, D. J.; Brigham, B.; Theile, C. S.; Charisse, K.; Akinc, A.; Guidry, E.; Pei, Y.; Strapps, W.; Cancilla, M.; Stanton, M. G.; Rajeev, K. G.; Sepp-Lorenzino, L.; Manoharan, M.; Meyers, R.; Maier, M. A.; Jadhav, V., 5'-(E)-Vinylphosphonate: A Stable Phosphate Mimic Can Improve the RNAi Activity of siRNA-GalNAc Conjugates. *Chembiochem* **2016,** *17* (11), 985-9.
230. Prakash, T. P.; Kinberger, G. A.; Murray, H. M.; Chappell, A.; Riney, S.; Graham, M. J.; Lima, W. F.; Swayze, E. E.; Seth, P. P., Synergistic effect of phosphorothioate, 5'-vinylphosphonate and GalNAc modifications for enhancing activity of synthetic siRNA. *Bioorg Med Chem Lett* **2016,** *26* (12), 2817-20.
231. Elkayam, E.; Parmar, R.; Brown, C. R.; Willoughby, J. L.; Theile, C. S.; Manoharan, M.; Joshua-Tor, L., siRNA carrying an (E)-vinylphosphonate moiety at the 5' end of the guide strand augments gene silencing by enhanced binding to human Argonaute-2. *Nucleic Acids Res* **2016**.
232. Ly, S.; Navaroli, D. M.; Didiot, M. C.; Cardia, J.; Pandarinathan, L.; Alterman, J. F.; Fogarty, K.; Standley, C.; Lifshitz, L. M.; Bellve, K. D.; Prot, M.; Echeverria, D.; Corvera, S.; Khvorova, A., Visualization of self-delivering hydrophobically modified siRNA cellular internalization. *Nucleic Acids Res* **2016**.
233. Alterman, J. F.; Hall, L. M.; Coles, A. H.; Hassler, M. R.; Didiot, M. C.; Chase, K.; Abraham, J.; Sottosanti, E.; Johnson, E.; Sapp, E.; Osborn, M. F.; Difiglia, M.; Aronin, N.; Khvorova, A., Hydrophobically Modified siRNAs Silence Huntingtin mRNA in Primary Neurons and Mouse Brain. *Mol Ther Nucleic Acids* **2015,** *4*, e266.
234. Birmingham, A.; Anderson, E.; Sullivan, K.; Reynolds, A.; Boese, Q.; Leake, D.; Karpilow, J.; Khvorova, A., A protocol for designing siRNAs with high functionality and specificity. *Nat Protoc* **2007,** *2* (9), 2068-78.
235. Birmingham, A.; Anderson, E. M.; Reynolds, A.; Ilsley-Tyree, D.; Leake, D.; Fedorov, Y.; Baskerville, S.; Maksimova, E.; Robinson, K.; Karpilow, J.; Marshall, W. S.; Khvorova, A., 3' UTR seed matches, but not overall identity, are associated with RNAi off-targets. *Nat Methods* **2006,** *3* (3), 199-204.
236. Ruegger, S.; Grosshans, H., MicroRNA turnover: when, how, and why. *Trends Biochem Sci* **2012,** *37* (10), 436-46.
237. Chatterjee, S.; Fasler, M.; Bussing, I.; Grosshans, H., Target-mediated protection of endogenous microRNAs in C. elegans. *Dev Cell* **2011,** *20* (3), 388-96.
238. Bail, S.; Swerdel, M.; Liu, H.; Jiao, X.; Goff, L. A.; Hart, R. P.; Kiledjian, M., Differential regulation of microRNA stability. *Rna* **2010,** *16* (5), 1032-9.
239. Chatterjee, S.; Grosshans, H., Active turnover modulates mature microRNA activity in Caenorhabditis elegans. *Nature* **2009,** *461* (7263), 546-9.
240. Zangari, J.; Ilie, M.; Rouaud, F.; Signetti, L.; Ohanna, M.; Didier, R.; Romeo, B.; Goldoni, D.; Nottet, N.; Staedel, C.; Gal, J.; Mari, B.; Mograbi, B.; Hofman, P.; Brest, P., Rapid decay of

engulfed extracellular miRNA by XRN1 exonuclease promotes transient epithelial-mesenchymal transition. *Nucleic Acids Res* **2016**.
241. Burgess, H. M.; Mohr, I., Cellular 5'-3' mRNA exonuclease Xrn1 controls double-stranded RNA accumulation and anti-viral responses. *Cell Host Microbe* **2015,** *17* (3), 332-44.
242. Trubetskoy, V. S.; Griffin, J. B.; Nicholas, A. L.; Nord, E. M.; Xu, Z.; Peterson, R. M.; Wooddell, C. I.; Rozema, D. B.; Wakefield, D. H.; Lewis, D. L.; Kanner, S. B., Phosphorylation-specific status of RNAi triggers in pharmacokinetic and biodistribution analyses. *Nucleic Acids Res* **2017,** *45* (3), 1469-1478.
243. Kenski, D. M.; Willingham, A. T.; Haringsma, H. J.; Li, J. J.; Flanagan, W. M., In vivo activity and duration of short interfering RNAs containing a synthetic 5'-phosphate. *Nucleic Acid Ther* **2012,** *22* (2), 90-5.
244. Coelho, T.; Adams, D.; Silva, A.; Lozeron, P.; Hawkins, P. N.; Mant, T.; Perez, J.; Chiesa, J.; Warrington, S.; Tranter, E.; Munisamy, M.; Falzone, R.; Harrop, J.; Cehelsky, J.; Bettencourt, B. R.; Geissler, M.; Butler, J. S.; Sehgal, A.; Meyers, R. E.; Chen, Q.; Borland, T.; Hutabarat, R. M.; Clausen, V. A.; Alvarez, R.; Fitzgerald, K.; Gamba-Vitalo, C.; Nochur, S. V.; Vaishnaw, A. K.; Sah, D. W.; Gollob, J. A.; Suhr, O. B., Safety and efficacy of RNAi therapy for transthyretin amyloidosis. *N Engl J Med* **2013,** *369* (9), 819-29.
245. Sehgal, A.; Barros, S.; Ivanciu, L.; Cooley, B.; Qin, J.; Racie, T.; Hettinger, J.; Carioto, M.; Jiang, Y.; Brodsky, J.; Prabhala, H.; Zhang, X.; Attarwala, H.; Hutabarat, R.; Foster, D.; Milstein, S.; Charisse, K.; Kuchimanchi, S.; Maier, M. A.; Nechev, L.; Kandasamy, P.; Kel'in, A. V.; Nair, J. K.; Rajeev, K. G.; Manoharan, M.; Meyers, R.; Sorensen, B.; Simon, A. R.; Dargaud, Y.; Negrier, C.; Camire, R. M.; Akinc, A., An RNAi therapeutic targeting antithrombin to rebalance the coagulation system and promote hemostasis in hemophilia. *Nat Med* **2015,** *21* (5), 492-7.
246. Wolfrum, C.; Shi, S.; Jayaprakash, K. N.; Jayaraman, M.; Wang, G.; Pandey, R. K.; Rajeev, K. G.; Nakayama, T.; Charrise, K.; Ndungo, E. M.; Zimmermann, T.; Koteliansky, V.; Manoharan, M.; Stoffel, M., Mechanisms and optimization of in vivo delivery of lipophilic siRNAs. *Nat Biotechnol* **2007,** *25* (10), 1149-57.
247. Lonn, P.; Kacsinta, A. D.; Cui, X. S.; Hamil, A. S.; Kaulich, M.; Gogoi, K.; Dowdy, S. F., Enhancing Endosomal Escape for Intracellular Delivery of Macromolecular Biologic Therapeutics. *Sci Rep* **2016,** *6* (32301), 32301.
248. Khvorova, A., Oligonucleotide Therapeutics - A New Class of Cholesterol-Lowering Drugs. *N Engl J Med* **2017,** *376* (1), 4-7.
249. Shen, W.; Liang, X. H.; Sun, H.; Crooke, S. T., 2'-Fluoro-modified phosphorothioate oligonucleotide can cause rapid degradation of P54nrb and PSF. *Nucleic Acids Res* **2015,** *43* (9), 4569-78.
250. Garber, K., Alnylam terminates revusiran program, stock plunges. *Nat Biotech* **2016,** *34* (12), 1213-1214.
251. Carroll, J. B.; Bates, G. P.; Steffan, J.; Saft, C.; Tabrizi, S. J., Treating the whole body in Huntington's disease. *Lancet Neurol* **2015,** *14* (11), 1135-42.
252. Albin, R. L., Out of one mutation, many Huntington's disease effects. *Lancet Neurol* **2015,** *14* (11), 1071-2.
253. Martin, B.; Golden, E.; Keselman, A.; Stone, M.; Mattson, M. P.; Egan, J. M.; Maudsley, S., Therapeutic perspectives for the treatment of Huntington's disease: treating the whole body. *Histol Histopathol* **2008,** *23* (2), 237-50.

254. Grapp, M.; Wrede, A.; Schweizer, M.; Huwel, S.; Galla, H. J.; Snaidero, N.; Simons, M.; Buckers, J.; Low, P. S.; Urlaub, H.; Gartner, J.; Steinfeld, R., Choroid plexus transcytosis and exosome shuttling deliver folate into brain parenchyma. *Nat Commun* **2013,** *4* (2123), 2123.
255. Yang, T.; Martin, P.; Fogarty, B.; Brown, A.; Schurman, K.; Phipps, R.; Yin, V. P.; Lockman, P.; Bai, S., Exosome Delivered Anticancer Drugs Across the Blood-Brain Barrier for Brain Cancer Therapy in Danio Rerio. *Pharm Res* **2015**, 22.
256. Haraszti, R. A. D., Marie-Cecile; Sapp, Ellen; Leszyk, John; Shaffer, Scott A ; Rockwell, Hannah E; Gao, Fei; Narain, Niven R; DiFiglia, Marian; Kiebish, Michael A; Aronin, Neil; Khvorova, Anastasia High-resolution proteomic and lipidomic analysis of exosomes and microvesicles from different cell sources. . *Journal of Exrtacellular Vesicles* **2016,** *In press*.
257. Leake, D.; Reynolds, A.; Khvorova, A.; Marshall, W.; Scaringe, S., Stabilized polynucleotides for use in RNA interference. Google Patents: 2004.
258. Nikan, M.; Osborn, M. F.; Coles, A. H.; Godinho, B. M.; Hall, L. M.; Haraszti, R. A.; Hassler, M. R.; Echeverria, D.; Aronin, N.; Khvorova, A.; Alterman, J. F.; Hall, L. M.; Coles, A. H.; Hassler, M. R.; Didiot, M. C.; Chase, K.; Abraham, J.; Sottosanti, E.; Johnson, E.; Sapp, E.; Osborn, M. F.; Difiglia, M.; Aronin, N.; Khvorova, A., Docosahexaenoic Acid Conjugation Enhances Distribution and Safety of siRNA upon Local Administration in Mouse Brain Hydrophobically Modified siRNAs Silence Huntingtin mRNA in Primary Neurons and Mouse Brain. *Mol Ther Nucleic Acids* **2016,** *5* (8), e344.
259. Morrissey, D. V.; Lockridge, J. A.; Shaw, L.; Blanchard, K.; Jensen, K.; Breen, W.; Hartsough, K.; Machemer, L.; Radka, S.; Jadhav, V.; Vaish, N.; Zinnen, S.; Vargeese, C.; Bowman, K.; Shaffer, C. S.; Jeffs, L. B.; Judge, A.; MacLachlan, I.; Polisky, B., Potent and persistent in vivo anti-HBV activity of chemically modified siRNAs. *Nat Biotechnol* **2005,** *23* (8), 1002-7.
260. Olearczyk, J.; Gao, S.; Eybye, M.; Yendluri, S.; Andrews, L.; Bartz, S.; Cully, D.; Tadin-Strapps, M., Targeting of hepatic angiotensinogen using chemically modified siRNAs results in significant and sustained blood pressure lowering in a rat model of hypertension. *Hypertens Res* **2014,** *37* (5), 405-12.
261. Petrova, N. S.; Chernikov, I. V.; Meschaninova, M. I.; Dovydenko, I. S.; Venyaminova, A. G.; Zenkova, M. A.; Vlassov, V. V.; Chernolovskaya, E. L., Carrier-free cellular uptake and the gene-silencing activity of the lipophilic siRNAs is strongly affected by the length of the linker between siRNA and lipophilic group. *Nucleic Acids Res* **2012,** *40* (5), 2330-44.
262. Geary, R. S.; Norris, D.; Yu, R.; Bennett, C. F., Pharmacokinetics, biodistribution and cell uptake of antisense oligonucleotides. *Adv Drug Deliv Rev* **2015,** *87*, 46-51.
263. Allerson, C. R.; Sioufi, N.; Jarres, R.; Prakash, T. P.; Naik, N.; Berdeja, A.; Wanders, L.; Griffey, R. H.; Swayze, E. E.; Bhat, B., Fully 2'-modified oligonucleotide duplexes with improved in vitro potency and stability compared to unmodified small interfering RNA. *J. Med. Chem.* **2005,** *48*, 901-904.
264. Nallagatla, S. R.; Bevilacqua, P. C., Nucleoside modifications modulate activation of the protein kinase PKR in an RNA structure-specific manner. *RNA* **2008,** *14*, 1201-1213.
265. Jackson, A. L.; Burchard, J.; Leake, D.; Reynolds, A.; Schelter, J.; Guo, J.; Johnson, J. M.; Lim, L.; Karpilow, J.; Nichols, K.; Marshall, W.; Khvorova, A.; Linsley, P. S., Position-specific chemical modification of siRNAs reduces "off-target" transcript silencing. *RNA* **2006,** *12*, 1197-1205.

266. Dovydenko, I.; Tarassov, I.; Venyaminova, A.; Entelis, N., Method of carrier-free delivery of therapeutic RNA importable into human mitochondria: Lipophilic conjugates with cleavable bonds. *Biomaterials* **2016,** *76*, 408-17.
267. Chen, Q.; Butler, D.; Querbes, W.; Pandey, R. K.; Ge, P.; Maier, M. A.; Zhang, L.; Rajeev, K. G.; Nechev, L.; Kotelianski, V.; Manoharan, M.; Sah, D. W., Lipophilic siRNAs mediate efficient gene silencing in oligodendrocytes with direct CNS delivery. *J Control Release* **2010,** *144* (2), 227-32.
268. Keerthikumar, S.; Chisanga, D.; Ariyaratne, D.; Al Saffar, H.; Anand, S.; Zhao, K.; Samuel, M.; Pathan, M.; Jois, M.; Chilamkurti, N.; Gangoda, L.; Mathivanan, S., ExoCarta: A Web-Based Compendium of Exosomal Cargo. *J Mol Biol* **2016,** *428* (4), 688-92.
269. Stremersch, S.; Brans, T.; Braeckmans, K.; De Smedt, S.; Raemdonck, K., Nucleic acid loading and fluorescent labeling of isolated extracellular vesicles requires adequate purification. *Int J Pharm* **2017**, 022.
270. Griffiths, S. G.; Cormier, M. T.; Clayton, A.; Doucette, A. A., Differential Proteome Analysis of Extracellular Vesicles from Breast Cancer Cell Lines by Chaperone Affinity Enrichment. *Proteomes* **2017,** *5* (4).
271. Simpson, R. J.; Jensen, S. S.; Lim, J. W., Proteomic profiling of exosomes: current perspectives. *Proteomics* **2008,** *8*, 4083-4099.
272. van Niel, G.; Porto-Carreiro, I.; Simoes, S.; Raposo, G., Exosomes: a common pathway for a specialized function. *J. Biochem.* **2006,** *140*, 13-21.
273. Henderson, M. C.; Azorsa, D. O., The genomic and proteomic content of cancer cell-derived exosomes. *Front Oncol.* **2012,** *2*, 1-9.
274. Valadi, H.; K., E.; Bossios, A.; Sjöstrand, M.; Lee, J. J.; Lötvall, J. O., Exosome-mediated transfer of mRNAs and microRNAs is a novel mechanism of genetic exchange between cells. *Nat. Cell Biol.* **2007,** *9*, 654-659.
275. Muralidharan-Chari, V.; Clancy, J. W.; Sedgwick, A.; D'Souza-Schorey, C., Microvesicles: mediators of extracellular communication during cancer progression. *J. Cell. Sci.* **2010,** *123*, 1603-1611.
276. Pitt, J. M.; Kroemer, G.; Zitvogel, L., Extracellular vesicles: masters of intercellular communication and potential clinical interventions. *J. Clin. Invest.* **2016,** *126*, 1139-1143.
277. Simons, M.; Raposo, G., Exosomes--vesicular carriers for intercellular communication. *Curr. Opin. Cell. Biol* **2009,** *21*, 575-581.
278. Nair, J. K.; Willoughby, J. L. S.; Chan, A.; Charisse, K.; Alam, M. R.; Wang, Q.; Hoekstra, M.; Kandasamy, P.; Kel'in, A. V.; Milstein, S.; Taneja, N.; O'Shea, J.; Shaikh, S.; Zhang, L.; van der Sluis, R. J.; Jung, M. E.; Akinc, A.; Hutabarat, R.; Kuchimanchi, s.; Fitzgerald, K.; Zimmermann, T.; van Berkel, T. J. C.; Maier, M. A.; Rajeev, K. G.; Manoharan, M., Multivalent N-acetylgalactosamine-conjugated siRNA localizes in hepatocytes and elicits robust RNAi-mediated gene silencing. *J. Am. Chem. Soc.* **2014,** *136*, 16958-16961.
279. Burnett, J. C.; Rossi, J. J.; Tiemann, K., Current progress of siRNA/shRNA therapeutics in clinical trials. *Biotechnol. J.* **2011,** *6*, 1130-1146.
280. Antimisiaris, S.; Mourtas, S.; Papadia, K., Targeted si-RNA with liposomes and exosomes (extracellular vesicles): How to unlock the potential. *Int. J. Pharm.* **2017,** *525*, 293-312.
281. Parlea, L.; Puri, A.; Kasprzak, W.; Bindewald, E.; Zakrevsky, P.; Satterwhite, E.; Joseph, K.; Afonin, K. A.; Shapiro, B. A., Cellular delivery of RNA nanoparticles. *ACS Comb. Sci.* **2016,** *18*, 527-547.

282. Xue, H. Y.; Liu, S.; Wong, H. L., Nanotoxicity: a key obstacle to clinical translation of siRNA-based nanomedicine. *Nanomedicine* **2014,** *9*, 295-312.
283. Akhtar, S., Cationic nanosystems for the delivery of small interfering ribonucleic acid therapeutics: a focus on toxicogenomics. *Expert Opin. Drug Metab. Toxicology* **2010,** *6*, 1347-1362.
284. Vader, P.; Mol, E. A.; Pasterkamp, G.; Schiffelers, R. M., Extracellular vesicles for drug delivery. *Adv. Drug. Deliv. Rev.* **2016,** *106*, 148-156.
285. Greco, K. A.; Franzen, C. A.; Foreman, K. E.; Flanigan, R. C.; Kuo, P. C.; Gupta, G. N., PLK-1 silencing in bladder cancer by siRNA delivered with exosomes. *Urology* **2016,** *91*, 241.e1-241.e7.
286. Didiot, M. C.; Hall, L. M.; Coles, A. H.; Haraszti, R. A.; Godinho, B. M.; Chase, K.; Sapp, E.; Ly, S.; Alterman, J. F.; Hassler, M. R.; Echeverria, D.; Raj, L.; Morrissey, D. V.; DiFiglia, M.; Aronin, N.; Khvorova, A., Exosome-mediated delivery of hydrophobically modified siRNA for Huntingtin mRNA silencing. *Mol. Ther.* **2016,** *24*, 1836-1847.
287. Wahlgren, J.; De L Karlson, T.; Brisslert, M.; Vaziri Sani, F.; Telemo, E.; Sunnerhagen, P.; Valadi, H., Plasma exosomes can deliver exogenous short interfering RNA to monocytes and lymphocytes. *Nucleic Acids Res.* **2012,** *40*, e130.
288. Alvarez-Erviti, L.; Seow, Y.; Yin, H.; Betts, C.; Lakhal, S.; Wood, M. J. A., Delivery of siRNA to the mouse brain by systemic injection of targeted exosomes. *Nat. Biotechnol.* **2011,** *29*, 341-345.
289. Lamichhane, T. N.; Raiker, R. S.; Jay, S. M., Exogenous DNA loading into extracellular vesicles via electroporation is size-dependent and enables limited gene delivery. *Mol. Pharmaceutics* **2015,** *12*, 3650-3657.
290. Akao, Y.; Iio, A.; Itoh, T.; Noguchi, S.; Y., I.; Ohtsuki, Y.; Naoe, T., Microvesicle-mediated RNA molecule delivery system using monocytes/macrophages. *Mol. Ther.* **2011,** *19*, 395-399.
291. Shtam, T. A.; Kovalev, R. A.; Varfolomeeva, E. Y.; Makarov, E. M.; Kil, Y. V.; Filatov, M. V., Exosomes are natural carriers of exogenous siRNA to human cells in vitro. *J. Cell Commun. Signal.* **2013,** *11*, 1-10.
292. Kooijmans, S. A.; Stremersch, S.; Braeckmans, K.; de Smedt, S. C.; Hendrix, A.; Wood, M. J.; Schiffelers, R. M.; Raemdonck, K.; Vader, P., Electroporation-induced siRNA precipitation obscures the efficiency of siRNA loading into extracellular vesicles. *J. Control release* **2013,** *172*, 229-238.
293. Nishina, K.; Unno, T.; Uno, Y.; Kubodera, T.; Kanouchi, T.; Mizusawa, H.; Yokota, T., Efficient in vivo delivery of siRNA to the Lliver by conjugation of α-tocopherol. *Molecular Therapy* **2008,** *16*, 734-740.
294. Murakami, M.; Nishina, K.; Watanabe, C.; Yoshida-Tanaka, K.; Piao, W.; Kuwahara, H.; Horikiri, Y.; Miyata, K.; Nishiyama, N.; Kataoka, K.; Yoshida, M.; Mizusawa, H.; Yokota, T., Enteral siRNA delivery technique for therapeutic gene silencing in the liver via the lymphatic route. *Scientific Reports* **2015,** *5:17035*.
295. Hassler, M. R.; Turanov, A. A.; Alterman, J. F.; Haraszti, R. A.; Coles, A. H.; Osborn, M. F.; Echeverria, D.; Nikan, M.; Salomon, W. E.; Roux, L.; Godinho, B. M. D. C.; Davis, S. M.; Morrissey, D. V.; Zamore, P. D.; Karumanchi, S. A.; Moore, M. J.; Aronin, N.; Khvorova, A., Comparison of partially and fully chemically-modified siRNA in conjugate-mediated delivery in vivo. *Nucleic Acids Res.* **2018,** *doi: 10.1093/nar/gky037*.

296. Geary, R. S.; Norris, D.; Yu, R.; Bennett, C. F., Pharmacokinetics, biodistribution and cell uptake of antisense oligonucleotides. *Adv. Drug. Deliv. Rev.* **2015,** *87*, 46-51.
297. Ly, S.; Navaroli, D. M.; Didiot, M. C.; Cardia, J.; Pandarinathan, L.; Alterman, J. F.; Fogarty, K.; Standley, C.; Lifshitz, L. M.; Bellve, K. D.; Prot, M.; Echeverria, D.; Corvera, S.; Khvorova, A., Visualization of self-delivering hydrophobically modified siRNA cellular internalization. *Nucleic Acids Res.* **2017,** *45*, 15-25.
298. Ma, J. B.; Yuan, Y. R.; Meister, G.; Pei, Y.; Tuschl, T.; Patel, D. J., Structural basis for 5'-end-specific recognition of guide RNA by the A. fulgidus Piwi protein. *Nature* **2005,** *434*, 666-670.
299. Frank, F.; Sonenberg, N.; Nagar, B., Structural basis for 5'-nucleotide base-specific recognition of guide RNA by human AGO2. *Nature* **2010,** *465*, 818-822.
300. Parmar, R.; Willoughby, J. L. S.; Liu, J.; Foster, D. J.; Brigham, B.; Theile, C. S.; Charisse, K.; Akinc, A.; Guidry, E.; Pei, Y.; Strapps, W.; Cancilla, M.; Stanton, M. G.; Rajeev, K. G.; Sepp-Lorenzino, L.; Manoharan, M.; Meyers, R.; Maier, M. A.; Jadhav, V., 5′-(E)-Vinylphosphonate: a stable phosphate mimic can improve the RNAi activity of siRNA–GalNAc conjugates. *ChemBioChem* **2016,** *17*, 987-989.
301. Lima, W. F.; Prakash, T. P.; Murray, H. M.; Kinberger, G. A.; Li, W.; Chappell, A. E.; Li, C. S.; Murray, S. F.; Gaus, H.; Seth, P. P.; Swayze, E. E.; Crooke, S. T., Single-stranded siRNAs activate RNAi in animals. *Cell* **2012,** *150*, 883-894.
302. Alterman, J. F.; Hall, L. M.; Coles, A. H.; Hassler, M. R.; Didiot, M. C.; Chase, K.; Abraham, J.; Sottosanti, E.; Johnson, E.; Sapp, E.; Osborn, M. F.; Difiglia, M.; Aronin, N.; Khvorova, A., Hydrophobically modified siRNAs silence Huntingtin mRNA in primary neurons and mouse brain. *Mol. Ther. Nucleic Acids* **2015,** *4*, e266.
303. van Meer, G.; Voelker, D. R.; Feigenson, G. W., Membrane lipids: where they are and how they behave. *Nat. Rev. Mol. Cell Biol.* **2008,** *9*, 112-124.
304. Smith, M.; Jungalwala, F. B., Reversed-phase high performance Iiquid chromatography of phosphatidylcholine: a simple method for determining relative hydrophobic interaction of various molecular species. *J. Lipid Res.* **1981,** *22*, 697-704.
305. Wolfrum, C.; Shi, S.; Jayaprakash, K. N.; Jayaraman, M.; Wang, G.; Pandey, R. K.; Rajeev, K. J.; Nakayama, T.; Charrise, K.; Ndungo, E. M.; Zimmermann, T.; Koteliansky, V.; Manoharan, M.; Stoffel, M., Mechanisms and optimization of in vivo delivery of lipophilic siRNAs. *Nat. Biotechnol.* **2007,** *25*, 1149-1157.
306. Lotvall, J.; Hill, A. F.; Hochberg, F.; Buzas, E. I.; Di Vizio, D.; Gardiner, C.; Gho, Y. S.; Kurochkin, I. V.; Mathivanan, S.; Quesenberry, P.; Sahoo, S.; Tahara, H.; Wauben, M. H.; Witwer, K. W.; Thery, C., Minimal experimental requirements for definition of extracellular vesicles and their functions: a position statement from the International Society for Extracellular Vesicles. *J Extracell Vesicles* **2014,** *3* (26913), 26913.
307. Haraszti, R. A.; Didiot, M.-C.; Sapp, E.; Leszyk, J.; Shaffer, S. A.; Rockwell, H. E.; Gao, F.; Narain, N. R.; DiFiglia, M.; Kiebish, M. A.; Aronin, N.; Khvorova, A., High-resolution proteomic and lipidomic analysis of exosomes and microvesicles from different cell sources. *J. Extracell Vesicles* **2016,** *5*, doi: 10.3402/jev.v5.32570.
308. Kramer-Albers, E. M., Ticket to Ride: Targeting Proteins to Exosomes for Brain Delivery. *Mol Ther* **2017,** *25* (6), 1264-1266.
309. Beltrami, C.; Besnier, M.; Shantikumar, S.; Shearn, A. I.; Rajakaruna, C.; Laftah, A.; Sessa, F.; Spinetti, G.; Petretto, E.; Angelini, G. D.; Emanueli, C., Human Pericardial Fluid

Contains Exosomes Enriched with Cardiovascular-Expressed MicroRNAs and Promotes Therapeutic Angiogenesis. *Mol Ther* **2017,** *25* (3), 679-693.
310. Yuyama, K.; Sun, H.; Mitsutake, S.; Igarashi, Y., Sphingolipid-modulated exosome secretion promotes clearance of amyloid-beta by microglia. *J Biol Chem* **2012,** *287* (14), 10977-89.
311. Kotzerke, K.; Mempel, M.; Aung, T.; Wulf, G. G.; Urlaub, H.; Wenzel, D.; Schon, M. P.; Braun, A., Immunostimulatory activity of murine keratinocyte-derived exosomes. *Exp Dermatol* **2013,** *22* (10), 650-5.
312. Sheng, H.; Hassanali, S.; Nugent, C.; Wen, L.; Hamilton-Williams, E.; Dias, P.; Dai, Y. D., Insulinoma-released exosomes or microparticles are immunostimulatory and can activate autoreactive T cells spontaneously developed in nonobese diabetic mice. *J Immunol* **2011,** *187* (4), 1591-600.
313. Heijnen, H. F.; Schiel, A. E.; Fijnheer, R.; Geuze, H. J.; Sixma, J. J., Activated platelets release two types of membrane vesicles: microvesicles by surface shedding and exosomes derived from exocytosis of multivesicular bodies and alpha-granules. *Blood* **1999,** *94* (11), 3791-9.
314. Skog, J.; Wurdinger, T.; van Rijn, S.; Meijer, D. H.; Gainche, L.; Sena-Esteves, M.; Curry, W. T., Jr.; Carter, B. S.; Krichevsky, A. M.; Breakefield, X. O., Glioblastoma microvesicles transport RNA and proteins that promote tumour growth and provide diagnostic biomarkers. *Nat Cell Biol* **2008,** *10* (12), 1470-6.
315. Korkut, C.; Li, Y.; Koles, K.; Brewer, C.; Ashley, J.; Yoshihara, M.; Budnik, V., Regulation of postsynaptic retrograde signaling by presynaptic exosome release. *Neuron* **2013,** *77* (6), 1039-46.
316. Abrami, L.; Brandi, L.; Moayeri, M.; Brown, M. J.; Krantz, B. A.; Leppla, S. H.; van der Goot, F. G., Hijacking multivesicular bodies enables long-term and exosome-mediated long-distance action of anthrax toxin. *Cell Rep* **2013,** *5* (4), 986-96.
317. Saha, B.; Momen-Heravi, F.; Kodys, K.; Szabo, G.; Momen-Heravi, F.; Saha, B.; Kodys, K.; Catalano, D.; Satishchandran, A.; Szabo, G., MicroRNA Cargo of Extracellular Vesicles from Alcohol-exposed Monocytes Signals Naive Monocytes to Differentiate into M2 Macrophages
Increased number of circulating exosomes and their microRNA cargos are potential novel biomarkers in alcoholic hepatitis. *J Biol Chem* **2016,** *291* (1), 149-59.
318. Zhang, S.; Chuah, S. J.; Lai, R. C.; Hui, J. H. P.; Lim, S. K.; Toh, W. S.; Willis, G. R.; Fernandez-Gonzalez, A.; Anastas, J.; Vitali, S. H.; Liu, X.; Ericsson, M.; Kwong, A.; Mitsialis, S. A.; Kourembanas, S.; Bai, L.; Shao, H.; Wang, H.; Zhang, Z.; Su, C.; Dong, L.; Yu, B.; Chen, X.; Li, X.; Zhang, X.; Monguio-Tortajada, M.; Roura, S.; Galvez-Monton, C.; Pujal, J. M.; Aran, G.; Sanjurjo, L.; Franquesa, M.; Sarrias, M. R.; Bayes-Genis, A.; Borras, F. E.; Wang, L.; Gu, Z.; Zhao, X.; Yang, N.; Wang, F.; Deng, A.; Zhao, S.; Luo, L.; Wei, H.; Guan, L.; Gao, Z.; Li, Y.; Wang, L.; Liu, D.; Gao, C.; Wen, D.; Peng, Y.; Liu, D.; Weizmann, Y.; Mahato, R. I.; Rebmann, V.; Konig, L.; Nardi Fda, S.; Wagner, B.; Manvailer, L. F.; Horn, P. A.; Hu, G. W.; Li, Q.; Niu, X.; Hu, B.; Liu, J.; Zhou, S. M.; Guo, S. C.; Lang, H. L.; Zhang, C. Q.; Wang, Y.; Deng, Z. F.; Amarnath, S.; Foley, J. E.; Farthing, D. E.; Gress, R. E.; Laurence, A.; Eckhaus, M. A.; Metais, J. Y.; Rose, J. J.; Hakim, F. T.; Felizardo, T. C.; Cheng, A. V.; Robey, P. G.; Stroncek, D. E.; Sabatino, M.; Battiwalla, M.; Ito, S.; Fowler, D. H.; Barrett, A. J., MSC exosomes mediate cartilage repair by enhancing proliferation, attenuating apoptosis and modulating immune reactivity

Mesenchymal Stromal Cell Exosomes Ameliorate Experimental Bronchopulmonary Dysplasia and Restore Lung Function through Macrophage Immunomodulation
Effects of Mesenchymal Stem Cell-Derived Exosomes on Experimental Autoimmune Uveitis
Nanosized UCMSC-derived extracellular vesicles but not conditioned medium exclusively inhibit the inflammatory response of stimulated T cells: implications for nanomedicine
Extracellular Vesicles Released from Human Umbilical Cord-Derived Mesenchymal Stromal Cells Prevent Life-Threatening Acute Graft-Versus-Host Disease in a Mouse Model of Allogeneic Hematopoietic Stem Cell Transplantation
Mesenchymal stem cell and derived exosome as small RNA carrier and Immunomodulator to improve islet transplantation
The Potential of HLA-G-Bearing Extracellular Vesicles as a Future Element in HLA-G Immune Biology
Exosomes secreted by human-induced pluripotent stem cell-derived mesenchymal stem cells attenuate limb ischemia by promoting angiogenesis in mice
Bone marrow-derived mesenchymal stromal cells harness purinergenic signaling to tolerize human Th1 cells in vivo. *Biomaterials* **2018,** *156* (1), 16-27.
319. Willis, G. R.; Fernandez-Gonzalez, A.; Anastas, J.; Vitali, S. H.; Liu, X.; Ericsson, M.; Kwong, A.; Mitsialis, S. A.; Kourembanas, S.; Bai, L.; Shao, H.; Wang, H.; Zhang, Z.; Su, C.; Dong, L.; Yu, B.; Chen, X.; Li, X.; Zhang, X.; Monguio-Tortajada, M.; Roura, S.; Galvez-Monton, C.; Pujal, J. M.; Aran, G.; Sanjurjo, L.; Franquesa, M.; Sarrias, M. R.; Bayes-Genis, A.; Borras, F. E.; Wang, L.; Gu, Z.; Zhao, X.; Yang, N.; Wang, F.; Deng, A.; Zhao, S.; Luo, L.; Wei, H.; Guan, L.; Gao, Z.; Li, Y.; Wang, L.; Liu, D.; Gao, C.; Wen, D.; Peng, Y.; Liu, D.; Weizmann, Y.; Mahato, R. I.; Rebmann, V.; Konig, L.; Nardi Fda, S.; Wagner, B.; Manvailer, L. F.; Horn, P. A.; Hu, G. W.; Li, Q.; Niu, X.; Hu, B.; Liu, J.; Zhou, S. M.; Guo, S. C.; Lang, H. L.; Zhang, C. Q.; Wang, Y.; Deng, Z. F.; Amarnath, S.; Foley, J. E.; Farthing, D. E.; Gress, R. E.; Laurence, A.; Eckhaus, M. A.; Metais, J. Y.; Rose, J. J.; Hakim, F. T.; Felizardo, T. C.; Cheng, A. V.; Robey, P. G.; Stroncek, D. E.; Sabatino, M.; Battiwalla, M.; Ito, S.; Fowler, D. H.; Barrett, A. J., Mesenchymal Stromal Cell Exosomes Ameliorate Experimental Bronchopulmonary Dysplasia and Restore Lung Function through Macrophage Immunomodulation
Effects of Mesenchymal Stem Cell-Derived Exosomes on Experimental Autoimmune Uveitis
Nanosized UCMSC-derived extracellular vesicles but not conditioned medium exclusively inhibit the inflammatory response of stimulated T cells: implications for nanomedicine
Extracellular Vesicles Released from Human Umbilical Cord-Derived Mesenchymal Stromal Cells Prevent Life-Threatening Acute Graft-Versus-Host Disease in a Mouse Model of Allogeneic Hematopoietic Stem Cell Transplantation
Mesenchymal stem cell and derived exosome as small RNA carrier and Immunomodulator to improve islet transplantation
The Potential of HLA-G-Bearing Extracellular Vesicles as a Future Element in HLA-G Immune Biology
Exosomes secreted by human-induced pluripotent stem cell-derived mesenchymal stem cells attenuate limb ischemia by promoting angiogenesis in mice
Bone marrow-derived mesenchymal stromal cells harness purinergenic signaling to tolerize human Th1 cells in vivo. *Am J Respir Crit Care Med* **2018,** *197* (1), 104-116.
320. Zhang, Q.; Fu, L.; Liang, Y.; Guo, Z.; Wang, L.; Ma, C.; Wang, H., Exosomes originating from MSCs stimulated with TGF-beta and IFN-gamma promote Treg differentiation. *J Cell Physiol* **2018,** *16* (10), 26436.

321. Bai, L.; Shao, H.; Wang, H.; Zhang, Z.; Su, C.; Dong, L.; Yu, B.; Chen, X.; Li, X.; Zhang, X.; Monguio-Tortajada, M.; Roura, S.; Galvez-Monton, C.; Pujal, J. M.; Aran, G.; Sanjurjo, L.; Franquesa, M.; Sarrias, M. R.; Bayes-Genis, A.; Borras, F. E.; Wang, L.; Gu, Z.; Zhao, X.; Yang, N.; Wang, F.; Deng, A.; Zhao, S.; Luo, L.; Wei, H.; Guan, L.; Gao, Z.; Li, Y.; Wang, L.; Liu, D.; Gao, C.; Wen, D.; Peng, Y.; Liu, D.; Weizmann, Y.; Mahato, R. I.; Rebmann, V.; Konig, L.; Nardi Fda, S.; Wagner, B.; Manvailer, L. F.; Horn, P. A.; Hu, G. W.; Li, Q.; Niu, X.; Hu, B.; Liu, J.; Zhou, S. M.; Guo, S. C.; Lang, H. L.; Zhang, C. Q.; Wang, Y.; Deng, Z. F.; Amarnath, S.; Foley, J. E.; Farthing, D. E.; Gress, R. E.; Laurence, A.; Eckhaus, M. A.; Metais, J. Y.; Rose, J. J.; Hakim, F. T.; Felizardo, T. C.; Cheng, A. V.; Robey, P. G.; Stroncek, D. E.; Sabatino, M.; Battiwalla, M.; Ito, S.; Fowler, D. H.; Barrett, A. J., Effects of Mesenchymal Stem Cell-Derived Exosomes on Experimental Autoimmune Uveitis
Nanosized UCMSC-derived extracellular vesicles but not conditioned medium exclusively inhibit the inflammatory response of stimulated T cells: implications for nanomedicine
Extracellular Vesicles Released from Human Umbilical Cord-Derived Mesenchymal Stromal Cells Prevent Life-Threatening Acute Graft-Versus-Host Disease in a Mouse Model of Allogeneic Hematopoietic Stem Cell Transplantation
Mesenchymal stem cell and derived exosome as small RNA carrier and Immunomodulator to improve islet transplantation
The Potential of HLA-G-Bearing Extracellular Vesicles as a Future Element in HLA-G Immune Biology
Exosomes secreted by human-induced pluripotent stem cell-derived mesenchymal stem cells attenuate limb ischemia by promoting angiogenesis in mice
Bone marrow-derived mesenchymal stromal cells harness purinergenic signaling to tolerize human Th1 cells in vivo. *Sci Rep* **2017,** *7* (1), 4323.
322. Du, Y. M.; Zhuansun, Y. X.; Chen, R.; Lin, L.; Lin, Y.; Li, J. G.; Tamura, R.; Uemoto, S.; Tabata, Y.; Zhang, S.; Chuah, S. J.; Lai, R. C.; Hui, J. H. P.; Lim, S. K.; Toh, W. S.; Willis, G. R.; Fernandez-Gonzalez, A.; Anastas, J.; Vitali, S. H.; Liu, X.; Ericsson, M.; Kwong, A.; Mitsialis, S. A.; Kourembanas, S.; Bai, L.; Shao, H.; Wang, H.; Zhang, Z.; Su, C.; Dong, L.; Yu, B.; Chen, X.; Li, X.; Zhang, X.; Monguio-Tortajada, M.; Roura, S.; Galvez-Monton, C.; Pujal, J. M.; Aran, G.; Sanjurjo, L.; Franquesa, M.; Sarrias, M. R.; Bayes-Genis, A.; Borras, F. E.; Wang, L.; Gu, Z.; Zhao, X.; Yang, N.; Wang, F.; Deng, A.; Zhao, S.; Luo, L.; Wei, H.; Guan, L.; Gao, Z.; Li, Y.; Wang, L.; Liu, D.; Gao, C.; Wen, D.; Peng, Y.; Liu, D.; Weizmann, Y.; Mahato, R. I.; Rebmann, V.; Konig, L.; Nardi Fda, S.; Wagner, B.; Manvailer, L. F.; Horn, P. A.; Hu, G. W.; Li, Q.; Niu, X.; Hu, B.; Liu, J.; Zhou, S. M.; Guo, S. C.; Lang, H. L.; Zhang, C. Q.; Wang, Y.; Deng, Z. F.; Amarnath, S.; Foley, J. E.; Farthing, D. E.; Gress, R. E.; Laurence, A.; Eckhaus, M. A.; Metais, J. Y.; Rose, J. J.; Hakim, F. T.; Felizardo, T. C.; Cheng, A. V.; Robey, P. G.; Stroncek, D. E.; Sabatino, M.; Battiwalla, M.; Ito, S.; Fowler, D. H.; Barrett, A. J., Mesenchymal stem cell exosomes promote immunosuppression of regulatory T cells in asthma
Immunosuppressive effect of mesenchymal stem cell-derived exosomes on a concanavalin A-induced liver injury model
MSC exosomes mediate cartilage repair by enhancing proliferation, attenuating apoptosis and modulating immune reactivity
Mesenchymal Stromal Cell Exosomes Ameliorate Experimental Bronchopulmonary Dysplasia and Restore Lung Function through Macrophage Immunomodulation
Effects of Mesenchymal Stem Cell-Derived Exosomes on Experimental Autoimmune Uveitis

Nanosized UCMSC-derived extracellular vesicles but not conditioned medium exclusively inhibit the inflammatory response of stimulated T cells: implications for nanomedicine
Extracellular Vesicles Released from Human Umbilical Cord-Derived Mesenchymal Stromal Cells Prevent Life-Threatening Acute Graft-Versus-Host Disease in a Mouse Model of Allogeneic Hematopoietic Stem Cell Transplantation
Mesenchymal stem cell and derived exosome as small RNA carrier and Immunomodulator to improve islet transplantation
The Potential of HLA-G-Bearing Extracellular Vesicles as a Future Element in HLA-G Immune Biology
Exosomes secreted by human-induced pluripotent stem cell-derived mesenchymal stem cells attenuate limb ischemia by promoting angiogenesis in mice
Bone marrow-derived mesenchymal stromal cells harness purinergenic signaling to tolerize human Th1 cells in vivo. *Exp Cell Res* **2017,** *23* (17), 30676-6.
323. Monguio-Tortajada, M.; Roura, S.; Galvez-Monton, C.; Pujal, J. M.; Aran, G.; Sanjurjo, L.; Franquesa, M.; Sarrias, M. R.; Bayes-Genis, A.; Borras, F. E., Nanosized UCMSC-derived extracellular vesicles but not conditioned medium exclusively inhibit the inflammatory response of stimulated T cells: implications for nanomedicine. *Theranostics* **2017,** *7* (2), 270-284.
324. Amarnath, S.; Foley, J. E.; Farthing, D. E.; Gress, R. E.; Laurence, A.; Eckhaus, M. A.; Metais, J. Y.; Rose, J. J.; Hakim, F. T.; Felizardo, T. C.; Cheng, A. V.; Robey, P. G.; Stroncek, D. E.; Sabatino, M.; Battiwalla, M.; Ito, S.; Fowler, D. H.; Barrett, A. J., Bone marrow-derived mesenchymal stromal cells harness purinergenic signaling to tolerize human Th1 cells in vivo. *Stem Cells* **2015,** *33* (4), 1200-12.
325. Skokos, D.; Botros, H. G.; Demeure, C.; Morin, J.; Peronet, R.; Birkenmeier, G.; Boudaly, S.; Mecheri, S., Mast cell-derived exosomes induce phenotypic and functional maturation of dendritic cells and elicit specific immune responses in vivo. *J Immunol* **2003,** *170* (6), 3037-45.
326. Kim, S. H.; Bianco, N. R.; Shufesky, W. J.; Morelli, A. E.; Robbins, P. D., Effective treatment of inflammatory disease models with exosomes derived from dendritic cells genetically modified to express IL-4. *J Immunol* **2007,** *179* (4), 2242-9.
327. Reiner, A. T.; Witwer, K. W.; van Balkom, B. W. M.; de Beer, J.; Brodie, C.; Corteling, R. L.; Gabrielsson, S.; Gimona, M.; Ibrahim, A. G.; de Kleijn, D.; Lai, C. P.; Lotvall, J.; Del Portillo, H. A.; Reischl, I. G.; Riazifar, M.; Salomon, C.; Tahara, H.; Toh, W. S.; Wauben, M. H. M.; Yang, V. K.; Yang, Y.; Yeo, R. W. Y.; Yin, H.; Giebel, B.; Rohde, E.; Lim, S. K., Concise Review: Developing Best-Practice Models for the Therapeutic Use of Extracellular Vesicles. *Stem Cells Transl Med* **2017,** *6* (8), 1730-1739.
328. Colao, I. L.; Corteling, R.; Bracewell, D.; Wall, I., Manufacturing Exosomes: A Promising Therapeutic Platform. *Trends Mol Med* **2018,** *12* (18), 30006-6.
329. Nordin, J. Z.; Lee, Y.; Vader, P.; Mager, I.; Johansson, H. J.; Heusermann, W.; Wiklander, O. P.; Hallbrink, M.; Seow, Y.; Bultema, J. J.; Gilthorpe, J.; Davies, T.; Fairchild, P. J.; Gabrielsson, S.; Meisner-Kober, N. C.; Lehtio, J.; Smith, C. I.; Wood, M. J.; El Andaloussi, S., Ultrafiltration with size-exclusion liquid chromatography for high yield isolation of extracellular vesicles preserving intact biophysical and functional properties. *Nanomedicine* **2015,** *11* (4), 879-83.

330. Corso, G.; Mager, I.; Lee, Y.; Gorgens, A.; Bultema, J.; Giebel, B.; Wood, M. J. A.; Nordin, J. Z.; Andaloussi, S. E., Reproducible and scalable purification of extracellular vesicles using combined bind-elute and size exclusion chromatography. *Sci Rep* **2017,** *7* (1), 11561.
331. Greening, D. W.; Xu, R.; Ji, H.; Tauro, B. J.; Simpson, R. J., A protocol for exosome isolation and characterization: evaluation of ultracentrifugation, density-gradient separation, and immunoaffinity capture methods. *Methods Mol Biol* **2015,** *1295*, 179-209.
332. Kowal, J.; Arras, G.; Colombo, M.; Jouve, M.; Morath, J. P.; Primdal-Bengtson, B.; Dingli, F.; Loew, D.; Tkach, M.; Thery, C., Proteomic comparison defines novel markers to characterize heterogeneous populations of extracellular vesicle subtypes. *Proc Natl Acad Sci U S A* **2016**, 201521230.
333. Wubbolts, R.; Leckie, R. S.; Veenhuizen, P. T.; Schwarzmann, G.; Mobius, W.; Hoernschemeyer, J.; Slot, J. W.; Geuze, H. J.; Stoorvogel, W., Proteomic and biochemical analyses of human B cell-derived exosomes. Potential implications for their function and multivesicular body formation. *J Biol Chem* **2003,** *278* (13), 10963-72.
334. van Wezel, A. L., The large-scale cultivation of diploid cell strains in microcarrier culture. Improvement of microcarriers. *Dev Biol Stand* **1976,** *37*, 143-7.
335. Grimm, K. M.; Trigona, W. L.; Heidecker, G. J.; Joyce, J. G.; Fu, T. M.; Shiver, J. W.; Keller, P. M.; Cook, J. C., An enhanced and scalable process for the purification of SIV Gag-specific MHC tetramer. *Protein Expr Purif* **2001,** *23* (2), 270-81.
336. Dizon-Maspat, J.; Bourret, J.; D'Agostini, A.; Li, F., Single pass tangential flow filtration to debottleneck downstream processing for therapeutic antibody production. *Biotechnol Bioeng* **2012,** *109* (4), 962-70.
337. Potter, M.; Lins, B.; Mietzsch, M.; Heilbronn, R.; Van Vliet, K.; Chipman, P.; Agbandje-McKenna, M.; Cleaver, B. D.; Clement, N.; Byrne, B. J.; Zolotukhin, S., A simplified purification protocol for recombinant adeno-associated virus vectors. *Mol Ther Methods Clin Dev* **2014,** *1* (14034), 14034.
338. Mannello, F.; Tonti, G. A., Concise review: no breakthroughs for human mesenchymal and embryonic stem cell culture: conditioned medium, feeder layer, or feeder-free; medium with fetal calf serum, human serum, or enriched plasma; serum-free, serum replacement nonconditioned medium, or ad hoc formula? All that glitters is not gold! *Stem Cells* **2007,** *25* (7), 1603-9.
339. Nave, J. F.; Taylor, D.; Tyms, S.; Kenny, M.; Eggenspiller, A.; Eschbach, A.; Dulworth, J.; Brennan, T.; Piriou, F.; Halazy, S., Synthesis, antiviral activity and enzymatic phosphorylation of 9-phosphonopentenyl derivatives of guanine. *Antiviral Res* **1995,** *27* (3), 301-16.
340. Lock, M.; Alvira, M.; Vandenberghe, L. H.; Samanta, A.; Toelen, J.; Debyser, Z.; Wilson, J. M., Rapid, simple, and versatile manufacturing of recombinant adeno-associated viral vectors at scale. *Hum Gene Ther* **2010,** *21* (10), 1259-71.
341. Lener, T.; Gimona, M.; Aigner, L.; Borger, V.; Buzas, E.; Camussi, G.; Chaput, N.; Chatterjee, D.; Court, F. A.; Del Portillo, H. A.; O'Driscoll, L.; Fais, S.; Falcon-Perez, J. M.; Felderhoff-Mueser, U.; Fraile, L.; Gho, Y. S.; Gorgens, A.; Gupta, R. C.; Hendrix, A.; Hermann, D. M.; Hill, A. F.; Hochberg, F.; Horn, P. A.; de Kleijn, D.; Kordelas, L.; Kramer, B. W.; Kramer-Albers, E. M.; Laner-Plamberger, S.; Laitinen, S.; Leonardi, T.; Lorenowicz, M. J.; Lim, S. K.; Lotvall, J.; Maguire, C. A.; Marcilla, A.; Nazarenko, I.; Ochiya, T.; Patel, T.; Pedersen, S.; Pocsfalvi, G.; Pluchino, S.; Quesenberry, P.; Reischl, I. G.; Rivera, F. J.; Sanzenbacher, R.; Schallmoser, K.; Slaper-Cortenbach, I.; Strunk, D.; Tonn, T.; Vader, P.; van Balkom, B. W.;

Wauben, M.; Andaloussi, S. E.; Thery, C.; Rohde, E.; Giebel, B., Applying extracellular vesicles based therapeutics in clinical trials - an ISEV position paper. *J Extracell Vesicles* **2015,** *4* (30087), 30087.
342. Jia, S.; Zocco, D.; Samuels, M. L.; Chou, M. F.; Chammas, R.; Skog, J.; Zarovni, N.; Momen-Heravi, F.; Kuo, W. P., Emerging technologies in extracellular vesicle-based molecular diagnostics. *Expert Rev Mol Diagn* **2014,** *14* (3), 307-21.
343. Long, J. D.; Sullivan, T. B.; Humphrey, J.; Logvinenko, T.; Summerhayes, K. A.; Kozinn, S.; Harty, N.; Summerhayes, I. C.; Libertino, J. A.; Holway, A. H.; Rieger-Christ, K. M., A non-invasive miRNA based assay to detect bladder cancer in cell-free urine. *Am J Transl Res* **2015,** *7* (11), 2500-9.
344. Ben-Dov, I. Z.; Whalen, V. M.; Goilav, B.; Max, K. E.; Tuschl, T., Cell and Microvesicle Urine microRNA Deep Sequencing Profiles from Healthy Individuals: Observations with Potential Impact on Biomarker Studies. *PLoS One* **2016,** *11* (1), e0147249.
345. Royo, F.; Zuniga-Garcia, P.; Torrano, V.; Loizaga, A.; Sanchez-Mosquera, P.; Ugalde-Olano, A.; Gonzalez, E.; Cortazar, A. R.; Palomo, L.; Fernandez-Ruiz, S.; Lacasa-Viscasillas, I.; Berdasco, M.; Sutherland, J. D.; Barrio, R.; Zabala-Letona, A.; Martin-Martin, N.; Arruabarrena-Aristorena, A.; Valcarcel-Jimenez, L.; Caro-Maldonado, A.; Gonzalez-Tampan, J.; Cachi-Fuentes, G.; Esteller, M.; Aransay, A. M.; Unda, M.; Falcon-Perez, J. M.; Carracedo, A., Transcriptomic profiling of urine extracellular vesicles reveals alterations of CDH3 in prostate cancer. *Oncotarget* **2016**.
346. Momen-Heravi, F.; Saha, B.; Kodys, K.; Catalano, D.; Satishchandran, A.; Szabo, G., Increased number of circulating exosomes and their microRNA cargos are potential novel biomarkers in alcoholic hepatitis. *J Transl Med* **2015,** *13* (261), 261.
347. Sohn, W.; Kim, J.; Kang, S. H.; Yang, S. R.; Cho, J. Y.; Cho, H. C.; Shim, S. G.; Paik, Y. H., Serum exosomal microRNAs as novel biomarkers for hepatocellular carcinoma. *Exp Mol Med* **2015,** *47*, e184.
348. Quinn, J. F.; Patel, T.; Wong, D.; Das, S.; Freedman, J. E.; Laurent, L. C.; Carter, B. S.; Hochberg, F.; Van Keuren-Jensen, K.; Huentelman, M.; Spetzler, R.; Kalani, M. Y.; Arango, J.; Adelson, P. D.; Weiner, H. L.; Gandhi, R.; Goilav, B.; Putterman, C.; Saugstad, J. A., Extracellular RNAs: development as biomarkers of human disease. *J Extracell Vesicles* **2015,** *4* (27495), 27495.
349. Hornick, N. I.; Huan, J.; Doron, B.; Goloviznina, N. A.; Lapidus, J.; Chang, B. H.; Kurre, P., Serum Exosome MicroRNA as a Minimally-Invasive Early Biomarker of AML. *Sci Rep* **2015,** *5* (11295), 11295.
350. Didiot, M. C.; Hall, L. M.; Coles, A. H.; Haraszti, R. A.; Godinho, B. M.; Chase, K.; Sapp, E.; Ly, S.; Alterman, J. F.; Hassler, M. R.; Echeverria, D.; Raj, L.; Morrissey, D. V.; DiFiglia, M.; Aronin, N.; Khvorova, A., Exosome-mediated Delivery of Hydrophobically Modified siRNA for Huntingtin mRNA Silencing. *Mol Ther* **2016**, 126.
351. Quesenberry, P. J.; Aliotta, J.; Deregibus, M. C.; Camussi, G., Role of extracellular RNA-carrying vesicles in cell differentiation and reprogramming. *Stem Cell Res Ther* **2015,** *6* (153), 153.
352. Holme, P. A.; Brosstad, F.; Solum, N. O., The difference between platelet and plasma FXIII used to study the mechanism of platelet microvesicle formation. *Thromb Haemost* **1993,** *70* (4), 681-6.

353. Lobb, R. J.; Becker, M.; Wen, S. W.; Wong, C. S.; Wiegmans, A. P.; Leimgruber, A.; Moller, A., Optimized exosome isolation protocol for cell culture supernatant and human plasma. *J Extracell Vesicles* **2015,** *4* (27031), 27031.
354. Aalberts, M.; van Dissel-Emiliani, F. M.; van Adrichem, N. P.; van Wijnen, M.; Wauben, M. H.; Stout, T. A.; Stoorvogel, W., Identification of distinct populations of prostasomes that differentially express prostate stem cell antigen, annexin A1, and GLIPR2 in humans. *Biol Reprod* **2012,** *86* (3), 82.
355. Raposo, G.; Stoorvogel, W., Extracellular vesicles: exosomes, microvesicles, and friends. *J Cell Biol* **2013,** *200* (4), 373-83.
356. Anderson, J. D.; Johansson, H. J.; Graham, C. S.; Vesterlund, M.; Pham, M. T.; Bramlett, C. S.; Montgomery, E. N.; Mellema, M. S.; Bardini, R. L.; Contreras, Z.; Hoon, M.; Bauer, G.; Fink, K. D.; Fury, B.; Hendrix, K. J.; Chedin, F.; El-Andaloussi, S.; Hwang, B.; Mulligan, M. S.; Lehtio, J.; Nolta, J. A., Comprehensive Proteomic Analysis of Mesenchymal Stem Cell Exosomes Reveals Modulation of Angiogenesis via Nuclear Factor-KappaB Signaling. *Stem Cells* **2016,** *34* (3), 601-13.
357. Kreimer, S.; Belov, A. M.; Ghiran, I.; Murthy, S. K.; Frank, D. A.; Ivanov, A. R., Mass-spectrometry-based molecular characterization of extracellular vesicles: lipidomics and proteomics. *J Proteome Res* **2015,** *14* (6), 2367-84.
358. Clark, D. J.; Fondrie, W. E.; Liao, Z.; Hanson, P. I.; Fulton, A.; Mao, L.; Yang, A. J., Redefining the Breast Cancer Exosome Proteome by Tandem Mass Tag Quantitative Proteomics and Multivariate Cluster Analysis. *Anal Chem* **2015,** *87* (20), 10462-9.
359. Wang, Z.; Hill, S.; Luther, J. M.; Hachey, D. L.; Schey, K. L., Proteomic analysis of urine exosomes by multidimensional protein identification technology (MudPIT). *Proteomics* **2012,** *12* (2), 329-38.
360. Sinha, A.; Ignatchenko, V.; Ignatchenko, A.; Mejia-Guerrero, S.; Kislinger, T., In-depth proteomic analyses of ovarian cancer cell line exosomes reveals differential enrichment of functional categories compared to the NCI 60 proteome. *Biochem Biophys Res Commun* **2014,** *445* (4), 694-701.
361. Vallejo, M. C.; Nakayasu, E. S.; Longo, L. V.; Ganiko, L.; Lopes, F. G.; Matsuo, A. L.; Almeida, I. C.; Puccia, R., Lipidomic analysis of extracellular vesicles from the pathogenic phase of Paracoccidioides brasiliensis. *PLoS One* **2012,** *7* (6), e39463.
362. Del Boccio, P.; Raimondo, F.; Pieragostino, D.; Morosi, L.; Cozzi, G.; Sacchetta, P.; Magni, F.; Pitto, M.; Urbani, A., A hyphenated microLC-Q-TOF-MS platform for exosomal lipidomics investigations: application to RCC urinary exosomes. *Electrophoresis* **2012,** *33* (4), 689-96.
363. Llorente, A.; Skotland, T.; Sylvanne, T.; Kauhanen, D.; Rog, T.; Orlowski, A.; Vattulainen, I.; Ekroos, K.; Sandvig, K., Molecular lipidomics of exosomes released by PC-3 prostate cancer cells. *Biochim Biophys Acta* **2013,** *1831* (7), 1302-9.
364. Duijvesz, D.; Burnum-Johnson, K. E.; Gritsenko, M. A.; Hoogland, A. M.; Vredenbregt-van den Berg, M. S.; Willemsen, R.; Luider, T.; Pasa-Tolic, L.; Jenster, G., Proteomic profiling of exosomes leads to the identification of novel biomarkers for prostate cancer. *PLoS One* **2013,** *8* (12), e82589.
365. Kalra, H.; Adda, C. G.; Liem, M.; Ang, C. S.; Mechler, A.; Simpson, R. J.; Hulett, M. D.; Mathivanan, S., Comparative proteomics evaluation of plasma exosome isolation techniques and assessment of the stability of exosomes in normal human blood plasma. *Proteomics* **2013,** *13* (22), 3354-64.

366. Ji, H.; Greening, D. W.; Barnes, T. W.; Lim, J. W.; Tauro, B. J.; Rai, A.; Xu, R.; Adda, C.; Mathivanan, S.; Zhao, W.; Xue, Y.; Xu, T.; Zhu, H. J.; Simpson, R. J., Proteome profiling of exosomes derived from human primary and metastatic colorectal cancer cells reveal differential expression of key metastatic factors and signal transduction components. *Proteomics* **2013,** *13* (10-11), 1672-86.
367. Graner, M. W.; Alzate, O.; Dechkovskaia, A. M.; Keene, J. D.; Sampson, J. H.; Mitchell, D. A.; Bigner, D. D., Proteomic and immunologic analyses of brain tumor exosomes. *Faseb J* **2009,** *23* (5), 1541-57.
368. Choi, D. S.; Kim, D. K.; Kim, Y. K.; Gho, Y. S., Proteomics, transcriptomics and lipidomics of exosomes and ectosomes. *Proteomics* **2013,** *13* (10-11), 1554-71.
369. Carayon, K.; Chaoui, K.; Ronzier, E.; Lazar, I.; Bertrand-Michel, J.; Roques, V.; Balor, S.; Terce, F.; Lopez, A.; Salome, L.; Joly, E., Proteolipidic composition of exosomes changes during reticulocyte maturation. *J Biol Chem* **2011,** *286* (39), 34426-39.
370. Evans, S. M.; Putt, M.; Yang, X. Y.; Lustig, R. A.; Martinez-Lage, M.; Williams, D.; Desai, A.; Wolf, R.; Brem, S.; Koch, C. J., Initial evidence that blood-borne microvesicles are biomarkers for recurrence and survival in newly diagnosed glioblastoma patients. *J Neurooncol* **2016**, 8.
371. Mathivanan, S.; Ji, H.; Simpson, R. J., Exosomes: extracellular organelles important in intercellular communication. *J Proteomics* **2010,** *73* (10), 1907-20.
372. Ostrowski, M.; Carmo, N. B.; Krumeich, S.; Fanget, I.; Raposo, G.; Savina, A.; Moita, C. F.; Schauer, K.; Hume, A. N.; Freitas, R. P.; Goud, B.; Benaroch, P.; Hacohen, N.; Fukuda, M.; Desnos, C.; Seabra, M. C.; Darchen, F.; Amigorena, S.; Moita, L. F.; Thery, C., Rab27a and Rab27b control different steps of the exosome secretion pathway. *Nat Cell Biol* **2010,** *12* (1), 19-30; sup pp 1-13.
373. Balaj, L.; Atai, N. A.; Chen, W.; Mu, D.; Tannous, B. A.; Breakefield, X. O.; Skog, J.; Maguire, C. A., Heparin affinity purification of extracellular vesicles. *Sci Rep* **2015,** *5* (10266), 10266.
374. Kalra, H.; Drummen, G. P.; Mathivanan, S., Focus on Extracellular Vesicles: Introducing the Next Small Big Thing. *Int J Mol Sci* **2016,** *17* (2), 170.
375. Zhang, B.; Asadi, S.; Weng, Z.; Sismanopoulos, N.; Theoharides, T. C., Stimulated human mast cells secrete mitochondrial components that have autocrine and paracrine inflammatory actions. *PLoS One* **2012,** *7* (12), e49767.
376. Sebastiani, G. D.; Iuliano, A.; Cantarini, L.; Galeazzi, M., Genetic aspects of the antiphospholipid syndrome: An update. *Autoimmun Rev* **2016,** *15* (5), 433-9.
377. Trajkovic, K.; Hsu, C.; Chiantia, S.; Rajendran, L.; Wenzel, D.; Wieland, F.; Schwille, P.; Brugger, B.; Simons, M., Ceramide triggers budding of exosome vesicles into multivesicular endosomes. *Science* **2008,** *319* (5867), 1244-7.
378. Phuyal, S.; Hessvik, N. P.; Skotland, T.; Sandvig, K.; Llorente, A., Regulation of exosome release by glycosphingolipids and flotillins. *Febs J* **2014,** *281* (9), 2214-27.
379. Zhang, P.; Zhang, L.; Qin, Z.; Hua, S.; Guo, Z.; Chu, C.; Lin, H.; Zhang, Y.; Li, W.; Zhang, X.; Chen, X.; Liu, G., Genetically Engineered Liposome-like Nanovesicles as Active Targeted Transport Platform. *Adv Mater* **2018,** *30* (7), 27.
380. Han, Y. D.; Bai, Y.; Yan, X. L.; Ren, J.; Zeng, Q.; Li, X. D.; Pei, X. T.; Han, Y., Co-transplantation of exosomes derived from hypoxia-preconditioned adipose mesenchymal stem cells promotes neovascularization and graft survival in fat grafting. *Biochem Biophys Res Commun* **2018,** *497* (1), 305-312.

381. Mleczko, J.; Ortega, F. J.; Falcon-Perez, J. M.; Wabitsch, M.; Fernandez-Real, J. M.; Mora, S., Extracellular Vesicles from Hypoxic Adipocytes and Obese Subjects Reduce Insulin-Stimulated Glucose Uptake. *Mol Nutr Food Res* **2018,** *2* (10), 201700917.
382. Guitart, K.; Loers, G.; Buck, F.; Bork, U.; Schachner, M.; Kleene, R., Improvement of neuronal cell survival by astrocyte-derived exosomes under hypoxic and ischemic conditions depends on prion protein. *Glia* **2016,** *64* (6), 896-910.
383. Xie, J. C.; Ma, X. Y.; Liu, X. H.; Yu, J.; Zhao, Y. C.; Tan, Y.; Liu, X. Y.; Zhao, Y. X., Hypoxia increases amyloid-beta level in exosomes by enhancing the interaction between CD147 and Hook1. *Am J Transl Res* **2018,** *10* (1), 150-163.
384. Sun, L.; Wang, H. X.; Zhu, X. J.; Wu, P. H.; Chen, W. Q.; Zou, P.; Li, Q. B.; Chen, Z. C., Serum deprivation elevates the levels of microvesicles with different size distributions and selectively enriched proteins in human myeloma cells in vitro. *Acta Pharmacol Sin* **2014,** *35* (3), 381-93.
385. Li, J.; Lee, Y.; Johansson, H. J.; Mager, I.; Vader, P.; Nordin, J. Z.; Wiklander, O. P.; Lehtio, J.; Wood, M. J.; Andaloussi, S. E., Serum-free culture alters the quantity and protein composition of neuroblastoma-derived extracellular vesicles. *J Extracell Vesicles* **2015,** *4* (26883), 26883.
386. King, H. W.; Michael, M. Z.; Gleadle, J. M., Hypoxic enhancement of exosome release by breast cancer cells. *BMC Cancer* **2012,** *12* (421), 421.
387. Pope, S. M.; Lasser, C., Toxoplasma gondii infection of fibroblasts causes the production of exosome-like vesicles containing a unique array of mRNA and miRNA transcripts compared to serum starvation. *J Extracell Vesicles* **2013,** *2* (2).
388. Oskowitz, A.; McFerrin, H.; Gutschow, M.; Carter, M. L.; Pochampally, R., Serum-deprived human multipotent mesenchymal stromal cells (MSCs) are highly angiogenic. *Stem Cell Res* **2011,** *6* (3), 215-25.
389. Aubertin, K.; Silva, A. K.; Luciani, N.; Espinosa, A.; Djemat, A.; Charue, D.; Gallet, F.; Blanc-Brude, O.; Wilhelm, C., Massive release of extracellular vesicles from cancer cells after photodynamic treatment or chemotherapy. *Sci Rep* **2016,** *6* (35376), 35376.
390. Taverna, S.; Ghersi, G.; Ginestra, A.; Rigogliuso, S.; Pecorella, S.; Alaimo, G.; Saladino, F.; Dolo, V.; Dell'Era, P.; Pavan, A.; Pizzolanti, G.; Mignatti, P.; Presta, M.; Vittorelli, M. L., Shedding of membrane vesicles mediates fibroblast growth factor-2 release from cells. *J Biol Chem* **2003,** *278* (51), 51911-9.
391. Haraszti, R. A.; Didiot, M. C.; Sapp, E.; Leszyk, J.; Shaffer, S. A.; Rockwell, H. E.; Gao, F.; Narain, N. R.; DiFiglia, M.; Kiebish, M. A.; Aronin, N.; Khvorova, A., High-resolution proteomic and lipidomic analysis of exosomes and microvesicles from different cell sources. *J Extracell Vesicles* **2016,** *5* (32570), 32570.
392. Kummel, D.; Ungermann, C., Principles of membrane tethering and fusion in endosome and lysosome biogenesis. *Curr Opin Cell Biol* **2014,** *29*, 61-6.
393. Nabhan, J. F.; Hu, R.; Oh, R. S.; Cohen, S. N.; Lu, Q., Formation and release of arrestin domain-containing protein 1-mediated microvesicles (ARMMs) at plasma membrane by recruitment of TSG101 protein. *Proc Natl Acad Sci U S A* **2012,** *109* (11), 4146-51.
394. Paulmann, M.; Arnold, T.; Linke, D.; Ozdirekcan, S.; Kopp, A.; Gutsmann, T.; Kalbacher, H.; Wanke, I.; Schuenemann, V. J.; Habeck, M.; Burck, J.; Ulrich, A. S.; Schittek, B., Structure-activity analysis of the dermcidin-derived peptide DCD-1L, an anionic antimicrobial peptide present in human sweat. *J Biol Chem* **2012,** *287* (11), 8434-43.

395. Delva, E.; Tucker, D. K.; Kowalczyk, A. P., The desmosome. *Cold Spring Harb Perspect Biol* **2009,** *1* (2), a002543.
396. Watson, K.; Koumangoye, R.; Thompson, P.; Sakwe, A. M.; Patel, T.; Pratap, S.; Ochieng, J., Fetuin-A triggers the secretion of a novel set of exosomes in detached tumor cells that mediate their adhesion and spreading. *FEBS Lett* **2012,** *586* (19), 3458-63.
397. Ikonen, E., Roles of lipid rafts in membrane transport. *Curr Opin Cell Biol* **2001,** *13* (4), 470-7.
398. Huijbregts, R. P.; Topalof, L.; Bankaitis, V. A., Lipid metabolism and regulation of membrane trafficking. *Traffic* **2000,** *1* (3), 195-202.
399. Cao, J.; Liu, Y.; Lockwood, J.; Burn, P.; Shi, Y., A novel cardiolipin-remodeling pathway revealed by a gene encoding an endoplasmic reticulum-associated acyl-CoA:lysocardiolipin acyltransferase (ALCAT1) in mouse. *J Biol Chem* **2004,** *279* (30), 31727-34.
400. Schlame, M.; Acehan, D.; Berno, B.; Xu, Y.; Valvo, S.; Ren, M.; Stokes, D. L.; Epand, R. M., The physical state of lipid substrates provides transacylation specificity for tafazzin. *Nat Chem Biol* **2012,** *8* (10), 862-9.
401. Jia, H.; Heymann, M.; Bernhard, F.; Schwille, P.; Kai, L., Cell-free protein synthesis in micro compartments: building a minimal cell from biobricks. *N Biotechnol* **2017,** *39* (Pt B), 199-205.
402. Li, Z.; Wei, H.; Liu, X.; Hu, S.; Cong, X.; Chen, X., LPA rescues ER stress-associated apoptosis in hypoxia and serum deprivation-stimulated mesenchymal stem cells. *J Cell Biochem* **2010,** *111* (4), 811-20.
403. Holcik, M.; Sonenberg, N.; Korneluk, R. G., Internal ribosome initiation of translation and the control of cell death. *Trends Genet* **2000,** *16* (10), 469-73.
404. Ghosh, H. S.; Reizis, B.; Robbins, P. D., SIRT1 associates with eIF2-alpha and regulates the cellular stress response. *Sci Rep* **2011,** *1* (150), 150.
405. Zhao, J.; Zhai, B.; Gygi, S. P.; Goldberg, A. L., mTOR inhibition activates overall protein degradation by the ubiquitin proteasome system as well as by autophagy. *Proc Natl Acad Sci U S A* **2015,** *112* (52), 15790-7.
406. Stavropoulou, A. V.; Mavrofrydi, O.; Saftig, P.; Efthimiopoulos, S., Serum Starvation Induces BACE1 Processing and Secretion. *Curr Alzheimer Res* **2017,** *14* (4), 453-459.
407. Llombart, V.; Garcia-Berrocoso, T.; Bech-Serra, J. J.; Simats, A.; Bustamante, A.; Giralt, D.; Reverter-Branchat, G.; Canals, F.; Hernandez-Guillamon, M.; Montaner, J., Characterization of secretomes from a human blood brain barrier endothelial cells in-vitro model after ischemia by stable isotope labeling with aminoacids in cell culture (SILAC). *J Proteomics* **2016,** *133*, 100-112.
408. Bochmann, I.; Ebstein, F.; Lehmann, A.; Wohlschlaeger, J.; Sixt, S. U.; Kloetzel, P. M.; Dahlmann, B., T lymphocytes export proteasomes by way of microparticles: a possible mechanism for generation of extracellular proteasomes. *J Cell Mol Med* **2014,** *18* (1), 59-68.
409. Lai, R. C.; Tan, S. S.; Teh, B. J.; Sze, S. K.; Arslan, F.; de Kleijn, D. P.; Choo, A.; Lim, S. K., Proteolytic Potential of the MSC Exosome Proteome: Implications for an Exosome-Mediated Delivery of Therapeutic Proteasome. *Int J Proteomics* **2012,** *2012* (10), 971907.
410. Choi, D. S.; Choi, D. Y.; Hong, B. S.; Jang, S. C.; Kim, D. K.; Lee, J.; Kim, Y. K.; Kim, K. P.; Gho, Y. S., Quantitative proteomics of extracellular vesicles derived from human primary and metastatic colorectal cancer cells. *J Extracell Vesicles* **2012,** *1* (1).
411. Overmiller, A. M.; Pierluissi, J. A.; Wermuth, P. J.; Sauma, S.; Martinez-Outschoorn, U.; Tuluc, M.; Luginbuhl, A.; Curry, J.; Harshyne, L. A.; Wahl, J. K., 3rd; South, A. P.; Mahoney, M.

G., Desmoglein 2 modulates extracellular vesicle release from squamous cell carcinoma keratinocytes. *Faseb J* **2017,** *31* (8), 3412-3424.
412. Dozio, V.; Sanchez, J. C., Characterisation of extracellular vesicle-subsets derived from brain endothelial cells and analysis of their protein cargo modulation after TNF exposure. *J Extracell Vesicles* **2017,** *6* (1), 1302705.
413. Keerthikumar, S.; Gangoda, L.; Liem, M.; Fonseka, P.; Atukorala, I.; Ozcitti, C.; Mechler, A.; Adda, C. G.; Ang, C. S.; Mathivanan, S., Proteogenomic analysis reveals exosomes are more oncogenic than ectosomes. *Oncotarget* **2015,** *6* (17), 15375-96.
414. Willms, E.; Johansson, H. J.; Mager, I.; Lee, Y.; Blomberg, K. E.; Sadik, M.; Alaarg, A.; Smith, C. I.; Lehtio, J.; El Andaloussi, S.; Wood, M. J.; Vader, P., Cells release subpopulations of exosomes with distinct molecular and biological properties. *Sci Rep* **2016,** *6* (22519), 22519.
415. Nemeth, A.; Orgovan, N.; Sodar, B. W.; Osteikoetxea, X.; Paloczi, K.; Szabo-Taylor, K. E.; Vukman, K. V.; Kittel, A.; Turiak, L.; Wiener, Z.; Toth, S.; Drahos, L.; Vekey, K.; Horvath, R.; Buzas, E. I., Antibiotic-induced release of small extracellular vesicles (exosomes) with surface-associated DNA. *Sci Rep* **2017,** *7* (1), 8202.
416. Lee, J.; Kim, J.; Jeong, M.; Lee, H.; Goh, U.; Kim, H.; Kim, B.; Park, J. H., Liposome-Based Engineering of Cells To Package Hydrophobic Compounds in Membrane Vesicles for Tumor Penetration. *Nano Lett* **2015**, 31.
417. Sato, Y. T.; Umezaki, K.; Sawada, S.; Mukai, S. A.; Sasaki, Y.; Harada, N.; Shiku, H.; Akiyoshi, K., Engineering hybrid exosomes by membrane fusion with liposomes. *Sci Rep* **2016,** *6* (21933), 21933.
418. Friend, D. S., Cytochemical staining of multivesicular body and golgi vesicles. *J Cell Biol* **1969,** *41* (1), 269-79.
419. Kolesnikova, L.; Berghofer, B.; Bamberg, S.; Becker, S., Multivesicular bodies as a platform for formation of the Marburg virus envelope. *J Virol* **2004,** *78* (22), 12277-87.
420. Nilsson, P.; Sekiguchi, M.; Akagi, T.; Izumi, S.; Komori, T.; Hui, K.; Sorgjerd, K.; Tanaka, M.; Saito, T.; Iwata, N.; Saido, T. C., Autophagy-related protein 7 deficiency in amyloid beta (Abeta) precursor protein transgenic mice decreases Abeta in the multivesicular bodies and induces Abeta accumulation in the Golgi. *Am J Pathol* **2015,** *185* (2), 305-13.
421. Nolan, J. P., Flow Cytometry of Extracellular Vesicles: Potential, Pitfalls, and Prospects. *Curr Protoc Cytom* **2015,** *73* (13), 13 14 1-16.
422. Nair, J. K.; Attarwala, H.; Sehgal, A.; Wang, Q.; Aluri, K.; Zhang, X.; Gao, M.; Liu, J.; Indrakanti, R.; Schofield, S.; Kretschmer, P.; Brown, C. R.; Gupta, S.; Willoughby, J. L. S.; Boshar, J. A.; Jadhav, V.; Charisse, K.; Zimmermann, T.; Fitzgerald, K.; Manoharan, M.; Rajeev, K. G.; Akinc, A.; Hutabarat, R.; Maier, M. A., Impact of enhanced metabolic stability on pharmacokinetics and pharmacodynamics of GalNAc-siRNA conjugates. *Nucleic Acids Res* **2017,** *45* (19), 10969-10977.